WANL-PR(LL)-022
September 30, 1968

Westinghouse Astronuclear Laboratory

SYNTHESIS OF CALCULATIONAL METHODS FOR THE DESIGN AND ANALYSIS OF RADIATION SHIELDS FOR NUCLEAR ROCKET SYSTEMS

Contract No. NAS-8-20414
Contract No. DCN-16-28-0029 (IF)

Volume 1

RADIATION MEASUREMENTS IN A NUCLEAR ROCKET PROPELLANT TANK MOCKUP USING SIMULATED LIQUID HYDROGEN

WANL-PR(LL)-022
September 30, 1968

Westinghouse Astronuclear Laboratory

SYNTHESIS OF CALCULATIONAL METHODS FOR THE DESIGN AND ANALYSIS OF RADIATION SHIELDS FOR NUCLEAR ROCKET SYSTEMS

Contract No. NAS-8-20414
Contract No. DCN-16-28-0029 (IF)

Volume 1

RADIATION MEASUREMENTS IN A NUCLEAR ROCKET PROPELLANT TANK MOCKUP USING SIMULATED LIQUID HYDROGEN

Prepared By:
H. C. Woodsum
J. Rowland

INFORMATION CATEGORY
Unclassified
C. M. Hinckley 9/25/68
AUTHORIZED CLASSIFIER DATE

Frontispiece

MODIFIED SATURN I B LOX TANK IN POSITION ABOVE THE PAX REACTOR

TABLE OF CONTENTS

TABLE OF CONTENTS (CONTINUED)

TABLE OF CONTENTS (CONTINUED)

TABLE OF CONTENTS (CONTINUED)

LIST OF ILLUSTRATIONS

LIST OF ILLUSTRATIONS (CONTINUED)

LIST OF ILLUSTRATIONS(CONTINUED)

LIST OF ILLUSTRATIONS (CONTINUED)

LIST OF ILLUSTRATIONS (CONTINUED)

LIST OF ILLUSTRATIONS (CONTINUED)

LIST OF TABLES

ABSTRACT

This report is Volume 1 of two volumes of the final report on "Synthesis of Calculational Methods for the Design and Analysis of Radiation Shields for Nuclear Rocket Systems." This work was performed for the George C. Marshall Space Flight Center (MSFC) under Contract NAS-8-20414, Modification 3.

This contract included the measurement and analysis of the radiation environment on and in a modified 72-inch diameter Saturn 1-B LOX tank suspended above a nuclear rocket critical assembly. Measurements were performed at the Westinghouse Astronuclear Experimental Facility (WANEF) with the tank filled with two different densities of polyethylene (0.59 and 0.14 gm/cc) to simulate, respectively, the neutron and photon transport properties in liquid hydrogen. A critical mockup of an NRX (NERVA Reactor Experiment) nuclear reactor provided a source of neutron and gamma radiation with the desired spectral characteristics. Two different shield mockups were interposed between the reactor and the propellant tank.

Measurements of neutron fluxes, fast neutron dose rates, and gamma dose rates were made in the propellant tank to provide data on neutron and photon transport properties. Thermal neutron fluxes and neutron spectra on the surface of the tank in a ground test environment were obtained for use in the evaluation of after-shutdown problems associated with activation of the propellant tank structure and for evaluation of radiation analysis methods. Some effects of test cell background were determined experimentally.

Comparisons of calculated and measured neutron and gamma radiation levels are included in this report. The two-dimensional discrete ordinates transport code, DOT, was employed to generate neutron fluxes throughout the reactor assembly; and the data processing code, NAGS, generated source data from those neutron fluxes for use in the point kernel and Monte Carlo analyses. Calculations in the propellant tank were performed utilizing the KAP-V point kernel code and the FASTER Monte Carlo code, both of which were previously provided to MSFC under this contract.

Volume 1 describes the experimental portion of the work, while Volume 2 presents an analysis of these measurements. A classified appendix to Volume 2 presents detailed geometrical and material descriptions of the reactor and shield mockups and listings of the computer code data employed in this analysis.

ACKNOWLEDGMENT

We appreciate the guidance provided by Mr. H. E. Stern, Deputy Manager, Nuclear and Space Science Division, George C. Marshall Space Flight Center, the Technical Monitor of the contract. We also appreciate the efforts of Mr. L. Katz of MSFC in providing the modified propellant tank and associated stress analysis and for performing the safety load test on the tank.

We acknowledge the permission of the Space Nuclear Propulsion Office to perform these measurements in conjunction with NERVA experiments and to utilize certain detector and electronic equipment. We appreciate the review and approval of M. Fleishman, SNPO/Cleveland.

The authors of this volume gratefully acknowledge the support given by the WANEF staff. Special thanks go to Mr. B. Jennings and Dr. V. S. Oblock for their consultation and guidance. Special thanks are also given to J. Shearer and E. A. Popyak for their assistance during the mechanical construction and data acquisition.

Thanks should also be given to the secretaries, Mrs. D. Christ and Mrs. P. A. Swanson, without whose patience this volume could not have been transcribed.

SECTION 1. INTRODUCTION

Under Contract No. NAS-8-20414 with the Marshall Space Flight Center, computer codes (1) were developed by the Westinghouse Astronuclear Laboratory for use in the radiation analysis of Nuclear Rocket Systems. These methods have been evaluated to some extent through comparisons of measured radiation environment data with similar experimental data obtained from previous NERVA low and high power reactor tests. However, this work indicated the serious lack of experimental data around the dome end of a nuclear rocket and, in particular, within a nuclear rocket propellant tank. These data are required especially to evaluate the accuracy of computer code methods, to predict radiation heating rates in the propellant tank and to predict propellant tank activation following a hot test firing in a simulated ground test environment.

Hence, the basic contract was extended, effective in January 1968, to include performance of limited radiation level measurements in a simulated propellant tank mockup and the evaluation of these results with the analytical methods developed under the contract. These measurements were made at the Westinghouse Astronuclear Experimental Facility (WANEF) using the PAX-E5 NERVA critical assembly with suitable shield mockups to provide the radiation source. The experiments were conducted simultaneously with scheduled NERVA shield experiments over a total time span of approximately one month. The results of these measurements are presented in this volume while the analytical results are covered in the second volume of this set.

In the performance of these experimental radiation measurements, a mockup propellant tank was mounted above the PAX-E5 reactor, a nuclear mockup of the NRX-A6 reactor, at a location characteristic of a flight nuclear rocket system. The tank is a surplus test fixture similar to a portion of a Saturn 1B-LOX tank and was modified, load tested, and furnished by Marshall Space Flight Center. The liquid hydrogen propellant was mocked up by two different densities of polyethylene to simulate neutron and gamma ray attenuation properties, respectively.

---

(1) "Synthesis of Calculational Methods for the Design and Analysis of Radiation Shields for Nuclear Rocket Systems," WANL-PR(LL)-010, Volumes 1-9, June 1967.

Three different radiation shields were imposed between the reactor core and the propellant tank. The first, known as Shield Configuration 4B, is a nuclear mockup of the reactor core support plate and plenum region of an unshielded NERVA engine. In the second shield, Configuration 7D, the above material is augmented with an 80 gm/cm^2 thick mockup of a boron-aluminum-titanium hydride shield. The total area density of the mockup is 140 gm/cm^2. A third shield which was also utilized, Configuration 11, was sufficiently thick (214 gm/cm^2) to provide a very high attenuation of the direct reactor radiation and was employed only for test cell background studies.

For these configurations, neutron and gamma ray dose measurements were made using active and passive dosimeters at various locations within the simulated propellant and on the outer surface of the mockup propellant tank. The results of these measurements will be used for comparison with analytical predictions performed on the detailed geometry and materials of the experimental conditions, are given in the companion volume of this report.

Section 2 contains the Conclusions derived from these experiments and gives recommendations for future work.

Section 3 contains a description of the Experimental Facilities, including the reactor, shield mockups, tank detection system and test cell.

Section 4 contains a listing of the test objectives.

Section 5 contains a description of the experimental plan.

Section 6 contains the experimental results and a discussion of these data.

The Appendices describe some of the details of the detector calibration, data reducing techniques, the results of chemical composition of the tank, and a comparison of these data with results obtained with LH_2 by General Dynamics/Fort Worth.

SECTION 2. CONCLUSIONS AND RECOMMENDATIONS

2.1 CONCLUSIONS

As a result of these experiments, the following conclusions are reached:

2.1.1 The fast neutron fluxes ($E > 1.5$ Mev and $E > 2.9$ Mev) and neutron dose rate distributions were measured in polyethylene of density 0.59 gm/cc (mocking up neutron transport dosimeters of LH_2) in a propellant tank above a mockup NRX reactor with two shield mockup configurations mounted on the reactor. Shield Configuration 4B consisted of a mockup of a support plate and plenum region for the R-1 reactor with total areal density of 59 gm/cm^2. Shield Configuration 11 consisted of a mockup of lead, polyethylene, and boral with total areal density of 214 gm/cm^2 to simulate a "thick" shield for measurement of test cell produced radiation background. The above noted neutron data have an accuracy of ± 10-15 percent. Because of the relatively small uncertainties and the significant difference in magnitude observed between the data for these two configurations, the "direct" (i.e., with test cell background removed) fast neutron dose rate can be obtained by a simple subtraction process (Configurations 4B-11) with only 15-30 percent uncertainty in the results. These data provide, by the method outlined in Section 3.6, an accurate measurement of neutron heating rates and provide the analyst a good check of the methods used to predict neutron heating throughout a simulated LH_2 propellant medium.

2.1.2 Comparison of present fast neutron flux distributions with the results of cryogenic hydrogen measurements by General Dynamics/Fort Worth(1) show qualitative agreement although differences in tank geometry preclude an exact comparison. Use of polyethylene in place of liquid hydrogen is concluded to adequately simulate the fast neutron ($E > 0.2$ Mev) transport properties of LH_2. The predicted fast neutron energy deposition (per watt of reactor power) as calculated from these dose measurements is 1.5×10^{-11} watts/cc of LH_2 at the bottom of the tank on the axial centerline.

---

(1) NASA CR-54078, "Nuclear Radiation Heating in Liquid Hydrogen,", Volume 1.

2.1.3 The gamma ray dose rate data for Shield Configuration 4B with polyethylene density of 0.59 gm/cc were also measured with active dosimetry to an accuracy of ± 9 percent, and these data can be used, by the method described in Section 3.6, to provide gamma heating rate data for this configuration. Comparison of these data with the Fort Worth cryogenic hydrogen measurements show good agreement in attenuation properties of polyethylene and liquid hydrogen. Hence, it is concluded that polyethylene adequately simulates the gamma attenuation properties of LH_2. Measurements of the gamma ray dose rates for Configurations 4B and 11 were also made to a reported accuracy of ± 17 percent (not including unknown neutron induced effects) using thermoluminescent dosimeters (TLD). In this case, since the subtraction of Configuration 11 from 4B data required the use of both the active and the passive TLD measurements the resultant "direct" dose rate is reported to an accuracy of 20 percent.

2.1.4 Neutron spectral data was obtained on the propellant tank surface using activation foil techniques to measure flux levels in certain broad energy bands, i.e., thermal energy, $E > 0.4$ev, $E \cong 5$ ev, $E > 0.5$Kev, $E > 1.5$ Mev, and $E > 2.9$ Mev. The accuracy of these data was generally within ± 13 percent except for the Pu-239 data which has an accuracy of ± 28 percent. These data provide a check of methods used to calculate neutron spectra.

2.1.5 Thermal neutron flux distributions were measured with a boron-lined ionization chamber in polyethylene of density 0.59 g/cc for Shield Configurations 4B and 11 and in polyethylene of density 0.14 g/cc for Shield Configurations 7D and 11 to within an accuracy of ± 9 percent. In addition, thermal neutron fluxes were measured on the surface of the propellant tank for the various configurations described above to an accuracy of ± 13 percent. These data will assist in analysis of thermal neutron induced secondary gamma sources and permit the accurate prediction of neutron induced activation for a propellant tank in the WANEF test cell geometry.

2.1.6 Gamma ray dose rate data were obtained with 0.14 gm/cc polyethylene (mocking up gamma transport characteristics of LH_2) in the propellant tank to an accuracy of

± 9 percent using ion chamber active dosimetry. Shield Configuration 7D was utilized which consisted of a mockup of support plate, plenum, and shield regions for the R-1 reactor with a total areal density of 140 gm/cm^2. However, because of the small differences noted in the data for Configurations 7D and 11, the direct dose rate data, obtained by subtracting 11 from 7D, provide only an order of magnitude accuracy and an upper limit to the "direct" dose rate values. Based upon those measurements, the deduced gamma energy deposition (per watt of reactor power) for LH_2 is 7.5×10^{-13} watts/cc ± 100 percent at the bottom of the tank on the axial centerline.

2.2 RECOMMENDATIONS FOR FUTURE EXPERIMENTAL WORK

Recommendations for future experimental work include the following:

1) Extend present measurements to include radiation mapping for shield configurations intermediate between Shield Configurations 4B and 7D (approximately 80 gm/cm^2) and with a variation of Shield Configuration 11 using both low and high density polyethylene in the tank in order to obtain a complete set of gamma and neutron dose rate data for a single shield configuration. Measurements should be made in the high density polyethylene with a tank filled to a greater height.

2) Experiments should be conducted with larger diameter tanks to reduce the edge effects in the smaller tank experiment. Measurements with various tank bottom shapes should be made to ascertain their effect upon the energy deposition in the tank.

3) Measurements should be made with mockups of proposed ground test module facilities performed to determine resultant test cell activation levels and effects upon propellant heating.

4) Measurements should be performed to provide better spatial resolution of radiation dose rates along the bottom of the tank for improved definition of heating rates.

5) A more detailed definition of the neutron and gamma spectra incident on the propellant tank mockup should be obtained.

6) Further measurements should be made to understand and reduce the difference obtained between the TLD passive dosimetry results and the CO_2 ionization

chamber results in a simulated propellant media. The passive dosimetry systems should be improved so that better agreement can be obtained with the active dosimetry results, both in consistency and in magnitude.

7) Additional measurements should be made in the presence of improved test cell background conditions. The test cell background should be reduced by lining the walls with suitable materials to permit measurement of shields with higher attenuations.

8) Measurements should be performed with and without a lithium containing liner surrounding the outer propellant tank walls in order to determine the magnitude of test cell induced thermal neutron capture gammas produced in the propellant tank walls.

9) Basic physics measurements should be made under the same conditions with both liquid hydrogen and polyethylene simulation to further verify their equivalence for the transport of gamma and fast neutron radiation.

SECTION 3. EXPERIMENTAL FACILITIES

3.1 WANEF FACILITY

The Marshall propellant tank radiation measurements were performed at the NERVA critical facility at the Westinghouse Astronuclear Experimental Facility (WANEF) located at Waltz Mill, Pennsylvania, approximately 20 miles southeast of Pittsburgh. The facility building houses two reactor assemblies, the PAX (Permanent Assembly Experiment) with which the reported measurements were performed, and the FCX (Flexible Critical Experiment) which was inactive during the performance of these measurements. An external view of WANEF is shown in Figure 3-1.

3.2 DESCRIPTION OF TEST CELL GEOMETRY

An isometric of the test cell in which the propellant tank experiments were conducted is shown in Figure 3-2. In addition to the PAX reactor which was used in the experiment, the test cell contains the Flexible Critical Experiment (FCX) reactor assembly.

Plan and elevation drawings of the WANEF test cell are shown in Figures 3-3 through 3-6. The height of the cell above the ground level is 52 feet and the basement depth is 22 feet 6 inches. Above ground level, the north and west walls are 4 feet 6 inches thick to a height of 20 feet. Above this, the west wall is cut back to a thickness of 2 feet and the north wall to 1 foot for the remaining height of the test cell. The 4-foot 6-inch north wall provides radiation shielding for personnel who may be working in an adjacent test cell during operation at WANEF. The east and south walls are 2 feet thick to a height of 20 feet above ground level and are then 1 foot thick above this level. The basement floor is a 6-inch thick concrete slab and the cell roof is 9-inch thick reinforced concrete covered with a mixture of tar and gravel. A 12-inch thick poured concrete slab on the north wall serves as a storage shelf for reactor fuel and miscellaneous experimental hardware for the WANEF facility. This storage shelf is 12 feet wide and extends the entire east-west length of the test cell.

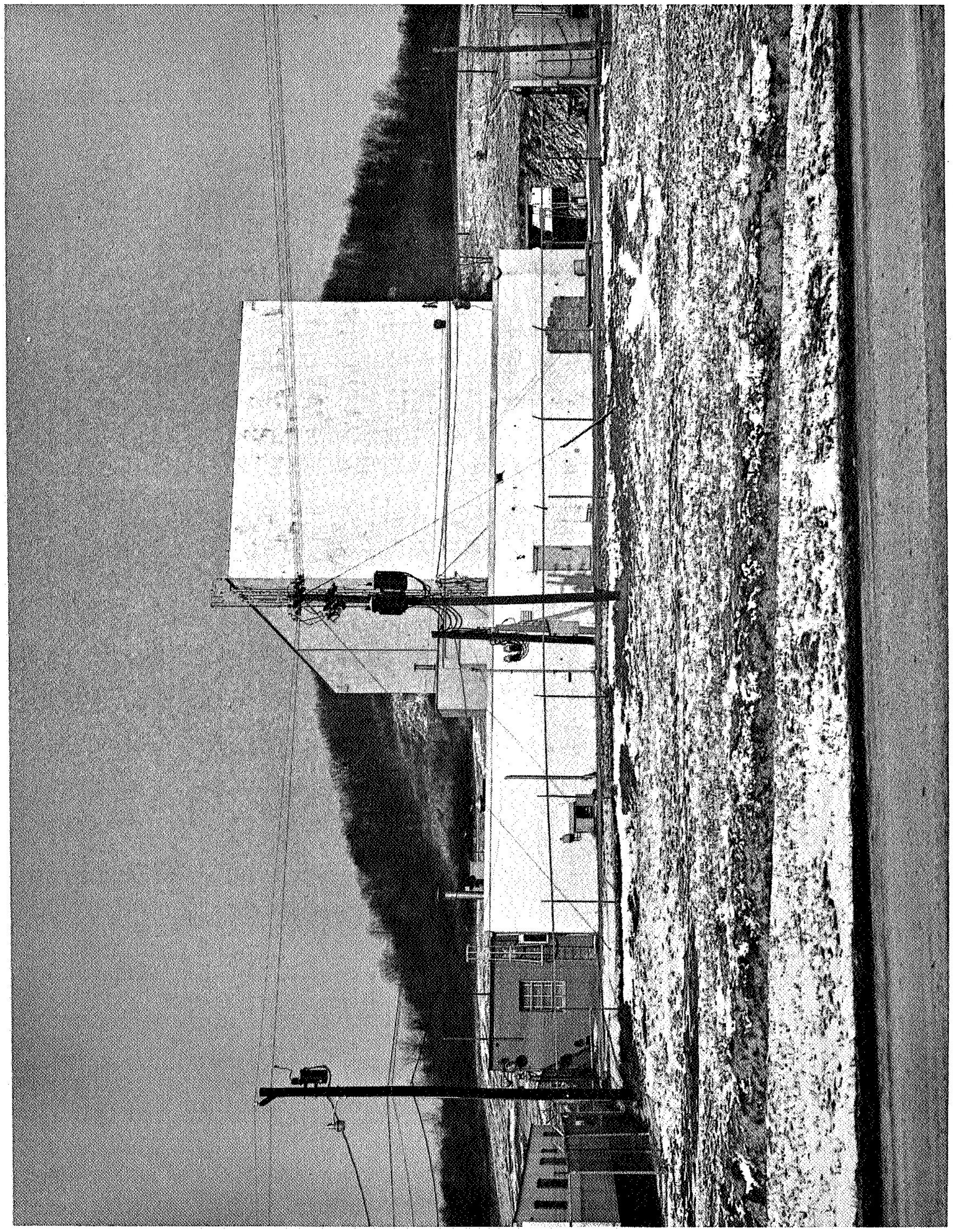

Figure 3. 1. The Westinghouse Astronuclear Experimental Facility

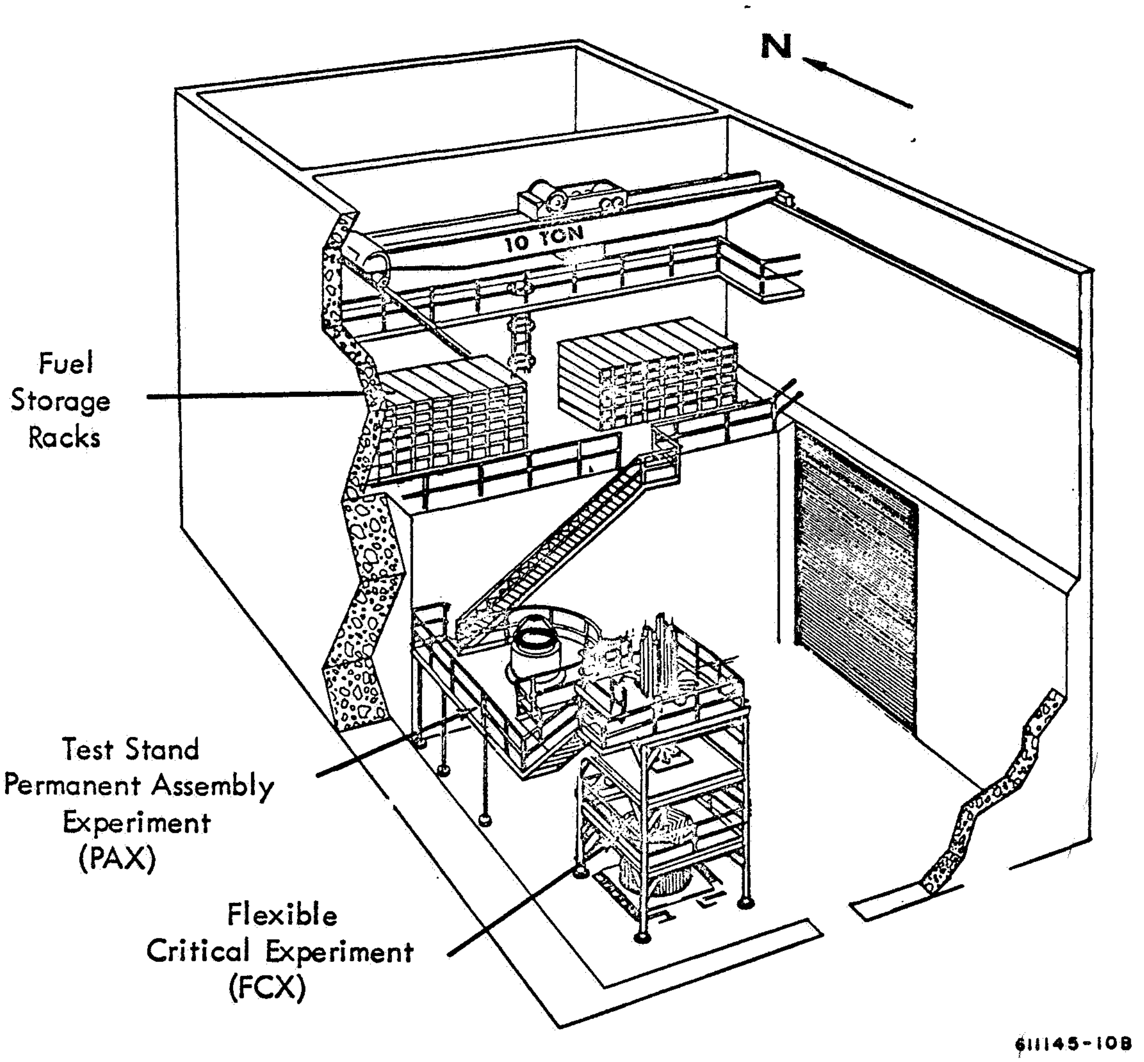

Figure 3-2. WANEF Test Cell - Isometric View

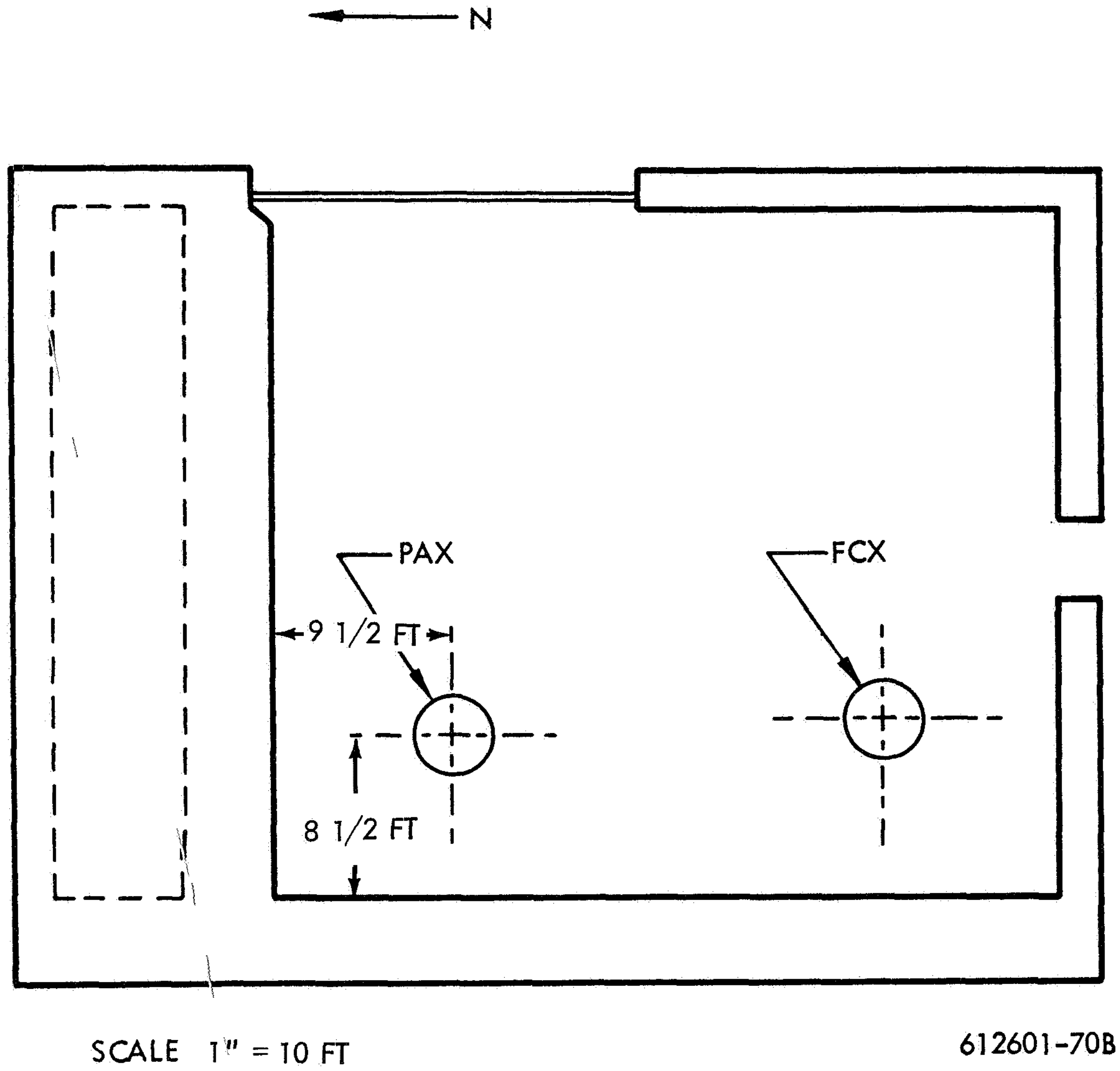

Figure 3-3. Plan View of WANEF Test Cell

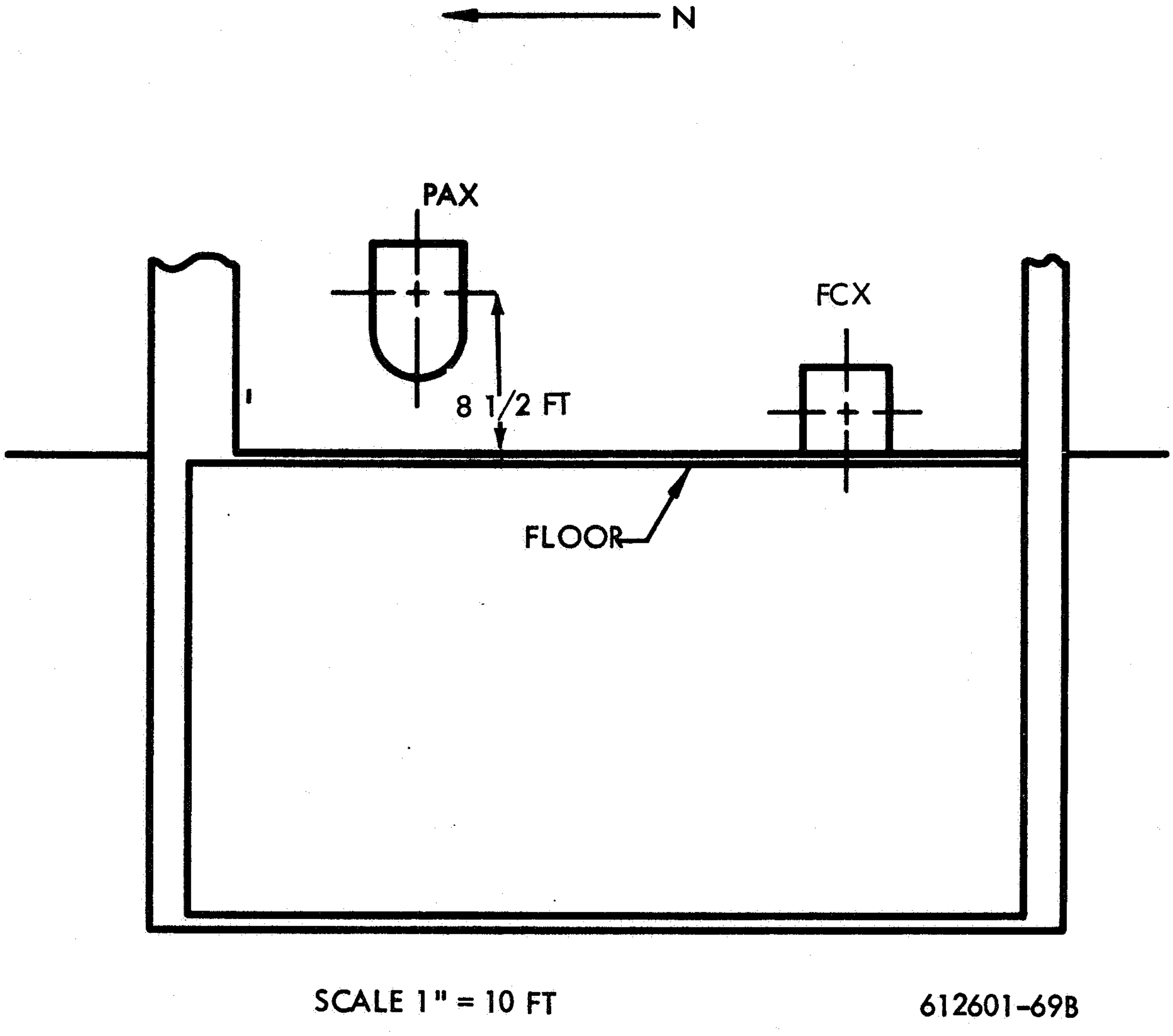

Figure 3-4. N-S Elevation View of WANEF Test Cell-Basement

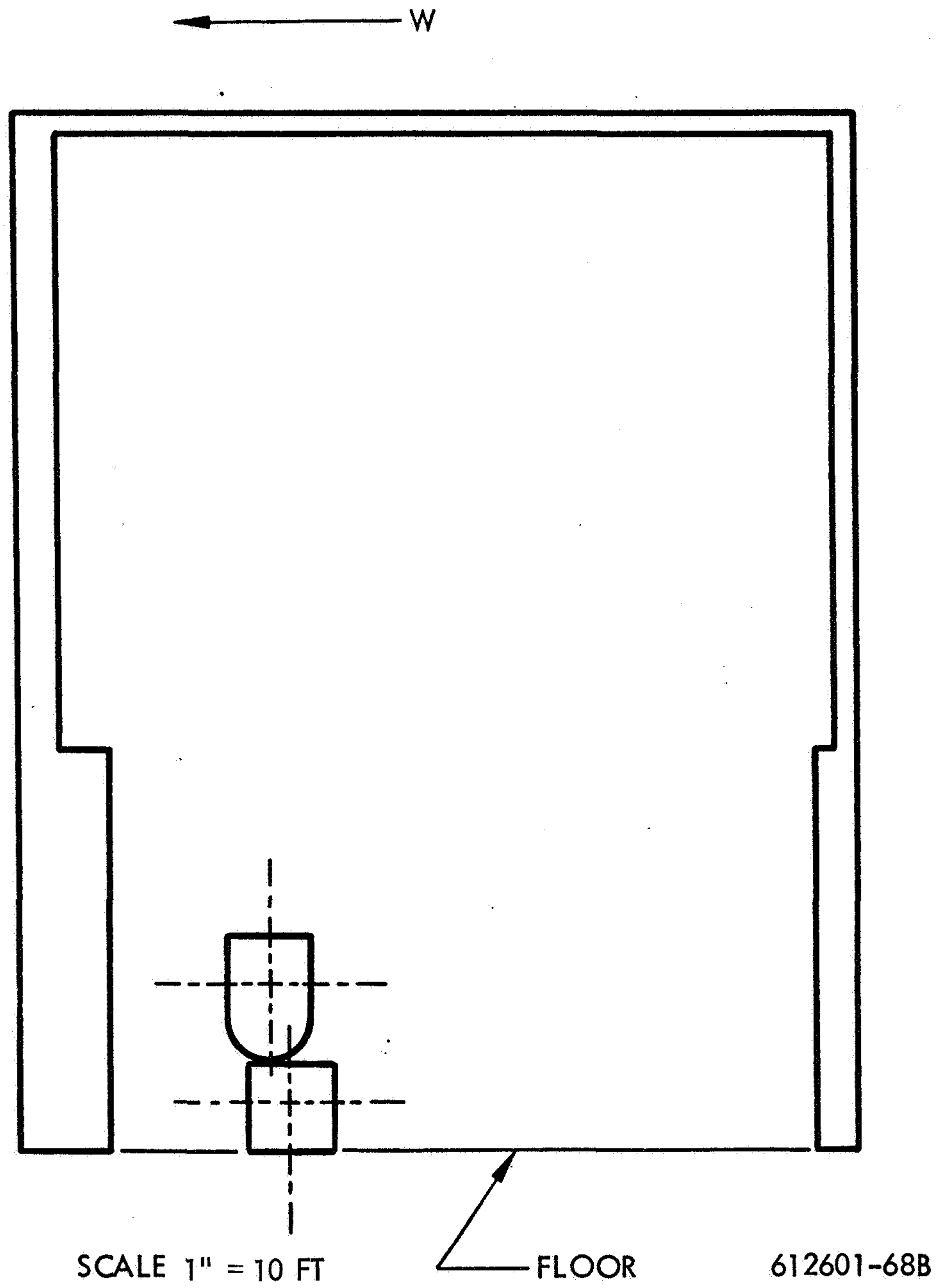

Figure 3-5. E-W Elevation View of WANEF Test Cell

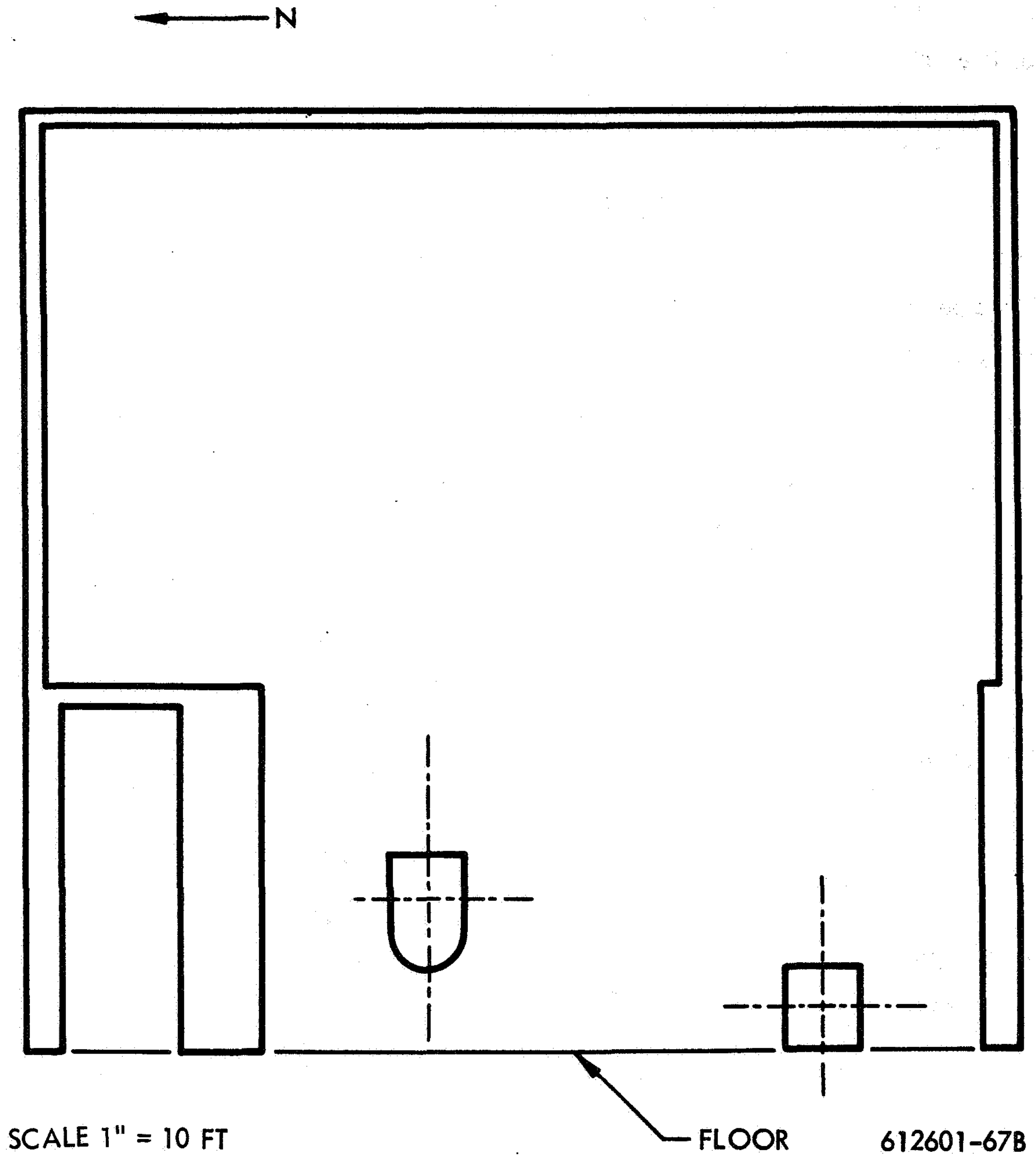

Figure 3-6. N-S Elevation View of WANEF Test Cell

Two doors provide access to the test cell: a 20 foot square electrically operated roll-up truck door, located in the east wall, and a personnel entrance, located in the south wall. The roll-up door is of 18 gauge galvanized metal with interlocking ribs. The personnel door is a "B" label hollow metal fire door which opens from the labyrinth into the cell.

The floor structure of the test cell is constructed of I-beams which are covered with metal checker plate. In order to permit trucks to enter the building, the north half of the floor has heavier construction, consisting of Type 14W43 I-beams located 1 foot - 11 1/2 inches on centers and covered with 1-inch thick checker plate. Allowable truck loading is 20 tons per axle. The south half of the floor is constructed more lightly to support 150 psf live load. This half of the floor is covered with 3/8-inch thick metal checker plate.

3.3 PAX REACTOR DESCRIPTION

3.3.1 PAX Assembly

The Permanent Assembly Experiment (PAX) critical assembly, shown in Figure 3-7, is a nuclear and mechanical mockup of the NRX reactor which is a part of the development program for the NERVA engine. The PAX-E5 assembly which was utilized in these measurements consists primarily of NRX components which are nuclearly equivalent to the NRX-A6 reactor.

The basic PAX assembly consists of the reactor subassembly, the radiation shield mockup, pressure vessel, control drum drives and test stand. The PAX reactor subassembly includes the core assembly, graphite inner reflector, beryllium outer reflector, and the lateral support. Clusters of graphite-uranium fuel elements, which constitute the core assembly, rest upon an aluminum core support plate which, in turn, is supported by the pressure vessel dome via a transition ring and the outer reflector support ring. A typical NRX-type dummy aluminum shield rests beneath the core support plate. Immediately surrounding the core assembly are three band and pulley mechanisms which provide lateral support for the PAX core. The beryllium outer reflector consists of twelve 30 degree sectors which are held vertically between the reflector support ring and the lower (forward) support ring by means of through-bolts. Each sector contains one rotating control drum. Surrounding the reactor subassembly is a dummy

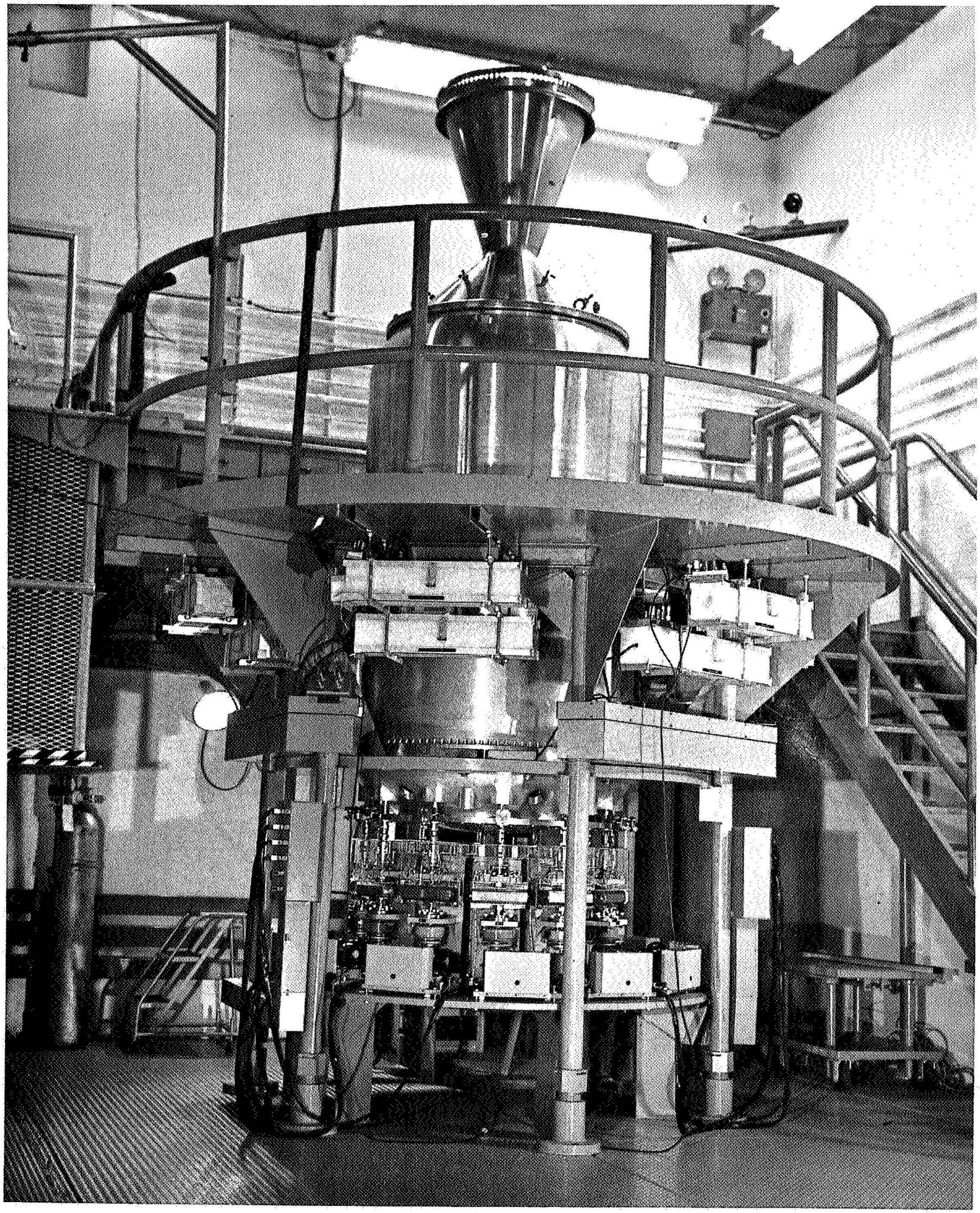

Figure 3-7. The PAX Reactor with Mockup Nozzle in Place

aluminum pressure vessel and a shield mockup which is comprised of three sections: the dome, which contains the core support plate, the cylinder body which contains the reactor subassembly, and a removable section at the nozzle end of the pressure vessel. The nozzle end mechanically supports either a protective cover, the dummy nozzle, or the components of end-on experiments. During these experiments a special adapter ring was used to support the shield mockup in place of the usual nozzle adapter section. That is, the nozzle end of the PAX was utilized and effectively converted into the inlet end of the reactor for these shield measurements.

3.3.2 PAX-E5 Reactor

The reactor configuration used for these experiments was the PAX-E5 reactor. In one quadrant of the reactor, three NRX-A3 type 30 degree beryllium sectors have been modified to closely simulate the NRX-A6 reflector. NRX-A6 reject fuel is used in this quadrant as well as the central circle. In the remaining 270 degrees, the reflector consists of 9 KIWI sectors augmented on the inner diameter with removable beryllium liner plates as shown in Figure 3-8 to provide the equivalent NRX-A6 beryllium area density. Since not enough NRX-A6 type fuel was available for the remaining 270 degree portion of the core, a mix of fueled and unfueled elements was used with the material number densities adjusted on a per element and per cluster basis by means of various types of wires placed in specified coolant channels. Hence, the PAX fuel elements are nuclearly equivalent to those in the current NRX-A6 design and are mechanically identical. Although the majority of the fuel elements in the PAX core are elements that have been rejected in manufacture, the causes for rejection are related to the mechanical or thermal specifications and do not affect their use in a reactor as a radiation source. Reactor power calibrations were derived from a fission flux map of the core and radiochemistry of selected fuel samples.

In order to keep this volume unclassified, the detailed specifications on the reactor are given in the classified appendix to Volume II.

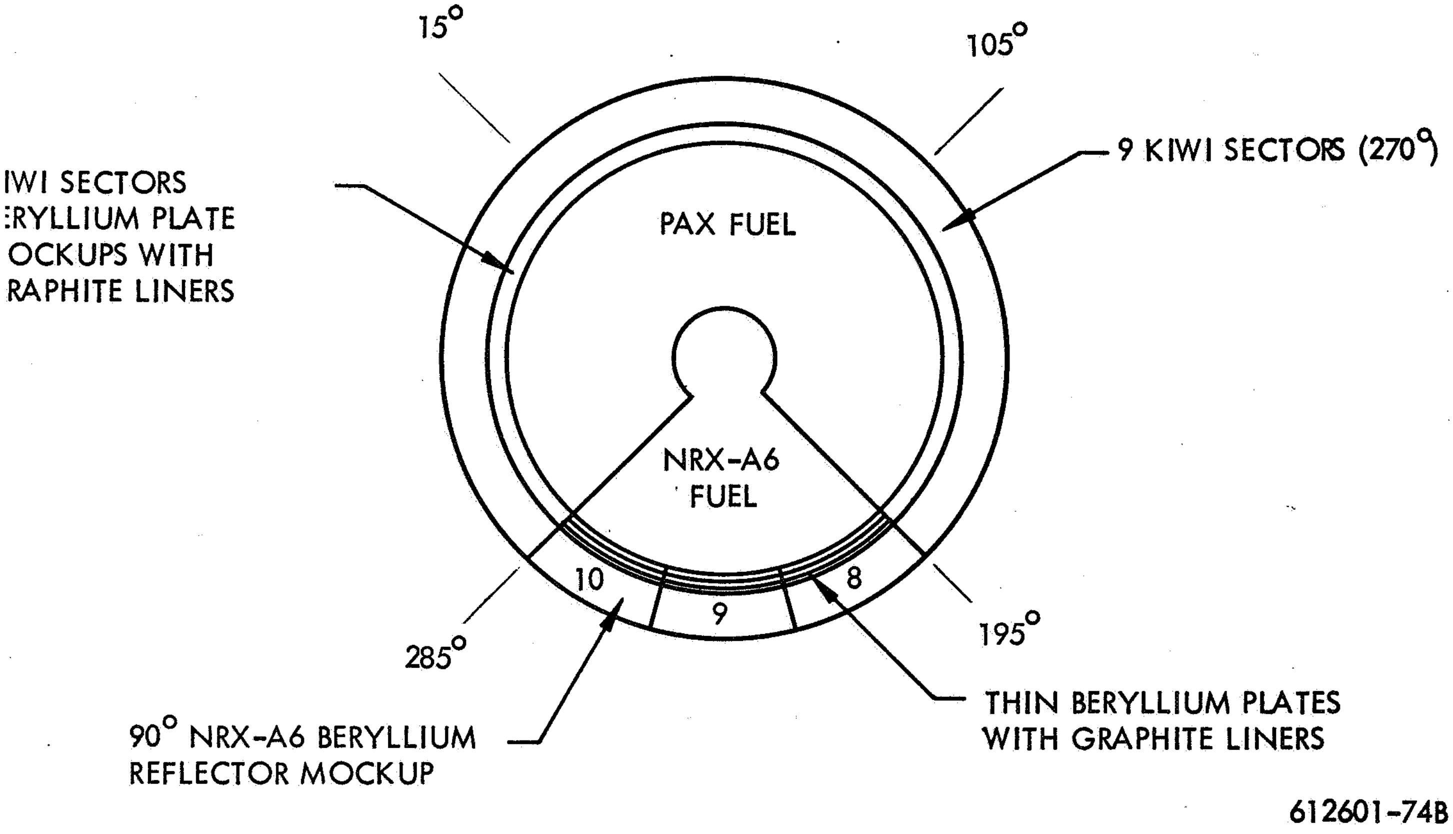

Figure 3-8. PAX-E5 Reactor Core and Reflector Configuration

3.4 SHIELD MOCKUPS

3.4.1 General Shield Configuration Descriptions

Three different configurations of materials on the end of the bare PAX-E5 reactor were employed in these experiments. These configurations are described as follows:

Shield Configuration Designation	Area Density, (gm/cm^2)	Description
4B	59.05	A bare PAX reactor with a mockup of a typical core support plate, plenum region, and pressure vessel on a NERVA type reactor.
7D	139.70	Configuration 4B with six BATH (Boron-Aluminum-Titanium-Hydride) shield modules interposed between the core support plate and the plenum-pressure vessel region.
11	213.93	A "thick" shield consisting of polyethylene, lead, and boral.

The materials* and areal densities are given in Table 3-1. It should be noted that all three configurations contained the 3/8 inch thick boral cluster plate mockup. Figures 3-9 and 3-10 show a breakdown of shield Configuration 4B, while Figures 3-11 and 3-12 contain the corresponding information for shield Configuration 7D. A breakdown of shield Configuration 11, the "thick" shield, is shown in Figures 3-13 and 3-14.

Small aluminum spacer bars were placed between the shielding materials at points of interest to permit NERVA measurements of neutron flux and dose rate inside the shield mockups by means of passive dosimeters. Two aluminum bars (3 feet x 1/2 inch x 1/4 inch) or rods (3 feet x 1/4 inch diameter) two inches apart were sandwiched centrally between two sheets of material in order to leave quarter-inch gaps. In addition, one-inch square aluminum bars, one quarter-inch thick, were also inserted at some of the corners and edges of these layers so that the materials could be kept as flat as possible. In all, 22 sets of spacers were used. Shield Configuration 11 employed no spacers between the various layers since no internal measurements were made.

---

*All aluminum used in the construction of the shield and dome and plenum region mockup was 2219 alloy to correspond to the actual alloy proposed for use in the R-1 reactor. All Inconel was type 718 and all Boral contained 23 w/o B_4C (of the total sheet).

TABLE 3.1

SHIELD COMPOSITIONS

Configuration 4B

Region Mockup Description	Material Thickness (Inch)	Material Thickness (cm)	Material	Density (gms/cc)	Area Density (gms/cm^2)
Cluster Plate	0.375	0.95	Boral 80 w/o Al 20 w/o B_4C	2.59	2.47
Support Plate	4.50	11.43	Al-2219	2.76	31.49
Hydrogen	1.25	3.18	$(CH_2)_n$	0.914	3.00
Plenum Support	0.75	1.91	Steel	8.35	15.91
Boral	0.25	0.64	Boral 80 w/o Al 20 w/o B_4C	2.59	1.64
Pressure Vessel	0.625	1.59	Al-2219	2.86	4.54
Total Material Thickness	7.75	19.70		Total Area Thickness	59.05

Configuration 7D

Region Mockup Description	Material Thickness (Inch)	Material Thickness (cm)	Material	Density* (gms/cc)	Area Density (gms/cm^2)
Cluster Plate, Support Plate, H_2, Plenum, Boral, PV	7.75	19.70	Configuration 4B (See Above)	3.00 (avg)	59.05
Shield	0.75	1.91	Inconel-718	8.75	16.71
Shield	1.50	3.81	Titanium	4.84	18.44
Shield	3.75	9.52	Al-2219	2.86	27.23
Shield	1.50	3.81	Polyethylene	0.914	3.48
Shield	2.25	5.71	Boral 80 w/o Al 20 w/o B_4C	2.59	14.79
Total Material Thickness	17.5	44.46		Total Area Density	139.70

Configuration 11

Region Mockup Description	Material Thickness (Inch)	Material Thickness (cm)	Material	Density* (gm/cc)	Area Density (gm/cm^2)
Cluster Plate	0.375	0.95	Boral 80 w/o Al) 20 w/o B_4C	2.59	2.47
Support	1.50	3.81	Al-2219	2.76	10.50
"Thick Shield"	2.06	5.08	B-(CH_2) n 35 w/o B_4C	0.942	4.79
"Thick Shield"	0.75 q	1.91	Boral 80 w/o Al 20 w/o B_4C	2.59	4.93
"Thick Shield"	6.00	15.24	Pb	11.33	172.67
"Thick Shield"	8.00	20.32	(CH_2) n	0.914	18.57
Total Material Thickness	18.63	47.31		Total Area Density	213.93

---

* As Measured.

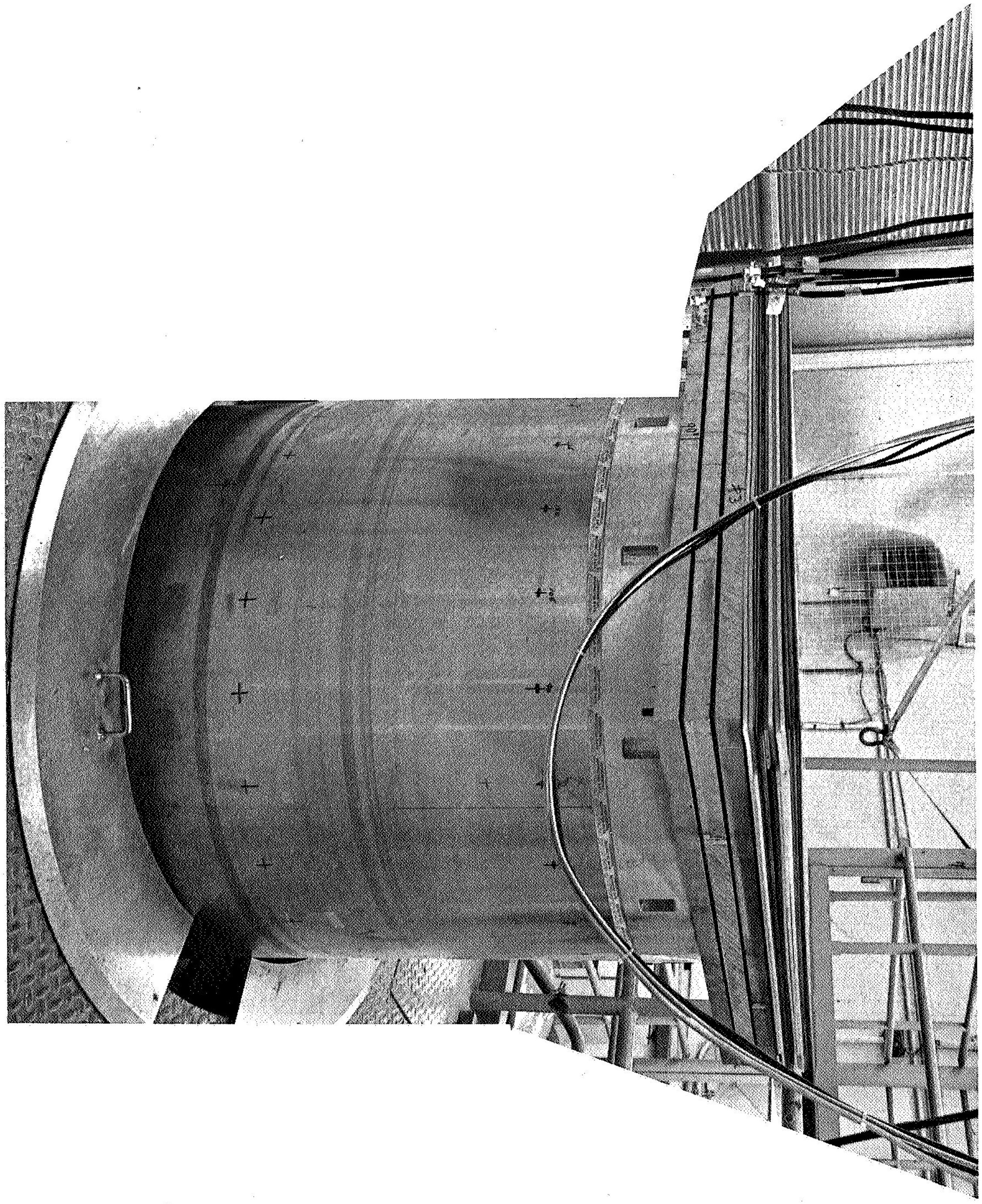

Figure 3-9. Shield Configuration 4B in Position Above PAX Reactor

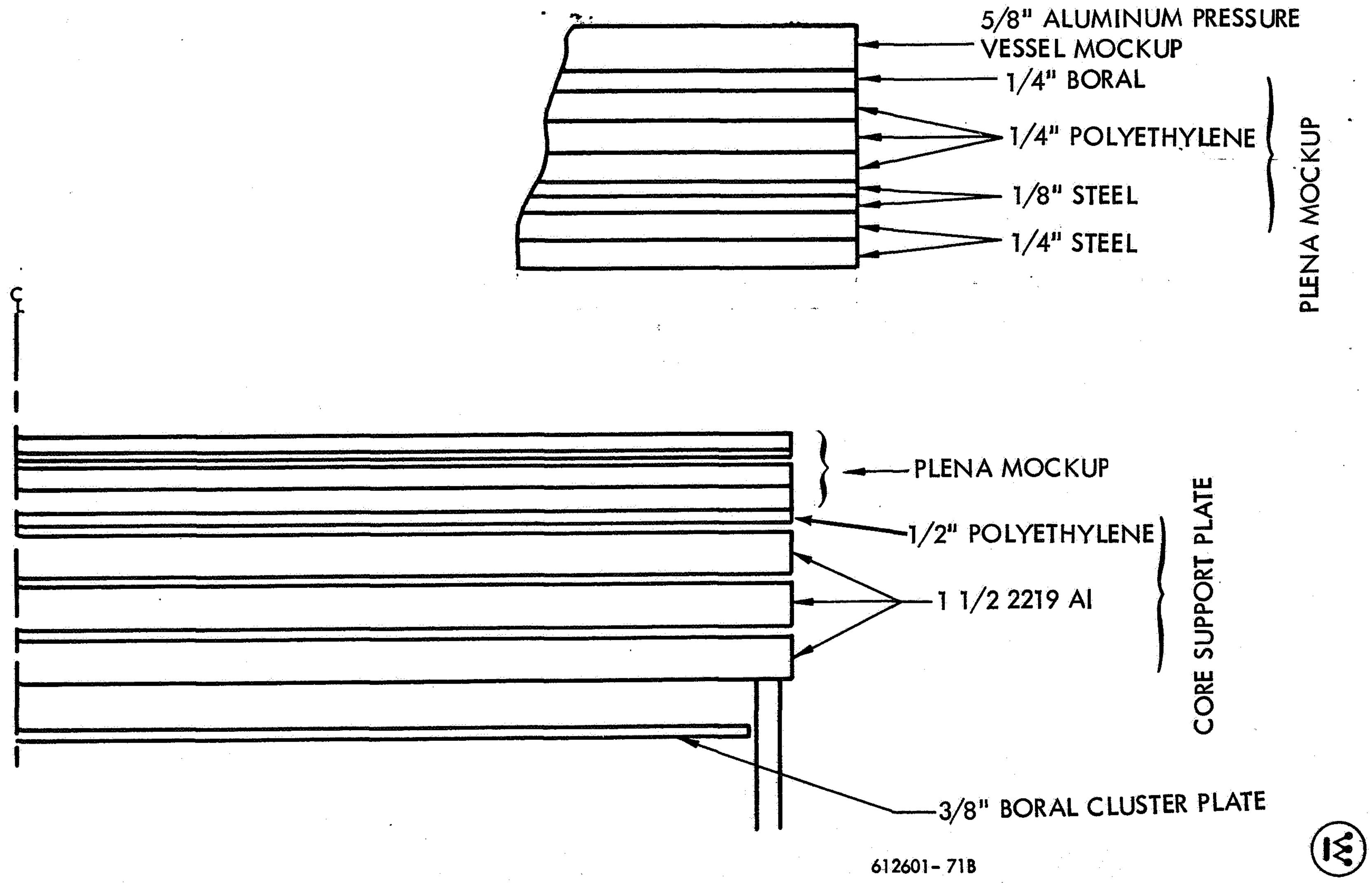

Figure 3-10. Schematic of Shield Configuration 4B

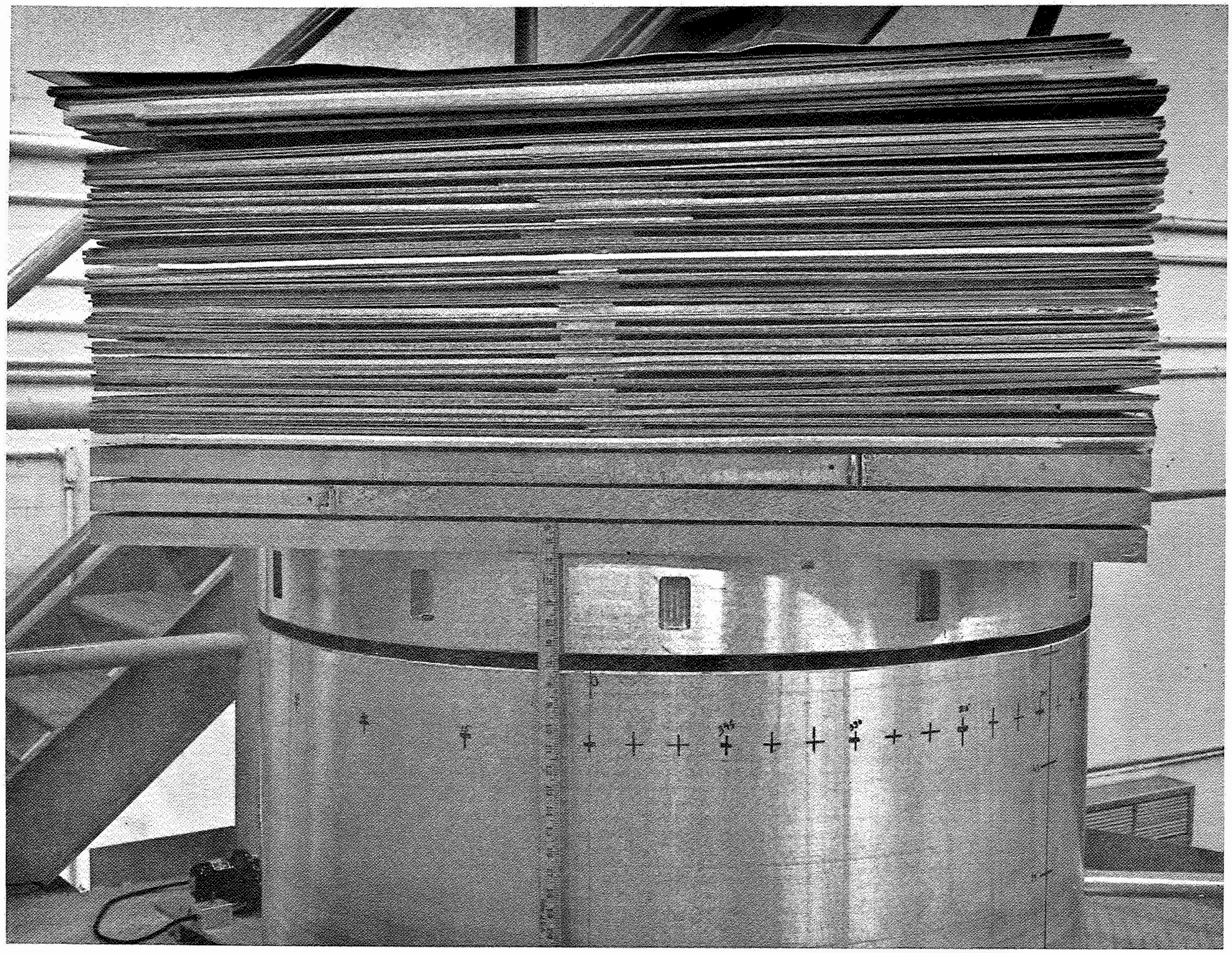

Figure 3-11. Shield Configuration 7D in Place Above the PAX Reactor

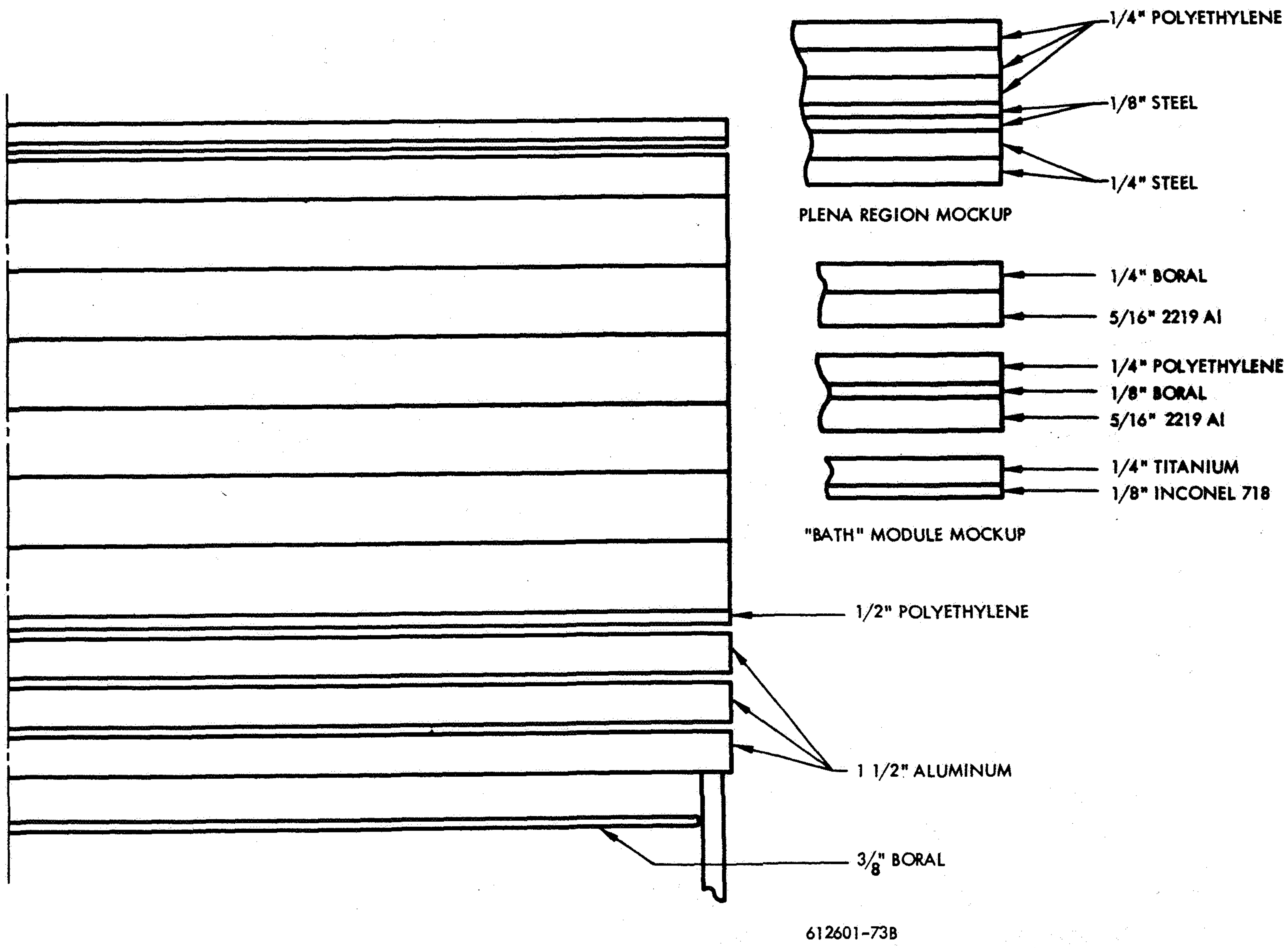

Figure 3-12. Schematic of Shield Configuration 7D

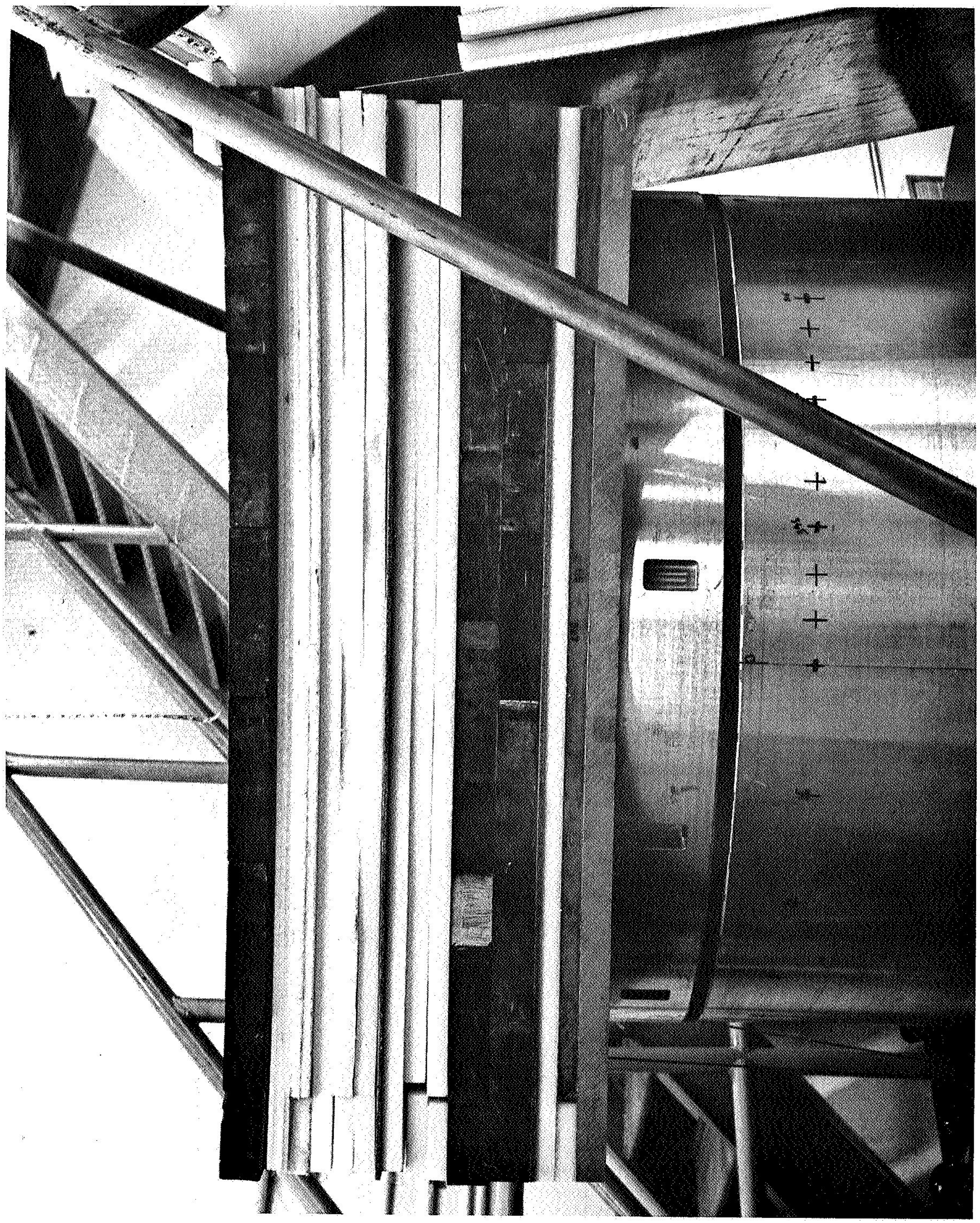

Figure 3-13. Shield Configuration 11 in Place Above the PAX Reactor

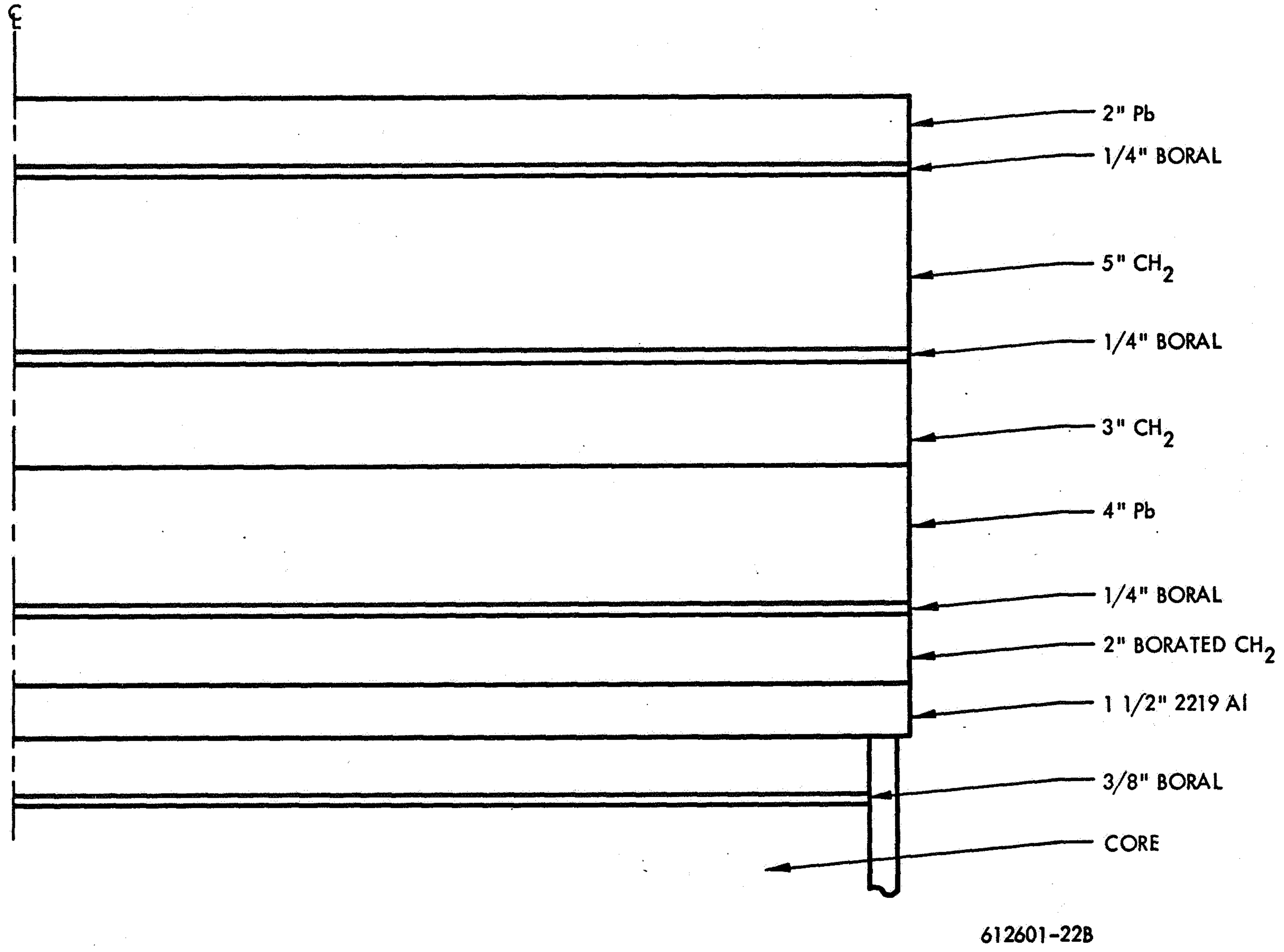

Figure 3-14. Schematic of Shield Configuration 11

Orientations of the shields with respect to the reactor are shown in Figures 3-15-1 and 3-15-2. The difference in angular orientation between Configurations 4B and 7D and Configuration 11 was dictated by the needs of specific NERVA experiments that were being performed at the same time.

3.5 PROPELLANT TANK ASSEMBLY

3.5.1 Propellant Tank

The tank used in this experiment was furnished by George C. Marshall Space Flight Center. Nameplate information on the tank skirt indicates a part number of 60 SKC3183-1 and a Serial Number of LTV-176. The manufacturer was Ling-Tempco-Vought under Contract NAS 8-4016. The tank is a duplicate of a Saturn 1B LOX tank except that it is not a full length tank. Appendix B contains information relating to the chemical composition of this tank.

MSFC modified the tank by providing lifting points consistent with WANEF's nuclear safety documentation and by drilling holes at specified locations in the walls of the tank. In accordance with WANEF safety requirements, MSFC also load tested the tank by filling it with water to give a total weight (tank plus water) of 4784 pounds and then lifting it by the specified lifting points*.

In order to provide a guide internal to the tank as well as to prevent the polyethylene pellets from flowing through the 4-1/4 inch diameter holes cut through the side of the tank, special tubing** was placed lengthwise through the diameter of the tank. Figures 3-17 and 3-18 give pertinent tank dimensions.

3.5.2 Active Dosimetry Traverse System

To permit remote operation for positioning the active dosimetry, 4-inch aluminum tubing was attached transversely across the Saturn 1-B tank at four locations, as shown in Figures 3-11 and Figure 3-12.

---

* A letter (R-SSL-NA) from Mr. Lester Katz (MSFC) to Mr. J. G. Gallagher (WANL) dated 10/25/67.

** 6063-T832 hard-coated cylinder tubing, 0.125 inch wall.

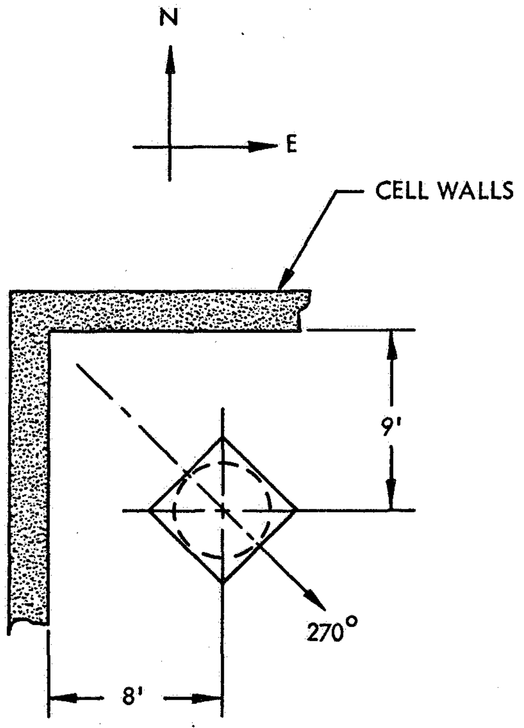

Figure 3-15-1. Orientation of Shields 4B and 7D with Respect to the Reactor Pressure Vessel and Core

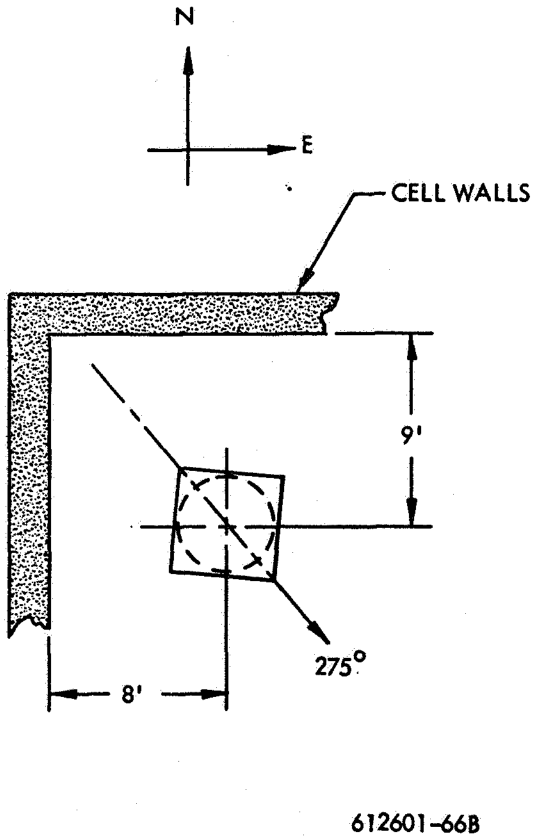

Figure 3-15-2. Orientation of Shield 11 with Respect to the Reactor Pressure Vessel and Core

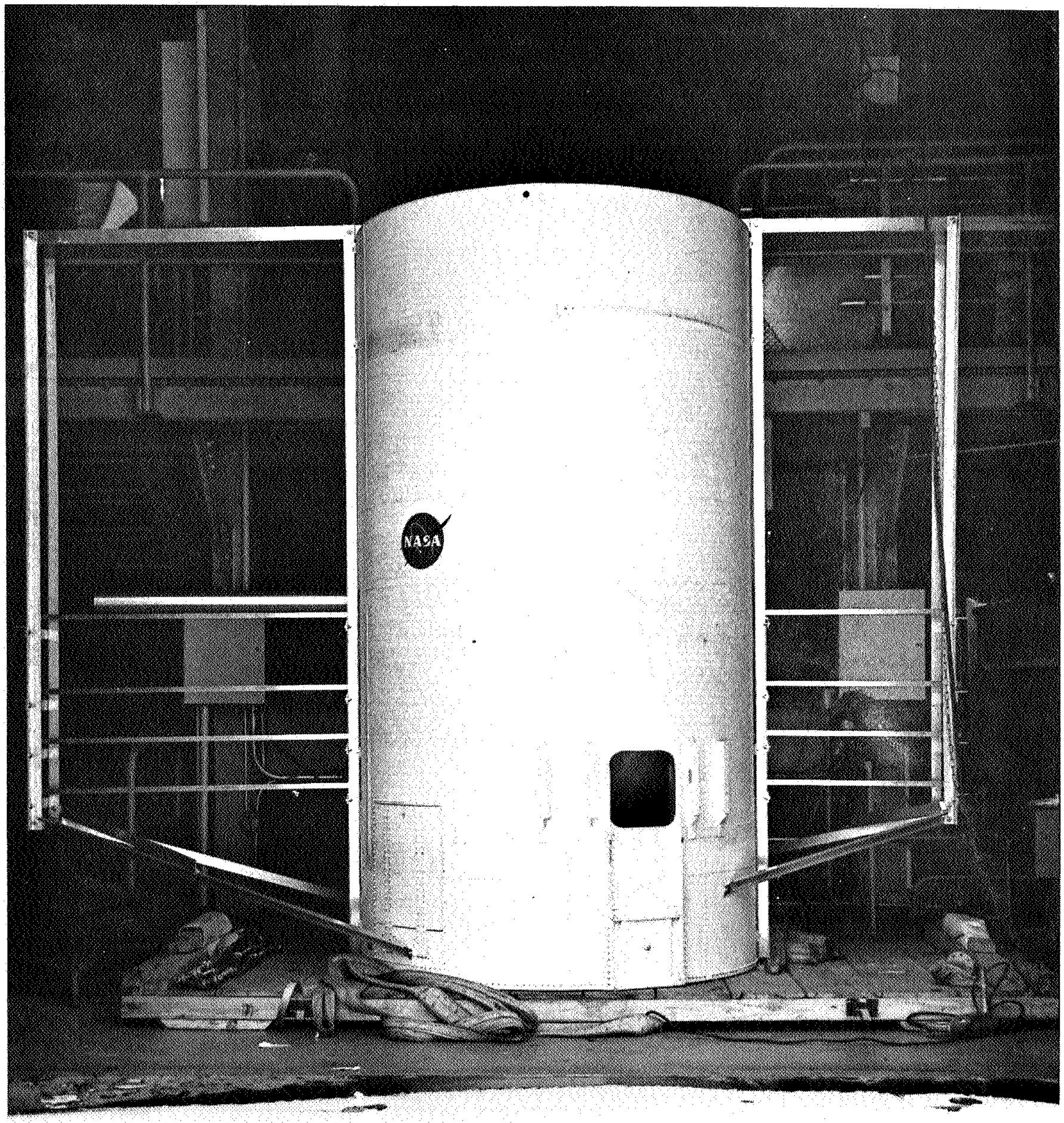

Figure 3-16. Tank Framework Under Construction

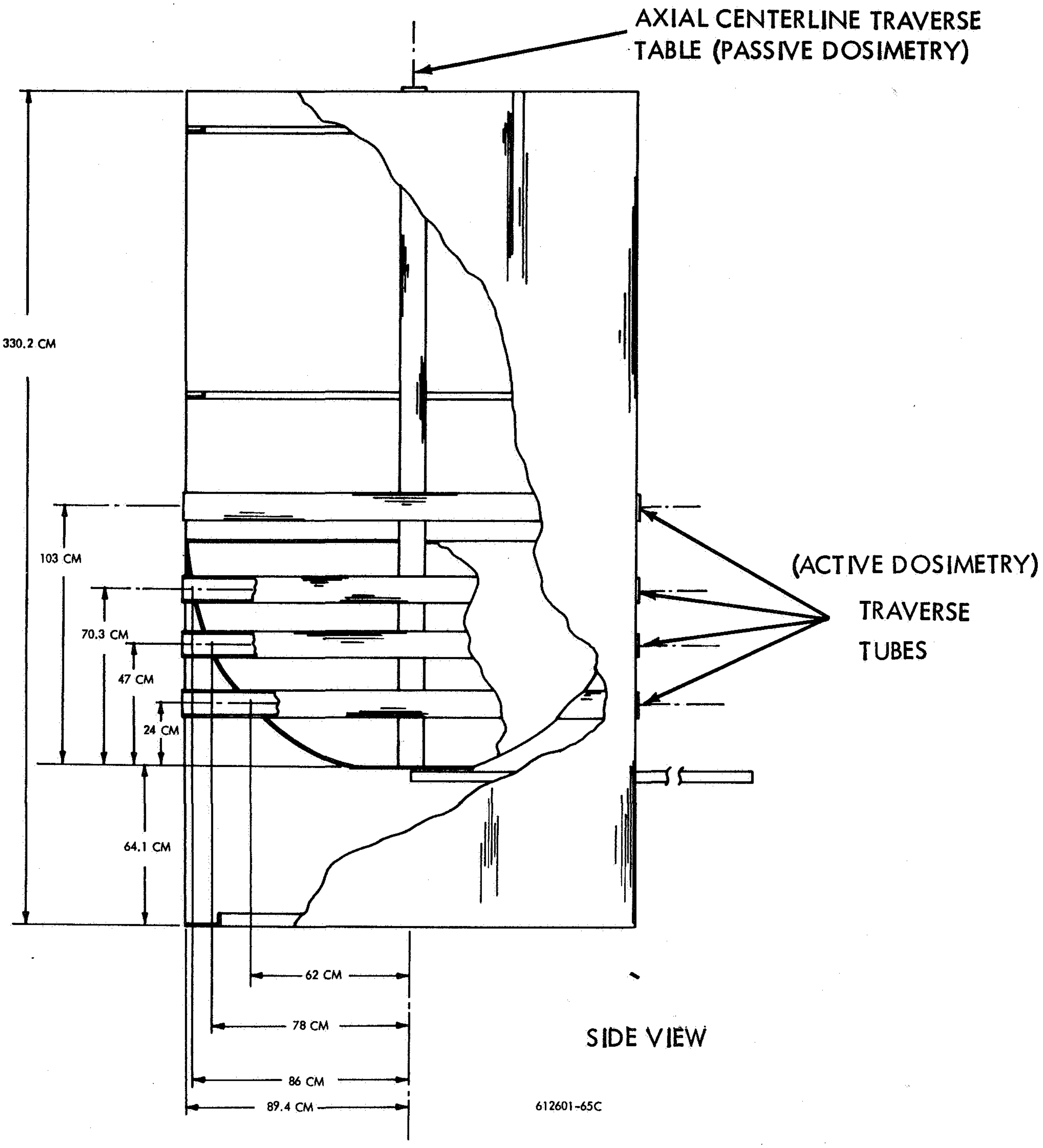

Figure 3-17. Pertinent Dimensions of Tank

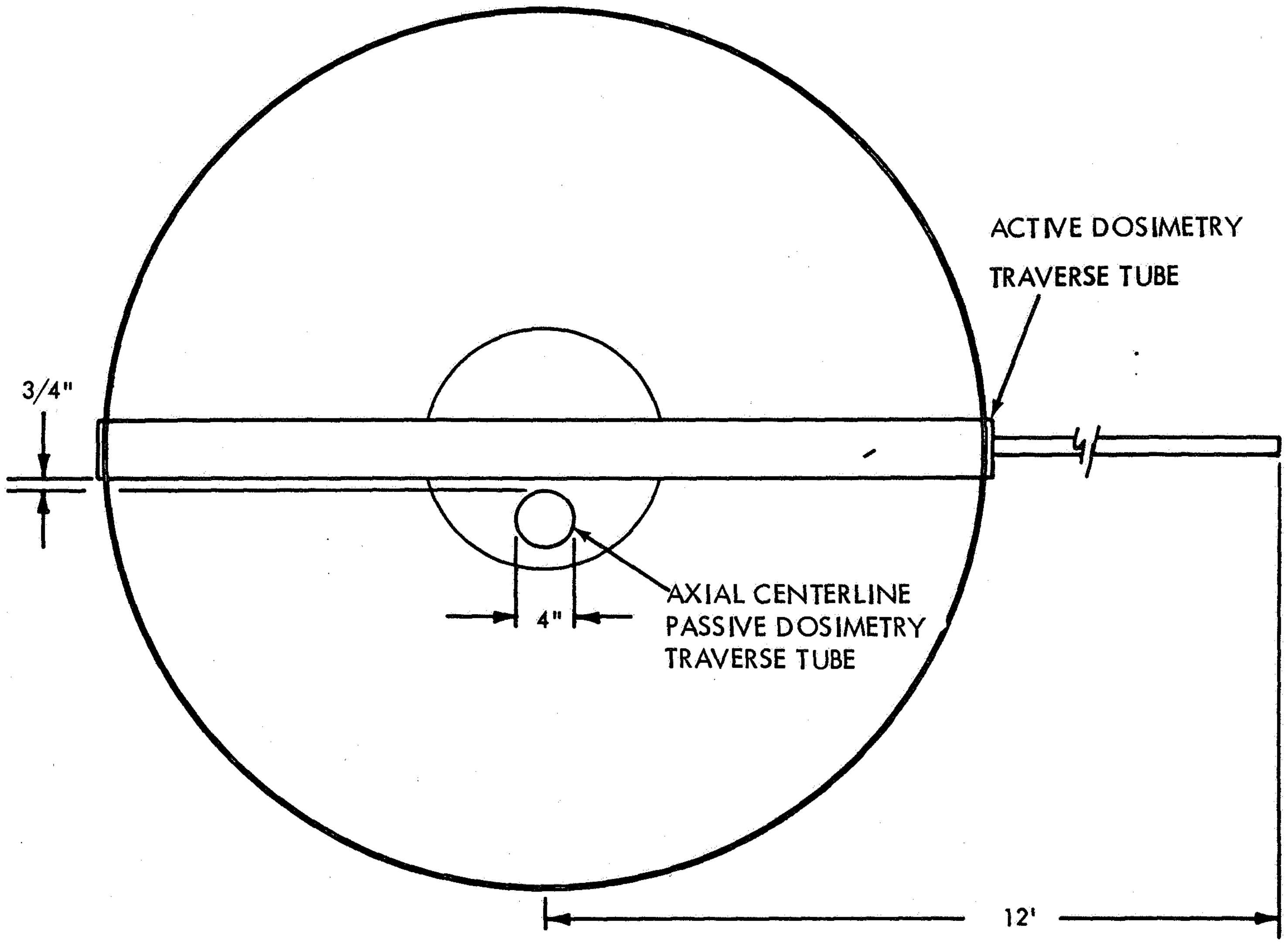

Figure 3-18. Top View of Tank

Aluminum pipe* was obtained in 12 foot lengths and turned down in a lathe (by approximately 0.050 inch) to such a size that they would slide freely through the tubing placed within the tank. The inside of the tubes was then given a liberal coating of a colloidal graphite lubricant while the pipes were coated with a Teflon lubricant in order to reduce friction and prevent galling.

In order to traverse the pipes (containing active dosimetry) through the tank, a framework of aluminum angle and channel was constructed. (This aluminum was either 6061 or 6063 alloy, depending upon availability.) A photograph of the nearly completed framework is shown in Figure 3-16. The framework had to be sufficiently rigid to support the traversing tubes as they were withdrawn and ball bearing wheels were provided for the purpose of reducing friction during withdrawal of the traverse tubes.

Actual motive power for the withdrawal of the tubes was provided by a pair of motor driven drums (see Figure 3-19) located above the top of the tank. The connection between the traversing pipes and the drums was made by 3/32 inch diameter plastic-covered aircraft cable. Pulleys were then located on special U-shaped parts which bolted on one end of the framework. Pulleys were also located on the main support channel. Although only two withdrawal mechanisms were provided, two pipes were often pulled by one mechanism through the simple expedient of connecting the cables together at a suitable location. Speed control of the motors was accomplished by a Variac located in the control room. Position indication was obtained by gearing a ten-turn precision potentiometer to the cable take-up drum and reading the voltage across the wiper arm. Readout was performed remotely by means of a digital voltmeter.

In order to fill the horizontal holes which were not used during a given run, an extra section of the traverse tubing were cut into 6 foot lengths. Although during certain runs, these tubes contained either passive or active dosimetry**, they were generally filled only with polyethylene of the appropriate density.

---

* 6061-T6 3-1/2 inch pipe, 1/4 inch walls.

** Where active data was taken under these conditions, it was taken only at one point (in the center of the tank) since the tube was not traversed.

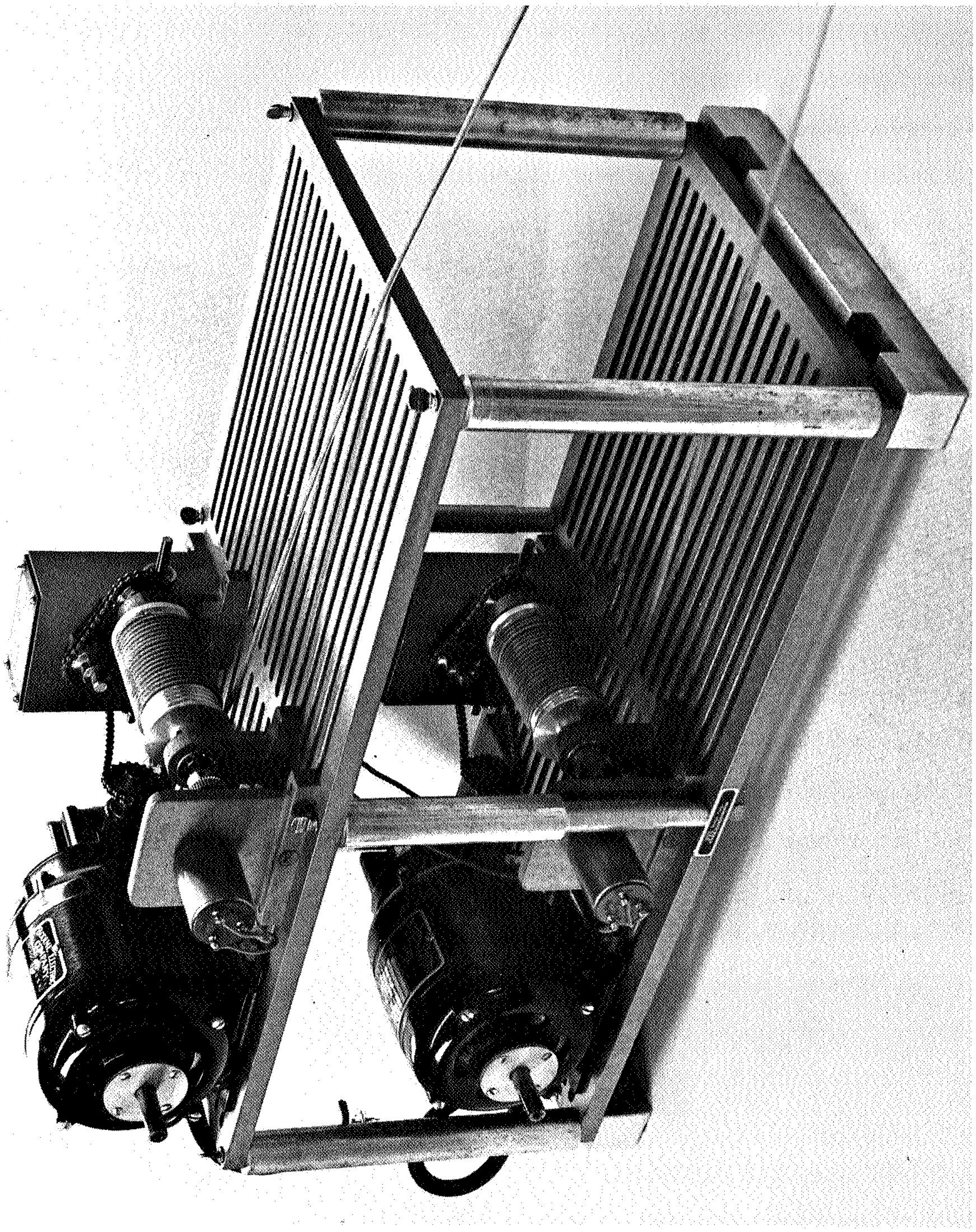

Figure 3-19. Withdrawal Mechanism for Traverse Tubes (Active Dosimetry)

Provision was also made for an axial traverse using passive dosimetry. A 4-inch piece of 6063-T6 aluminum pipe having 0.072-inch thick walls was positioned as shown in Figure 3-18 and was welded in place at the bottom. A close fitting acrylic plastic tube having 3-3/4-inch OD with 1/8-inch thick walls and a 1/8-inch thick removable bottom plate was constructed. This tube was then loaded with passive dosimetry and the proper density polyethylene.

3.6 SIMULATION OF PROPELLANT TANK LIQUID HYDROGEN

3.6.1 Simulation of Photon and Neutron Transport Properties

Since liquid hydrogen is costly, hazardous, and difficult to maintain, various densities of polyethylene were used to simulate its neutron and photon transport properties. This was analytically investigated and found to be acceptable. The choice of polyethylene $(CH_2)_n$ as a liquid hydrogen ($\rho = 0.07$ gm/cc) substitute was made based on its high hydrogen to carbon ratio, ease of handling, safety, and availability. Two material densities were selected for the mockup based on: (a) equating electron densities of polyethylene with that of liquid hydrogen to mockup the photon transport properties, yielding a density of 0.12 gm/cc, and (b) equating hydrogen atom densities with liquid hydrogen to mockup the neutron transport properties of liquid hydrogen, yielding a density of 0.48 gm/cc. In the actual experiment, these densities were approximated with materials having densities of 0.14 and 0.59 gm/cc for reasons of availability.

Monte Carlo calculations had been performed* to determine the adequacy of simulating the high energy neutron and photon properties of liquid hydrogen. Within the uncertainties associated with the statistical variations associated with calculations at each position, one cannot say that there is a significant difference between the photon transport properties of 0.12 gm/cc polyethylene and those of liquid hydrogen. It does appear, however, that the 0.12 gm/cc polyethylene produces a gamma dose rate which is too high by approximately

---

* WANL-TME-1560, "Justification for the NSX Radiation and Shielding Program at WANEF", February 1967.

10–15 percent. Therefore, it was expected that a slightly higher density polyethylene provides a better simulation of the photon gamma transport properties of LH_2. Polyethylene with a density of 0. 14 gm/cc is commercially available in the form of a low density solid foam. Therefore, this material was chosen to provide photon simulation of liquid hydrogen. Figure 3-20 shows a photograph of this material. Hydrogen and carbon have a constant ratio of mass energy absorption coefficients (Figure 3-21) over the energy range of 0. 1 Mev to 5 Mev. At 6 Mev, there is an approximate 8 percent decrease in the ratio of energy absorption coefficients and at 10 Mev, the decrease is approximately 16 percent for carbon relative to hydrogen. Hence, from Figure 3-21 (within a very small uncertainty), the translation from rads (carbon) into rads (hydrogen) can be made, i.e., rads (hydrogen) is equal to 1. 93 rads (carbon). (The rad is a unit of absorbed energy from ionizing radiation equal to 100 ergs/g in a specified material.) A carbon wall CO_2 filled ionization chamber would then be suitable for measuring rads (carbon).

To simulate fast neutron transport and energy deposition in liquid hydrogen, an average polyethylene density of 0. 48 gm/cc was desired to obtain an equivalent hydrogen density of 0. 07 gm/cc. It was found possible to approximate this with commercially available polyethylene pellets having an approximate bulk density of 0. 59 gm/cc (equivalent to 0. 086 gm/cc hydrogen) as shown in Figure 3-22. This material should provide a reasonably good nuclear simulation (0. 1 Mev E 10 Mev) of the neutron transport properties of liquid hydrogen; the slight differences in the hydrogen density and the effects of the unwanted carbon can be accounted for by the analytical corrections.

The high density polyethylene used was obtained from Eastman Chemical Products, Inc., in the form of small pellets. The pellets were roughly right circular cylinders with a height and a diameter of 1/8 inch. The material designation was Natural Low Density (0. 918 gm/cc) 800A and was a special low density polyethylene. (The density quoted in this report, 0. 59 gm/cc, refers to a bulk density and is not the density of an individual pellet.) The tank was filled with polyethylene to a height of approximately 112 cm.

Figure 3-20. Low Density Polyethylene (As Cut to Fit the Bottom of the Propellant Tank Hemisphere for LH_2 Gamma Simulation)

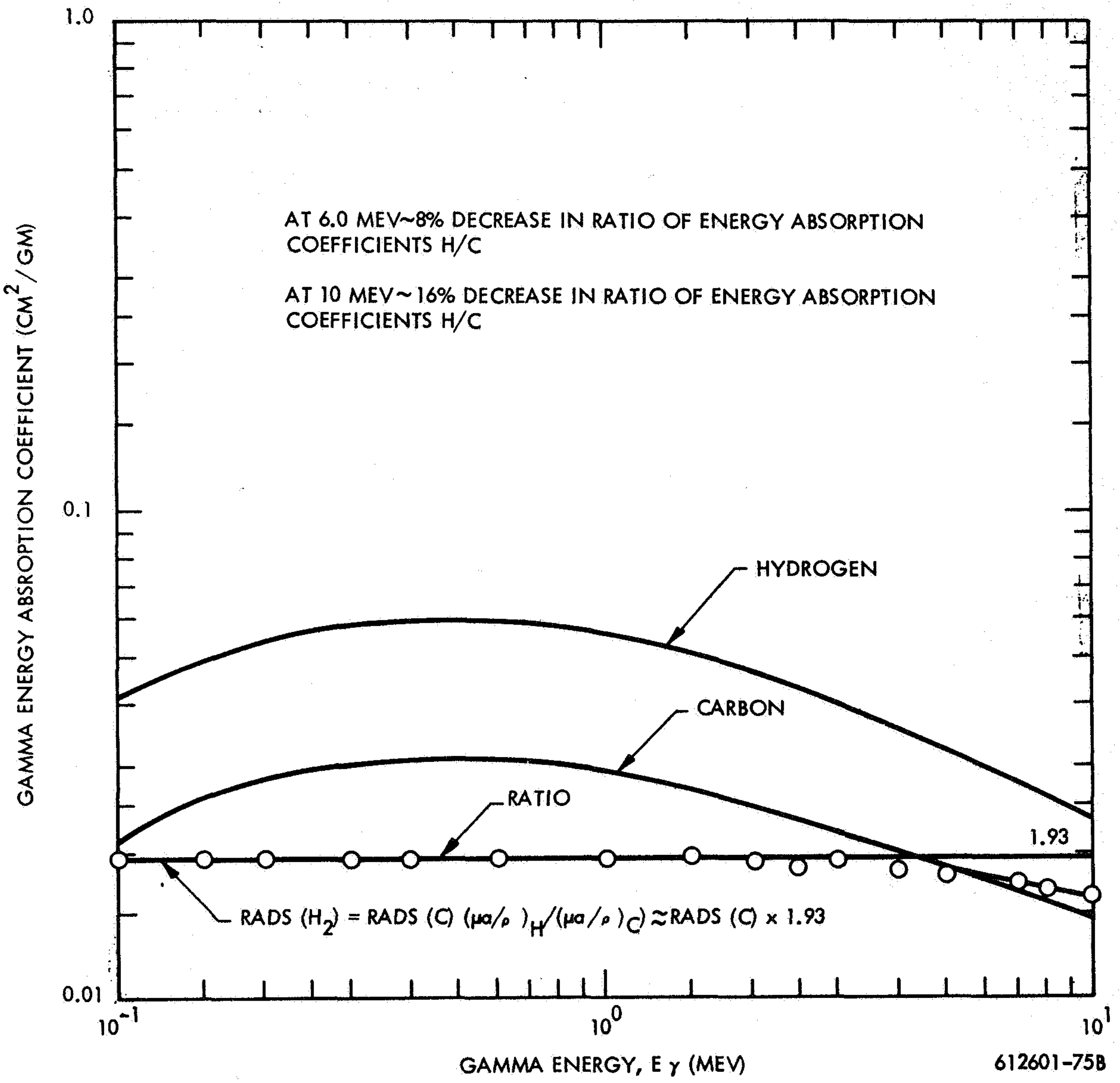

Figure 3-21. Comparative Gamma Energy Absorption Coefficients in Hydrogen and Carbon

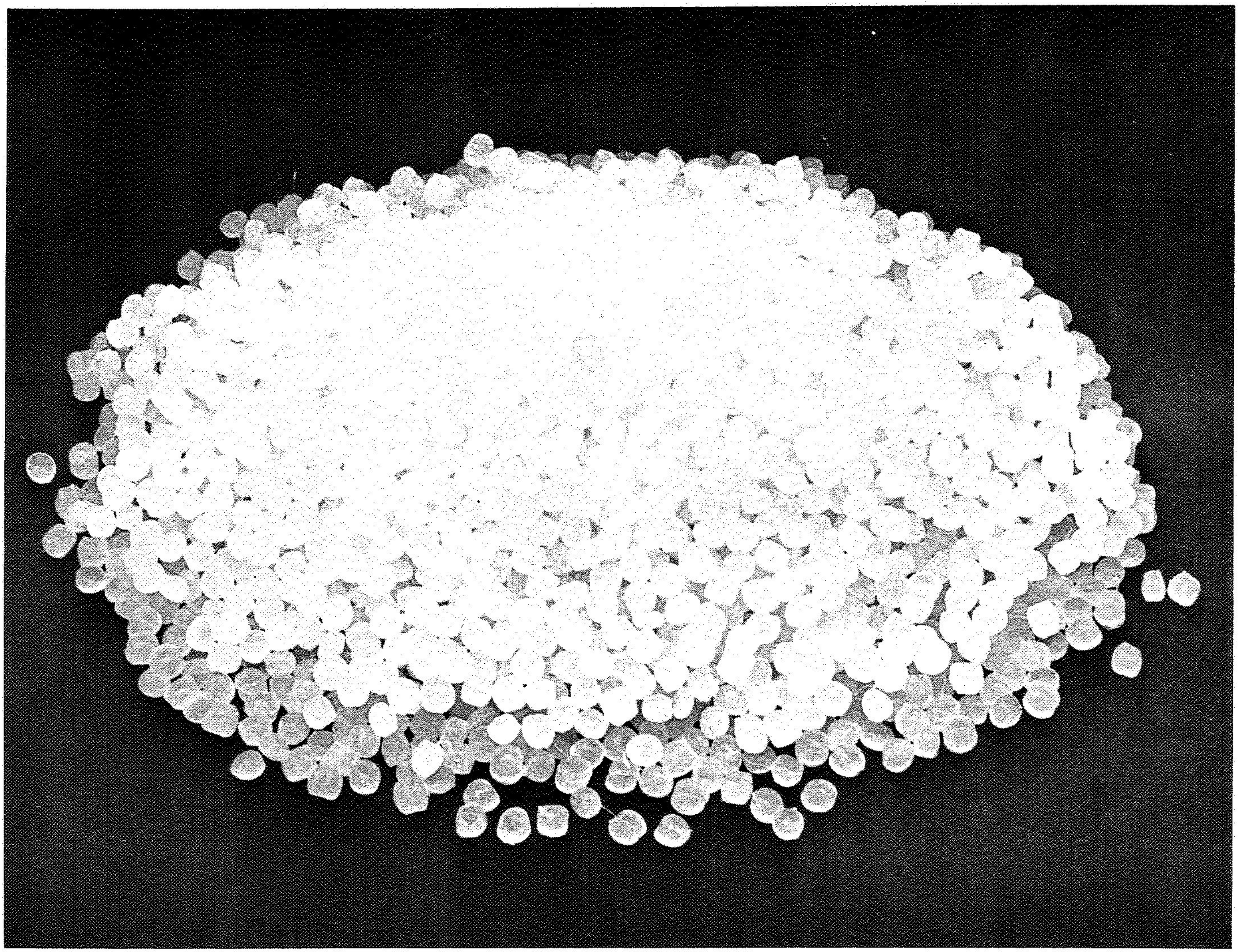

Figure 3-22. High Density Polyethylene Pellets

The polyethylene foam was purchased from Dow Chemical Company in the form of rectangular slabs 2 inches x 15 inches x 10 feet. The material as furnished was quite nonuniform in cross section and had to be machined before use. Ordinary woodworking tools were successfully employed for this task. The bulk density of the polyethylene foam was determined to be 0.14 gm/cc. It was stacked in the tank to a height of approximately 212 cm.

3.6.2 Conversion of Dose Rates to Heating Rates

In the case of the low density polyethylene, the measurement of energy from w/cc polyethylene $(CH_2)_n$ in terms of w/cc in liquid hydrogen is given as follows:

$$\text{w/cc } LH_2 = \text{w/cc polyethylene} \times 1.93 \, \frac{\text{rads (H)}}{\text{rads (C)}} \times \frac{\rho_{LH_2}}{\rho_{\text{polyethylene}}}$$

$$= \text{w/cc polyethylene} \times 1.93 \times \frac{0.070}{0.14}$$

$$= 0.965 \text{ w/cc polyethylene}$$

A conversion factor for the conversion of gamma dose rate to gamma heating rate in polyethylene (ρ=0.14 gm/cc) is given by:

$$\frac{\text{watts/cc polyethylene}}{\text{watts (reactor power)}} =$$

$$\frac{\text{rads (carbon)}}{\text{hr-w (reactor power}} \times \frac{\text{100 erg/gm polyethylene}}{\text{rad (polyethylene)}} \times \frac{\text{0.14 gm polyethylene}}{\text{cc}} \times \frac{\text{1 joule}}{10^7 \text{ ergs}} \times \frac{\text{1 hou}}{\text{3600 se}}$$

$$= 3.89 \times 10^{-10} \text{ rads (carbon)/hr-watt}$$

$$\therefore \text{ w/cc } LH_2 = 3.75 \times 10^{-10} \text{ rads (carbon)/hr-watt}$$

The only additional correction factor which might be required here is for differences in thermal neutron induced secondary gammas produced in the tank, especially for those produced by thermal neutrons arriving from scattering or thermalization by the test cell wall

A Hurst neutron dosimeter was used to measure the fast neutron energy deposition in rads-(ethylene)*. The ratio of rads (hydrogen) to rads (ethylene) is independent of neutron energy to within 5 percent within the energy interval 10 Kev to 20 Mev as shown in Figure 3-23. Therefore, the direct measurement of energy deposition in terms of rads-(tissue) provides data which can be converted to rads (hydrogen) with a minimal uncertainty.

The corresponding conversion from neutron dose rate to neutron heating rate in polyethylene is then easily obtained from first principles as follows:

$$\frac{\text{(watts/cc polyethylene)}}{\text{watt (reactor power)}} = \frac{\text{rads (tissue)}}{\text{hr-w (reactor power)}} \times \frac{1.42\text{ rads (polyethylene)}}{\text{rad (tissue)}}$$

$$\times \frac{100\text{ ergs/gm polyethylene}}{\text{rad (poly)}} \quad \frac{0.59\text{ gm polyethylene}}{\text{cc}} \times \frac{1\text{ joule}}{10^{7}\text{ ergs}} \times \frac{1\text{ hour}}{3600\text{ sec}}$$

$$= 2.3 \times 10^{-9} \times \text{rads (tissue)/hr-w}$$

Since

the heating rate produced by the carbon is estimated to be less than one percent of the heating rate produced by the hydrogen, the equivalent heating rate at the bottom edge of the propellant is given approximately by the ratio of hydrogen densities multiplied by the heating rate in polyethylene or,

$$\text{watts/cc}_{\text{LH}_2} = \frac{\text{watts}}{\text{cc polyethylene}} \times \frac{0.07\text{ gm/cc LH}_2}{2/14 \times 0.59\text{ gm H/cc polyethylene}}$$

$$= 0.833\text{ watts/cc polyethylene}$$

$$\therefore\ \text{watts/cc}_{\text{LH}_2} = 0.833 \times 2.3 \times 10^{-9}\ \frac{\text{rads (tissue)}}{\text{hr-watt}}$$

$$= 1.9 \times 10^{-9} \times \frac{\text{rads (tissue)}}{\text{hr-watt}}$$

---

* The Hurst dosimeter is actually calibrated in units of rads (tissue)but the conversion from rads (tissue) to rads (ethylene) is approximately a constant factor of 1.42 ± 0.07.

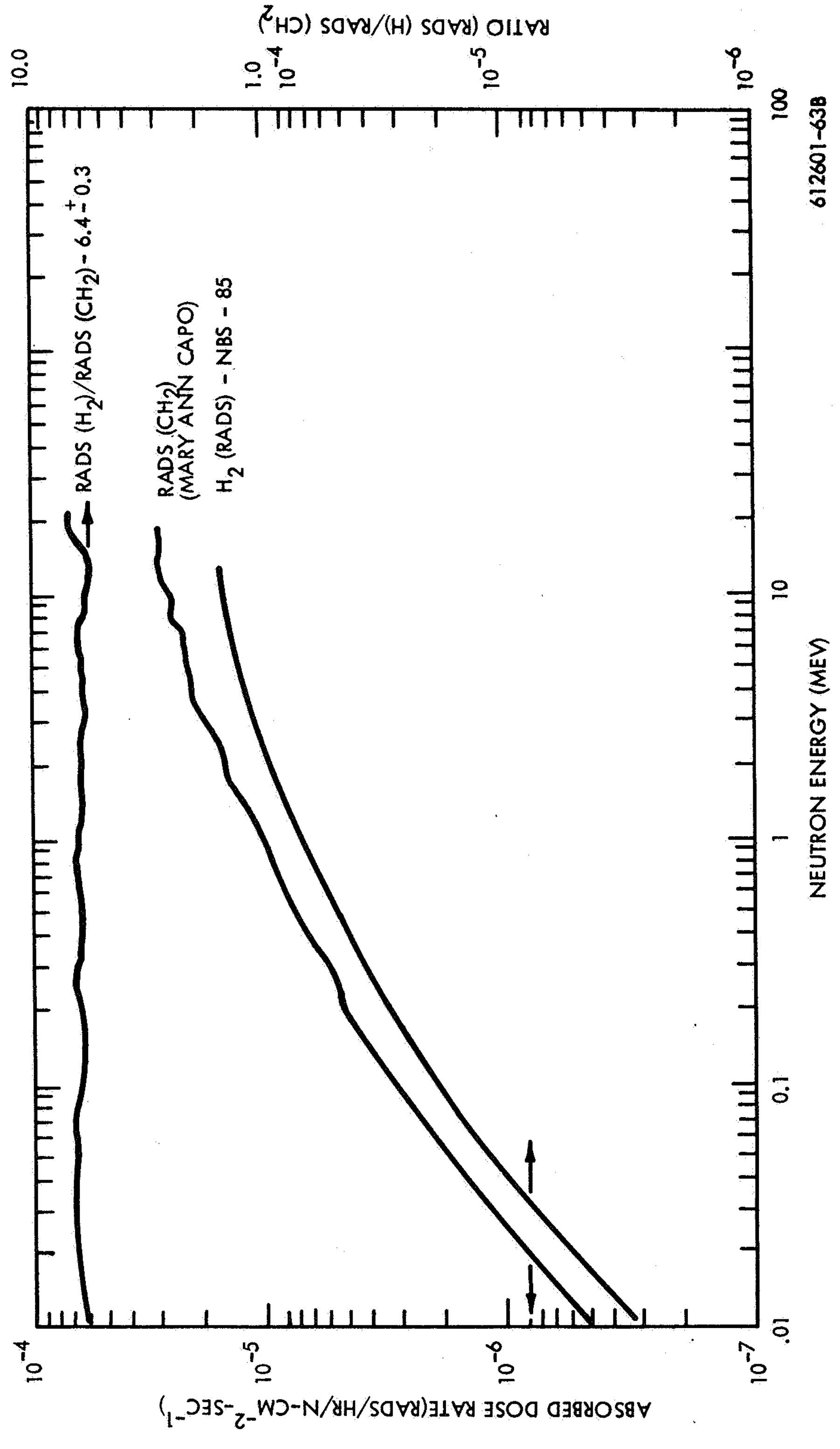

Figure 3-23. Comparison of Dose Conversion Factors for Ethylene and Hydrogen

In order to convert this heating rate to heating rate in liquid hydrogen, analytical corrections will have to be performed to remove the carbon and to reduce the hydrogen density to the desired value of 0.07 gm/cc.

3.7 ACTIVE DOSIMETRY SYSTEMS

Four different types of active detectors were employed to measure fast neutron dose, thermal neutron flux, fast neutron flux and gamma dose rate. The detectors employed for these measurements are described in the next section. Details on calibration are given in Appendix A of this volume.

3.7.1 Fast Neutron Dose

The RSN-48 is a Hurst proportional counter made by Reuter Stokes and is patterned after an Oak Ridge design*. Figure 3.24 gives details of this detector. Figure 3-25 shows the RSG-8A and its associated electronic instrumentation while Figure 3-26 is a block diagram of the instrumentation interconnections.

The fast neutron dose rate is obtained by an integration of pulse heights, yielding the number of ion pairs produced in the gas, rather than the usual ionization chamber measurement of charge or current. This procedure permits the integration of only those pulses resulting from neutrons while rejecting the lower energy caused by gamma rays. A requirement of this method, however, is that measured pulse height be proportional to the number of ion pairs.

The counter design is based on the Bragg-Gray cavity principle (same wall and gas composition). Both ethylene, C_2H_4, and cyclopropane, C_3H_6, have the same atomic composition as polyethylene walls, $(CH_2)_n$. Cyclopropane is preferred due to lower operating voltage.

The polyethylene wall inner surface is coated with a "very thin" conducting layer of aquadag (graphite) and serves as outer electrode of the counter. The central

---

* ORNL-LR-DWG-14076

TAKEN FROM
ORNL-LR-DWG. 14076
UNCLASSIFIED

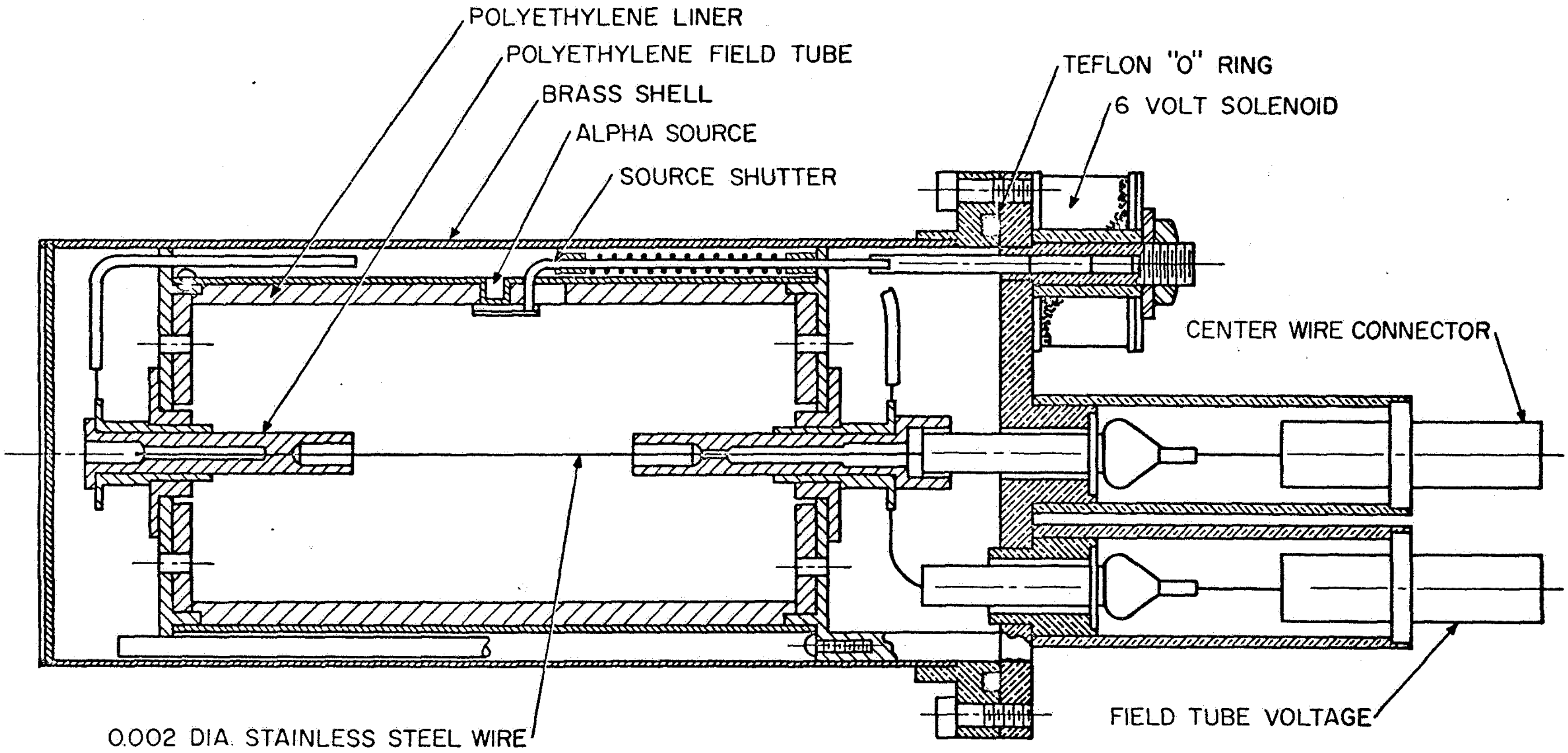

FULL SCALE

Figure 3-24. Standard Fast Neutron Dosimeter

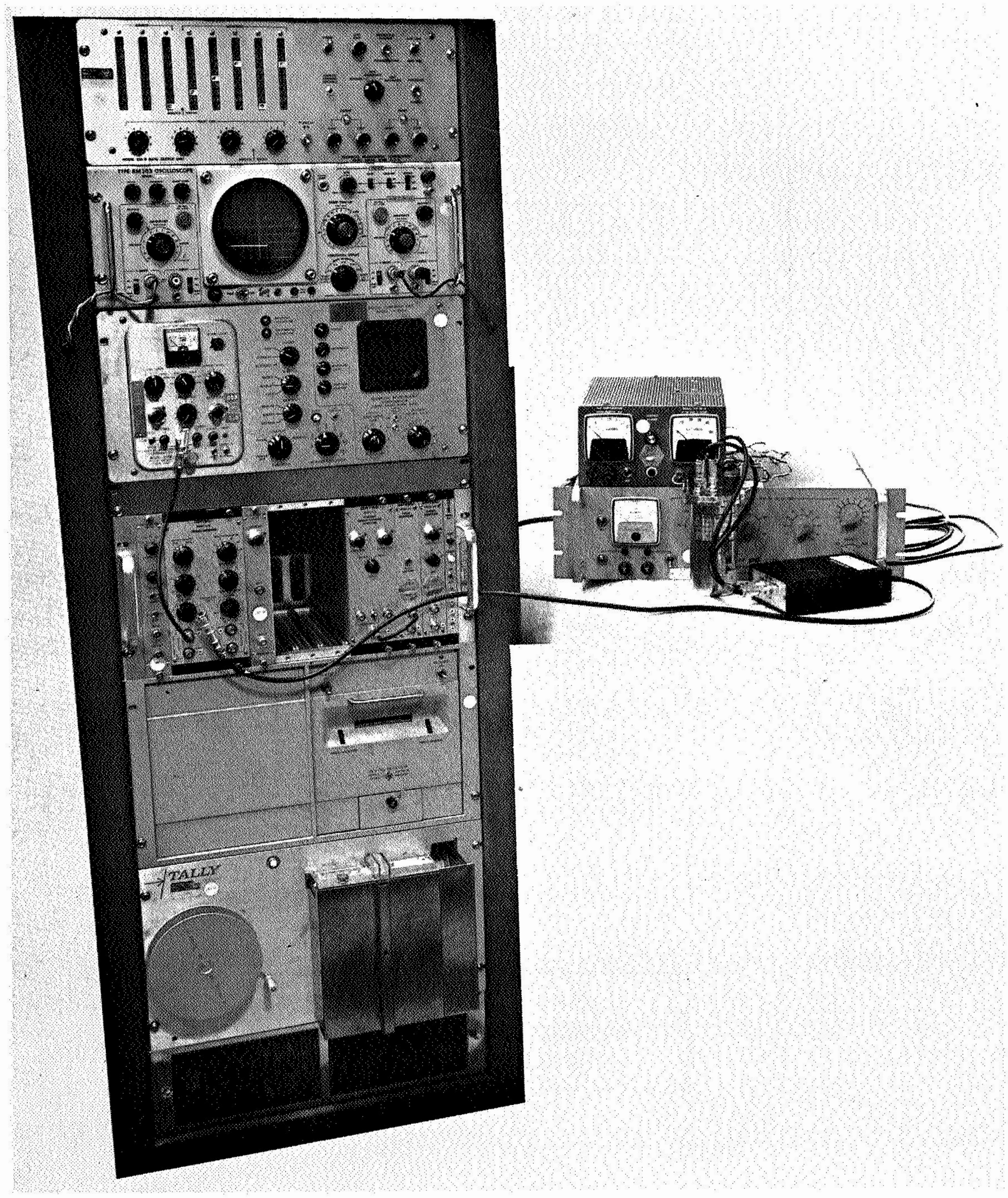

Figure 3-25. RSN-48A Hurst Detector and Associated Electronics

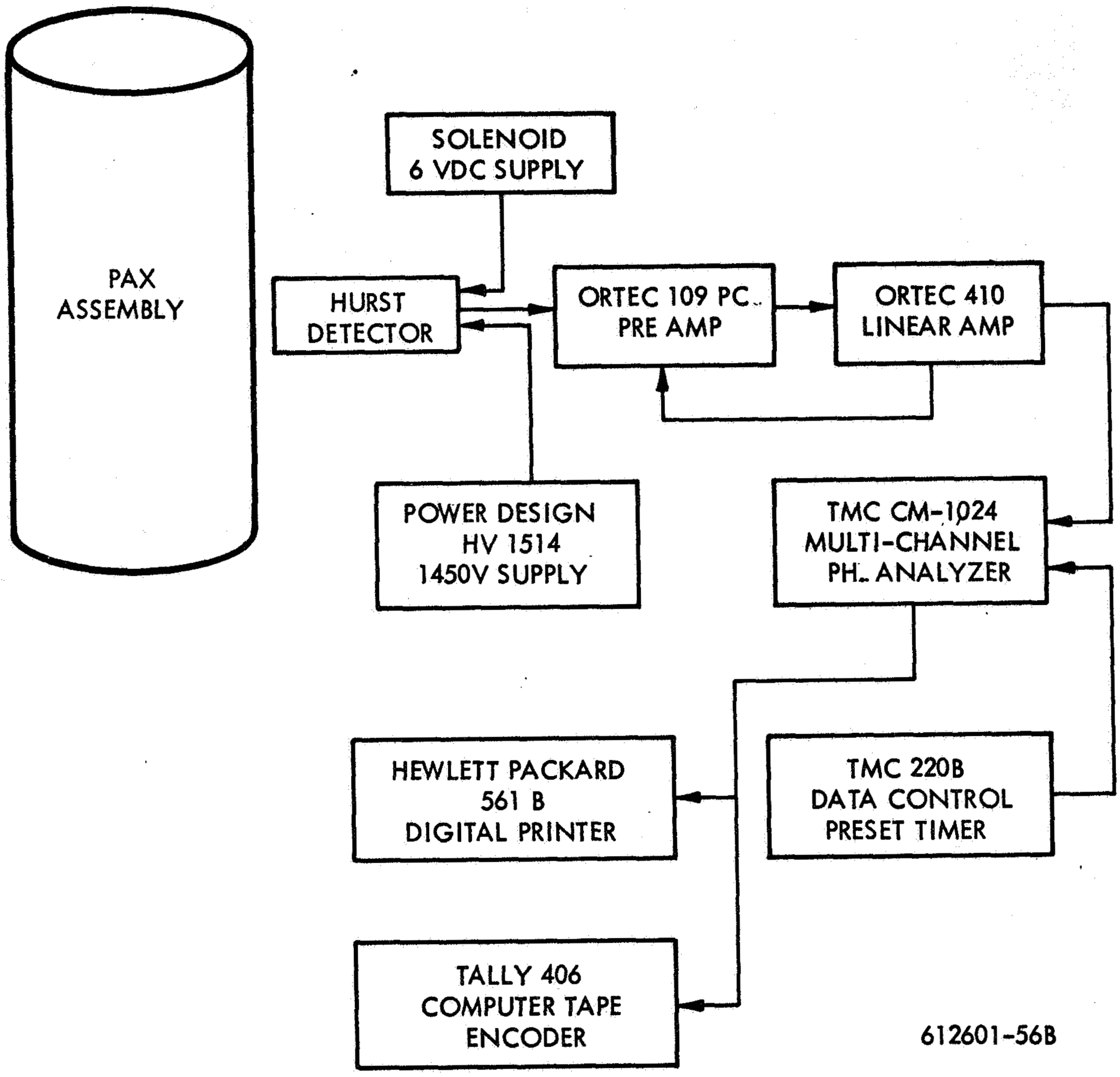

Figure 3-26. A Block Diagram Showing the Interconnections Between the RSN-48A Hurst Detector and Its Associated Electronics

electrode consists of a 0.002 inch diameter stainless steel wire. Counter sensitive volume is defined by field tubes (around the central electrode) and is approximately 60 cm^3. The sealed counters containing cyclopropane are initially fillled to a pressure of 840 mm of Hg at room temperature (22°C). The equilibrium pressure (after ingassing into the wall liner) is approximately 690 mm of Hg. The mass of cyclopropane contained in the sensitive volume is therefore 0.094 grams. This mass is a nominal value and may vary for different counters; hence, a correction factor must be evaluated for each counter. The potential applied to the central electrode is 1450 volts (positive) with one-third of this voltage being applied to the field tubes. A Pu^{239} alpha source is contained within the counter to provide a means of calibrating the energy absorbed. This calibration source is covered by a shutter shield when not in use; the shutter can be opened by applying a voltage to the solenoid on the counter exterior.

3.7.2 Thermal Neutron Flux

The WX-5362 (shown in Figure 3-27) detector, manufactured by Westinghouse, Elmira, is a B-10 lined compensated ion chamber originally developed* for NERVA applications. Figure 3-28 shows the WX-5362 and its associated electronic instrumentation while Figure 3-29 contains a block diagram of the instrumentation interconnections.

The three electrodes are of beryllium metal and the radial spacing between the high voltage electrode and the signal electrode is one millimeter. The facing areas of these electrodes are coated with 92 percent enriched boron - 10 to an area density of 0.5 mg/cm^2. The total area is 150 cm^2 of boron, or 75 cm^2 of facing electrode area. The gamma compensating electrode is machined finally as required to give exacting compensation, which is determined empirically for each individual detector.

The signal electrode is only 0.020 inches in thickness, which allows close proximity of the neutron and gamma compensating volumes. This assures nearly the same gamma intensities for both volumes even in high gradient fields. The high voltage electrode of the neutron sensitive volume is 0.060 inch thick rather than the 0.020 inches indicated. This thickness is required to obtain a beryllium gamma dose rate in the neutron sensitive volume, as otherwise, recoil electrons from the titanium case may penetrate this electrode.

---

*WANL-TME-527, "Design of Neutron Detectors for NERVA"

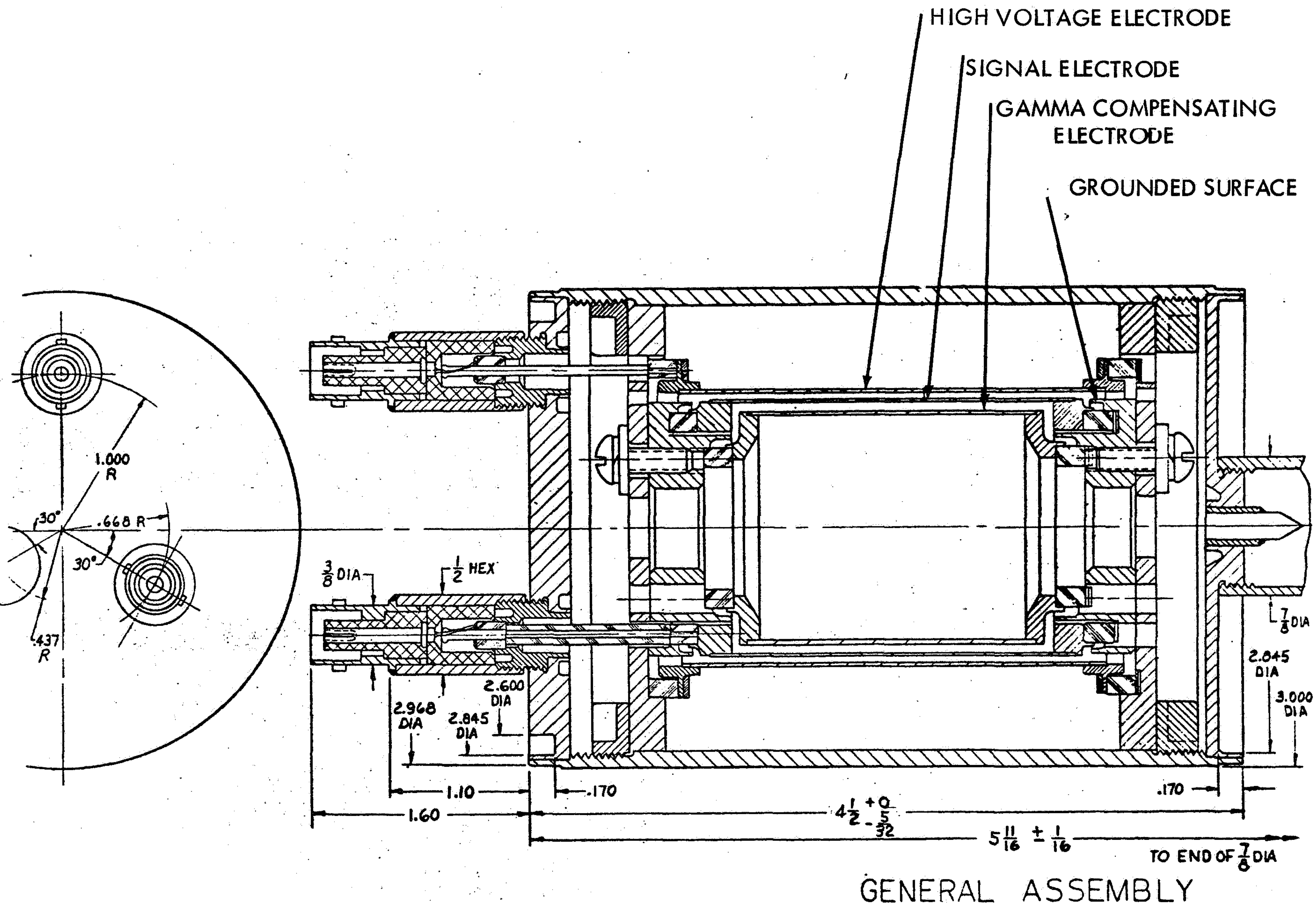

Figure 3-27. Pertinent Details of WX-5362 Boron-Lined Compensated Ion Chamber

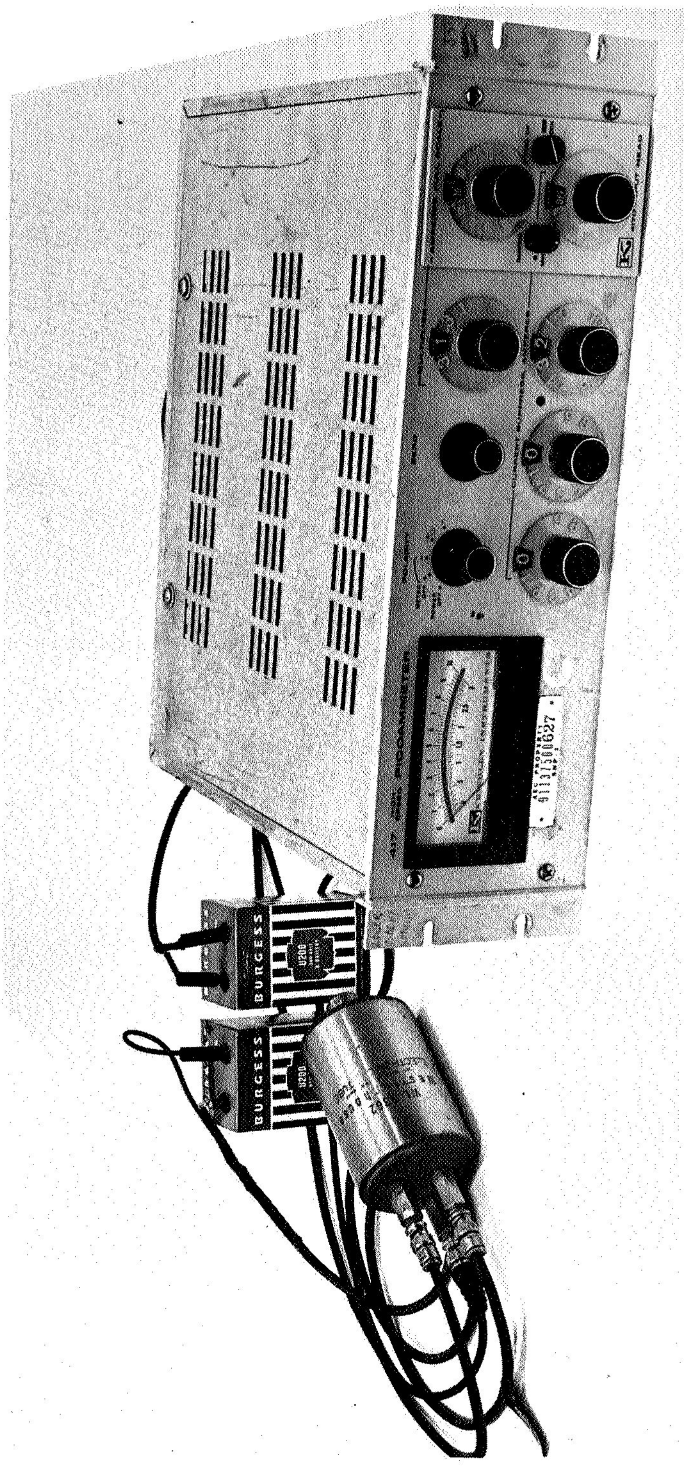

Figure 3-28. WX-5362 Boron-Lined Compensated Ion Chamber and Associated Electronics

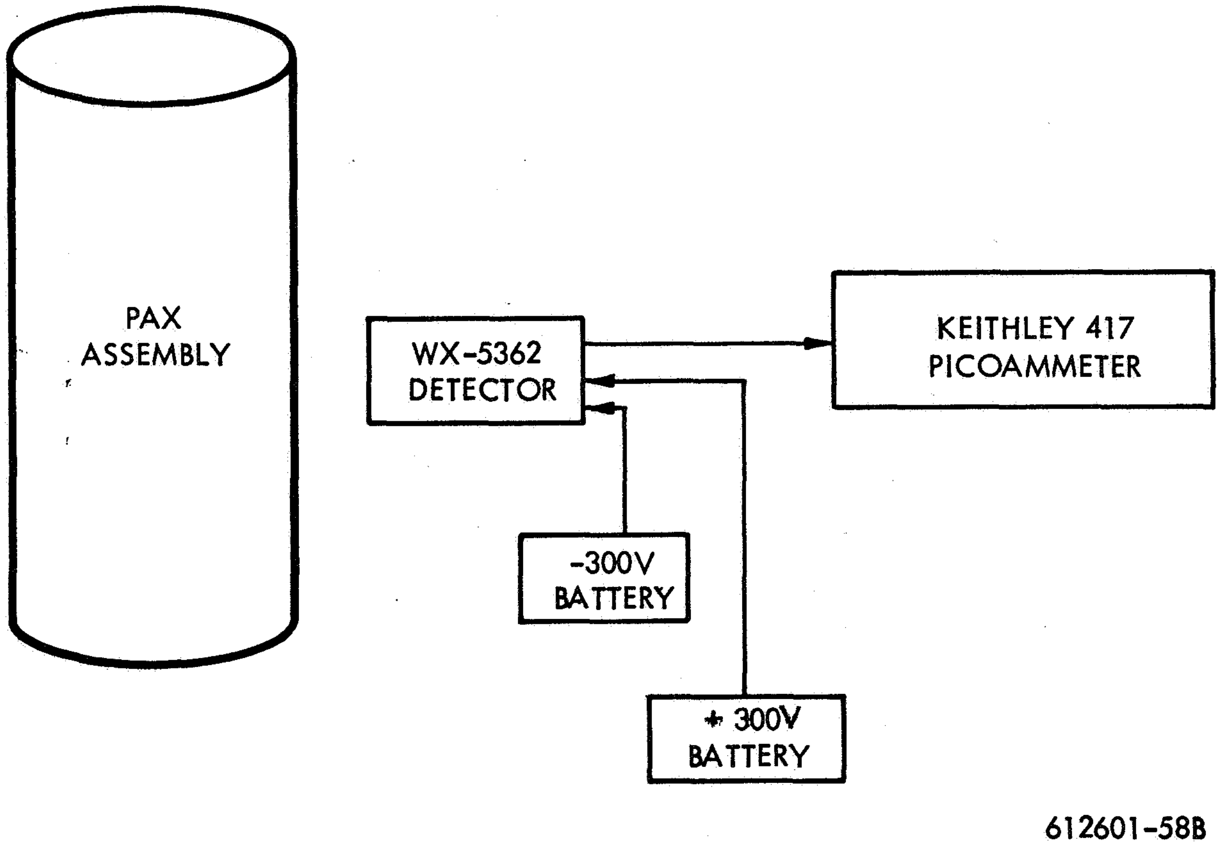

Figure 3-29. Block Diagram Showing the Interconnections Between the WX-5362 Boron-Lined Compensated Ion Chamber and Its Associated Electronics

Another design feature is the continuation of the signal electrode surface plane by a grounded surface. This clearly defines the volumetric edge of the detector and maintains a uniform electric field gradient at the edge, to reduce any non-linearity due to diffusion of charges from the sensitive volume. This part also shields the ceramic insulator from the electric field and hence, the collection of charges on the insulator surface. The same piece defines the compensating volume edge.

The signal electrode is connected to the signal connector by a lead that is shielded and insulated from direct view of surfaces at high potential. In addition, the gas volume around this lead is minimized. This is an important feature, because thermal potentials or other voltage sources may be present on the signal electrode, and currents could flow through any existing end volumes of gas.

Almost all the metallic parts of the WX-5362 are of titanium, except the beryllium electrodes largely because the neutron activation of titanium is small.

All insulators in the WX-5362 are of high purity alumina. The insulation resistance of each of the electrodes to ground is greater than 5×10^{13} ohms at room temperature.

3.7.3 Fast Neutron Threshold Flux

The WX-30748 (Figure 3-30)fast fission detector, manufactured by Westinghouse, Elmira, contains approximately 2 grams of U-238 having a U-235 content of 2 parts per million. Pertinent details of the detector are given in Figure 3-19. Figure 3-31 shows the WX-30748 and its associated electronic instrumentation while Figure 3-32 is a block diagram showing the interconnections of this instrumentation.

During all measurements, the detector was wrapped in a 0.020 inch cadmium blanket and then encased in a can consisting of two 1/8 inch thick layers of Boral. The seams in the Boral layers were oriented so that direct streaming through the gaps did not occur.

3.7.4 Gamma Dose Rate

The Reuter-Stokes RSG-8A is a carbon wall gamma sensitive ionization chamber. This particular one is filled with CO_2 gas and is designed to obey the Bragg-Gray law.

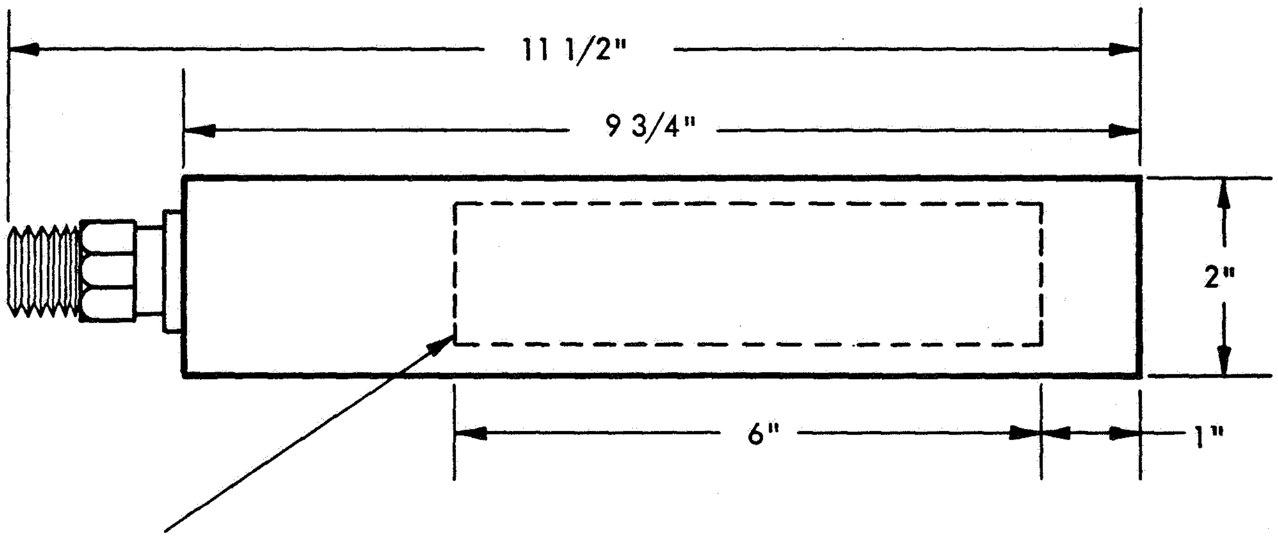

THE ACTIVE VOLUME IS COMPOSED OF A SERIES OF CONCENTRIC SHELLS UPON WHICH THE URANIUM IS PLATED. THE MAXIMUM O.D. OF THE ACTIVE VOLUME IS 1.4" WHILE THE MINIMUM I.D. IS 0.5".

612601-61B

Figure 3-30. Pertinent Details of WX-30748 Fast Fission Detector

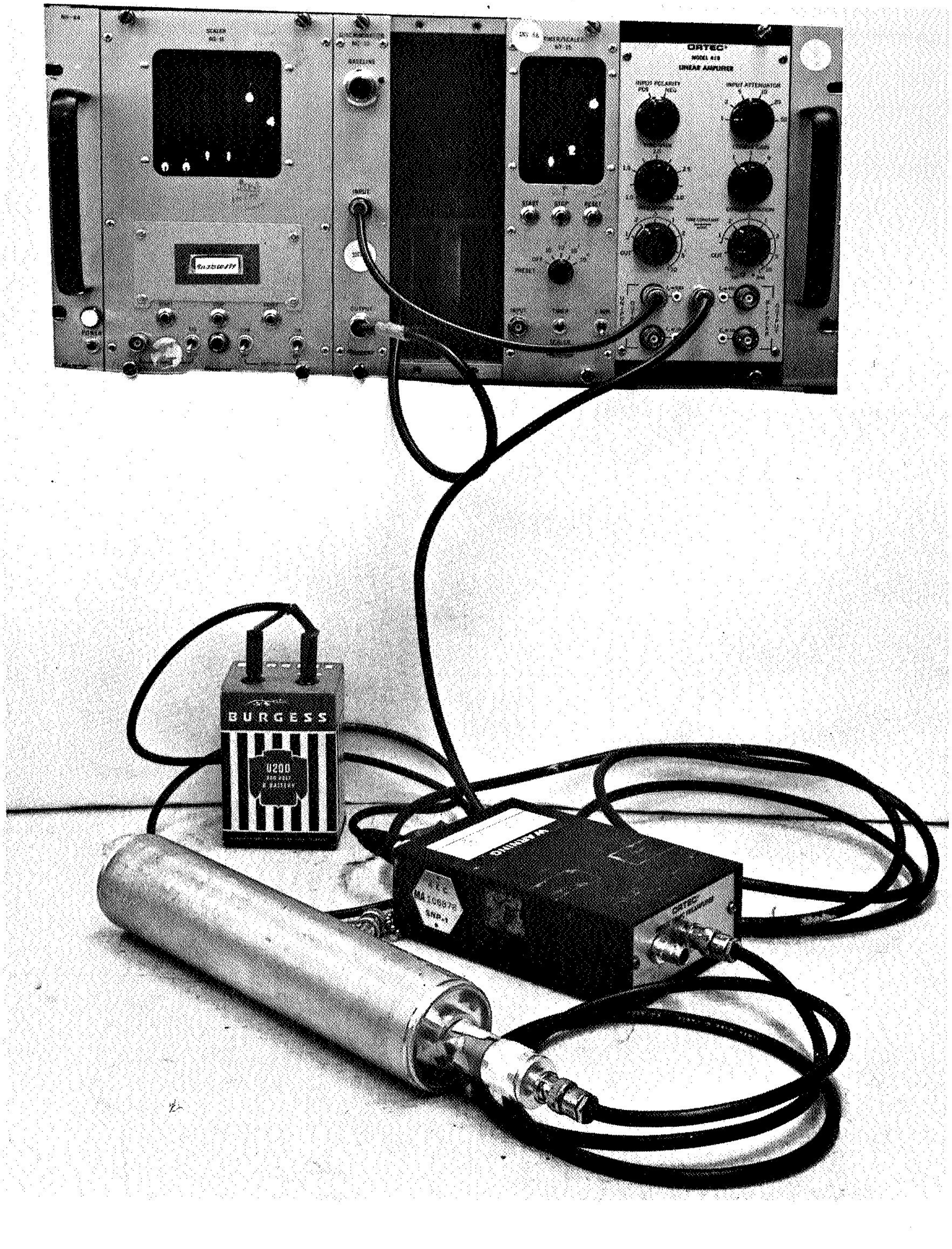

Figure 3-31. WX-30748 Fast Fission Chamber and Associated Electronics

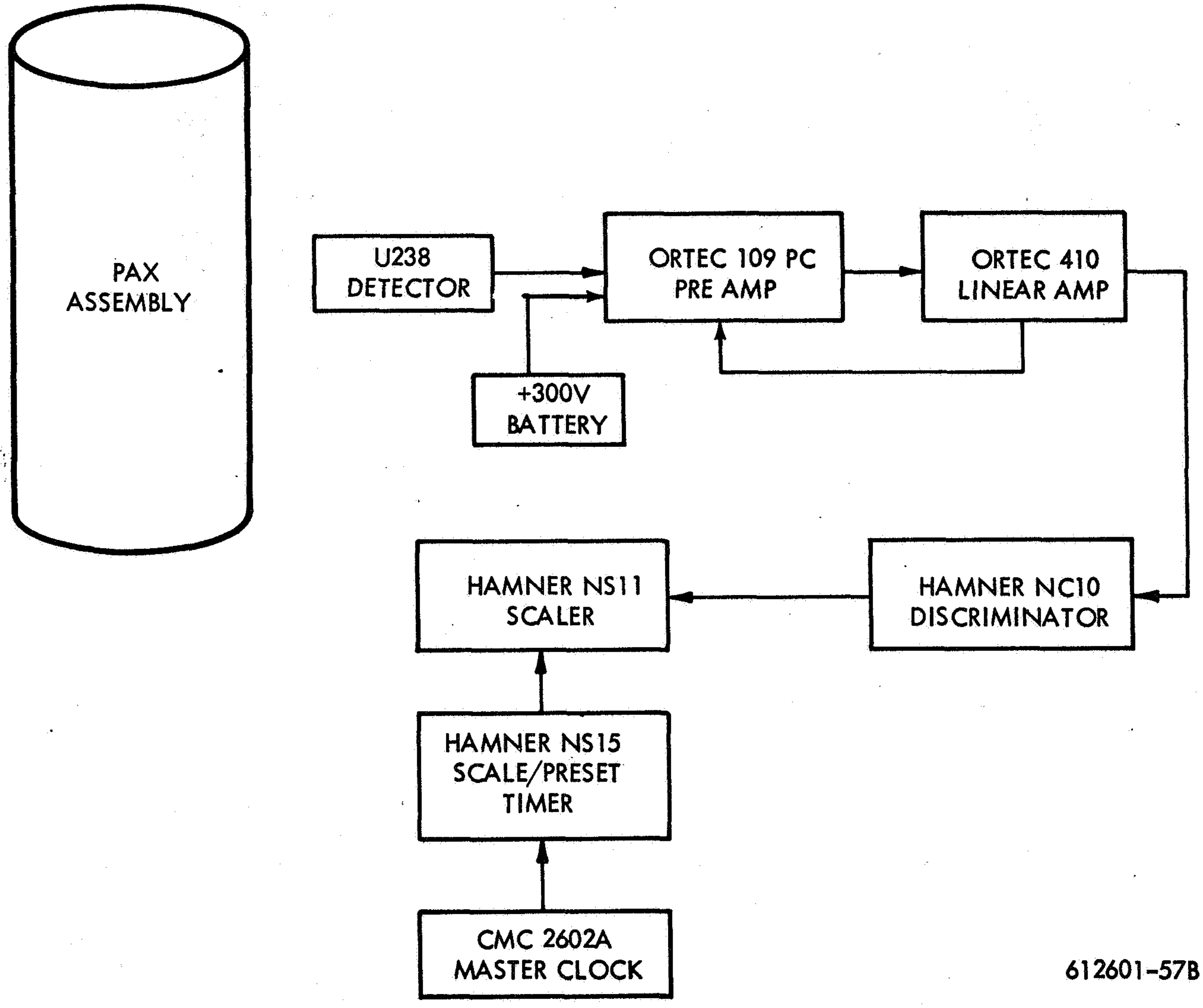

Figure 3-32. Block Diagram Showing the Interconnections Between the WX-30748 Fast Fission Counter and Its Associated Electronics

Actual calibration, therefore, is a measure of the absorbed dose in carbon. Details of the chamber are shown in Figure 3-33. Figure 3-34 shows the RSG-8A and its associated electronic instrumentation while Figure 3-35 is a block diagram showing the interconnections of this instrumentation.

3.7.5 Signal Routing

All preamplifiers required for detectors were mounted underneath the track for the appropriate traverse tube. The high voltage batteries were fastened to one of the main support posts on the traversing framework. All signal cables were routed to a strain relief attachment at the center of the main framework support channel on top of the tank. From there, they were tied to the lifting fixture in order to avoid friction on the sharp tank edge. Another strain relief connection was made at the top of the FCX test stand. This served the additional purpose of keeping the cables from underfoot. From these cables, the signals were then routed through the coax patch panels in the test cell to the appropriate data acquisition instrumentation (Figure 3-36) in the control room or the counting room.

3.8 PASSIVE DOSIMETERS

The passive dosimeters were chosen to provide information on the neutron fast and thermal fluxes and dose rates and gamma dose rates. Passive dosimetry was generally used at locations where active dosimetry was impractical, although one traverse was made with both active and passive to obtain an intercomparison. Figures 3-37 and 3-38 is a view of typical passive dosimetry used for these experiments. 3-37 and 3-38 is a view of typical passive dosimetry used for these experiments. Dysprosium, gold, sulfur, thermoluminescent detectors, Phylatrons, and Pu-239 were the passive detectors employed.

3.8.1 Dysprosium Foils

The Dy foils were used to obtain thermal neutron flux information at selected locations. They were exposed both bare and with Cd covers*. The foil dimensions were

---

* All cadmium covers used for the various foils were 0.020 inches thick.

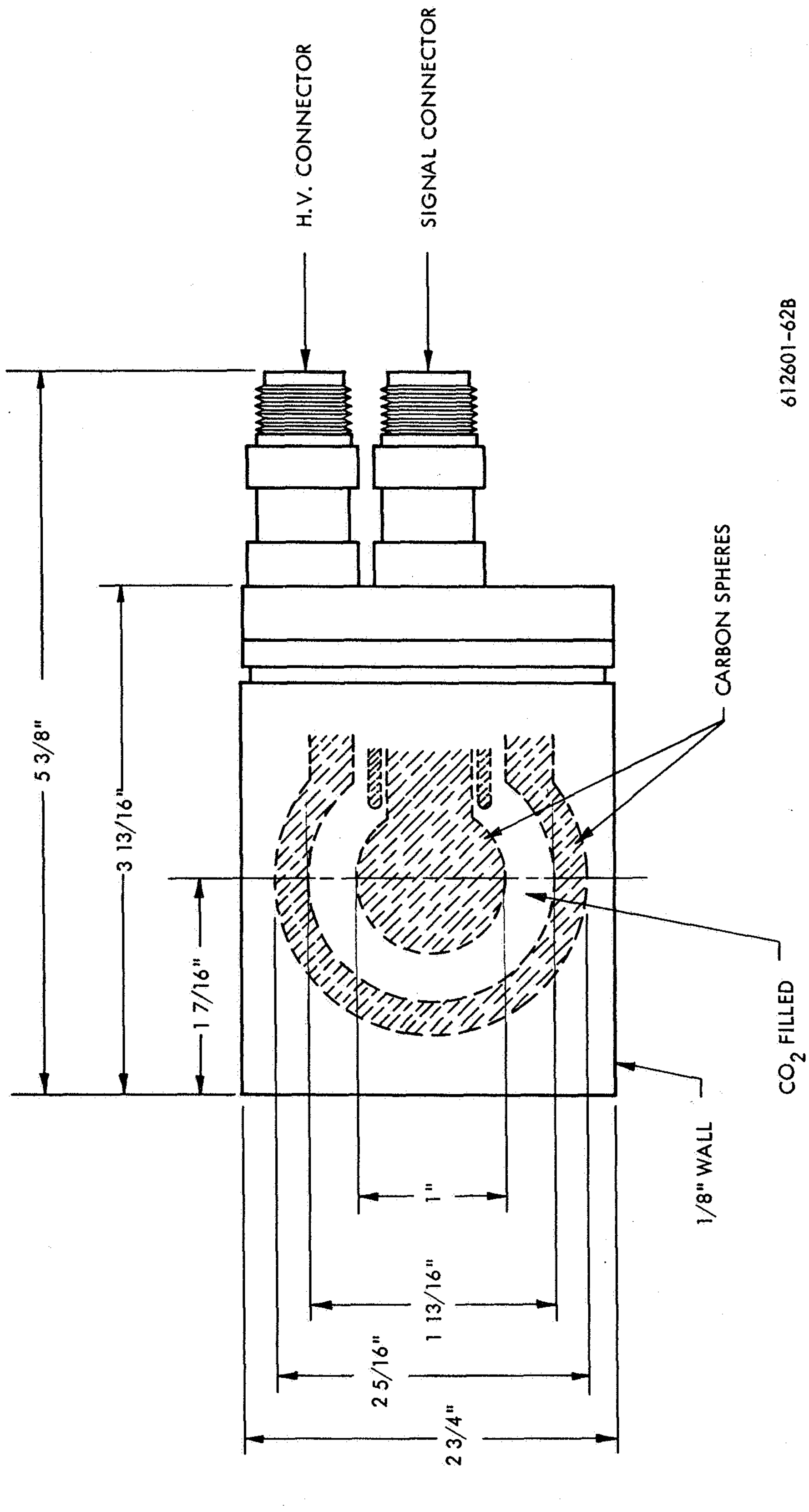

Figure 3-33. Pertinent Details of the RSG-8A Carbon Wall Ion Chamber

Figure 3-34. RSG-8A Carbon Wall Chamber and Associated Electronics

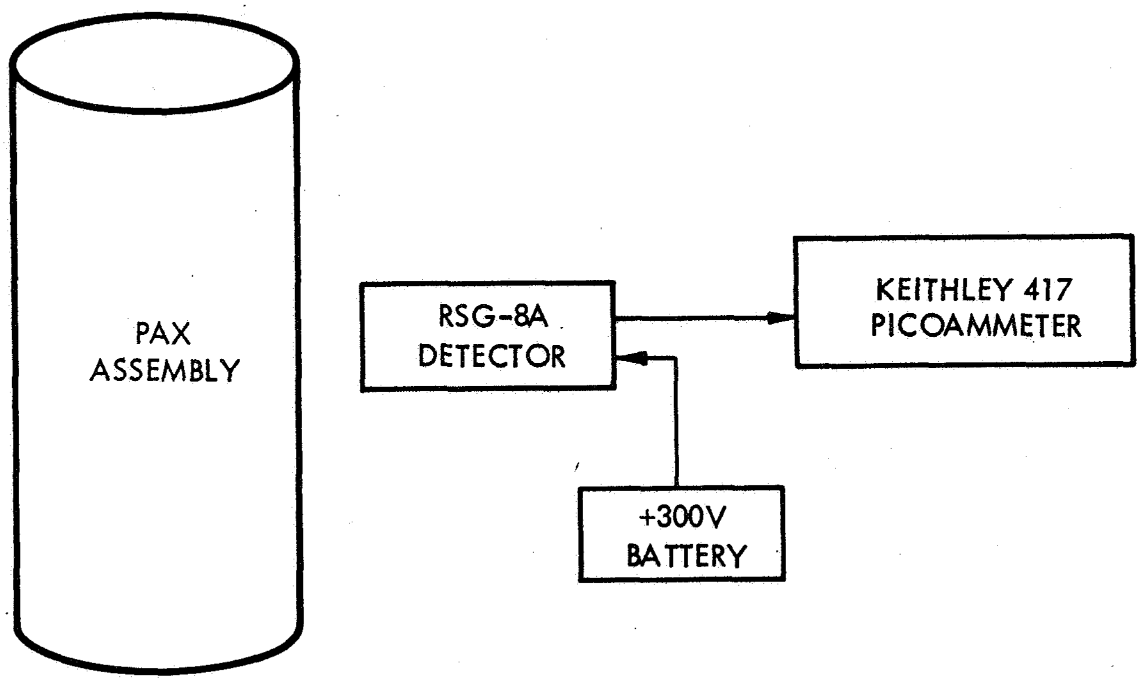

612601-59B

Figure 3-35. Block Diagram Showing the Interconnections Between the RSG-8A Carbon Wall Chamber and Its Associated Electronics

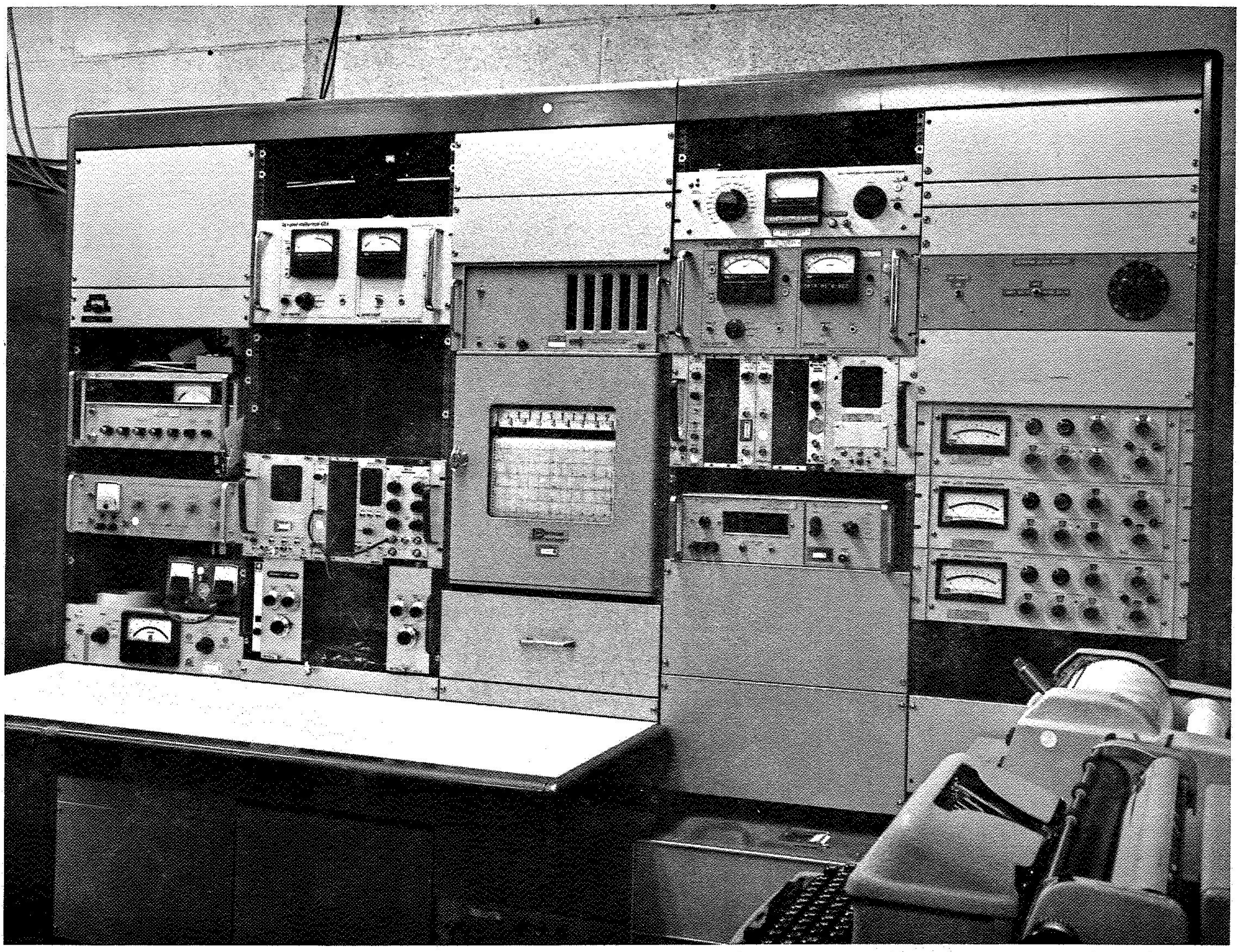

Figure 3-36. Data Acquisition Instrumentation

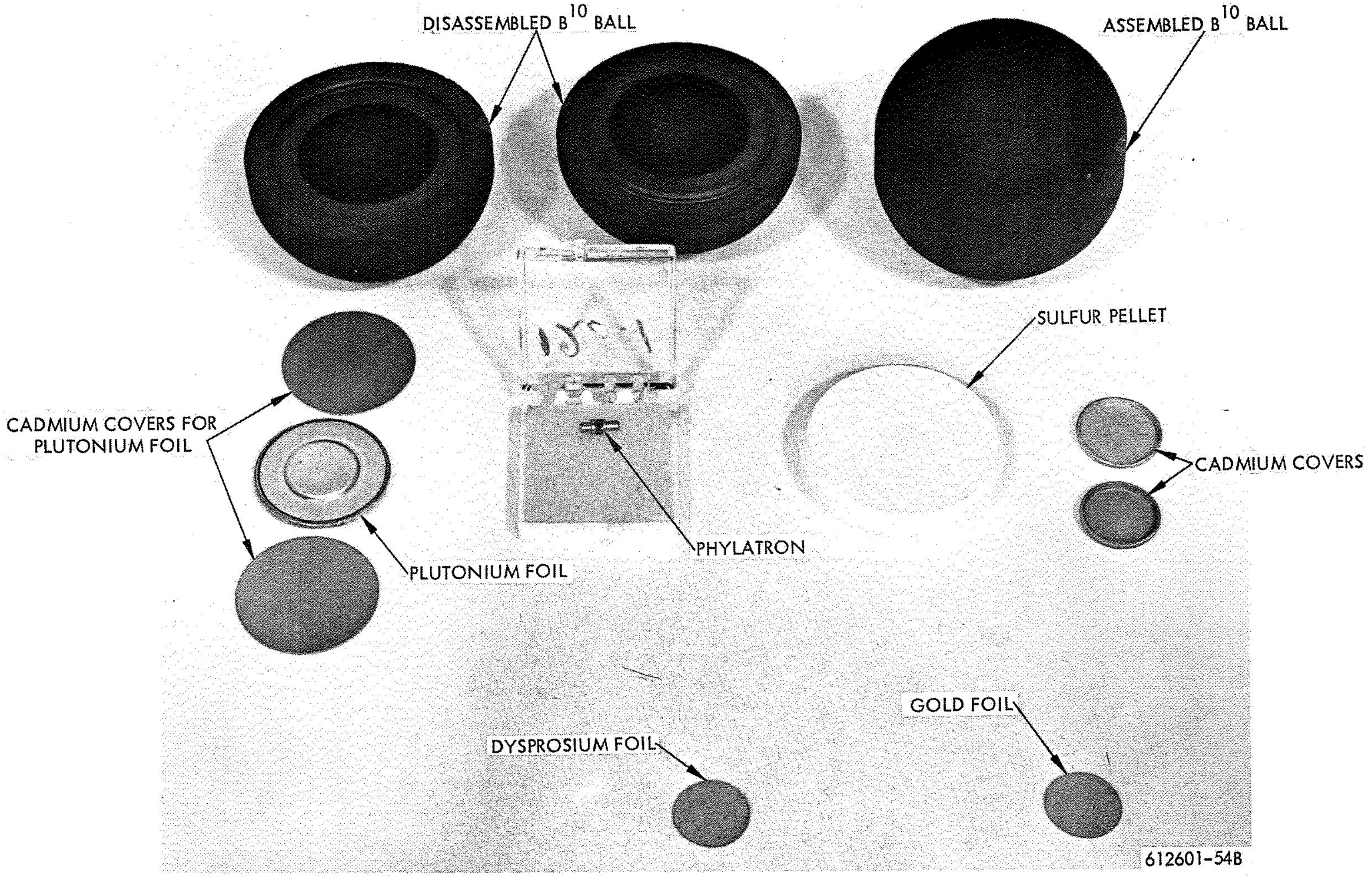

Figure 3-37. Typical Passive Dosimeters

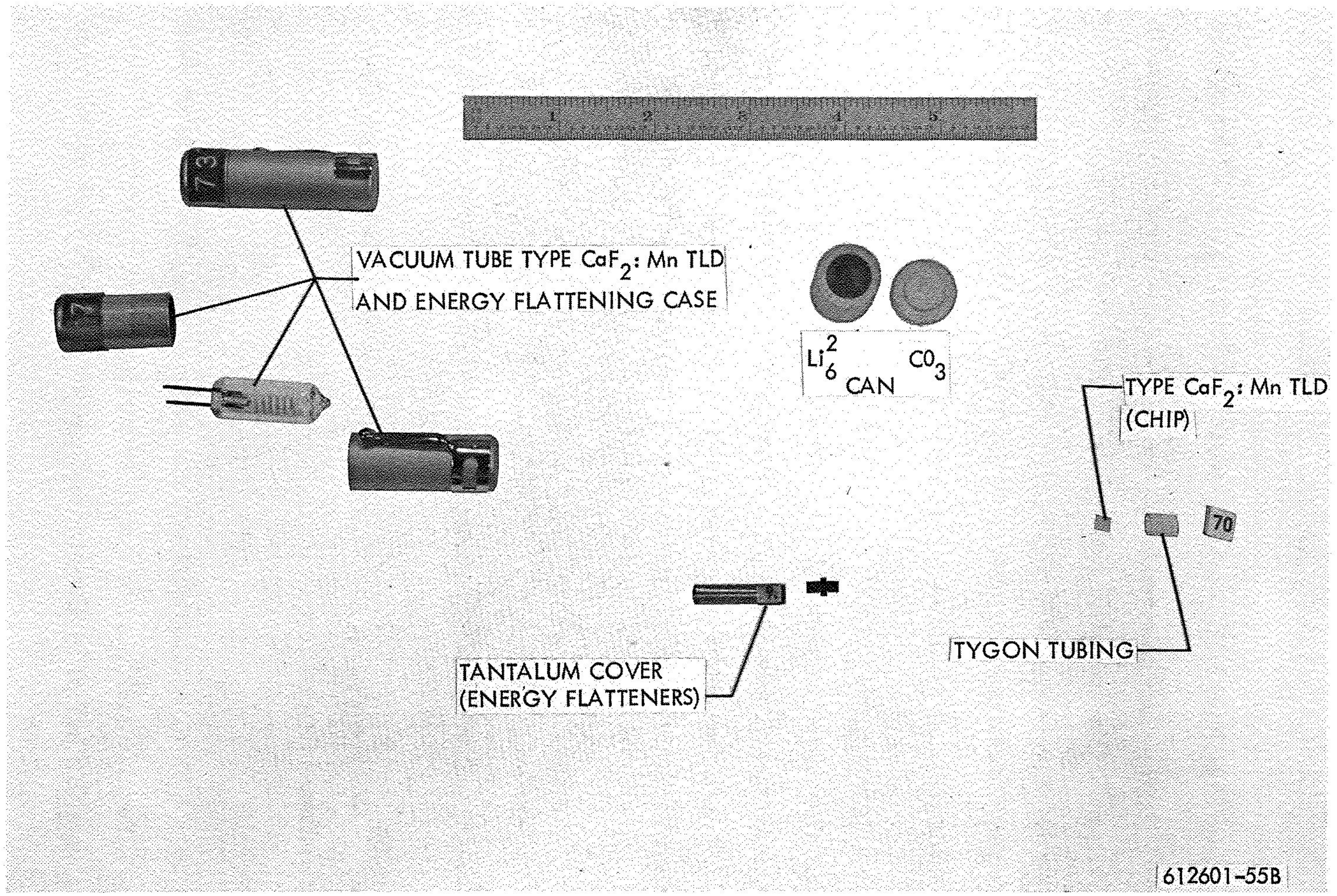

Figure 3-38. Typical TLD's and Energy Response Compensators

0.005 inch thick x 0.500 inch diameter and contained 3.75 w/o dysprosium in an aluminum matrix. The nuclear reaction used to monitor neutron flux is:

$$Dy^{164} + {}_{o}n' \longrightarrow Dy^{165}$$

Dy^{165} emits a 1.25 Mev β^- particle with $T_{1/2}$ = 2.32 hours.

The Dy^{165} isotope was counted for β^- activity using the NC-8010 gas-flow proportional counter system. (The isometric state of Dy^{165} with the half-life of 1.3 minutes was permitted to decay for a sufficient time before counting; also, there are no effects from the irradiation of the additional stable isotopes of dysprosium or aluminum present in the foil.)

3.8.2 Gold Foils

The Au foils were used to obtain a spectral indication by exposing both bare and Cd-covered foils. Due to the large activation resonance at 4.9 ev, most of the captures of the Cd-covered foil are due to this resonance. Therefore, a spectral indication in this region is obtained. The foil dimensions were 0.005 inch thick by 0.500 inch in diameter with the material consisting of 24 K gold. The nuclear reaction used in this case to monitor neutron flux is

$$Au^{197} + {}_{o}n^{1} \longrightarrow Au^{198}$$

Au^{198} emits a 0.96 Mev β^- particle and 0.412 Mev gamma ray with $T_{1/2}$ = 64.8 hours.

The Au^{198} was counted for the β^- activity using the NC-8010 gas-flow proportional counter system.

3.8.3 Pu-239 Foils

The Pu-239 foils were used to obtain a neutron spectral indication at the bottom of the tank. (Fluxes within the tank were so low as to preclude measurement with this detector.) The foils were 0.5 inches in diameter and weight 1.5 to 2.1 gm each. They were encapsulated in an aluminum case that has a diameter of 0.988 inches and a thickness of 0.120 inches. There was 8.54 ± 0.08 w/o Pu-240 present in the foil. During irradiation, the foils were irradiated under cadmium covers which were placed inside B-10 balls. A view of the assembly is shown in Figure 3-39. The 1 cm thick B-10 makes the Pu-239 foils into detectors with an effective threshold of ~1/2 Kev. The nuclear reaction used to monitor neutron flux is

$$\text{Pu-239} \pm {}_o n^1 \longrightarrow \text{fission products}$$

The gamma rays emitted by the fission products were counted with an NaI gamma counting system.

3.8.4 Sulfur Pellets

The S pellets were used to obtain the fast neutron flux information. The effective threshold of detection is ~2.9 Mev. The pellet dimensions were 0.218 inch thick x 1.5 inches in diameter. The nuclear reaction used to monitor the fast neutron flux is

$$S^{32} + {}_o n^1 \longrightarrow P^{32} + p^+$$

The P^{32} emits a 1.71 Mev β particle with $T_{1/2}$ = 14.3 days. The P^{32} disintegration rate was measured with a low background gas-flow proportional counter system.

3.8.5 Phylatrons

Phylatrons were used to measure fast neutron dose internal to and on the surface of the tank. They are essentially a wide-based p-i-n silicon diode approximately 7 mm long by 3 mm in diameter. Figure 3-40 shows a schematic description of the diode structure. The dosimeters are manufactured from the Phylatron Corporation, Columbus, Ohio. The basic principle of operation is that the fast neutron dose to which the device is exposed changes the minority carrier lifetime of the base region. When the device is operated with a forward bias current sufficient to modulate the conductivity of the base, the voltage drop across the diode is very sensitive to the minority carrier lifetime.

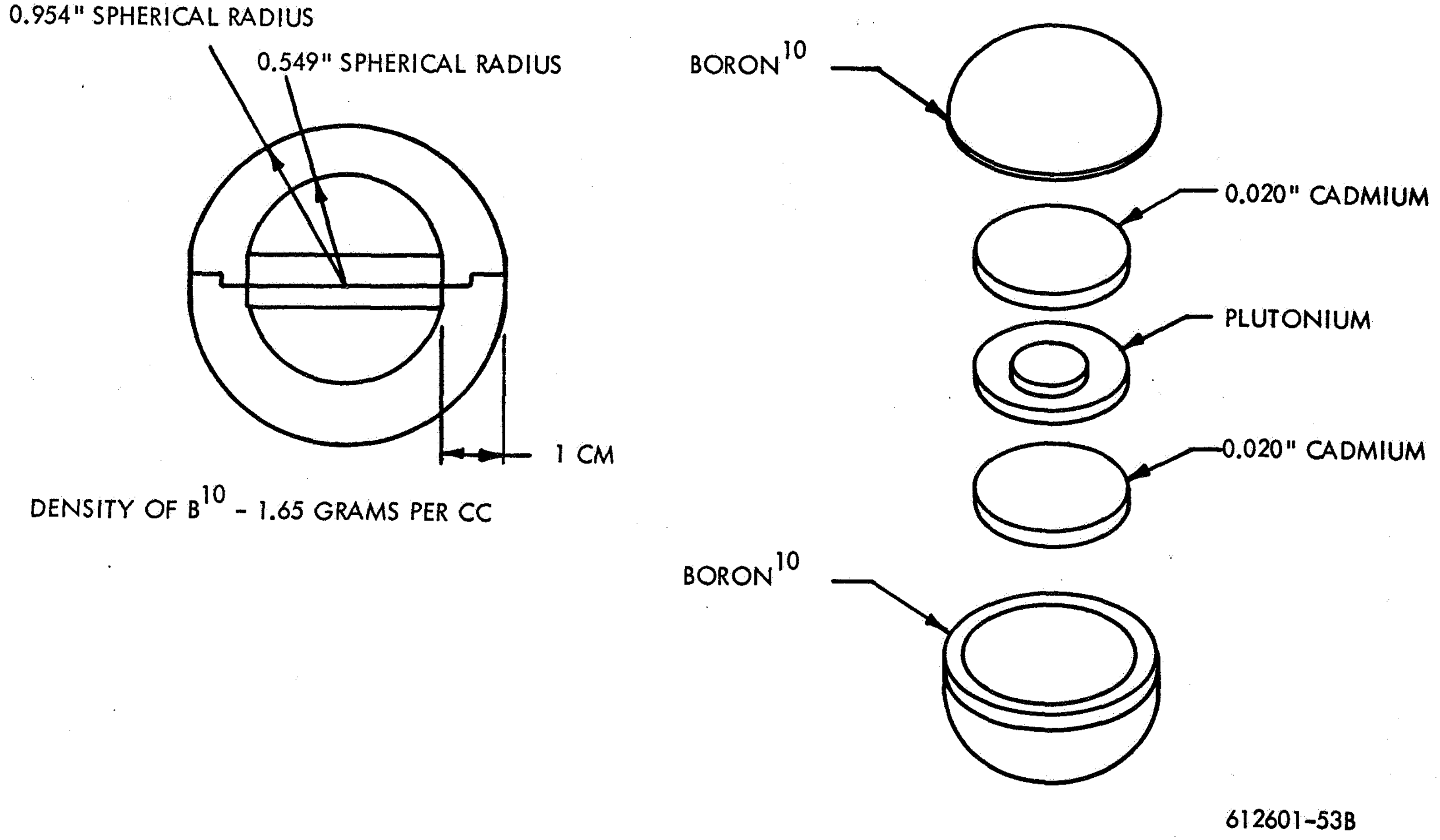

Figure 3-39. Exploded View of B^{10} Container Used for Neutron Energy Compensation on Pu-239 Foils

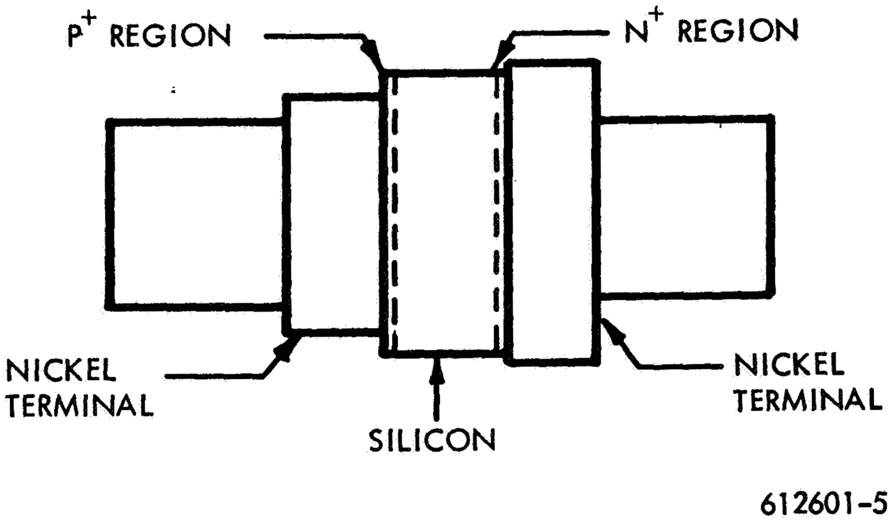

Figure 3-40. Phylatron Structure

The SNDR-2 Phylatron dosimeter reader supplies the constant current and measures the forward voltage drop by a null method. The manufacturer supplies calibration curves for the dosimeters which relate forward voltage change versus neutron dose. The range of the dosimeters can be purchased to span the region of 5-15,000 Rads (tissue). The specific diodes used for this experiment had a total dosage range of 700 Rads.

Exposure to 3.6×10^6 R of Co^{60} radiation produced no significant neutron dose indication. It was thus assumed that Phylatrons are insensitive to gamma radiation for purposes of these experiments.

3.8.6 Thermoluminescent Dosimeters (TLD)

The CaF_2: Mn* hot pressed chips (EG&G Model TL-3B) were used to monitor gamma dose in and on the surface of the propellant tank. The chips were mounted inside 1/64 inch thick Tygon tubing. The mechanism of gamma detection is that ionizing radiation incident upon the material produces metastable energy states in the chip. When the material is heated the release of the stored energy produces detectable photons. The quantity of photons released during heating, as a function of time, can be related to the amount of energy deposited in the chip by appropriate calibration** methods. The TLD's were annealed at a temperature of 350°C for approximately 1-1/2 hours prior to irradiation. This removed any residual metastable states present in the dosimeter. After irradiation, the accumulated energy deposition was obtained by readout with an Edgerton, Germeshausen and and Grier (EG&G) Model TL-3 reader unit.

3.9 COUNTING EQUIPMENT

3.9.1 NC-8010 System

The Dy and Au foil β^- activities were counted on the 2π gas-flow proportional detector. The system is completely automated for efficiency and for reducing errors involved in handling large volumes of data. The NC-8010, was built to WANEF specifications by the

---

* 3 mole percent MnF_2.

** Thermal neutron sensitivity given by the manufacturer is 1.41×10^{-10} R/n/cm^2.

Nuclear-Chicago Corporation, and uses solid-state circuitry. A photo of the system is shown in Figure 3-41.

The principle of operation may be summarized as follows. The NC-8010 system consists of three sample changing mechanisms, appropriate amplifiers, scalers, timers, logic and control units, and output devices (printer and paper tape punch). The detector is a 2 flow proportional counter, with interchangeable end windows of aluminum-coated Mylar and uses P-10 gas (90 percent argon and 10 percent methane). Samples up to two inches in diameter can be accommodated.

Each sample changer holds up to 50 samples on planchets in the loading chute; upon command (there is a choice of manual or automatic command from the logic control), the new sample is withdrawn from the bottom of the loading chute and positioned under the radiation detector.

The three scalers and pre-set timer are located in a single-unit chassis which has a single display. The elapsed timer and memory storage unit provides a timer that may be used as an elapsed timer or as a time normalizer.

An additional detector was used with the NC-8010 system to provide a normalizer channel. The system was then set in the pre-set count mode in order to automatically trigger a sample change. This mode of operation automatically corrects for sample decay during counting. Data output is recorded on one-inch wide paper punch tape in a form compatible with the Raytheon 250 computer which was programmed to reduce the data.

3.9.2 Gamma Counting System

The gamma counting system consists of three detectors using Harshaw two-inch diameter, two-inch high NaI (Ti) scintillation crystals and integrally mounted RCA 6342A photomultiplier tubes. The detectors were operated at 1105 volts, with a FWHM resolution of approximately 8 percent at 0.661 Mev. The output of each detector is fed into a Hamner Model 338 linear amplifier with a differential and integral pulse height discriminator. The pulse height discriminator outputs are fed, in turn, into scalers having binary coded decimal

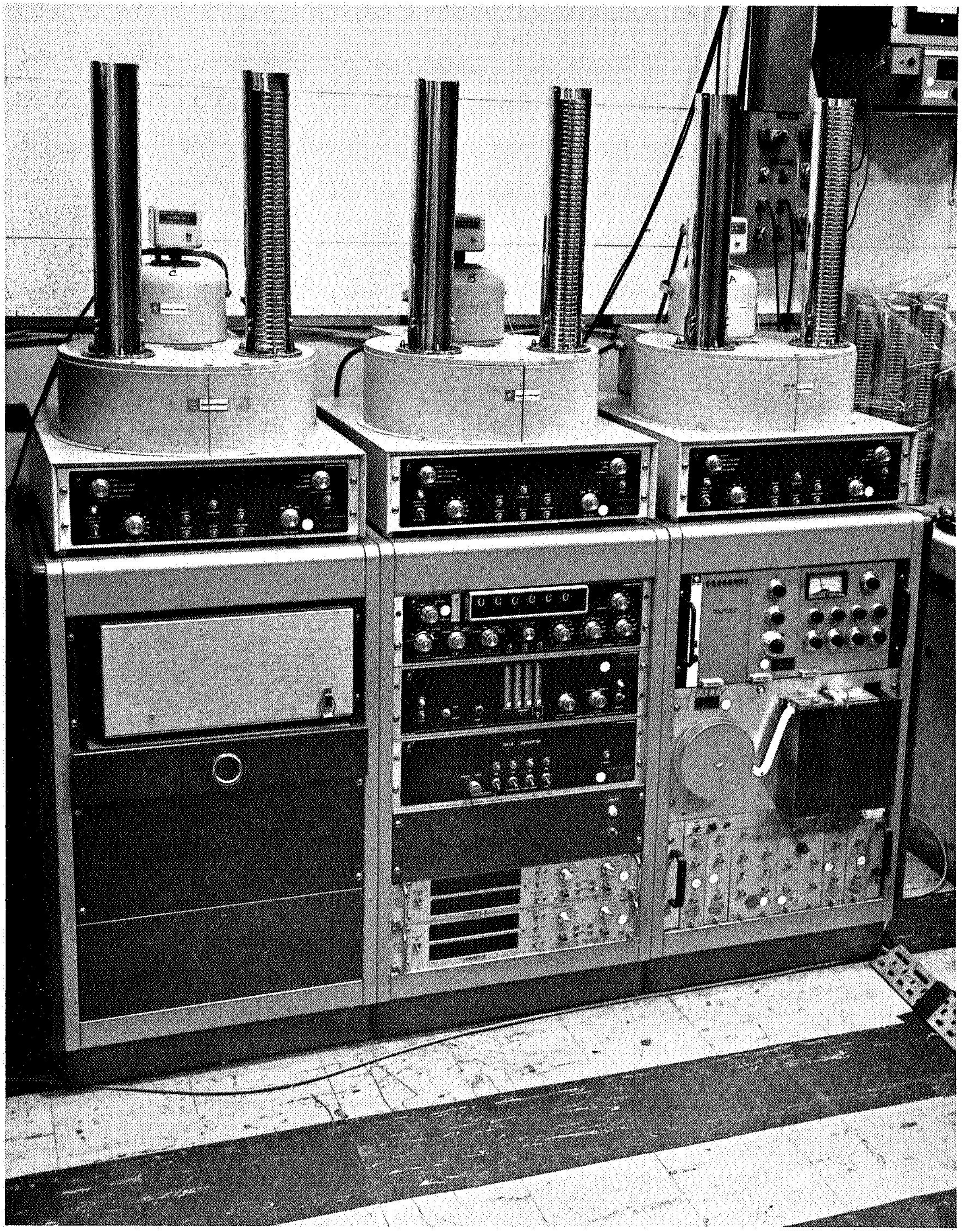

Figure 3-41. The NC-8010 $2\pi\beta$ Counting System

outputs. These scaler outputs, along with interval and elapsed times from two timers and a manually set two-digit identification output, were recorded automatically on punched paper tape by a specially modified Friden Flexowriter, which is an integral part of the system. A photo of the system is shown in Figure 3-42-1 and 3-42-2.

The Pu-239 fission foils were counted with an integral discriminator setting of 1.2 Mev. The discriminator settings were calibrated with Co^{60} and Cs^{137} gamma rays. One channel was used as a normalizer to provide decay correction information. Another channel was used to monitor background changes during counting. The third channel was used to count the foils.

3.9.3 Low Background Beta Counter

The sulfur pellets were counted in the low background beta system shown in Figure 3-43. This system is a fully automatic, one-channel, beta-counting system for counting solid samples having a low specific activity. It incorporates a guard counter which detects the charged particles resulting from cosmic ray background, and anti-coincidence circuits that cause this background to be ignored. The system, which can count samples up to two inches in diameter, automatically cycles through up to 150 of these at one time, counting each in succession. The results were automatically recorded on both printed and punched tape formats and reduced by the Raytheon 250 computer.

3.9.4 P-I-N Silicon Diode Readout

The irradiated Phylatrons are inserted into the dosimeter holder of the SNDR-2 reader shown in Figure 3-44. The change in forward voltage with irradiation is then obtained from the instrument. Calibration curves of forward voltage change versus dose supplied by the manufacturer are used to obtain the dose.

The dosimeter readout instrument consists of a 100 ma transistorized constant current source. A Zener diode regulated ten-turn potentiometric voltage adjustment (located on front panel of reader) is used for bucking out any forward voltage drop of the dosimeter.

Figure 3-42-1. Gamma Counting System Detectors and Shields

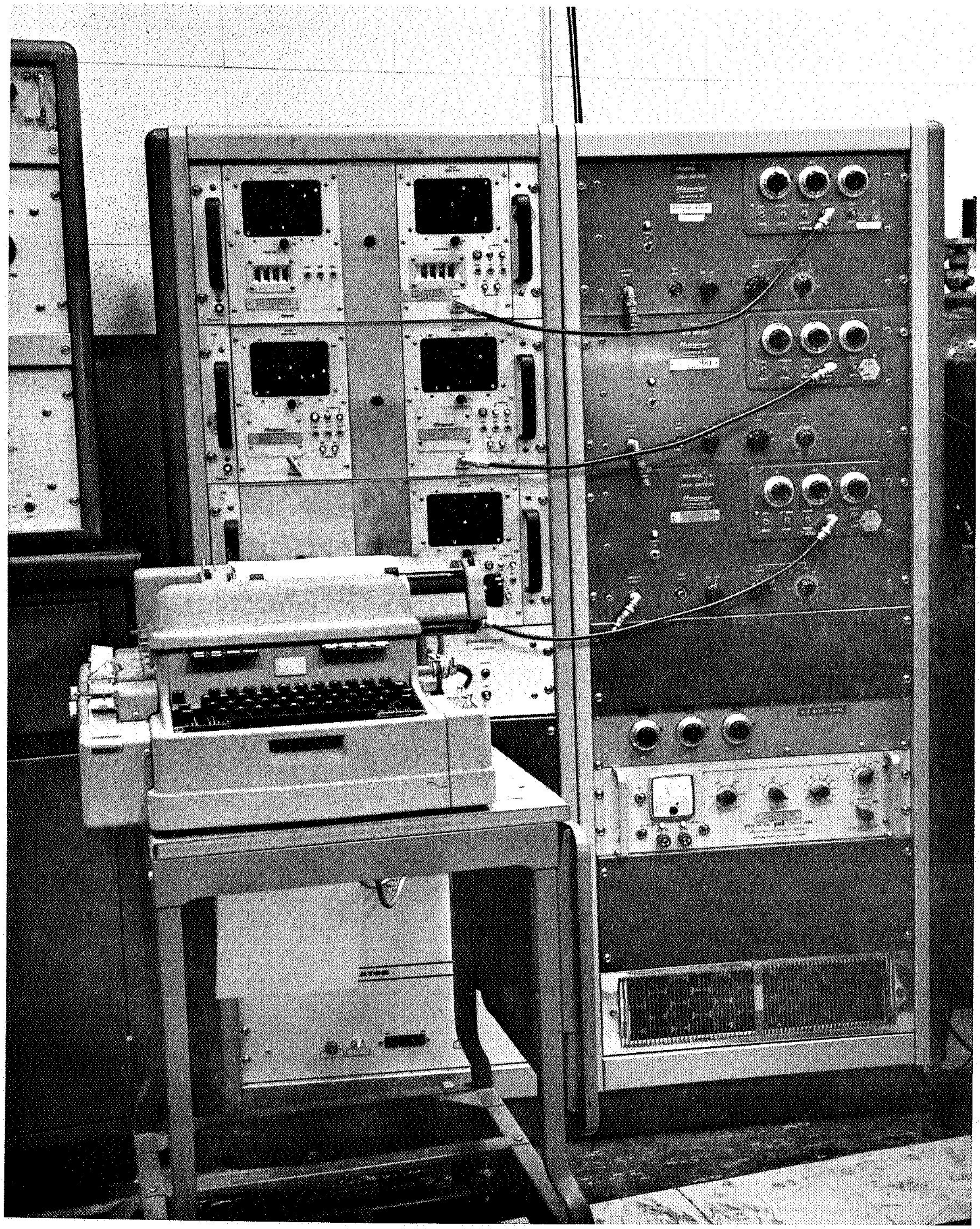

Figure 3-42-2. Gamma Counting System Electronics

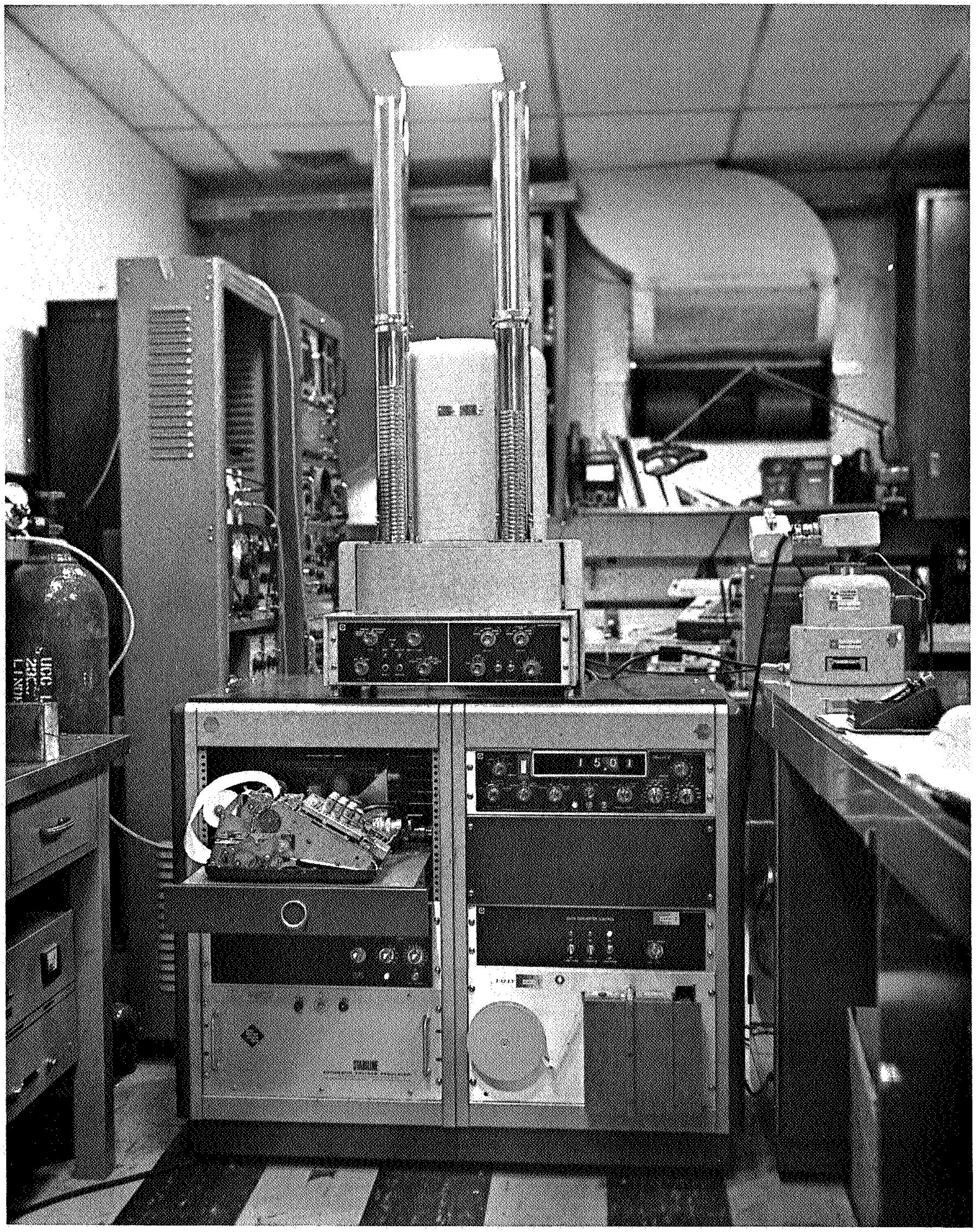

Figure 3-43. Low Background β Counter

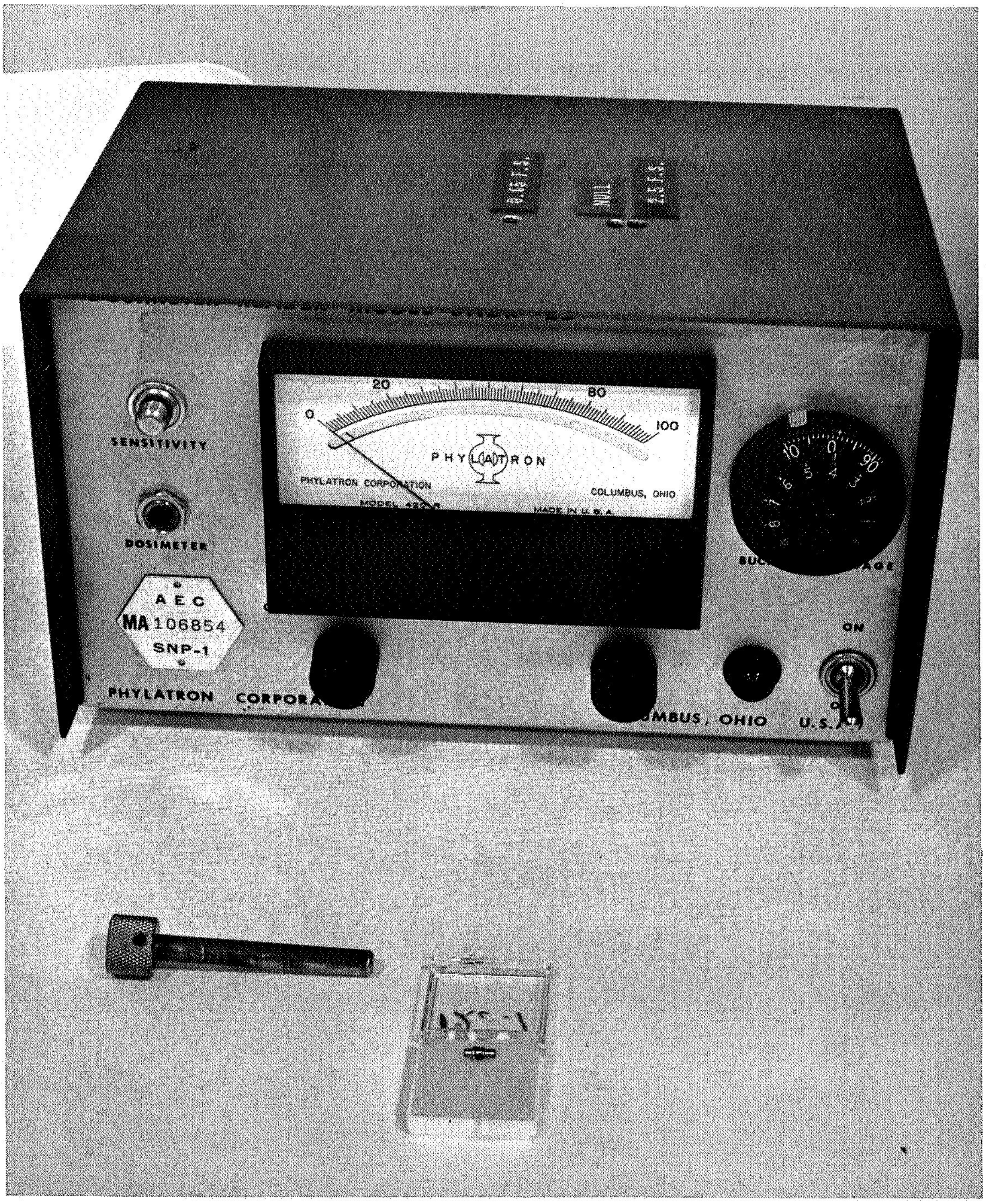

Figure 3-44. SNDR-2 Phylatron Reader

The reader meter is calibrated by a 25 Ω resistor which is in the circuit with no dosimeter in the holder. The full scale deflection of the meter in this position is 2.5 Volts. Prior to any irradiation, the dosimeter forward voltage is recorded. This is obtained by placing the dosimeter in the reader and bucking out the forward voltage with the ten-turn potentiometer. The scale on the potentiometer reads percent of 2.5 volts. The potentiometer is varied until the meter deflection is zero. The potentiometer reading gives the forward voltage drop across the resistor.

After irradiation, the process is repeated. The forward voltage prior to any irradiation is subtracted from the irradiated forward voltage, which gives a change in forward voltage. The change in forward voltage versus dose curves supplied by the manufacturer permits the dose to be obtained. The dosimeters can be used again if the range of the dose is not exceeded. The forward voltage prior to any subsequent irradiation must be recorded and this residual dose is subtracted to obtain a net dose during the subsequent irradiation.

Due to transients in the diode immediately following irradiation and slight annealing processes in the dosimeter with time, the dosimeters were read during the period of 2 - 2-1/2 hours after irradiation. This is when the manufacturer recommends readout. The dose decay during the 1/2 hour period is negligible.

3.8.5 Thermoluminescent Detector Readout System

The energy deposited in the CaF_2: Mn thermoluminescent dosimeter is readout on an EG&G thermoluminescent dosimeter reader Model TL-3B (shown in Figure 3-45-1). The dosimeter is surrounded by a heating coil in (Figure 3-45-2) the reading head. The reading head is then placed in a light tight chamber. When the dosimeters are heated, the photons emitted by the dosimeter are observed with a photomultiplier tube. The current from the PM tube operates a chart recorder with automatic range selection. The variation of light intensity with time is recorded on the chart paper. From the peak of the curve and the number of range changes that occurred, the energy deposited in the dosimeter can be obtained. Absolute calibration of the instrument is obtained by reading TLD's irradiated in a known Co^{60} gamma field.

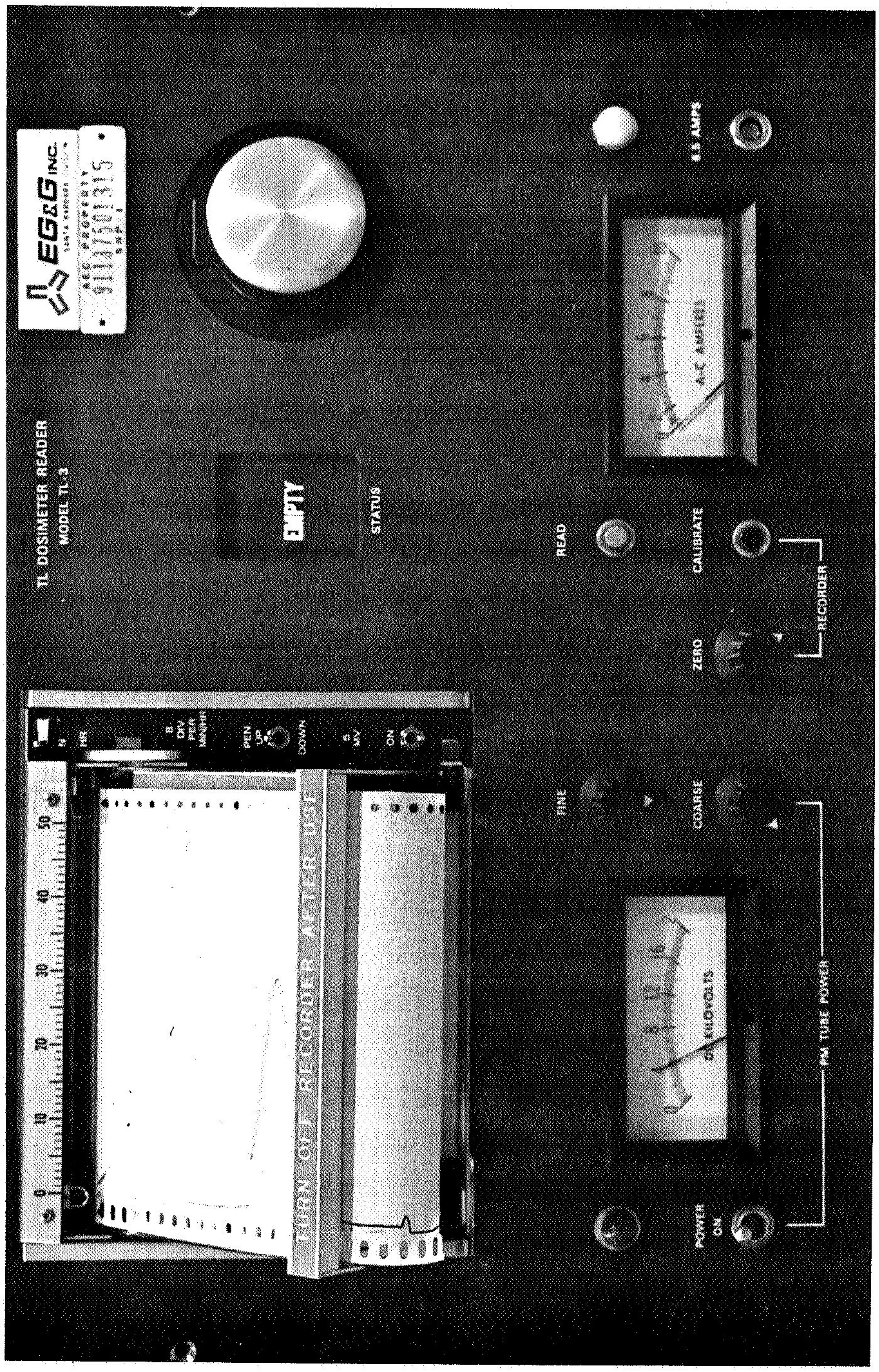

Figure 3-45-1. EG&G TLD Reader

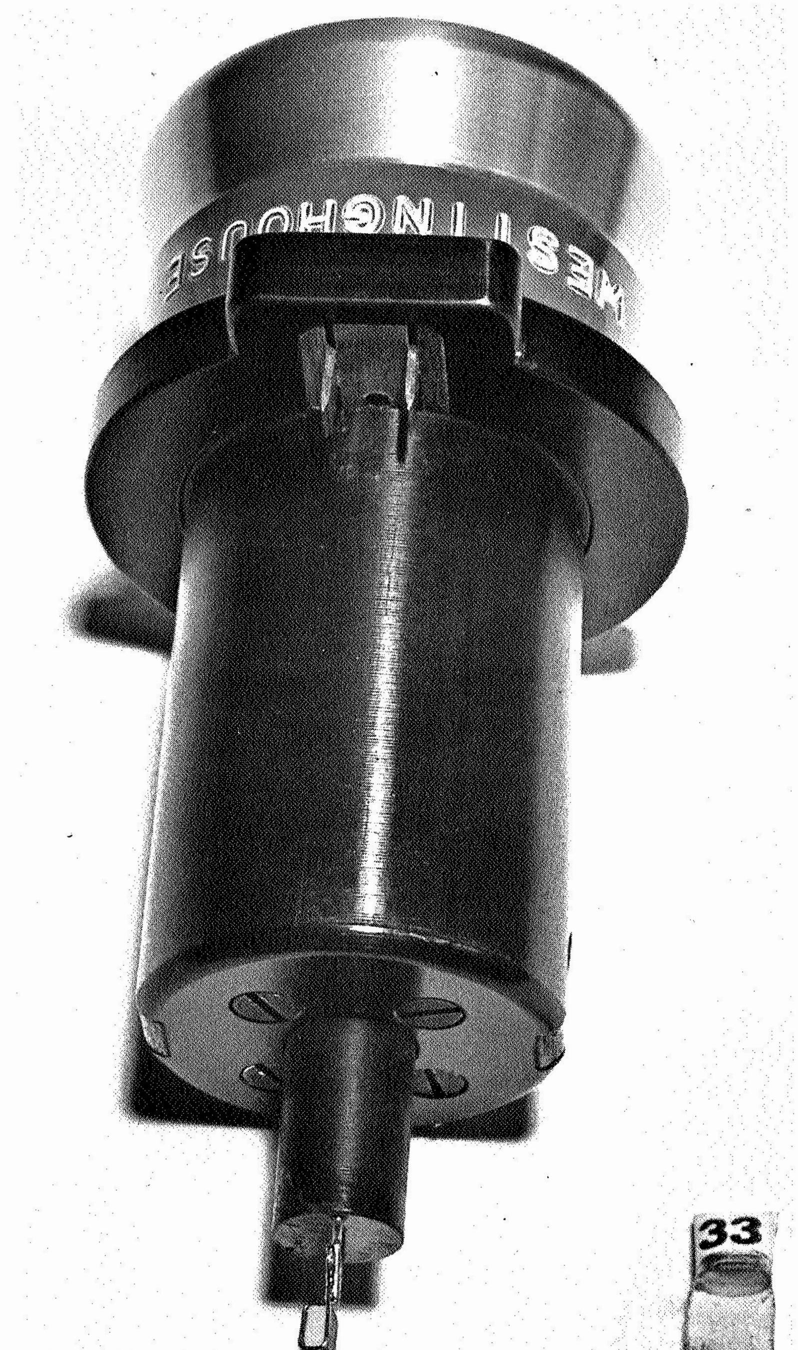

Figure 3-45-2. TLD Reader Head with CaF_2: Mn TLD in Place in Heating Coil and Tygon Irradiation Packet

The stability of the system during readout is periodically checked with a reference light that enables the system to be adjusted, if required. The reference light contains a small amount of β^- emitting C^{14}. The radiation causes the fluoride material of the reference light to emit a reproducible glow which can be used to adjust the readout system.

SECTION 4. TEST OBJECTIVES

The test objectives are best summarized in Exhibit D. Additional Scope of Work for Contract NAS-8-20414 is as follows:

"The contractor will conduct experiments, using the Permanent Assembly Experiment (PAX) reactor at the Westinghouse Astronuclear Experimental Facility (WANEF), to determine heating rates in a simulated liquid hydrogen environment, will analyze the experiments using standard shield calculation methods, and will compare and evaluate the experimental and calculated results." It was further stated in the scope of work that two types of reduced density polyethylene to simulate neutron and gamma ray transport properties, respectively, in liquid hydrogen would be provided by the contractor and would be loaded into a propellant tank mockup to approximately a depth of 3 feet for neutrons and 6 feet for gamma rays. MSFC, in turn, agreed to furnish the propellant tank mockup suitably modified for the contractor. The data which was required included "a good definition of gamma ray, fast, and thermal neutron radiation environment throughout the tank."

Also, "where possible, spectral measurements of the radiation should be taken on the surface of the tank."

Based on these requirements, a test plan for the experimental portion of the program was formulated subject to the following constraints:

1) All reactor runs were to be made "piggy-back" (i.e., simultaneous) with NERVA runs on a non-interference basis.

2) Because of the extra fabrication and installation time required, the low density polyethylene was to be run first.

3) Because of limitations on the counting facilities, the number of short-lived foils available, i.e., dysprosium, was determined consistent with NERVA requirements.

In addition to the above limitations and requirements, it was decided that measurements on the two different densities of polyethylene were to be taken with a "thick" shield, i.e., Configuration 11, in an attempt to permit an experimentally determined background from test cell produced radiation.

The following section discusses how these test objectives were implemented for these experiments.

SECTION 5. EXPERIMENTAL PLANS

This section describes runs made with both active and passive dosimetry as well as their placement on and in the tank. Positioning of the propellant tank above the reactor is also discussed.

5.1 ACTIVE DOSIMETRY

A detailed listing of the actual runs made together with the active dosimetry types and locations is given in Table 5-1. In order to avoid an excessive number of runs required to gather adequate active dosimetry, some runs were made with two detectors in some of the traverse tubes. Because of the limited travel of the tube, one detector was only traversed slightly more than half way through the tank. However, since the radiation environment in the propellant tank should be nearly symmetrical about the tank axial centerline (except for effects caused by the test cell), this condition was deemed acceptable. If necessary, it was felt corrections for the test cell effects could be derived from passive dosimetry.

All active dosimetry was placed in one or more of the three twelve foot long aluminum traverse tubes or, in a few cases, in one of the 6 foot long dummy traverse tubes. For the low density polyethylene foam, an attempt was made to place the center of detection of each detector approximately 74 inches from the drawn end of the traverse tube. Placement at this position assured that the detector would traverse from one side of the tank to the other since the tank ID is approximately 70 inches. In the case of the polyethylene foam, foam shells were constructed to maintain proper spacing of the detectors within the tubes. Detector spacing within the pellet (high density polyethylene) filled tubes was maintained by small pieces of polyfoam glued to the detector walls. The remaining space around the detector was filled with the poly pellets. Except for the space occupied by the detector(s) and the associated leads, the entire inside of each traverse tube was filled with polyethylene of the appropriate density. Figure 5-1 shows a partially disassembled traverse tube, RSG-8A detector, polyethylene foam, detector cables and end cap.

TABLE 5-1

ACTIVE DOSIMETRY LOCATIONS

LIST OF ACTIVE DETECTOR RUNS

			DETECTOR TYPE AND HORIZONTAL TRAVERSE TUBE LOCATION[++]			
Run No.	Density of Poly In Tank	Shield Configuration	Hurst (RSN-48)	Fast Fission (WX-30748)	Carbon Wall Detector (RSG-8 A)	Boron-Lined Compensated Ion Chamber (WX-5362)
1	Low(ρ= 0.14 gm/cc)	7D		-	1 & 2	3
2	Low	7D		-	3 & 4	1
3	Low	7D			-	2 & 4
4	Low	11	-	-	1 & 3	2
5	Low	11	-	-	2	1 & 3
6	High (ρ=0.59 gm/cc)	11	2 & 3	1		2[+] & 3[+]
7	High	4B	2 & 3	1		2[+] & 3[+]
8	High	4B	4	3	1	1 & 4
9	High	4B	1	2	3	-

[+] Data exists for 5/8 of the tank width

[++] These are tank position designations with the axial distance between horizontal centerline being 9 inches, 9 inches and 13 inches between Tubes 1 and 2, 2 and 3, and 3 and 4, respectively. Tube 1 is 9-5/8 inches above the outside bottom of the tank. The tubes run between azimuth 90 degrees and 270 degrees.

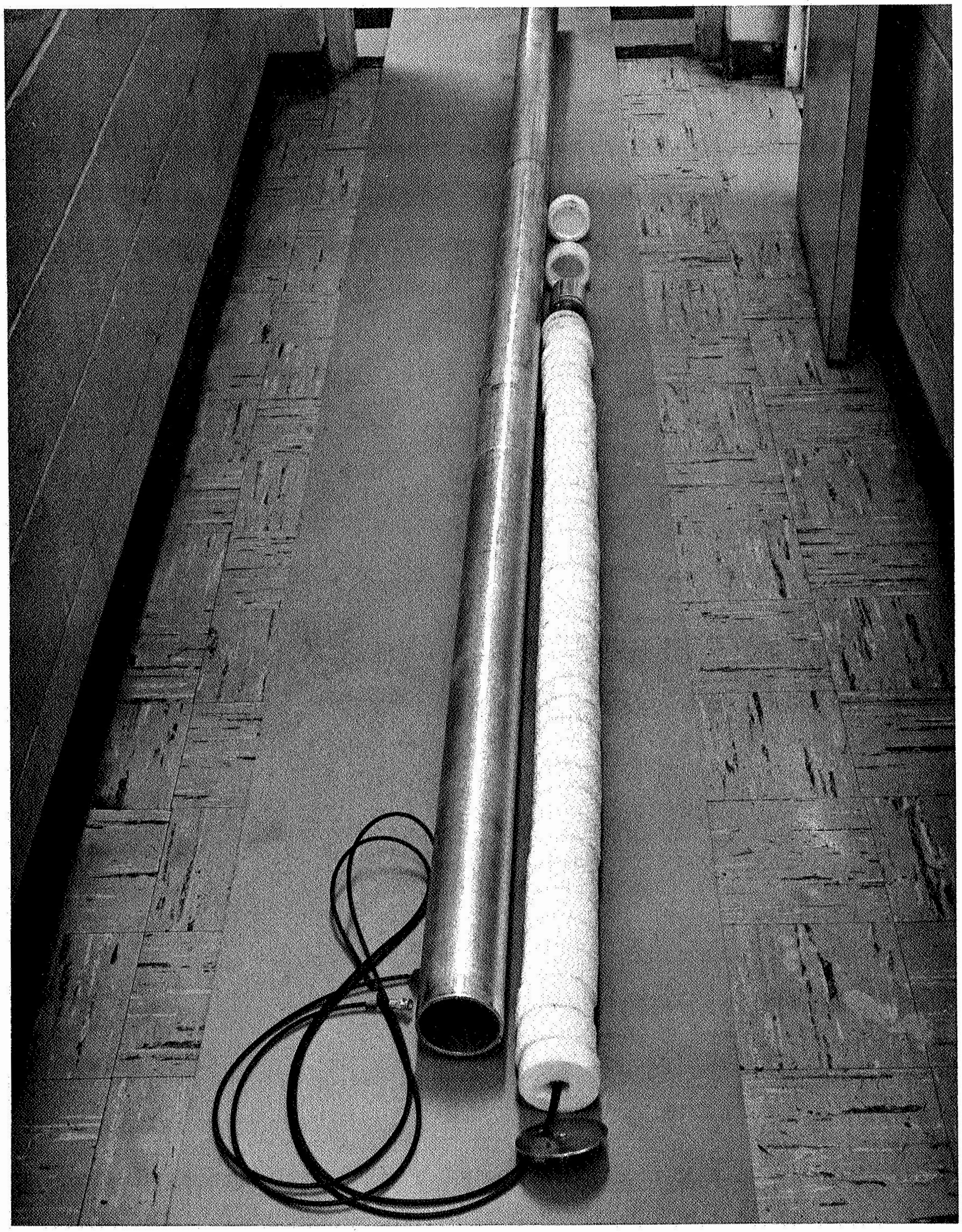

Figure 5-1. A Partially Disassembled Traverse Tube Showing One of RSG-8A Chambers and the Method of Assembly

When two detectors were placed in the same traverse tube, the center of detection of each detector was placed approximately 12 inches from the original 74 inch mark, assuring a detector separation distance of about 2 feet. To compensate for this change, the traverse tube was recessed approximately one foot before the start of the run.

In order to check the linearity of the withdrawal mechanism a series of measurements was taken of indicated voltage versus tube position. These measurements agreed quite well with the calculated positions.

Prior to the beginning of each run, all traverse tubes were reset to their proper position and the ten-turn potentiometers were reset to the position of maximum rotation. Since potentiometer power was supplied by batteries, this maximum voltage was recorded for each traverse mechanism. This value was then used as a normalizer for each run. This voltage was 6.340 volts at the beginning of the series of measurements but decreased to 6.140 by the time of the last run, a total time span of approximately one month.

All detectors were checked immediately prior to any given run with an appropriate radiation source. The corresponding high voltage batteries were also checked occasionally and replaced when necessary.

Because of the extreme sensitivity of the RSN-48 detector - 190 PC preamp combination to input cable capacitance, special subminiature coaxial cable was used. Tests proved that as much as 12 feet of this cable did not provide enough capacity to noticeably degrade the internal a calibration spectrum.

5.2 PASSIVE DOSIMETRY

5.2.1 Passive Dosimetry Types

A detailed listing of the types of passive dosimetry employed for each density polyethylene and each shield is given in Table 5-2. Reactor power levels used remained constant during any given run but varied between runs by from 150 to 750 watts. Integrated powers ranged from 150 to 1500 watt-hours.

TABLE 5-2

PASSIVE DOSIMETRY TYPES

		PASSIVE DOSIMETRY LOCATIONS		
Density of Poly in Tank	Shield Config.	Tank Axial[+++]	Tank Circumferential[+]	Tank Hemisphere[++]
Low	7D	TLD, Dy, CdDy	TLD, Dy, CdDy	TLD, Dy, CdDy, Pu* Au, CdAu
Low	11	TLD, Dy, CdDy TLD***	TLD	S*, Pu*, Au*, CdAu*, TLD, Dy, CdDy
High	11	TLD, Dy, CdDy	TLD, Dy, CdDy	
High	4B	TLD, Dy, CdDy, S, Dy**, CdDy**, TLD**	TLD, Dy, CdDy, S	TLD, Dy, CdDy, S, Pu*, Au*, CdAu*, P*

Au = bare gold

CdAu = cadmium-covered gold

Dy = dysprosium

CdDy = Cadmium-covered dysprosium

TLD = thermoluminescent detector (CaF_2 : Mn)

P = Phylatron

Pu = Pu-239 in B-10 ball

---

[*] Bottom of hemisphere only.

[**] Axial on tank exterior. Data taken at azimuth of 225 and 315 degrees

[***] Data taken radially at Station 103 cm.

[+] Data taken at Station +80 cm and -42 cm where the station is measured positively upward from the bottom of the hemispherical tank section.

[++] Data taken on the outside tank surface on an azimuthal plane (vertical) going between 90 and 270 degrees.

[+++] Unless otherwise noted, data taken on an axial traverse is r = 11.75 cm, azimuth = 0 degrees for varying stations.

5.2.2 Foil Placement

5.2.2.1 Axial Traverse in Tank

The vertical traverse within the tank was accomplished by placing dosimeters within the removable, clear acrylic tube which fitted inside of the vertical aluminum tube running the length of the tank. In the tank coordinate system, the center of the tube was at a radius of 11.75 centimeters at 0 degrees azimuth.

For the low density polyethylene case this tube was filled with discs of polyfoam with a press-fit. The passive dosimeters used on any one run were taped to discs of lightweight cardboard of the same diameter as the polyfoam discs. These were then inserted between the polyfoam discs where desired, with the foils on the surface of the cardboard. Axial spacing of the discs was measured after the acrylic tube was loaded. The sulfur pellets, because of their thickness, were recessed into the polyfoam disc above the cardboard by melting cylindrical depressions of the correct diameter and depth, into the polyfoam using a modified soldering iron. Sulfur and bare Dy were placed on the centerline of the tube while cadmium-covered dysprosium and TLD's were placed off-axis 180 degrees apart. Figure 5-2 shows the dosimetry loading as described above.

For the high-density polyethylene case using polyethylene pellets, the acrylic tube was filled with pellets to the same height on the rest of the tank. To provide a positioning structure (Figure 5-3) for the dosimeters, a 5/16-inch diameter Plexiglas rod was drilled with horizontal holes into which 0.055-inch diameter, 3.5 inch long steel tube was pressed. The azimuth of the holes varied so that the end of the sections of tubing described a spiral around and up the rod. The rod could then be inserted into the acrylic tube and positioned in the axis of the tube. The steel tubing cross piece served for dosimeter mounting and also kept the rod positioned on the tube axis. Dosimeters were taped to pieces of light cardboard which were then taped to the underside of the steel tubing with the dosimeters on the lower side of the cardboard. The cadmium-covered foils were placed on one side of the rod and the bare foils and TLD's on the other.

5.2.2.2 Horizontal Traverse Through Tank

A horizontal traverse through the tank was performed with dysprosium and TLD's and with the polyfoam in the horizontal traverse tube at a station of 103.19 cm. Foil placement techniques were identical to those in the tank axial traverse except that the polyfoam discs formed a press fit into a 1/2 length section of the aluminum traverse tube rather than an acrylic tube. For this reason the foil placement had to be measured before the tube was loaded rather than after. In order to do this the stack of polyfoam discs and of cardboard discs containing dosimeters was assembled and then compressed to the required length that it would have after loading into the tube. The dosimeter locations were then measured while the discs were compressed.

5.2.2.3 Circumferential Traverse Around Tank

Circumferential traverses were made on the tank surface at two stations (+82.07 cm and -40.64 cm), with dosimeters placed at a minimum spacing of 45 degrees. Sulfur dosimeters were taped directly to the tank surface. Other dosimeter types were first taped to pieces of lightweight cardboard which were then taped to the tank. Where both Dy and TLD dosimeters were to be placed at the same time on a given point, the bare dysprosium foil was placed on the exact point desired, the cadmium-covered dysprosium placed at 1.09 degrees (1.70 cm) greater azimuth, and the TLD's at 1.09 degrees lesser azimuth. Where sulfur and either bare dysprosium or TLD's were to be placed on the same point, the Dy or TLD's were placed at the exact point desired, and the sulfur at 1.65 degrees (2.58 cm) greater azimuth.

5.2.2.4 Axial on Tank Surface

In the high density polyethylene loading utilizing Shield Configuration 4B, two axial traverses were made on the surface of the tank at azimuths of 125 degrees and 215 degrees. Dy and TLD dosimeters were used. Foil placement techniques were similar to those for the circumferential traverses. The bare Dy foils were placed on the exact azimuth desired, the TLD's at 0.54 degrees (0.84 cm) greater azimuth and the Cd-covered Dy at 1.09 degrees greater azimuth than the bare Dy.

5.2.2.5 Traverses on Tank Hemisphere

A number of traverses were performed on the surface of the tank hemispherical bottom from the axis of the tank outward to its circumference. Except for the S pellets, dosimeters were taped to strips of lightweight cardboard before being taped to the tank. Where there was more than one type of foil being used simultaneously, the bare Dy or Au foil was taped to the exact point desired, the cadmium-covered Dy or Au foil to a greater azimuth, and the TLD at a lesser azimuth. Center-to-center spacing of the dosimeters was 1.5 cm. Figure 5-4 shows the relationship between radius and station number for the dosimetry position on the tank hemisphere.

5.3 PROPELLANT TANK POSITIONING

Care was expended to insure accurate positioning of the tank above the reactor and shield. A plumb bob suspended from the bottom center of the tank hemisphere was used to indicate the position of the tank axial centerline on the top of the shield. Because of the frequent movement of shield materials, the axial centerline of the reactor was located on top of the shield immediately prior to the final tank positioning. This positioning of the tank in this manner was found to be reproducible to ± 1.0 inch.

Angular positioning of the tank was determined by two rods; one clamped to the top of the FCX test stand on the south and the other fastened to the west wall. The latter rod was fixed for the entire series of runs but the former was removed and replaced as required for handling reasons. It was later determined that the angular position of the tank was slightly in error. However, it was decided not to correct this error but continue to reproduce the same position throughout the series of runs. In order to correct for this error, 5 degrees should be subtracted from the tank dosimetry angular positions. Hence, tank position 0 degrees corresponds to reactor position 5 degrees.

The tank was positioned (see frontispiece) so that the bottom of the tank hemisphere was at Reactor Station (164 ± 2) inches. This uncertainty was caused by the uncertainty in initial positioning as well as some tilting of the tank. The latter effect was caused by the shifting center of gravity resulting from the withdrawal of the traverse tubes.

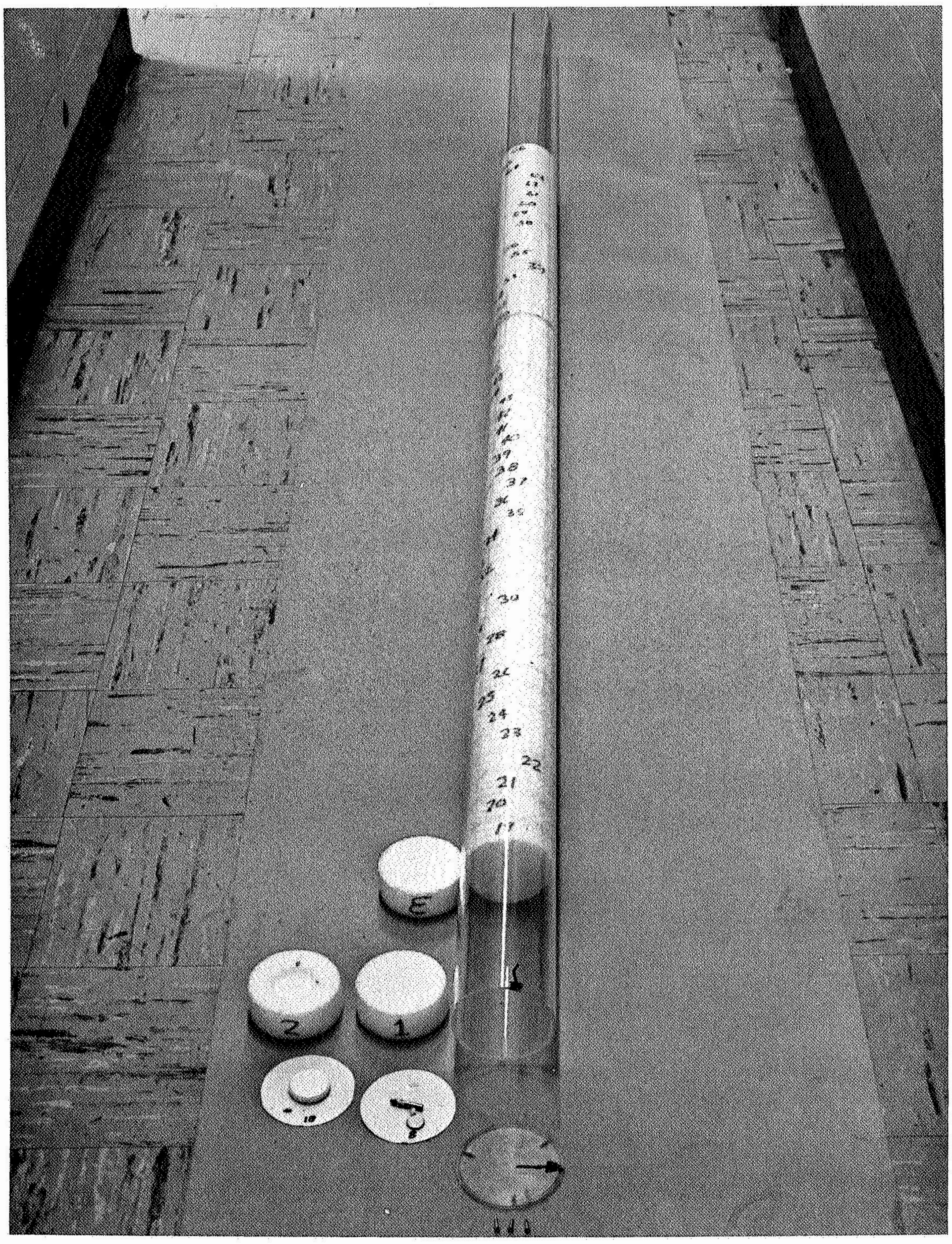

Figure 5-2. Axial Tube Passive Dosimetry Loading

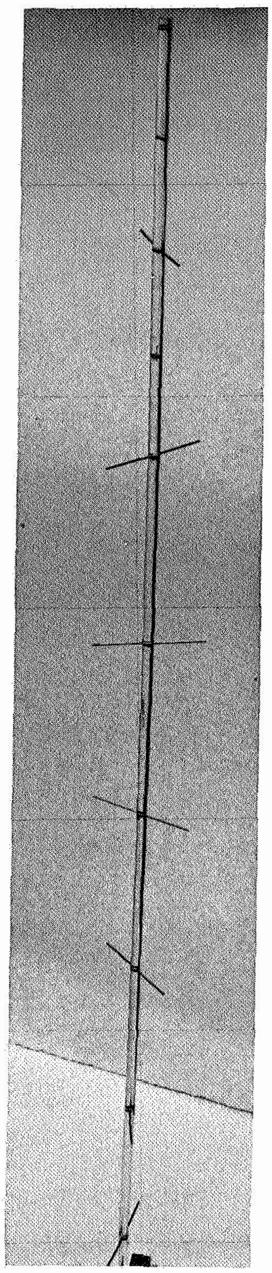

Figure 5-3. Passive Dosimetry Support Structure Used in the Axial Tube for the High Density Polyethylene

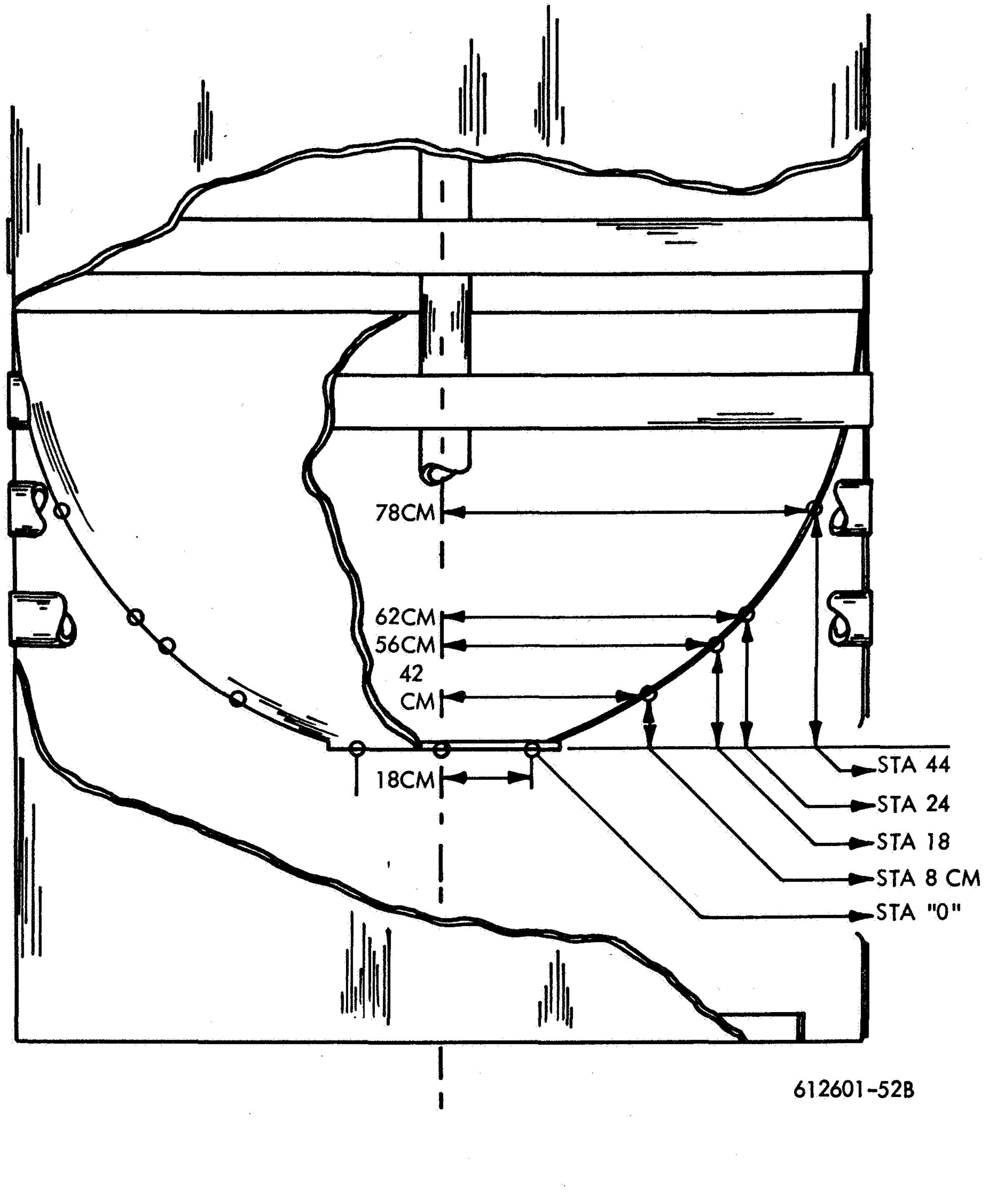

Figure 5-4. Distance Conversion Factors for Passive Dosimetry Loading in the Tank Hemisphere

It was greatly reduced during the last few runs by erecting a tank support structure above the reactor.

If the tank was initially vertical at the beginning of the test, the shifting center of gravity during withdrawal of the first tube would cause the remaining tubes to traverse under the influence of gravity. Thus, the lifting fixture turn-buckles were adjusted so that the bottom of the skirt at the 270 degree position of the tank was approximately 3 inches higher than in the 90 degree position when all three traverse tubes were reset. When the tubes were then withdrawn to their maximum distance, the tank axis was nearly vertical.

SECTION 6. EXPERIMENTAL RESULTS

This section presents the data taken during this experiment and gives a discussion of these data. Section 6.1 presents the results obtained with high density ($\rho = 0.59$ gm/cc) polyethylene used to simulate the neutron transport properties of liquid hydrogen. Section 6.2 presents the results using low density poly ($\rho = 0.14$ gm/cc) used to simulate the photon transport properties of liquid hydrogen. Neutron spectral data obtained with foil activation techniques at the surface of the propellant tank are discussed in Section 6.3. Section 6.4 discusses the measurement uncertainties. Section 6.5 contains calculations of the experimental heating rates.

A general description of the specific configurations is shown in Table 6-1. All data are presented on a per watt (of reactor power) basis. The Configuration 11 data for the respective high and low density polyethylene simulation is included in an effort to determine test cell background.

TABLE 6-1

GENERAL DESCRIPTION OF SHIELD-TANK CONFIGURATIONS

Shield Configuration	Shield Mass Thickness (gm/cm^2)	Total Mass Thickness* (gm/cm^2)	Polyethylene Density (gm/cc)	Simulation Property of LH_2
4B	0	59	0.59	Neutron Transport in LH_2
11	214	214	0.59	Neutron Transport in LH_2
11	214	214	0.14	Photon Transport in LH_2
7D	81	140	0.14	Photon Transport in LH_2

*Including support structure mockup.

6.1 MEASUREMENTS WITH HIGH DENSITY POLYETHYLENE IN TANK

The types of active dosimetry measurements performed with the high density polyethylene simulation in the propellant tank are described in Table 5-1 by runs 6, 7, 8 and 9. The types of passive dosimetry measurements which were made at the same time, are described in Table 5-2. The emphasis, as mentioned previously, was on obtaining neutron data (as opposed to gamma ray data) since the poly simulation was intended to more closely represent the neutron properties of liquid H_2. The fast neutron flux and dose rate measurements are presented in Section 6.1.1; the thermal neutron flux measurements are presented in Section 6.1.2. Some gamma dose rate measurements were also taken and are presented in Section 6.1.3

Standard conventions have been adhered to in reporting detector positions in that all positive positions on the tank hemisphere and in the traverse tubes referred to radii measured towards the test cell corner, i.e., towards $\theta = 90$ degrees, while the negative positions represent radii measured in the opposite direction, i.e., towards the center of the test cell ($\theta = 270$ degrees). All positive directions (stations) measured on the axial centerline and axially into the tank refer to elevations greater than the bottom of the tank hemisphere while negative directions refer to distances below the outside bottom of the tank hemisphere. A sketch of this coordinate reference system and an indication of the traverses taken is given in Figure 6-1.

6.1.1 Fast Neutron Measurements

Four different types of detectors were used to obtain fast neutron data. Two of these, a Hurst proportional counter and Phylatron solid-state dosimeters, measure fast neutron dose rate. The other two, a U-238 fast fission chamber and sulfur pellets, measure fast neutron threshold flux. Lack of sensitivity precluded the use of any U-238 fission foils and the use of the Plutonium-239 fission foil at any place except on the outside bottom of the tank on the hemisphere.

Plutonium data is presented in Section 6.3 where it is used to obtain spectral information.

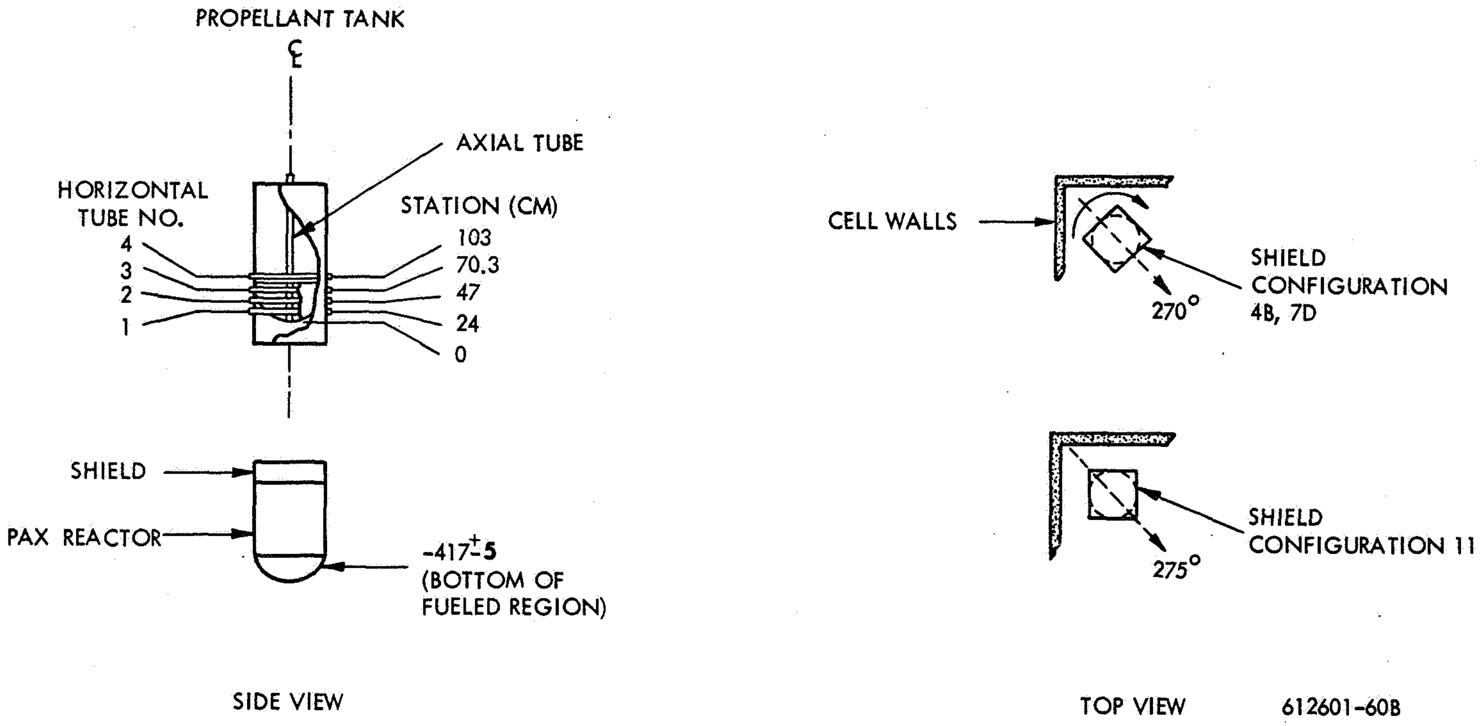

Figure 6-1. Reference Coordinate System

6.1.1.1 Fast Neutron Dose Rate as Measured with a Hurst Detector

The Hurst detector was the primary data acquisition instrument for fast neutron dose rate data. The data obtained with the Hurst detector for Shield Configuration 4B with the high density polyethylene in the tank are shown in Figure 6-2 for all four traverse tubes. Traverse Tube 4 is within a few centimeters of the top of the polyethylene. Thus, measurements in this tube were largely affected by test cell background and the non-uniformity of the polyethylene top surface. Figure 6-3 gives the Hurst fast neutron dose rate for Shield Configuration 11. Traverses were obtained only for Tubes 2 and 3 because of the problems experienced in Tube 4 for Configuration 4B. It should be noted that for both Configuration 4B and 11, the dose rate is higher at the outside of the tank towards the test cell corner. Figure 6-4 contains a comparison of the fast neutron dose rate in traverse Tube 2 for Shield Configurations 11 and 4B. The difference between these two curves, which should represent the "direct" contribution in a space environment, is also shown. Thus, Figure 6-5 gives the direct fast neutron dose rate for Tubes 1, 2 and 3 in the manner discussed above. Although no Hurst data was available in Tube 1 to obtain background, it is felt that the ratio of the background to the direct for this particular tube is very small because of the short attenuation distance into the poly. The extra point included in this curve was obtained with a Hurst detector at essentially the location of the bottom of the hemisphere on the tank axial centerline. It should be noted that the agreement between this point and the Traverse 1 data at locations external to the tank is quite good. The steep gradients near the tank wall in the direction toward the test cell corner caused some difficulty in defining the curves in this region. Hence, the curves that apply to these areas are shown dotted in Figure 6-5.

6.1.1.2 Fast Neutron Dose as Measured with Phylatrons

One point was obtained at essentially the bottom of the tank hemisphere using Phylatron dosimeters. The fast neutron dose rate, as measured with this device, amounted to 16.3 ± 4.0 mrads (tissue)/hr/watt. A corresponding number measured by the Hurst detector is 12 ± 1 mrads (tissue)/hr/watt.

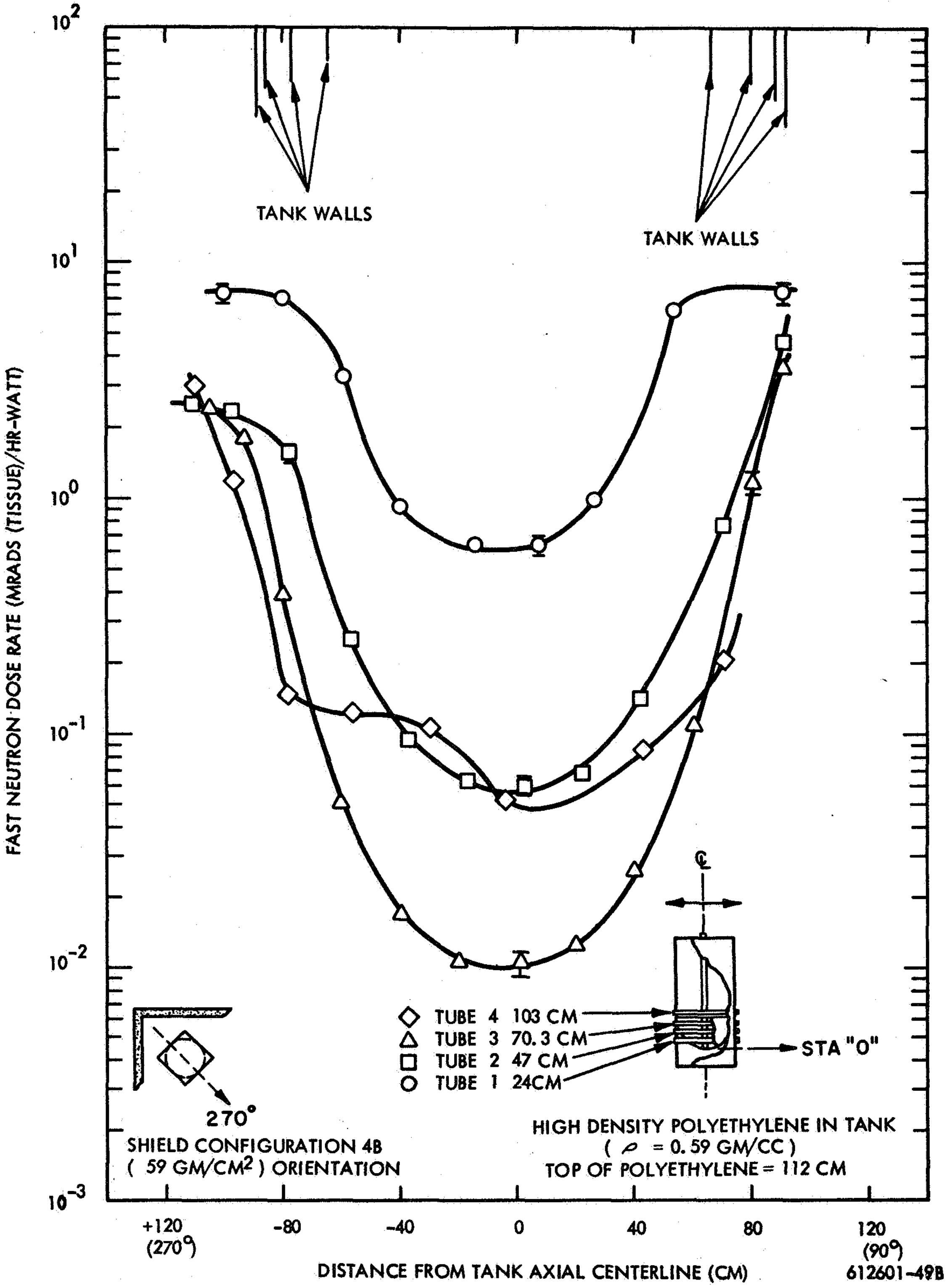

Figure 6-2. Fast Neutron Dose Rate as Measured with a Hurst Detector vs Distance from Tank Axial Centerline

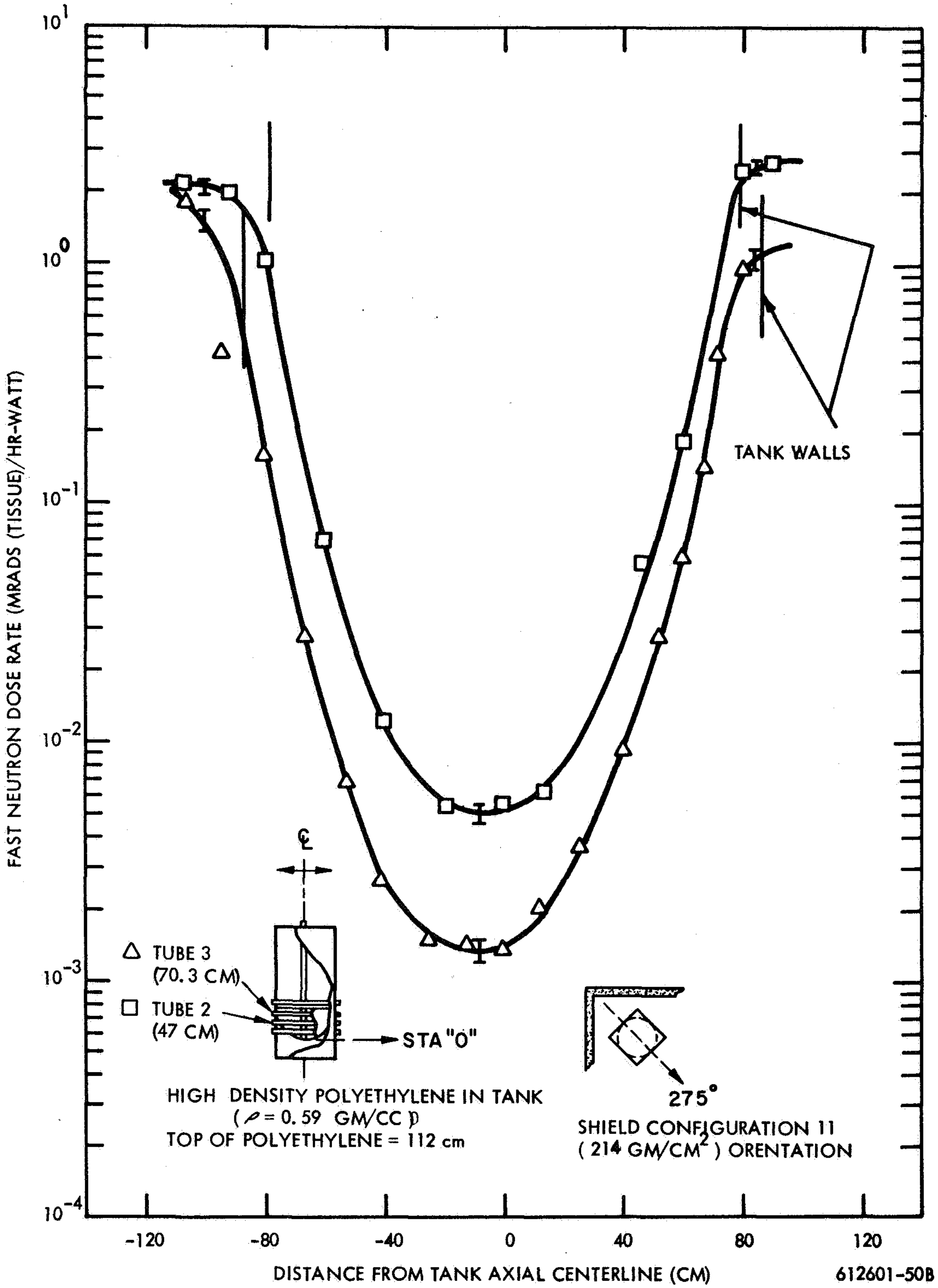

Figure 6-3. Fast Neutron Dose Rate as Measured with a Hurst Detector vs Distance from Tank Axial Centerline

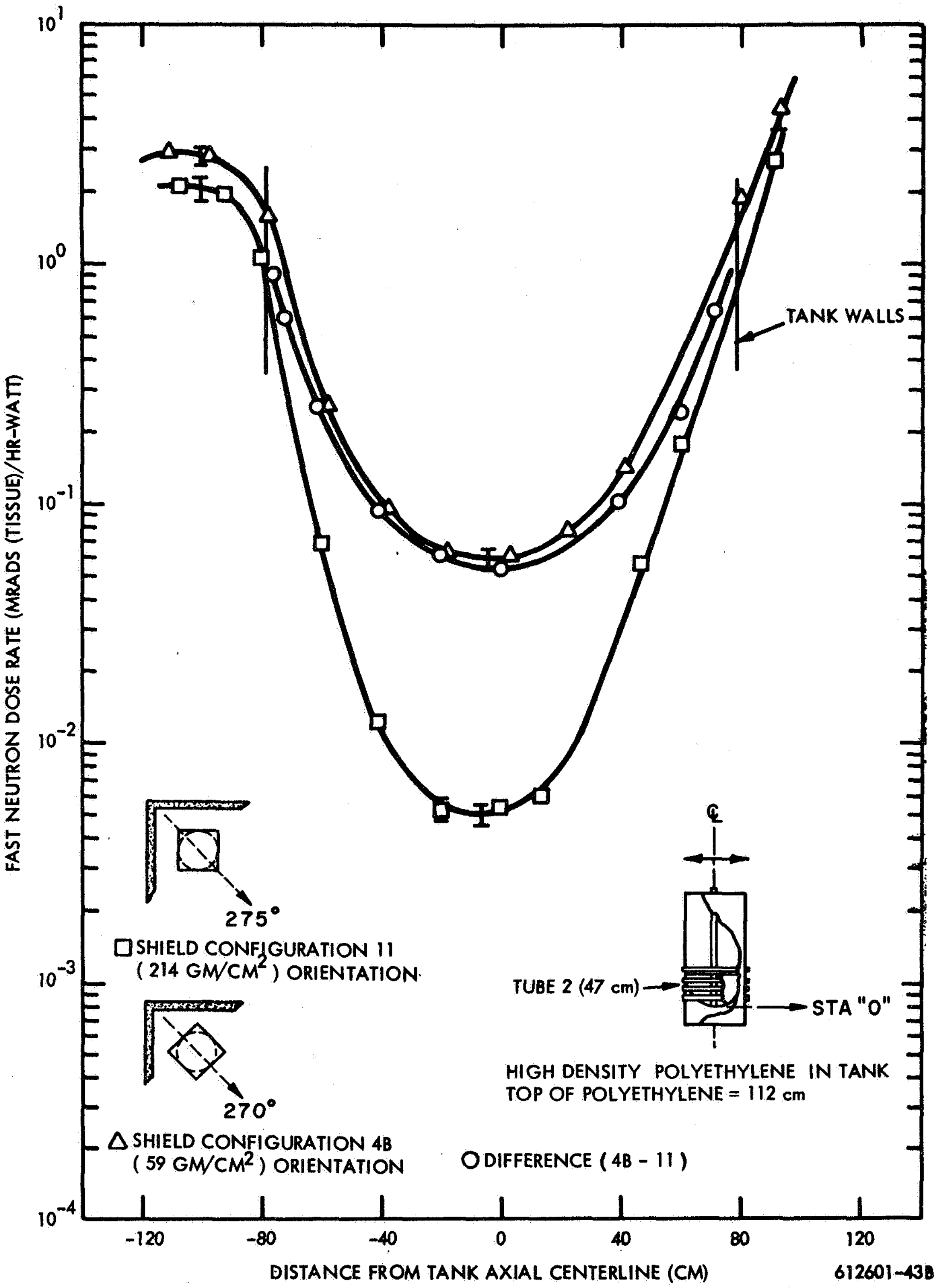

Figure 6-4. Fast Neutron Dose Rate as Measured with a Hurst Detector vs Distance from Tank Axial Centerline (Tube 2)

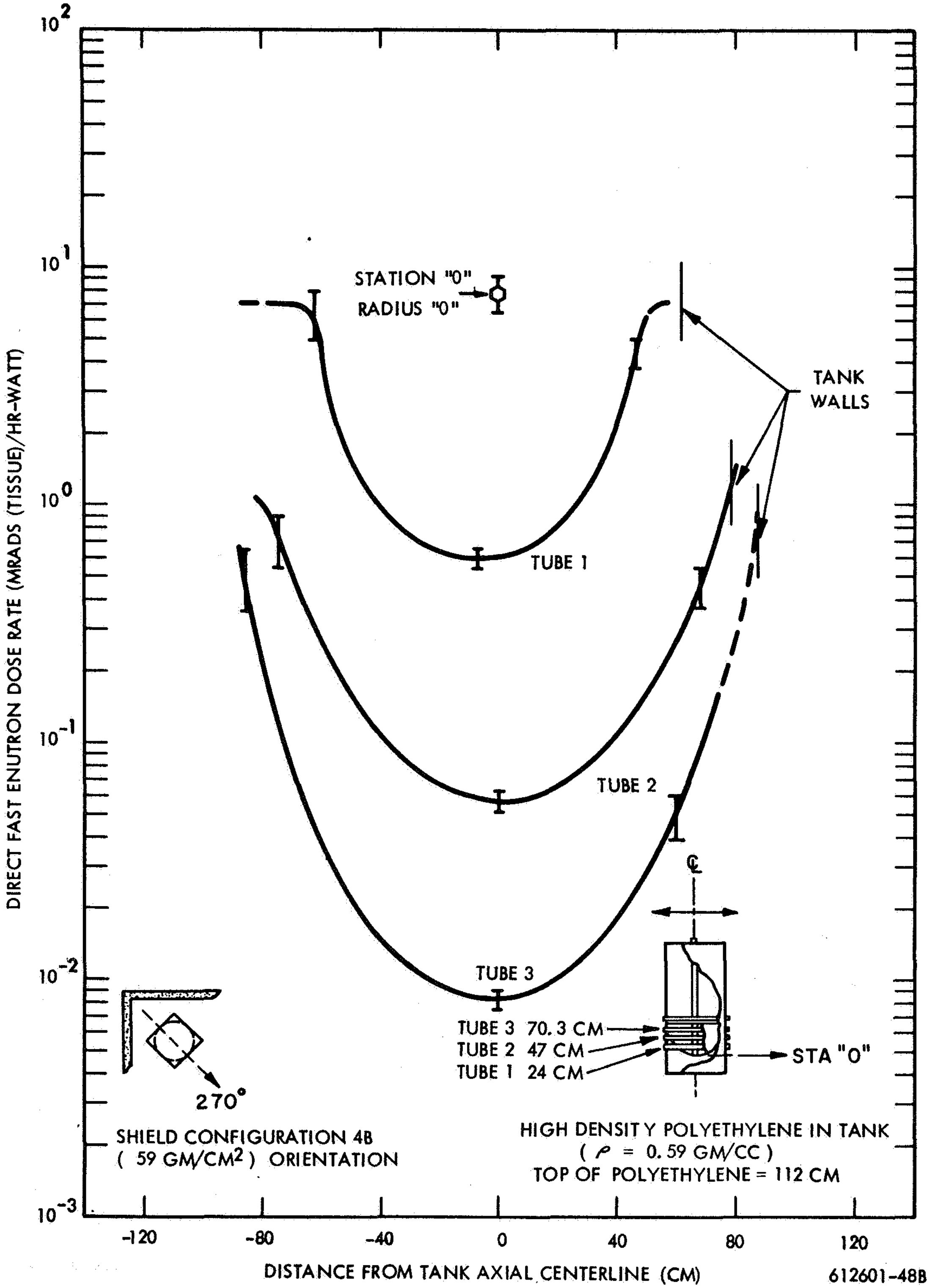

Figure 6-5. Direct Fast Neutron Dose Rate as Measured with a Hurst Detector vs Distance from Tank Axial Centerline

6.1.1.3 Fast Neutron Flux (E > 1.5 Mev) as Measured with the WX-30748 U-238 Fast Fission Chamber

The data obtained during the traverses in Tubes 1, 2 and 3 for Shield Configuration 4B and in Tube 1 for Shield Configuration 11 are shown in Figure 6-6. Again, it should be noted that the flux at the outside of the tank, as measured in the positive direction, is greater than the value at a corresponding distance in a negative direction. Upon inspection of these curves, it is noted that they do not decrease nearly as greatly as do the Hurst data as one goes from the outside of the tank into the center. This is felt to be partially due to the great length of the detector sensitive volume, i.e., 6 inches, partially due to "streaming" of thermal neutrons through the cable connector, and possibly due to photofissions in the U-238.

Upon inspection of Figure 6-6, it is also apparent that a certain degree of asymmetry is evident about the axial centerline. In Section 3.6.3, it was mentioned that the fast fission detector was first wrapped with 20-mil cadmium and then encased in two layers of Boral, each 1/8 inch thick. However, this cadmium and Boral covering had a substantial hole (about 3/4 inch in diameter) for the electrical connections. Thus, a substantial penetration existed which allowed the entrance of thermal neutrons. Thus, each of the fast fission curves presented in Figure 6-6 is believed to be a composite of three individual effects. The first is the desired fast neutron flux curve, e.g., that flux above 1.5 Mev. The second effect is due to thermal neutron streaming. The third effect is postulated to be produced by high energy gammas which cause photofission in the U-238. It should be noted that the thermal neutron population, which is being sampled, occurs near the hole in the covering approximately 13 cm (in the 270 degree direction) away from the detector center. Thus, it is possible for a point on a curve to be slightly higher for the negative distance than for the point on the curve corresponding to the same positive distance. A close examination of the data supports this conclusion, except in the case of Tube 1 for Shield Configuration 11. It is felt for this case, however, that direct streaming from outside becomes more important or that somehow a void may have occurred somewhere in the traverse tube in the polyethylene just behind the detector.

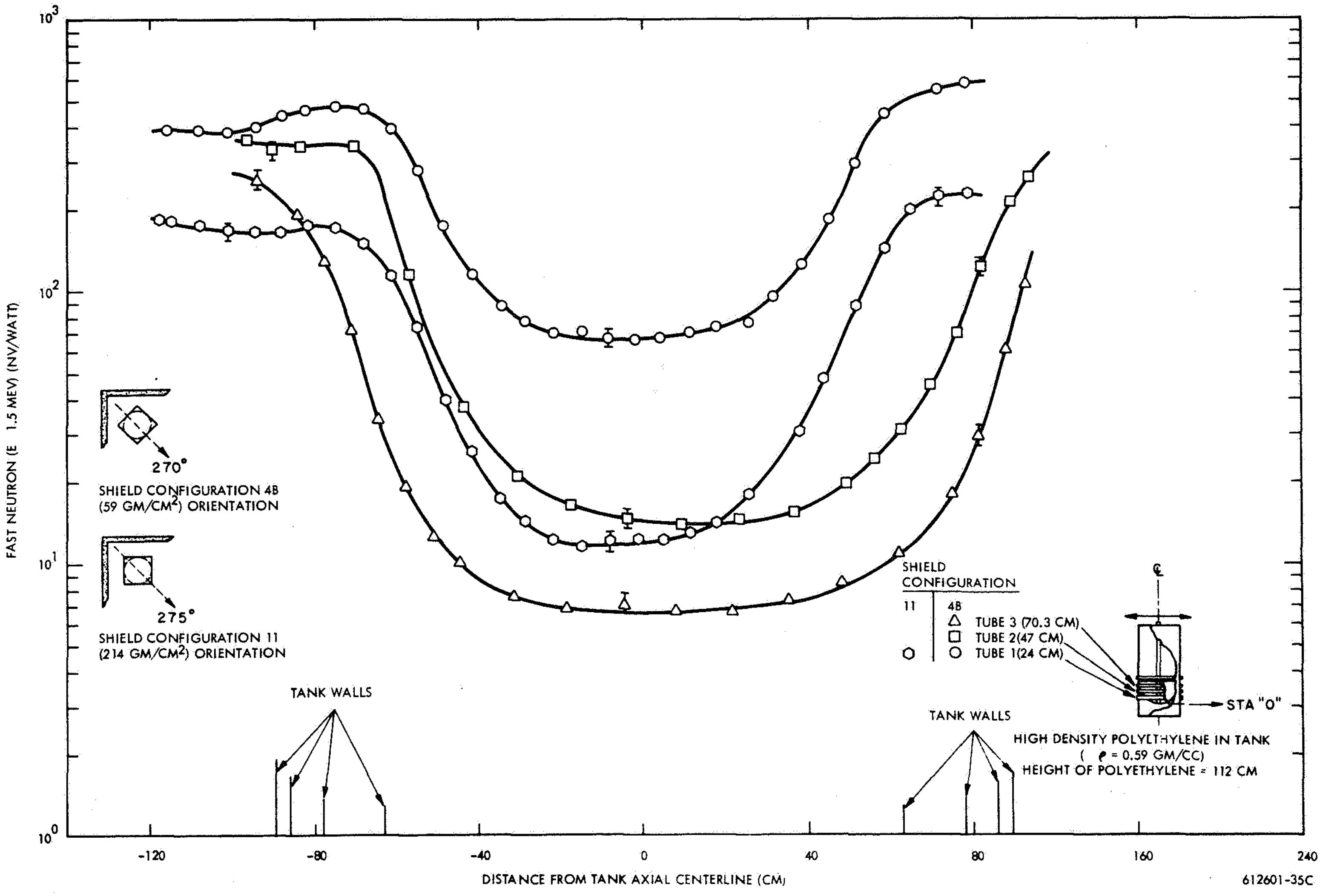

Figure 6-6. Fast Neutron (E > 1.5 Mev) Flux as Measured with a WX-30748 Fast Fission Chamber vs Distance from Tank Axial Centerline

6.1.1.4 Fast Neutron Flux as Measured with Sulfur (E > 2.9 Mev)

Figure 6-7 presents the fast neutron flux as obtained by sulfur pellets vs axial distance into the tank. It should be noted that the flux first decreases rapidly for the first 60 cm or so and then sharply increases from 108 to 123 cm. Since the high density poly only extended to a height of approximately 112 cm, the last two points were actually above the poly and the point at 108 cm was barely below the surface. Thus, the last two points effectively measured the test cell background and the point at 108 cm was influenced by this background.

Figure 6-8 gives the fast neutron flux as measured with sulfur pellets versus radial distance from the tank axial centerline on the tank hemisphere. Figure 6-9 shows the fast neutron flux as measured with sulfur pellets vs azimuth for two different stations on the tank external skin. Of particular interest is the data for Station 82.07 cm. This curve appears to have a peak around 135 degrees or in the direction approximately perpendicular to the north wall. Unfortunately, this curve is comprised of only 4 points and so precise definition is not available.

One possible explanation for the large fast neutron flux at the upper surface of the polyethylene as well as the increase in fast neutron flux measured around the circumference of the tank at Station 82.07 cm at an azimuth of 135 degrees is a source of fast neutrons produced in the fuel storage racks located on the test cell shelf. This source would be generated by the large thermal neutron background of the test cell causing fissions in the stored fuel.

No significant increase occurs in the sulfur data measured around the azimuth at Station - 40.64 cm which is located well below the upper shelf and is thus shielded by the edge of the shelf.

6.1.1.5 A Comparison of the Fast Neutron Results

Figure 6-10 contains the axial centerline attenuation curves for the Hurst proportional counter, the sulfur pellets, and the U-238 fast fission chamber. Additionally, the single point is noted at the surface of the tank hemisphere for the Phylatron dosimeter.

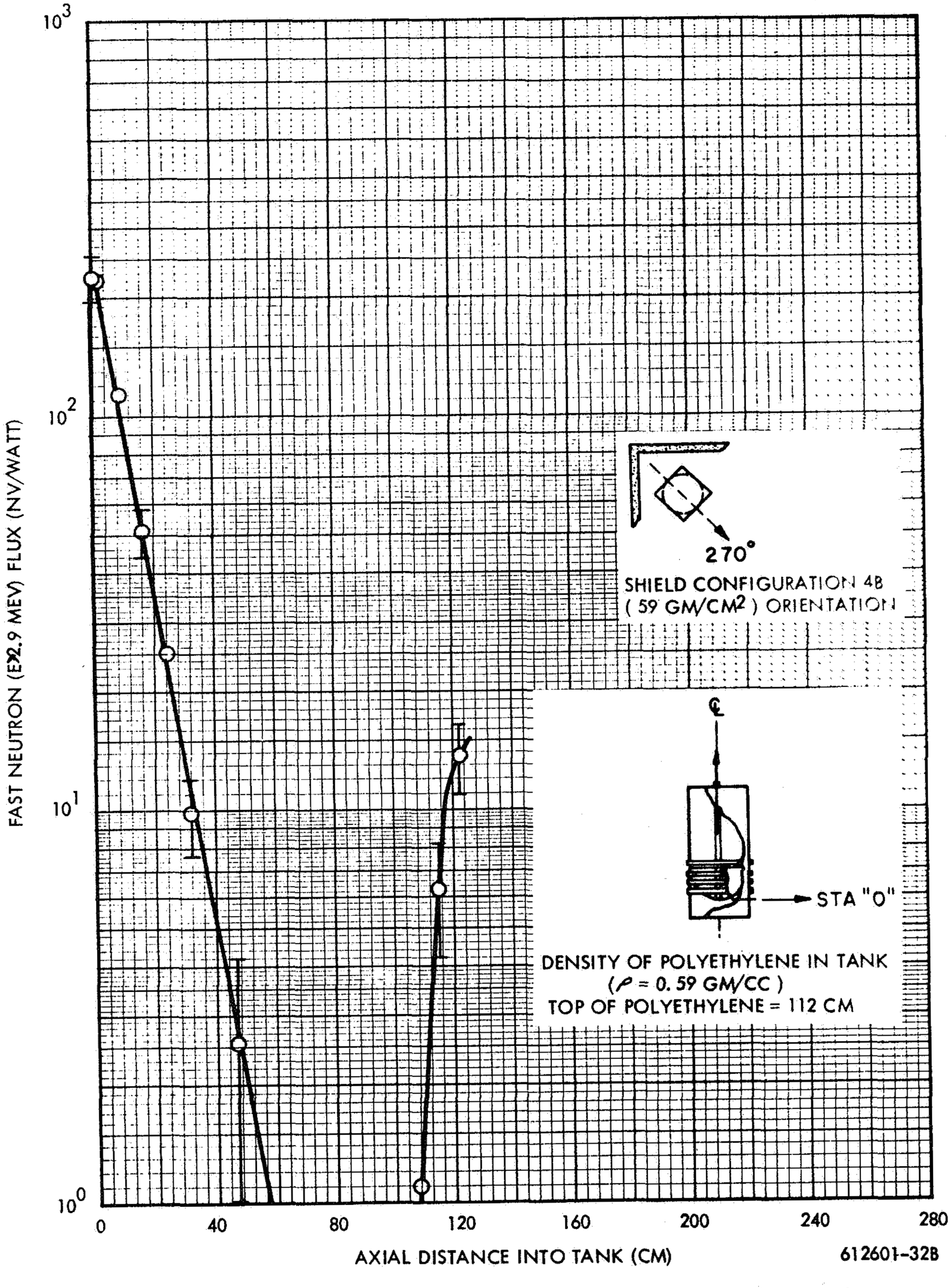

Figure 6-7. Fast Neutron (E > 2.9 Mev) Flux as Measured with Sulfur Pellets vs Axial Distance into Tank

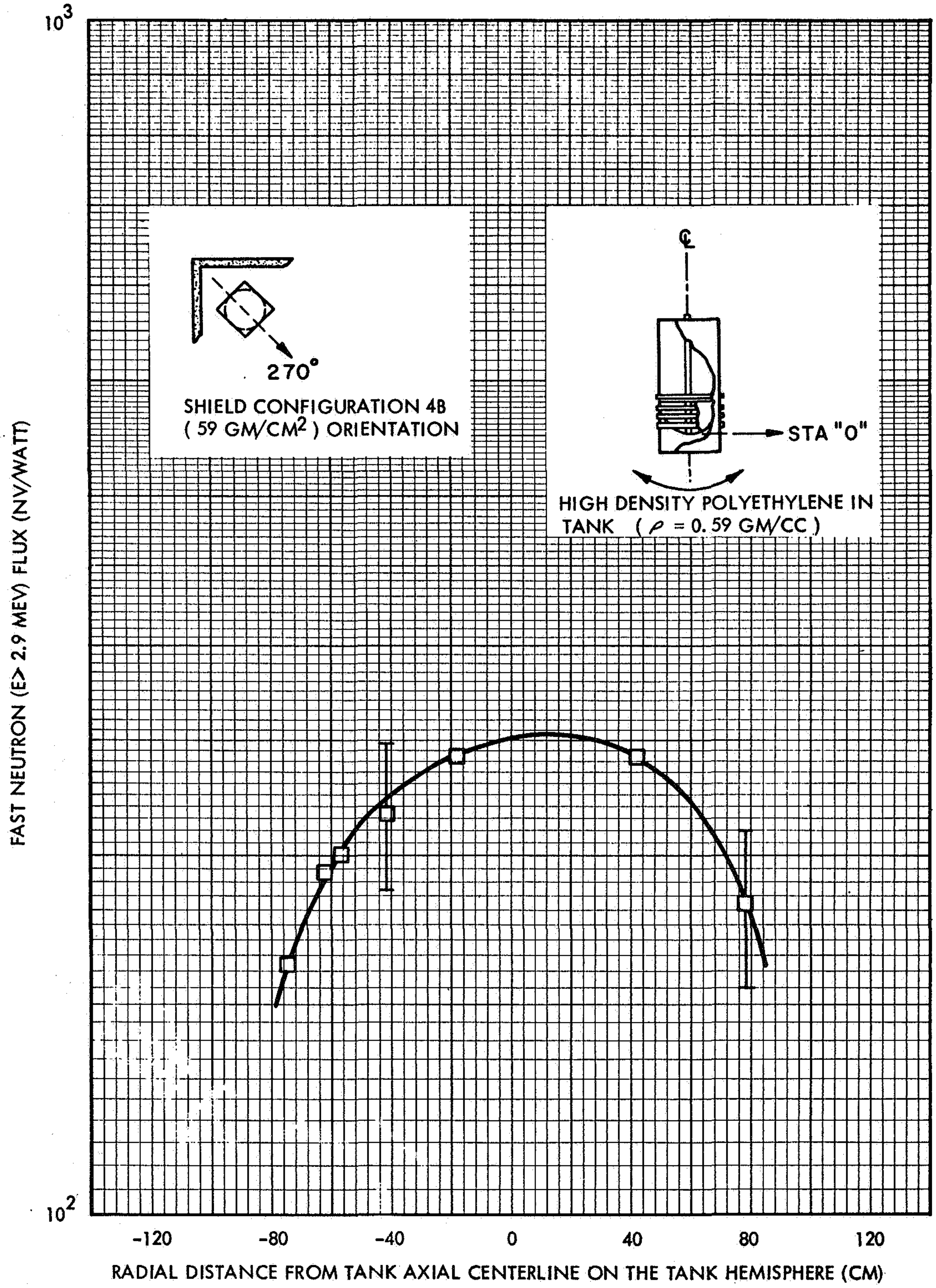

Figure 6-8. Fast Neutron (E > 2.9 Mev) Flux as Measured with Sulfur Pellets vs Radial Distance from the Tank Centerline on the Tank Hemisphere

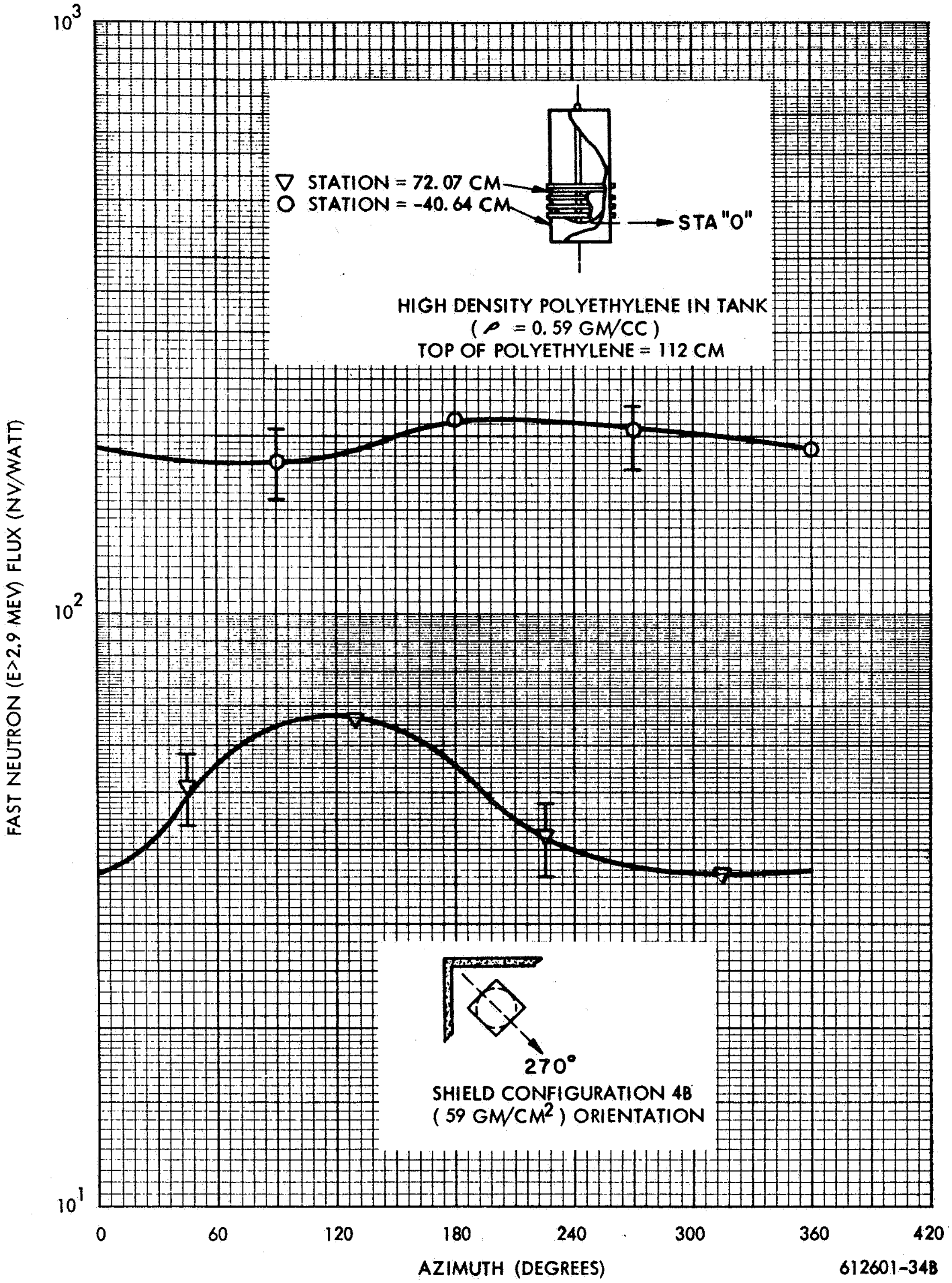

Figure 6-9. Fast Neutron (E > 2.9 Mev) Flux as Measured with Sulfur Pellets vs Azimuth on Tank External Skin

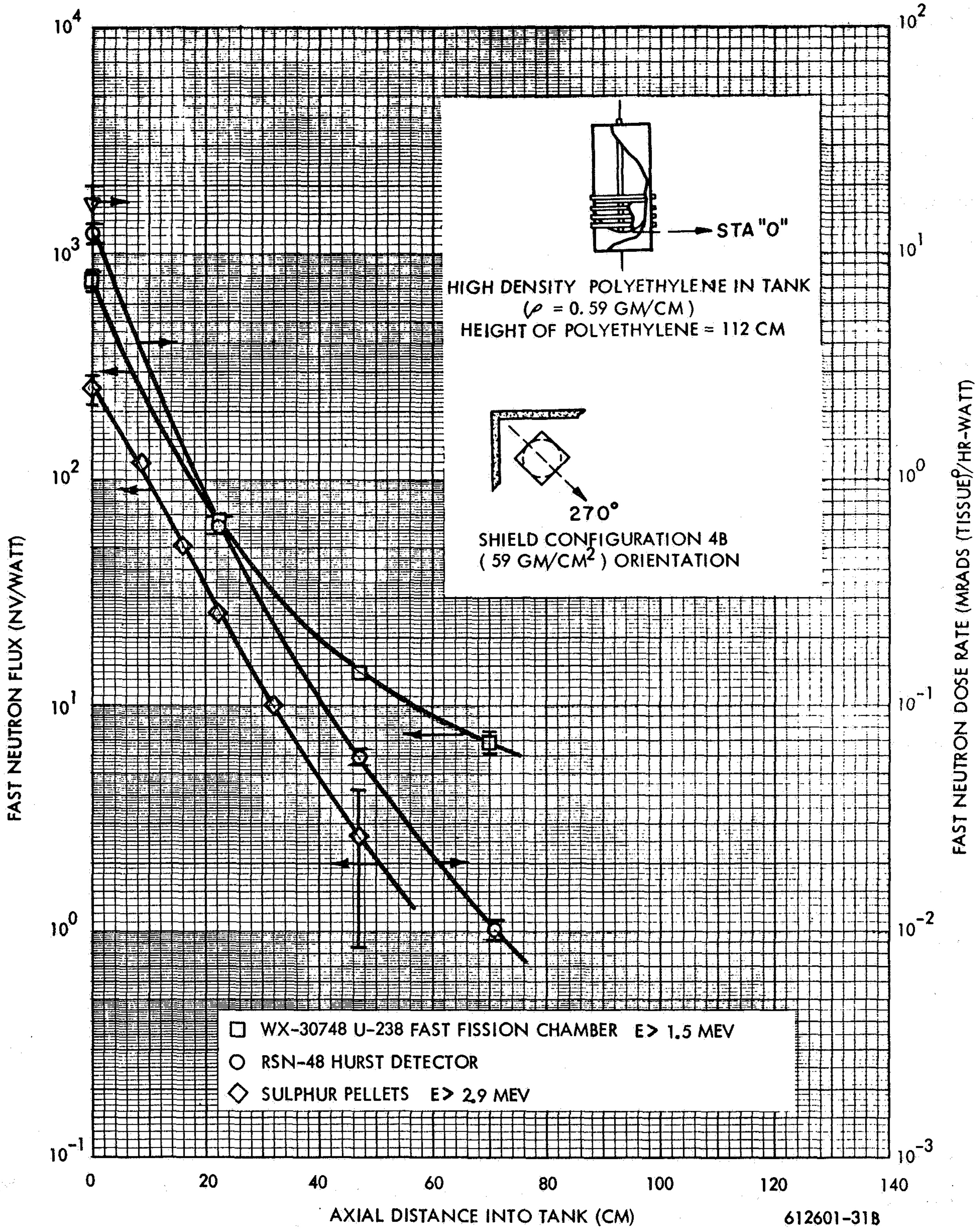

Figure 6-10. Fast Neutron Flux and Dose vs Axial Distance into Tank

Of primary interest are the curves from the fast neutron flux and the Hurst detectors; as may be seen upon inspection of the figure, they are practically parallel. The fast fission chamber data appears to be in good agreement for at least the first two data points. The data at 47 and 70 cm appears to be higher than would be expected based on the Hurst and sulfur data. However, if one subtracts a number proportional to the relative gamma dose rate at these last two positions, much better agreement is obtained, again suggesting a significant number of photofission reactions occurring in the fast fission chamber.

A rough calculation of the order of magnitude of the photo fission effect indicates that it could be of the order of the desired fast fission response if the gamma spectra were hard enough, i.e., if most of the gamma dose rate came from gammas with energies greater than 6 Mev. This is because the photo fission cross-section threshold is about 5.5 Mev.

6.1.2 Thermal Neutron Flux Measurements

Thermal neutron flux measurements were performed with both active and passive detection techniques to provide data for calculating material activation source strengths and to permit better understanding of the fast neutron and the gamma ray dose rate enivornment. The WX-5362 boron-lined compensated ion chamber was utilized to measure fluxes within the propellant tank, while dysprosium foils were utilized both in the tank and on the surfaces of the propellant tank for both Shield Configurations 4 B and 11.

6.1.2.1 Thermal Neutron Flux Measured with a Boron-Lined Compensated Ion Chamber

The thermal neutron flux, as measured by a compensated ion chamber as a function of distance from the tank axial centerline for various heights is shown in Figures 6-11 and 6-12. The first figure represents the response obtained with Shield Configuration 4B and includes the response of the detector to both the direct radiation through the shield and that of the test cell environment. Figure 6-12 represents the response with Shield Configuration 11 which considerably reduces the direct neutrons from the reactor. The curves show a characteristic decrease in flux level from the sides of the tank to the centerline. Except for the measurement through Tube 4, the flux also decreases as a function of the station of the traverse tube.

The direct thermal flux with Shield Configuration 4B is obtained by subtracting the data obtained with Configuration 11 from that obtained with Configuration 4B. This data is plotted in Figure 6-13 for traverses in Tubes 2 and 3. Comparable data for the other tubes was not obtained. Because of detector positioning requirements, the distance traversed was not the same in all cases. This was a result of the requirement that two detectors be placed in the same traverse tube as well as the limited distance obtainable with the traverse tube withdrawal mechanism. However, subtractions have been performed where comparable data exists. As indicated by the fairly smooth curve through the centerline, the subtraction process gives a fairly significant difference between 4B and 11. In this region, it is felt that the thermal flux in the tank is fairly well defined in these experiments. Out at the walls of the tank the data becomes more scattered, which is due to the fact that the data obtained there with Configuration 11 was comparable to that obtained with Configuration 4B.

6.1.2.2. Thermal Neutron Flux Measurements with Dysprosium Foils

Thermal flux measurements were also obtained with dysprosium foils both in and on the tank. Figure 6-14 shows the thermal flux as measured by dysprosium vs the axial distance into the tank along the tank centerline. Both bare dysprosium and cadmium-covered dysprosium results are shown for Shield Configuration 4B and 11. The bare and cadmium-covered foil fluxes fall off smoothly with axial distance into the tank, reach a minimum between 60 and 80 cm and then rise rapidly again towards the top of the polyethylene which is approximately 112 cm. This effect at the top of the tank was observed for the Boron-lined compensated ion chamber results and is presumably due to the high cell background above the polyethylene. Also, plotted on this figure are the compensated ion chamber results extracted from Figure 6-11. The ion chamber results are similar to the bare dysprosium results.

Dysprosium measurements were obtained on the bottom hemisphere of the tank in the direction of the 90 - 270 degree azimuth. Figure 6-15 is a plot of the bare and cadmium foil results as a function of the radial distance from the axial centerline. Note that for radii greater than 0, there is a corresponding increasing axial position above Station 0. The data is somewhat asymmetric with respect to the centerline with the data being higher in the positive direction. This is in the direction towards the corner of the test cell walls and presumably in

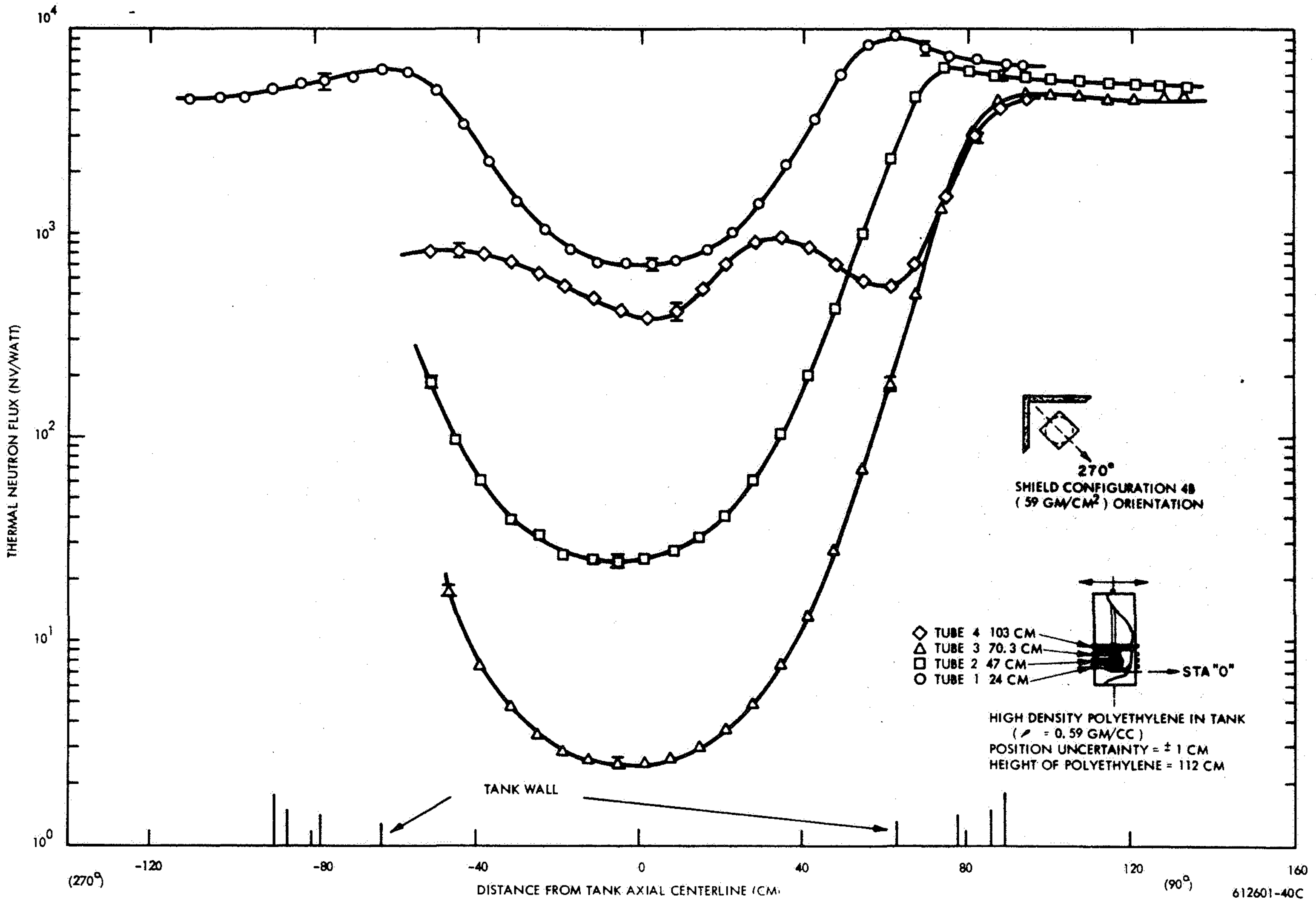

Figure 6-11. Thermal Neutron Flux as Measured with a WX-5362 Boron-Lined Compensated Ion Chamber vs Distance from Tank Axial Centerline

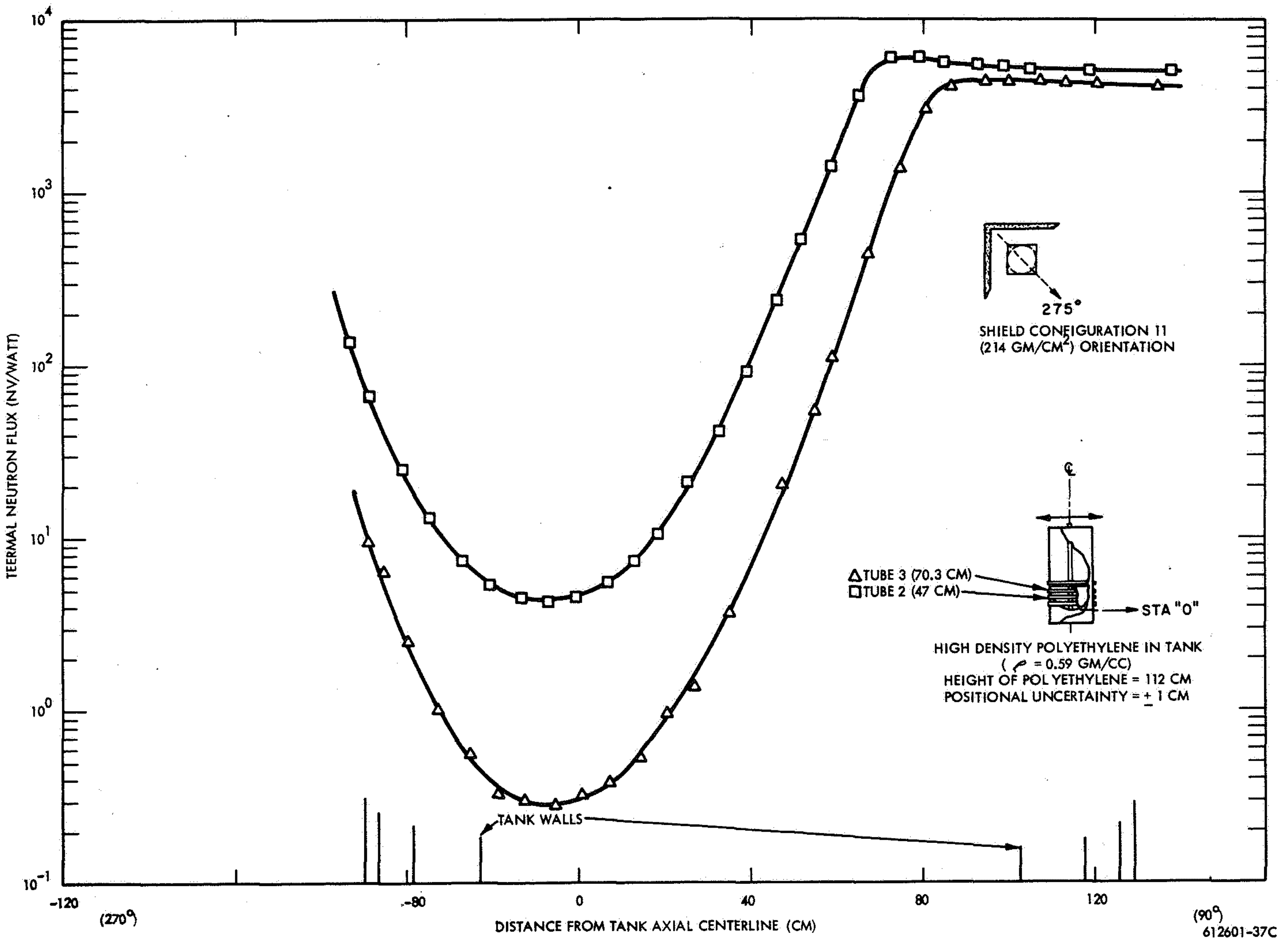

Figure 6-12. Thermal Neutron Flux as Measured with a WX-5362 Boron-Lined Compensated Ion Chamber vs Distance from Axial Centerline of Tank

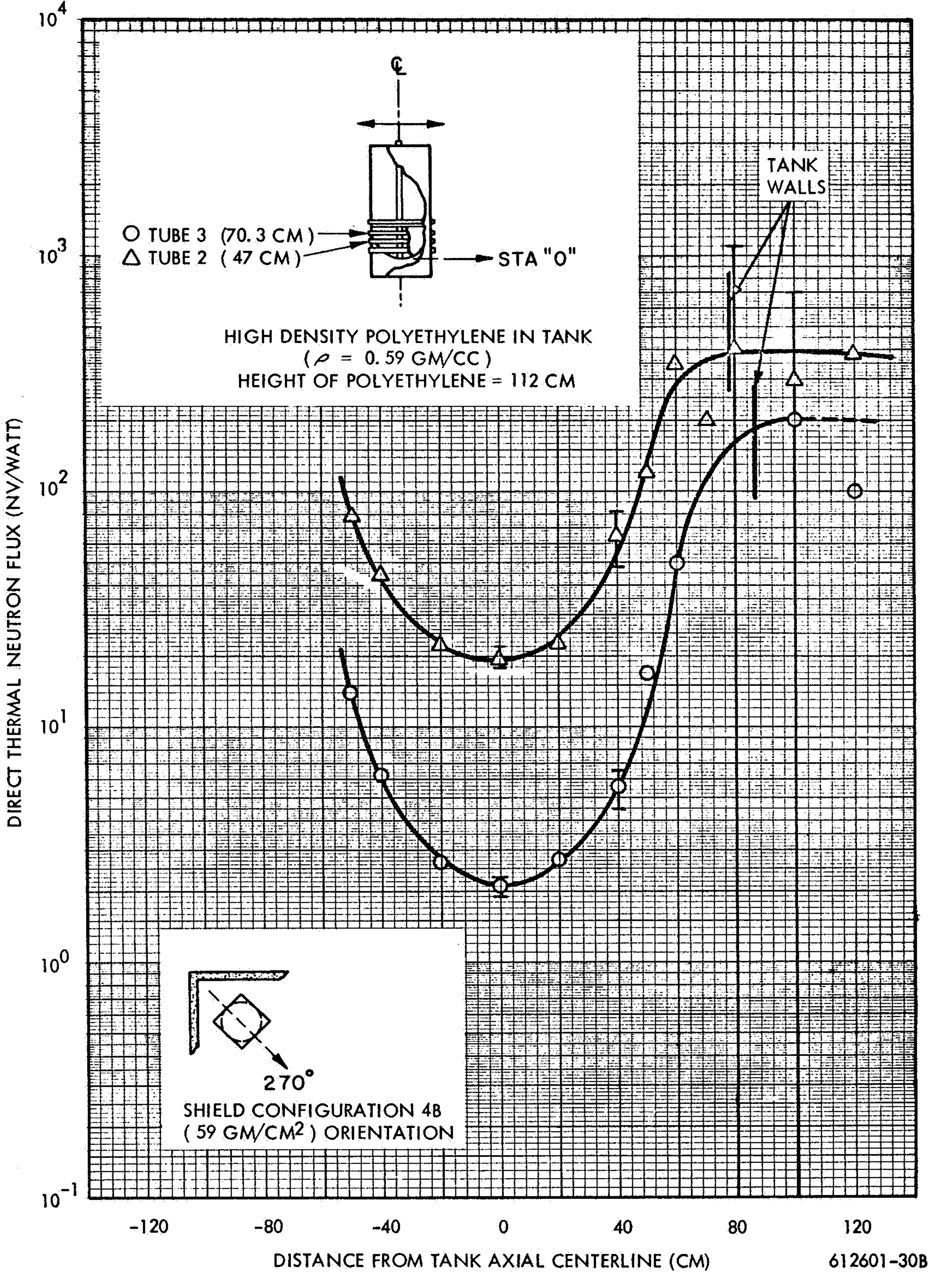

Figure 6-13. Direct Thermal Neutron Flux as Measured with a WX-5362 Boron-Lined Compensated Ion Chamber vs Distance from Tank Axial Centerline

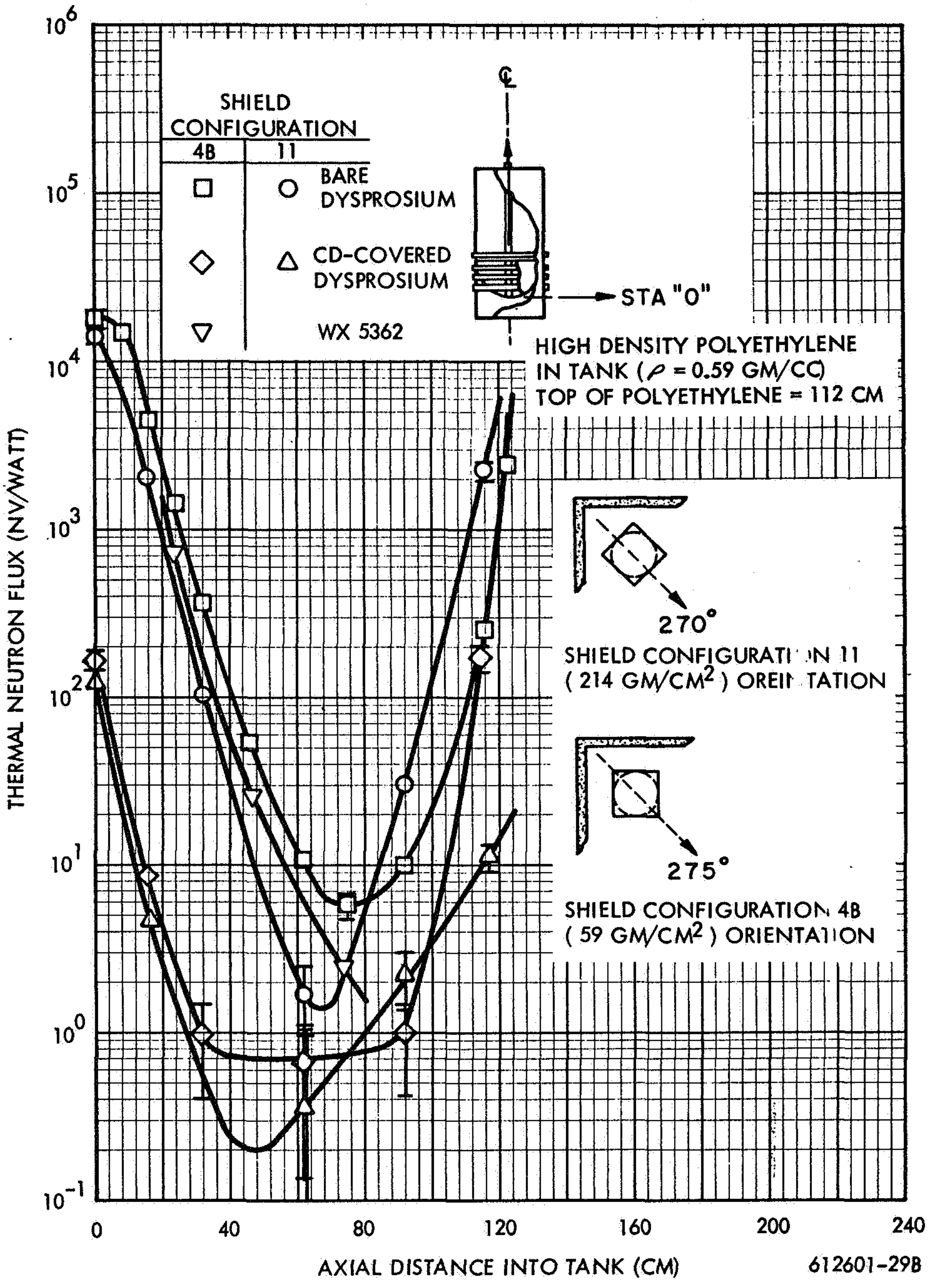

Figure 6-14. Thermal Neutron Flux as Measured vs Axial Distance into Tank

this case, the increase is due to the presence of a significant amount of test cell background.

Dysprosium measurements of the thermal neutron flux on the surface of the tank as a function of axial position were obtained and the results are plotted in Figure 6-16. Foils were irradiated at two azimuthal locations from the bottom of the skirt at Station - 40 cm to 244 cm. Both bare and cadmium-covered foils were utilized. The thermal fluxes measured on the surface do not fall off with distance as rapidly as the measurements made in the tank, as shown in Figure 6-14. Here again, the test cell background is the governing source for the thermal flux on the surface of the tank. It can be seen that the measurements made at the azimuthal position of 315 degrees for both the bare and cadmium-covered foils are slightly but systematically higher than the data obtained at the azimuth of 225 degrees. It is believed that the reason for this is the slightly closer proximity of the west wall compared to the north wall. The centerline is approximately 9 feet 2 inches from the north wall, while it is only 8 feet 2 inches from the west wall. The west wall is in the direction of approximately 45 degrees and the north wall, in the 135 degree direction. Uncertainties on the bare and cadmium-covered foil results are approximately ± 13 and ± 14 percent, respectively.

Measurements of the thermal neutron flux on the tank surface as a function of azimuthal angle exhibits a scalloped behavior which is most likely due to test cell radiation environment. Figure 6-17 shows the flux as measured by bare and cadmium-covered dysprosium foils with Shield Configuration 4B. The bare foil data at two stations show a pronounced peaking at 90 degrees and a depression at 270 degrees as would be expected if the cell walls were contributing a sizable neutron flux to the walls of the tank. Figure 6-18-1 shows similar results with Configuration 11. The cadmium-covered foil data indicates some scalloping but not as extensive as the bare data. Uncertainties in these data are approximately ± 13 percent.

6.1.2.3 A Comparison of the Thermal Neutron Results

Figure 6-18-2 contains the axial centerline thermal neutron fluxes as measured by the WX-5362 and bare and cadmium-covered dysprosium foils. The WX-5362 and bare dysprosium foil results have approximately the same attenuation behavior. Their slope is

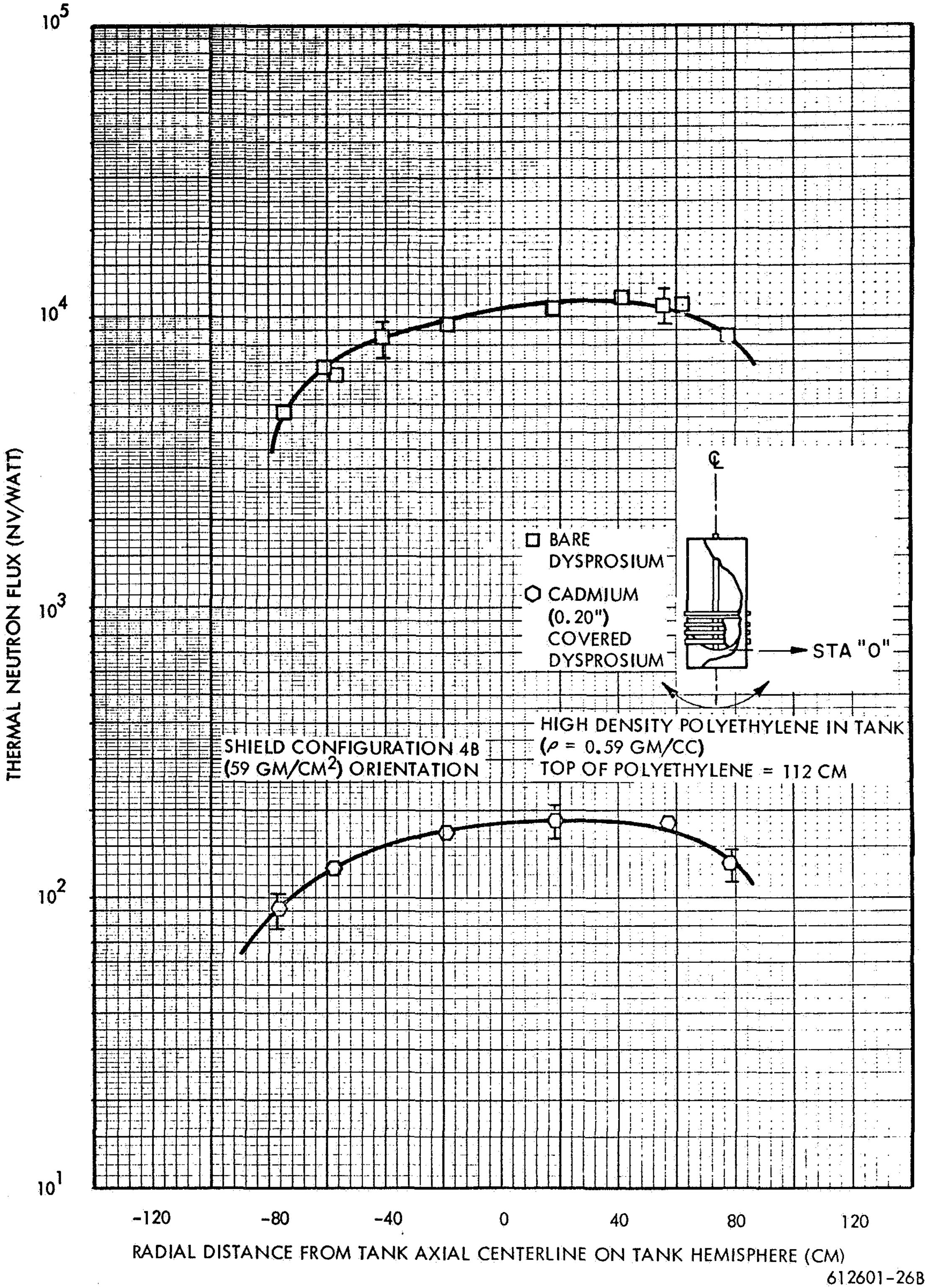

Figure 6-15. Neutron Flux as Measured with Dysprosium vs Radial Distance from Tank Axial Centerline on Tank Hemisphere

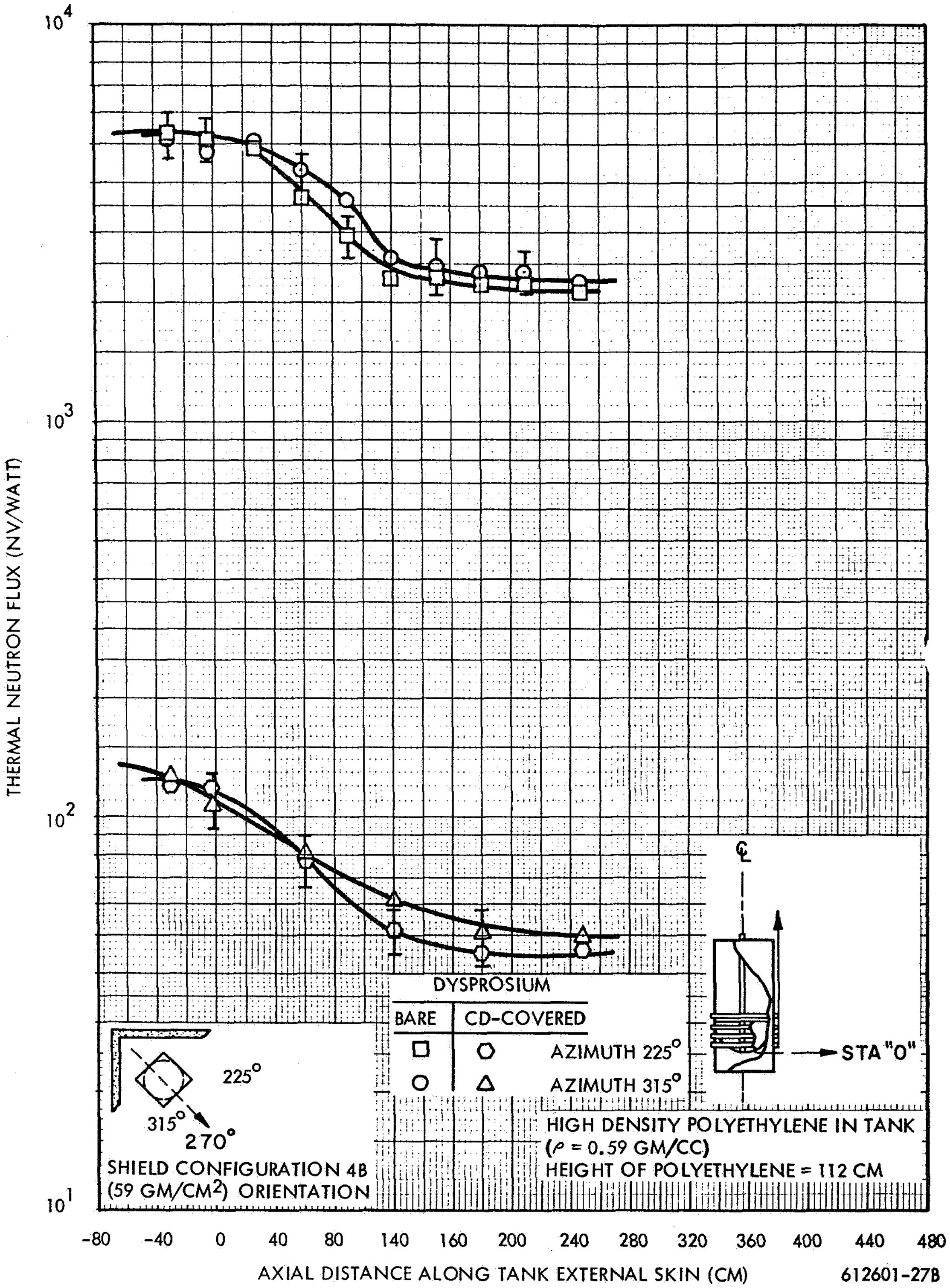

Figure 6-16. Thermal Neutron Flux as Measured with Dysprosium vs Axial Distance Along Tank External Skin

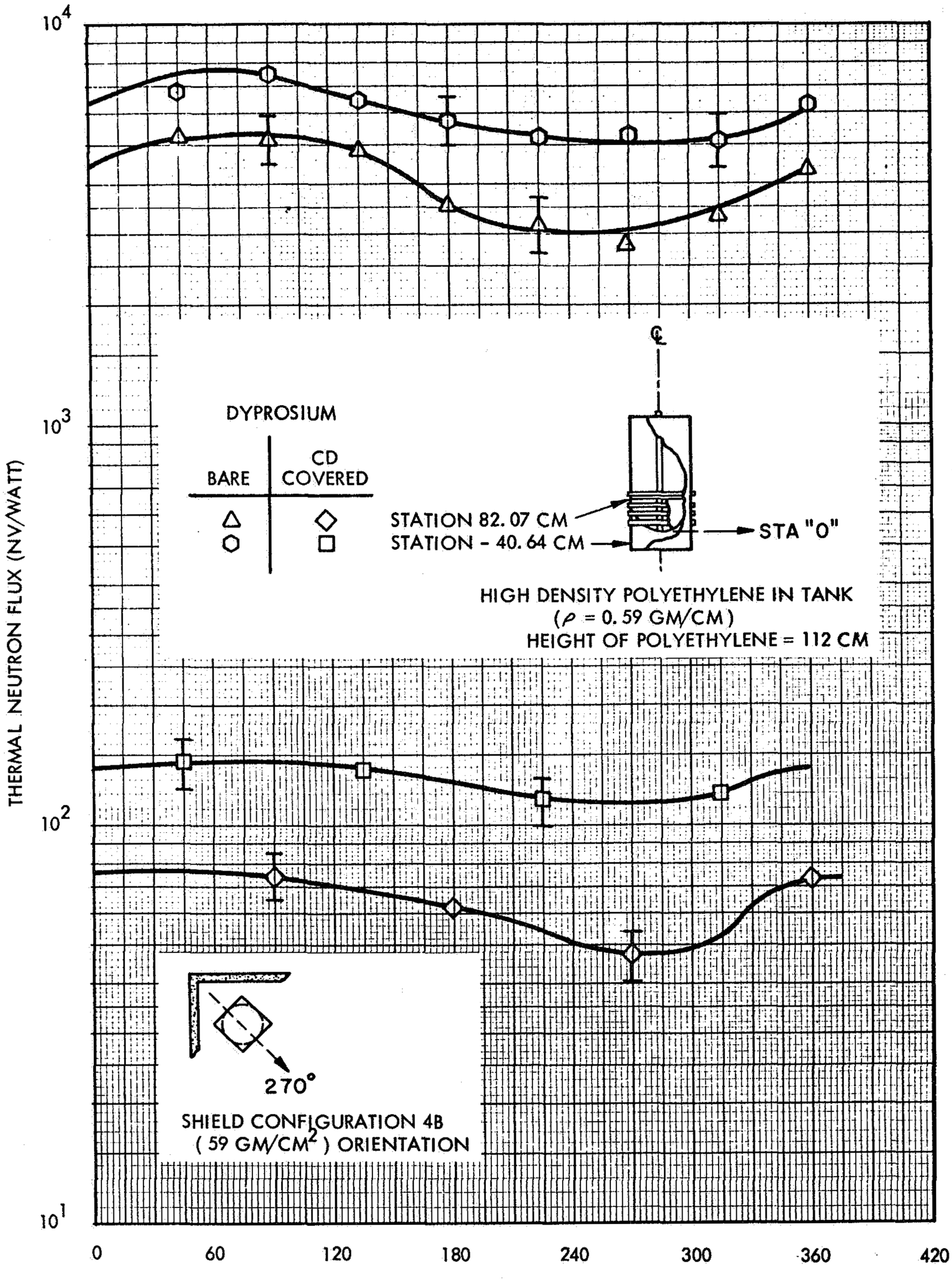

Figure 6-17. Thermal Neutron Flux as Measured with Dysprosium vs Azimuth on Tank External Skin

steeper than the fast neutron data shown in Figure 6-10. The cadmium-covered dysprosium foil exhibits a slightly steeper slope than the bare dysprosium and appears to level out at about 50 cm. The reason for this behavior is not entirely clear. The U-238 fast fission chamber data in Figure 6-10 showed a similar tendency. At least part of this behavior may be attributed to the large uncertainties involved in this region.

6.1.3 Gamma Dose Rate Measurements

Gamma ray dose rate information was obtained during the portion of the test when high density polyethylene was present in the tank as part of the overall data acquisition process. These data cannot be used to infer gamma ray transmission properties of the low density polyethylene or heating rates in liquid hydrogen; however, it may serve as a basis for an evaluation of the analytical techniques.

6.1.3.1 Gamma Dose Rate Measurements with a CO_2 Ionization Chamber

Gamma ray dose rate data was obtained for the high density polyethylene in the tank, on Shield Configurations 4B and 11. Figure 6-19 shows two radial traverses through the high density polyethylene in the tank for Shield Configuration 4B using the CO_2 ionization chamber. Similar data was not obtained for Shield Configuration 11; thus, no direct determination of the direct gamma radiation environment (with the test cell background removed) within the tank, is possible for the CO_2 chamber data by itself. However, additional gamma dose rate data was obtained for both shield configurations, i.e., 4B and 11, using CaF_2:Mn TLD's on the external tank surface and in an axial tube located just off the tank centerline at r= 11.75 cm and $\Theta = 0$ degrees. These data are discussed in the following section.

6.1.3.2 Gamma Dose Rate Measurements with CaF_2:Mn Thermoluminescent Dosimeters

Figure 6-20 presents gamma dose rate data obtained with CaF_2:Mn TLD's on the propellant tank hemisphere. The distribution is asymmetrical about the tank centerline axis skewed in a direction toward the test cell walls. This distribution is caused by test cell wall scattering effects along with the test cell wall produced secondary gammas. Figure 6-21 presents gamma dose rate data obtained with CaF_2:Mn TLD's located axially on the propellant

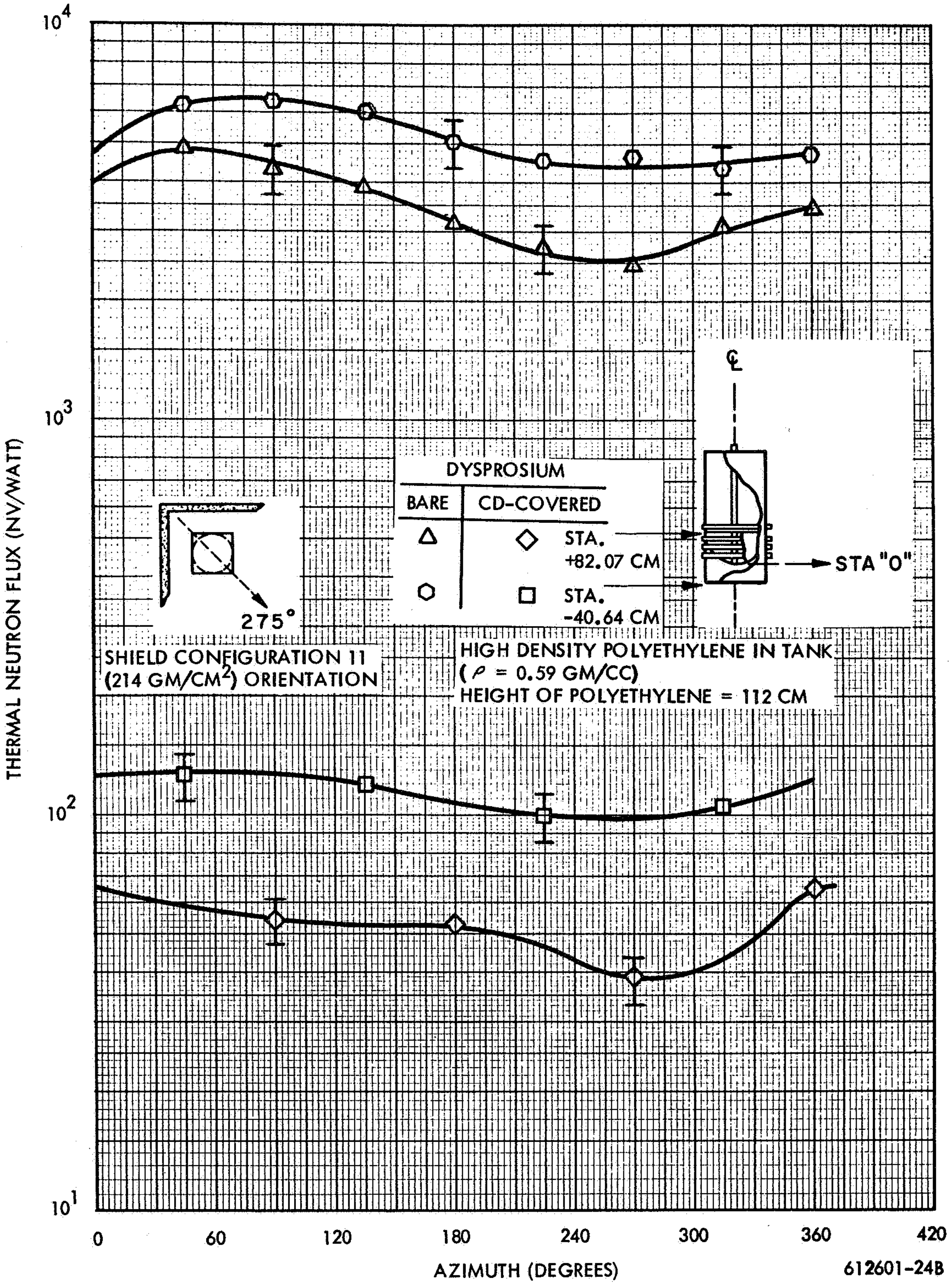

Figure 6-18-1. Thermal Neutron Flux Measured with Dysprosium vs Azimuth on Tank External Skin

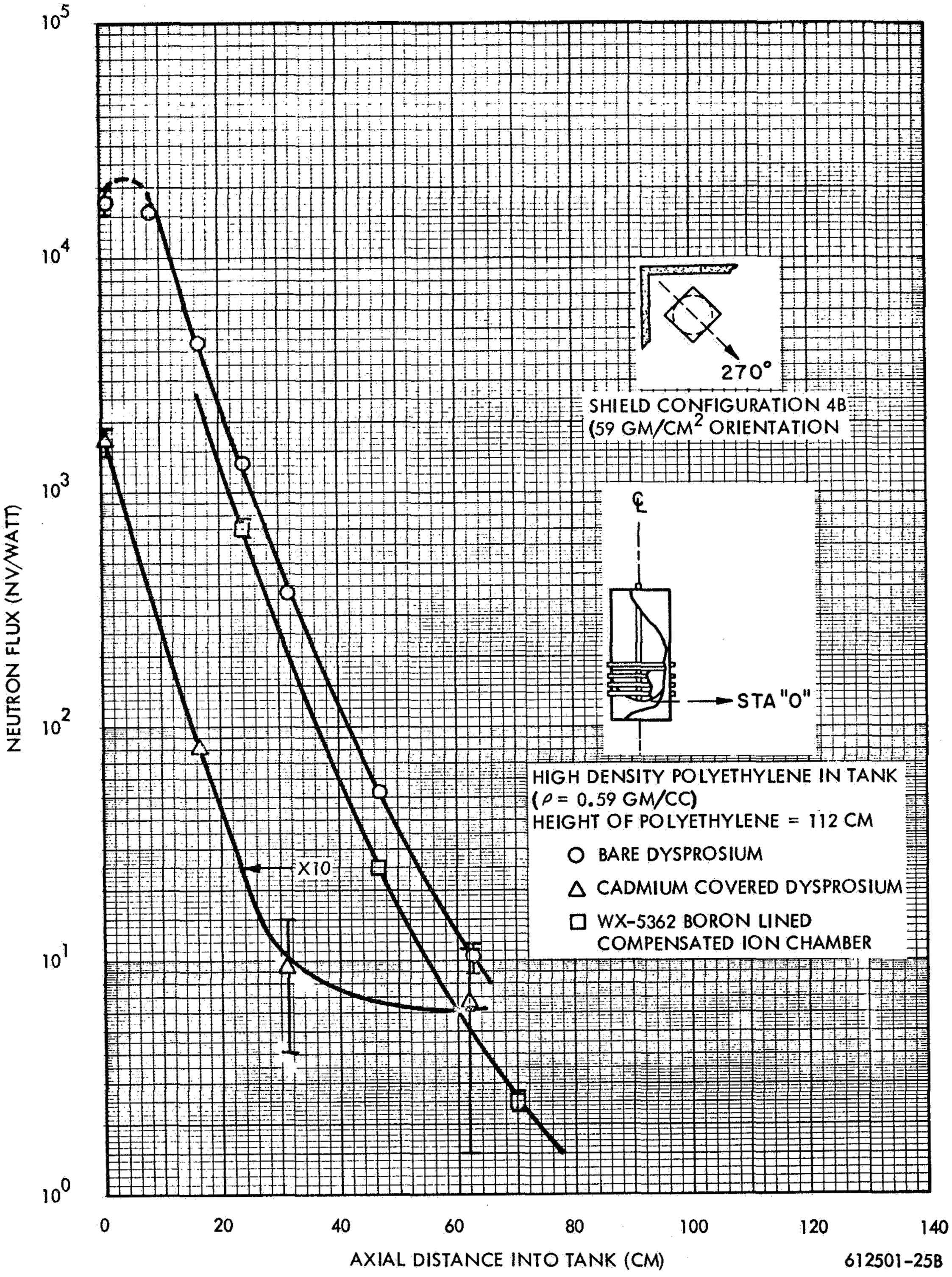

Figure 6-18-2. Neutron Flux vs Axial Distance into Tank

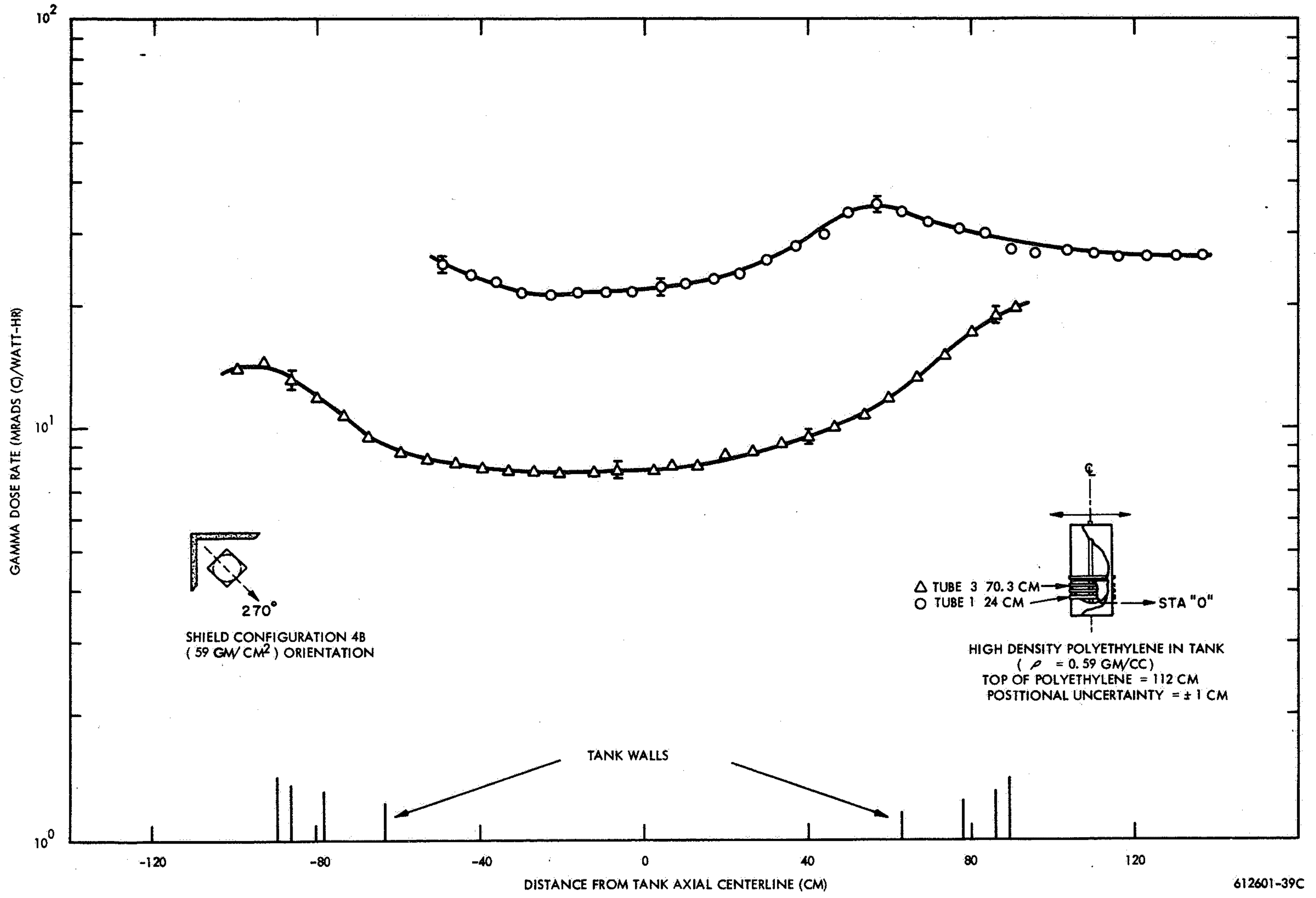

Figure 6-19. Gamma Dose Rate as Measured with a RSG-8A Carbon Wall Ion Chamber vs Distance from Tank Axial Centerline

tank external skin at two different azimuthal locations. This data was obtained from axial locations from near the bottom of the tank skirt to the top of the tank. The two traverses cross over at a station of approximately 100 cm. This location coincides approximately with the top of the high density polyethylene located in the tank. The discontinuous curve shape at 100 cm is due probably to the lack of high density polyethylene in the tank past 112 cm. Below that level the polyethylene serves to shield the cell wall radiation sources. Figure 6-22 presents the gamma dose rate data obtained with CaF_2:Mn TLD's located on the propellant tank external skin at two different axial heights vs azimuthal position on the skin for two different shield configurations, 4B and 11. The data obtained at station = -40.64 cm is located on the tank skirt below the tank hemisphere, while the data obtained at station = 82.07 cm is located slightly above the middle of the high density polyethylene on the external skin of the tank.

The data for both shield configurations has the same relative shape for the same station location but the curve shapes are entirely different for the two station locations. The data for shield configuration 4B is higher, as it should be, than the data for shield Configuration 11. The curve shape for the data taken at station = 82.07 cm, for both shield configurations is explained by noting the relationship between the azimuthal location of the peak values and the relationship between these points and the shortest distance to the test cell walls which occurs at the same location. Thus, the peaks are caused by the presence of the test cell walls. The curve shape for the data taken at station = -40.64 cm is not as easy to explain, however. One would expect to see the same general curve shape as discussed previously due to the test cell walls. The shape, however, does not have two humps, but rather only one which occurs approximately at an azimuthal angle of 135 degrees, apparently the same location as one of the humps in the station = 82 cm data. However, this data is much more pronounced, possibly due to the close presence of a steel staircase which passes alongside the propellant tank at this location. No other explanation for this curve shape is available at the present time.

Figure 6-23 shows gamma dose rates obtained for both configurations 4B and 11 in an axial tube located just off the tank centerline at r = 11.75 cm and azimuthal angle

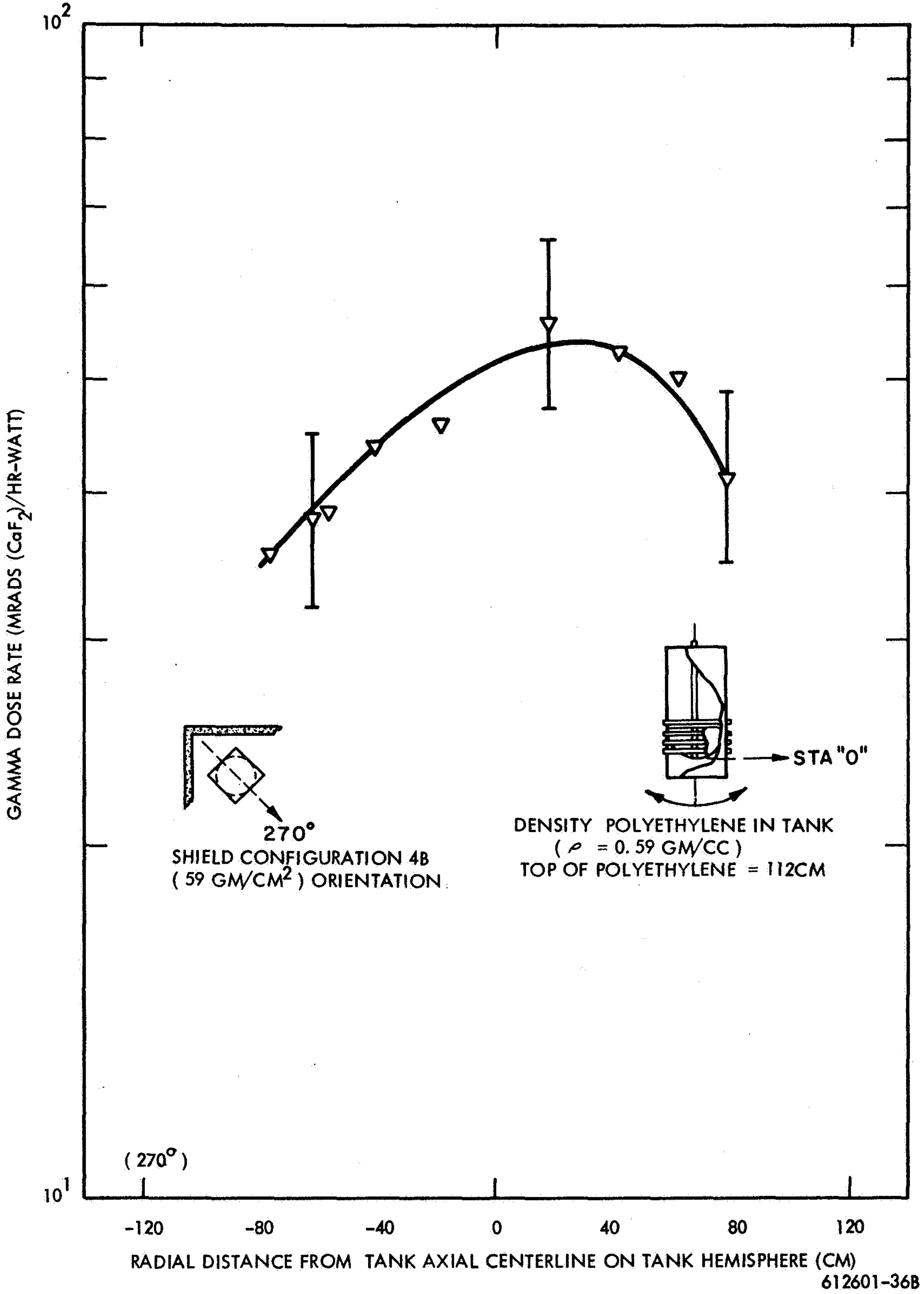

Figure 6-20. Gamma Dose Rate as Measured with CaF_2:Mn TLD's vs Radial Distance from Tank Centerline on Tank Hemisphere

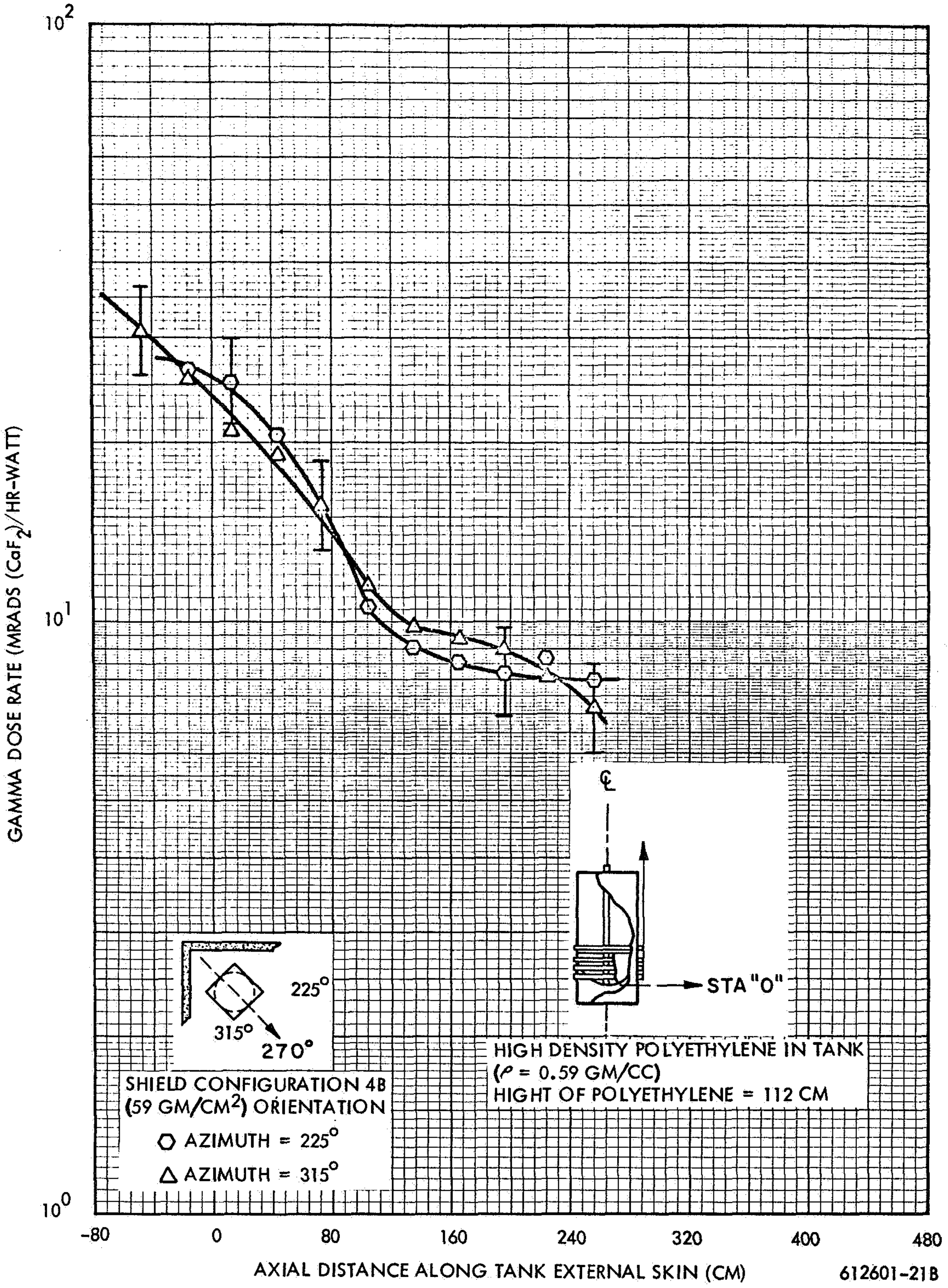

Figure 6-21. Gamma Dose Rate as Measured with CaF_2:Mn TLD's vs Axial Distance Along Tank External Skin

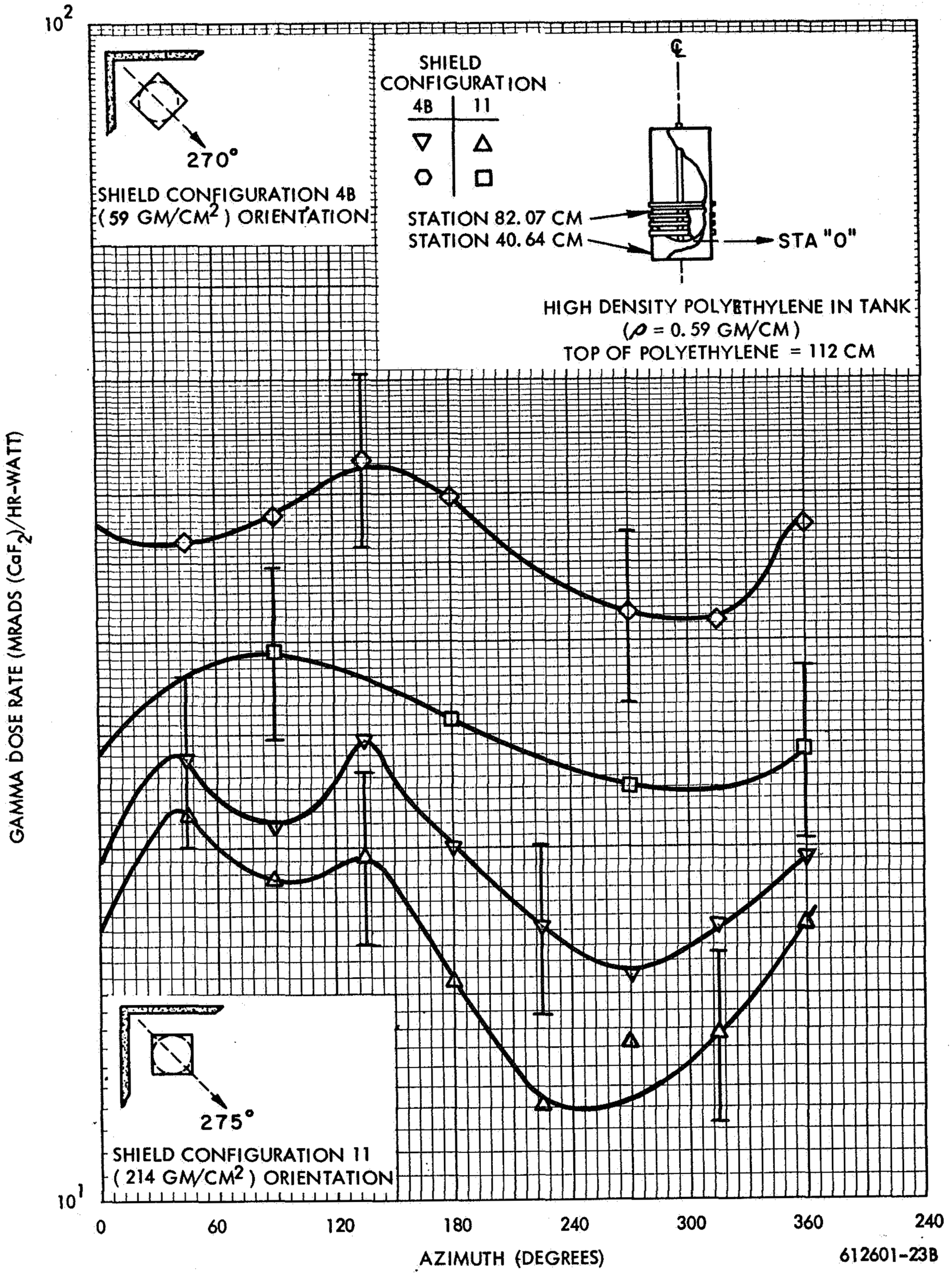

Figure 6-22. Gamma Dose Rate as Measured with CaF_2:Mn TLD's vs Azimuth on Tank External Skin

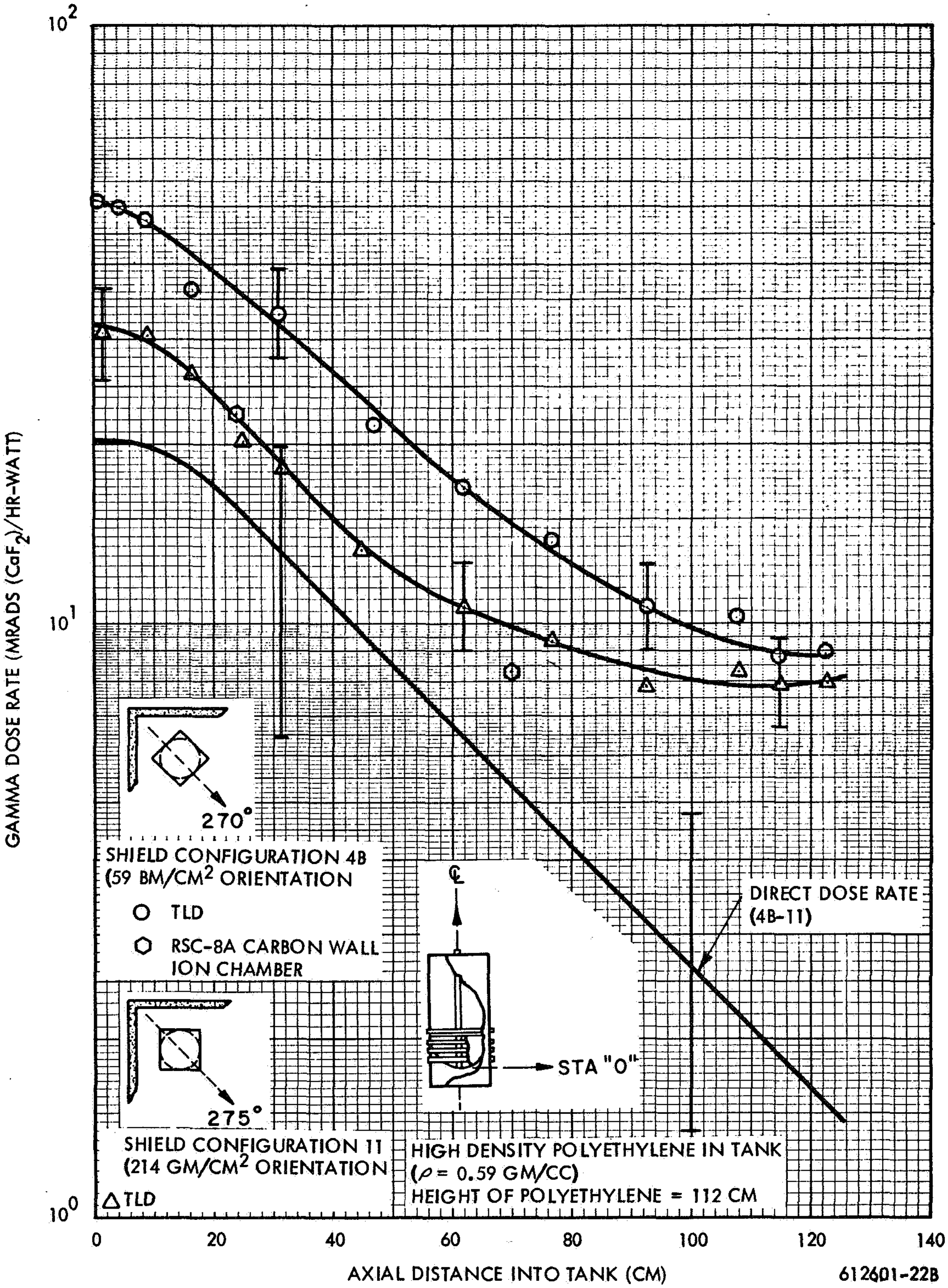

Figure 6-23. Gamma Dose Rate as Measured with CaF_2:Mn TLD's vs Axial Distance into Tank

$\theta = 0$ degrees. This data shows a significant difference between the dose rates measured for these two configurations although the detectors above an axial distance of 108 cm showed a much smaller difference than the detectors located below this station. This is due to the fact that the detectors above 108 cm were near or above the top surface of the polyethylene, which occurred at approximately 112 cm and, thus, were less self-shielded from the test cell background radiation. The difference between the Configurations 4B and 11 sets of data has been obtained as indicated on Figure 6-23 as "direct" gamma dose rate for Configuration 4B.

6.1.3.3 A Comparison of Gamma Dose Rate Results

The data obtained as a function of depth into the tank as shown in Figure 6-23 was primarily obtained using CaF_2:Mn TLD dosimeters for Configuration 11 and Configuration 4B, as indicated. Also shown on this figure are two CO_2 data points cross plotted from Figure 6-19 obtained for Configuration 4B. Note the factor of 2 difference beteen the CO_2 data and the CaF_2:Mn TLD data. The reason for the apparent discrepancy has not been determined but at least two possibilities exist. They are: 1) a non-flat TLD energy response to gamma ray energies less than 0.2 Mev and greater than 5 Mev, 2) a significant TLD neutron response, especially to thermal neutrons. This discrepancy is emphasized in the recording of the data by presenting the TLD dose response in units of rads (CaF_2) rather than rads (C). Further discussion of the TLD response is given in Section 6.2.1.

Figure 6-24 presents a comparison of the gamma dose rate data obtained with CaF_2:Mn TLD's and also the CO_2 chamber for two different axial locations within the high density polyethylene as a function of the radial distance from the tank centerline, for both shield Configurations 4B and 11. The CO_2 data was obtained only on shield Configuration 4B and an attempt is made using the data in this figure to obtain an approximate distribution for CO_2 data on shield Configuration 11. This would allow the determination, by subtraction, of the Configuration 11 data from the 4B data, of the direct gamma component in the tank. A percentage correction was applied to the CO_2 data for shield Configuration 4B, based upon the TLD data for 4B and 11 to determine the dashed CO_2 curve for shield Configuration 11. The "direct" gamma ray dose rate data thus obtained for the two axial locations as a function of radial position within the high density polyethylene is presented in Figure 6-25.

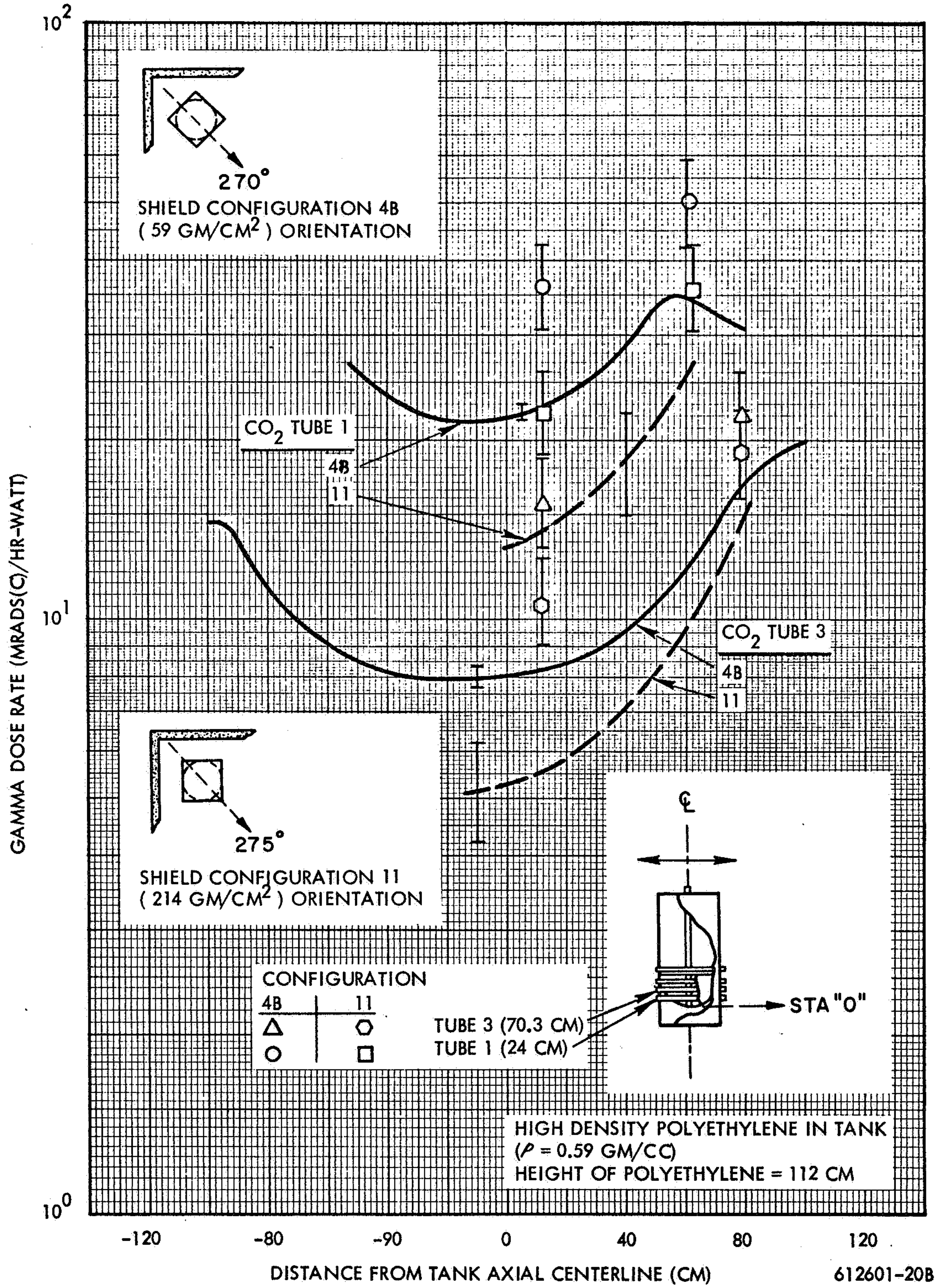

Figure 6-24. Gamma Dose Rate vs Distance from Tank Axial Centerline

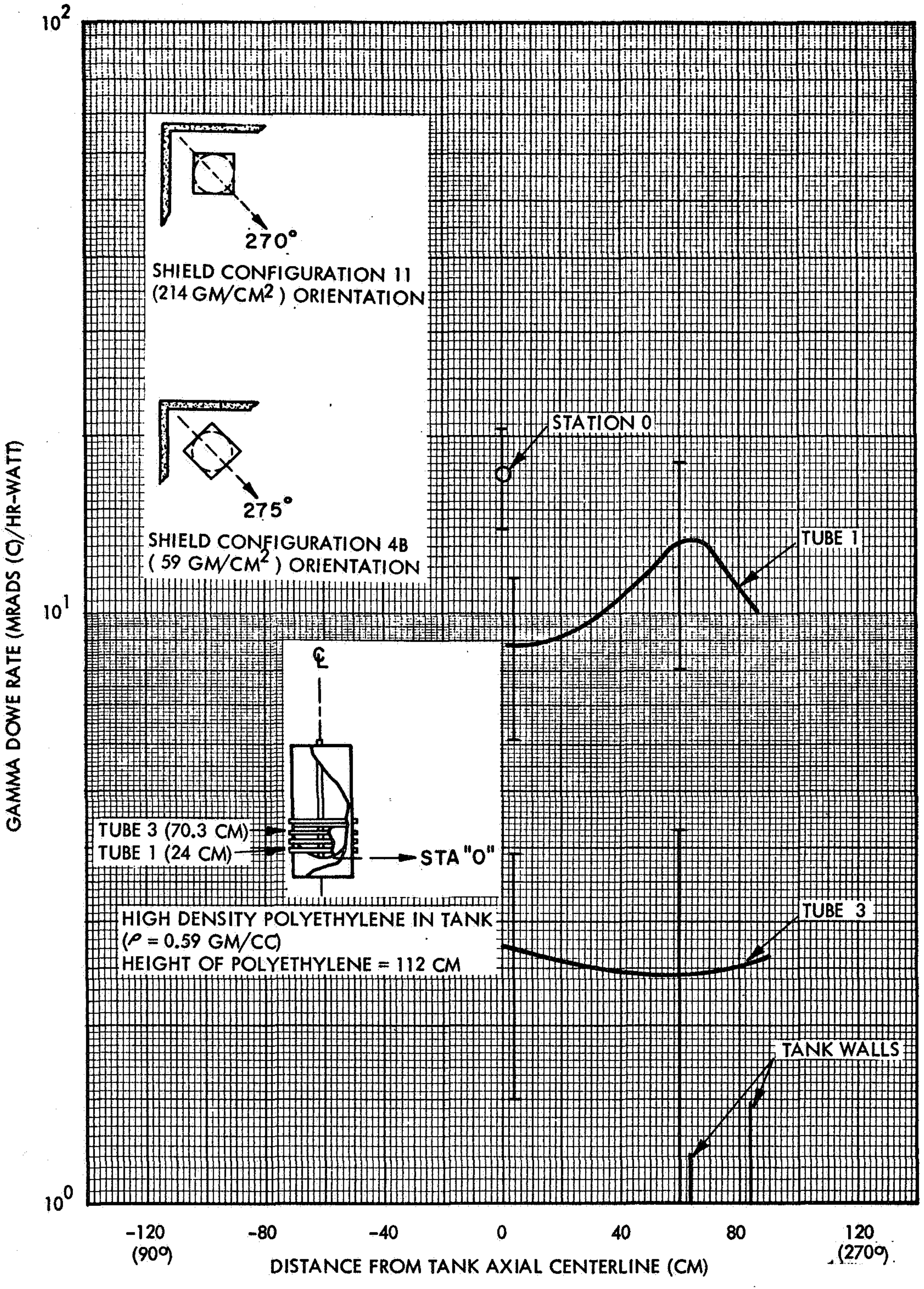

Figure 6-25. Direct Gamma Dose Rate vs Distance from Tank Axial Centerline

6.2 MEASUREMENTS WITH LOW DENSITY POLYETHYLENE IN TANK

This density polyethylene was used to obtain a simulation of gamma transport properties of liquid hydrogen. Because of the NERVA R-1 shield measurement requirements and schedule, these measurements were primarily taken with Shield Configuration 7D, a mockup of shield and support structure having a total thickness density of 140 gms/cm^2, and the corresponding background measurement with Configuration 11. As was anticipated, the gamma background due to the test cell environment is much more significant in this case than for Configuration 4B. Therefore, the subtraction of Configuration 11 data from analogous Configuration 7D data yields a larger uncertainty in these results than for the neutron data or the gamma dose rate data obtained with Configuration 4B. Gamma dose rate measurements are presented in Section 6.2.1 and supporting thermal flux measurements are given in Section 6.2.2.

6.2.1 Gamma Dose Rate Measurements

Gamma dose rate measurements were made with low density polyethylene in the tank for both Configurations 7D and 11 using the CO_2 ionization chamber in Traverse Tubes 1, 2, 3 and 4 for Configuration 7D and in Tubes 1, 2 and 3 for Configuration 11 and are described in Section 6.2.1.1.

In addition, passive type dosimetry measurements were made with CaF_2:Mn thermoluminescent dosimeters through Traverse Tube 4 for Configuration 11 through the axial tube, and on the surface of the tank. These data are described in Section 6.2.1.2.

6.2.1.1 Gamma Dose Rate Measurements with a CO_2 Ion Chamber

Figure 6-26 gives a series of measurements of the gamma dose rate for the four different traverses into the tank as taken with the carbon wall CO_2 filled ionization chamber. In each case, it may be noted that the gamma dose rate is significantly higher near that portion of the tank wall which is closest to the test cell corner, i.e., in the positive direction. Figure 6-27 presents similar data for Shield Configuration 11.

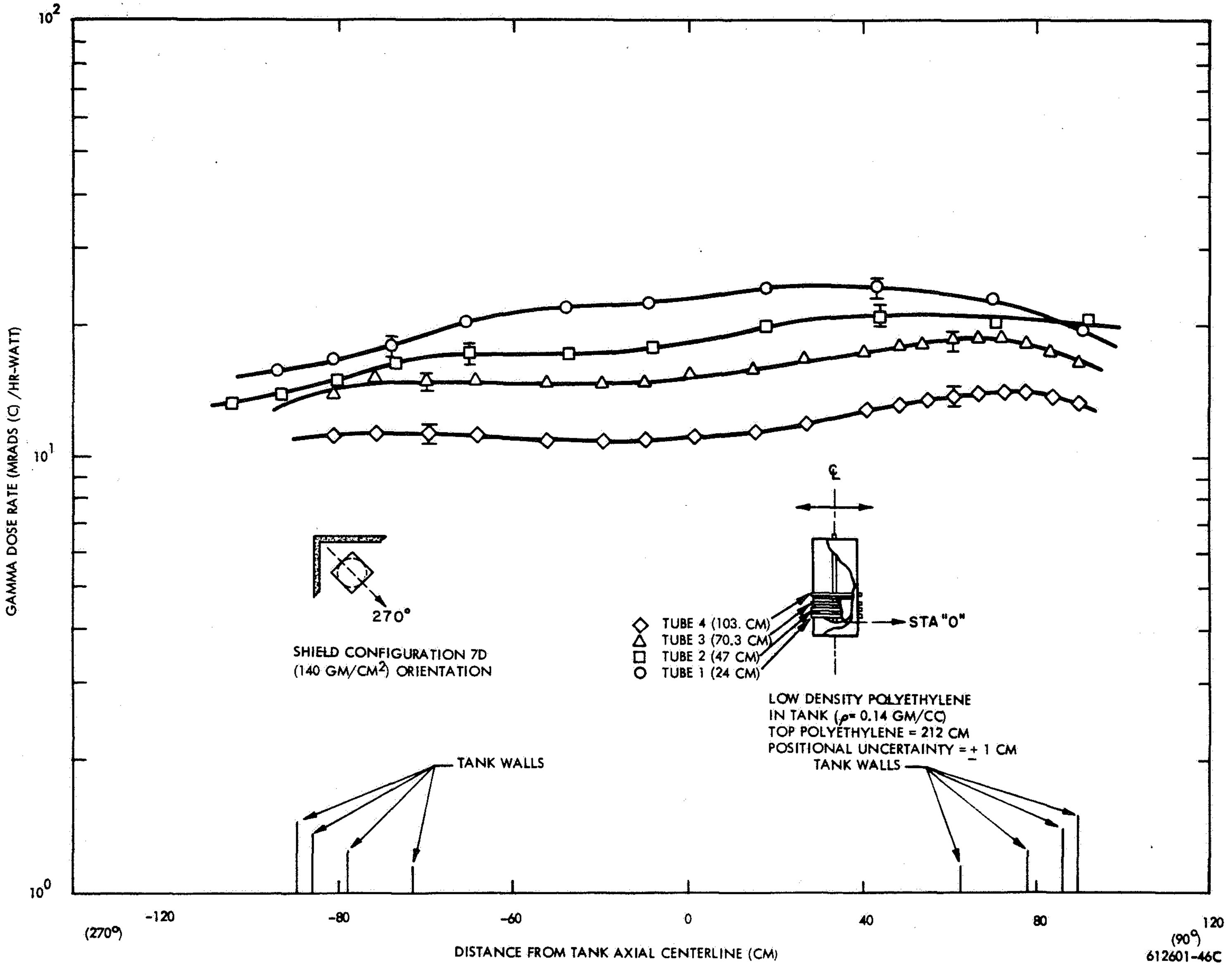

Figure 6-26. Gamma Dose Rate as Measured with an RSG-8A Carbon Wall Ion Chamber Vs Distance from Tank Axial Centerline

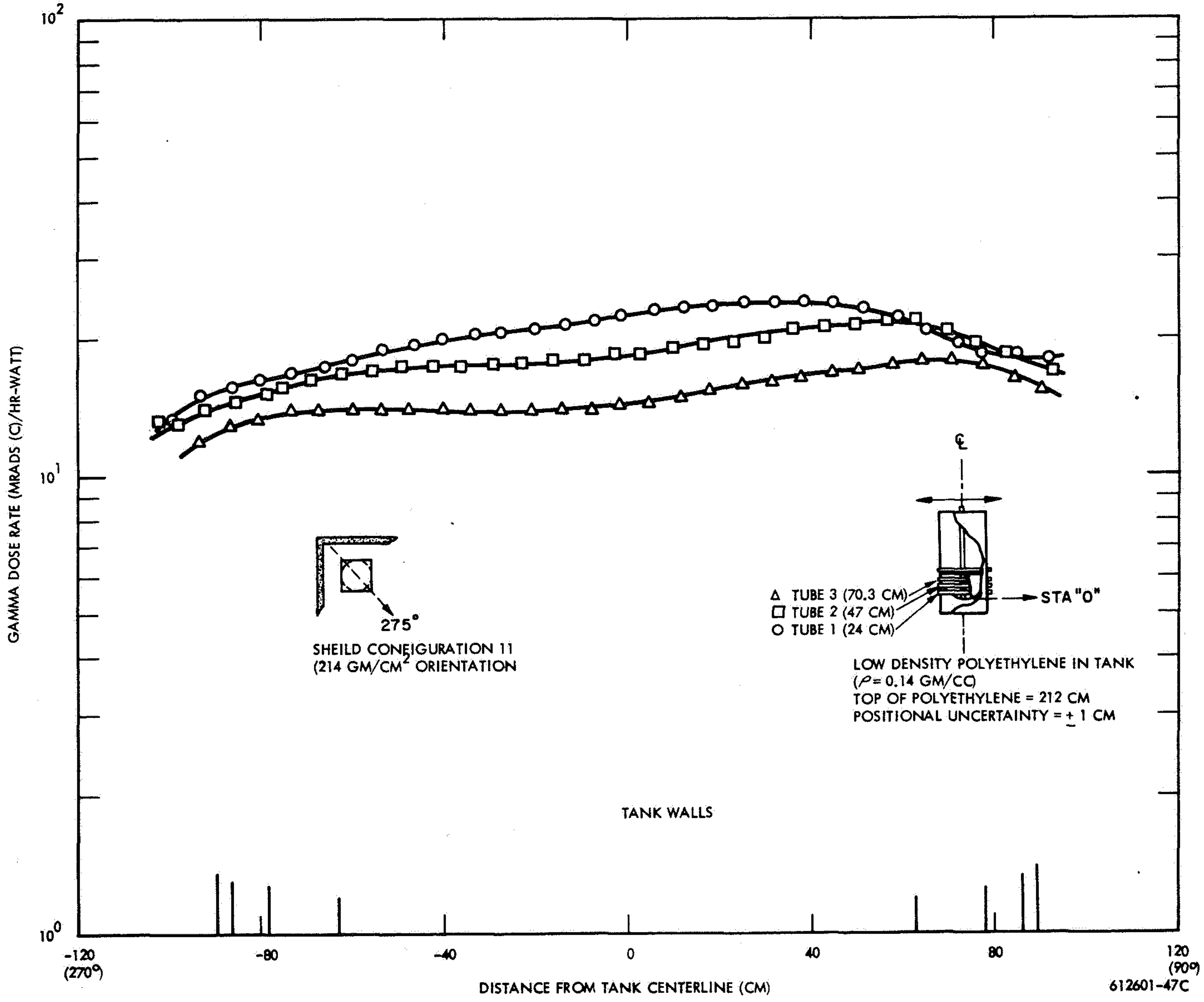

Figure 6-27. Gamma Dose Rate as Measured with an RSG-8A Carbon Wall Ion Chamber Vs Distance from Axial Centerline of Tank

6.2.1.2 Gamma Dose Rate Measurements with Thermoluminescent Dosimeters

Figure 6-28 shows the gamma dose rate as measured with CaF_2:Mn TLD's in a traverse type arrangement through Traverse Tube No. 4. The corresponding curve for the CO_2 chamber from Configuration 7D (since there is no essential difference between 7D and 11 results) is also plotted in Figure 6-28. It may be noted that the TLD data is approximately 60 percent higher than the corresponding CO_2 data. Also, the scatter in the TLD data is considerably greater than that in the CO_2 data. Figure 6-29 shows the gamma dose rate, as measured with calcium fluoride TLD's, on an axial traverse into the tank. The curve basically consists of three sections: 1) an initial increase which corresponds to the peaking effect of thermal flux due to a high capture gamma component in the bottom of the tank, 2) a fairly exponential attenuation from 20 to about 100 cm, and a third exponential attenuation with a different slope from approximately 100 cm to the top of the polyethylene. Figure 6-30 indicates the gamma dose rate as measured with CaF_2:Mn TLD's for various locations on the tank hemisphere. As is expected, the points are somewhat higher in the positive direction (corresponding to distances measured toward the test cell corner) than in the opposite direction. Again, there appears to be no significant difference between Configuration 7D and 11 data. Figure 6-31 indicates the gamma dose rate as measured on the outside tank skin at two elevations vs azimuth for Configurations 7D and 11. Because of the large uncertainties, no significance may be attached to any possible spatial effects. Figure 6-32 gives the gamma dose rate vs axial distance into the tank. Data is presented at five different positions for each of three different TLD configurations. All positions contain CaF_2:Mn TLD's; no lithium fluoride TLD's were considered because of their high neutron sensitivity. Figure 6-33 indicates the energy response of the CaF_2:Mn TLD's in both the unshielded and the commercial tantalum shield used for some of these measurements. In order to determine if the higher values of the TLD data as opposed to the CO_2 data could be caused by the TLD increased low energy response, one of the CaF_2:Mn TLD configurations was run with the TLD placed within a 1/64 inch thick piece of Tygon tubing. The second TLD configuration was made with the CaF_2:Mn TLD's placed inside a commercial tantalum case. The third TLD configuration was made with the TLD placed inside a commercial tantalum case which was, in turn, placed within an Li^6

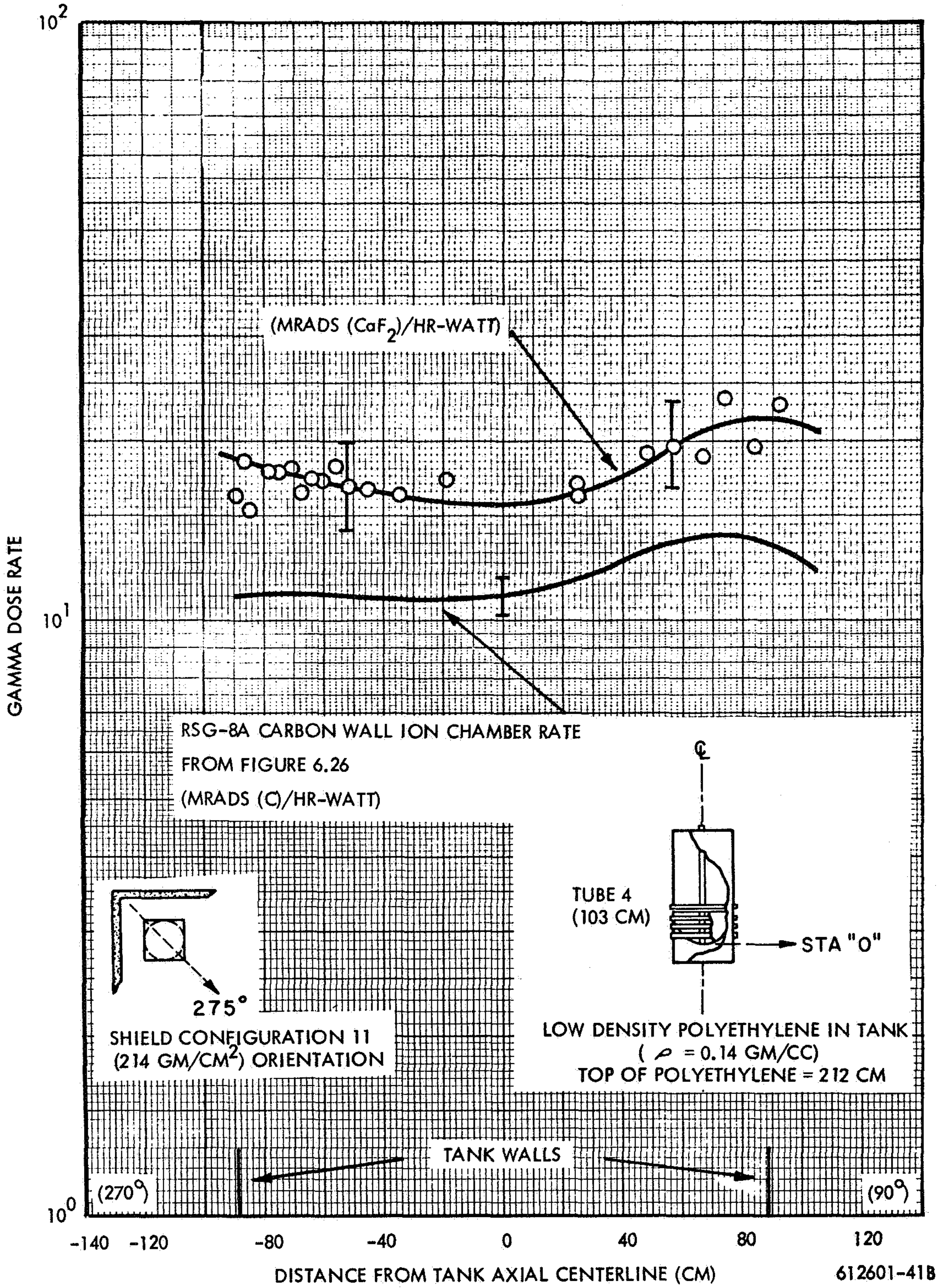

Figure 6-28. Gamma Dose Rate as Measured with CaF_2:Mn TLD's Vs Distance from Tank Axial Centerline

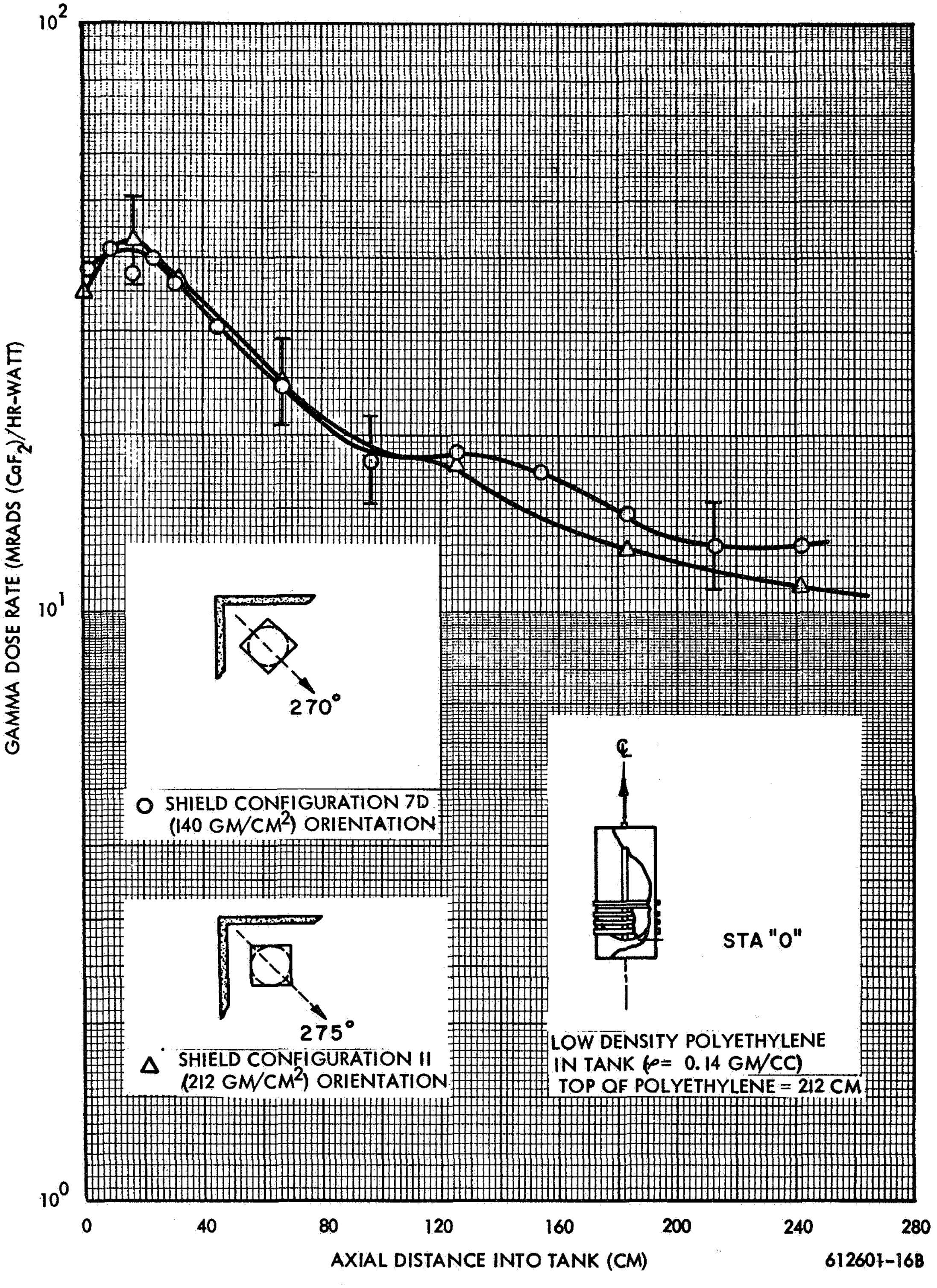

Figure 6-29. Gamma Dose Rate as Measured with CaF_2:Mn TLD's vs Axial Distance into Tank

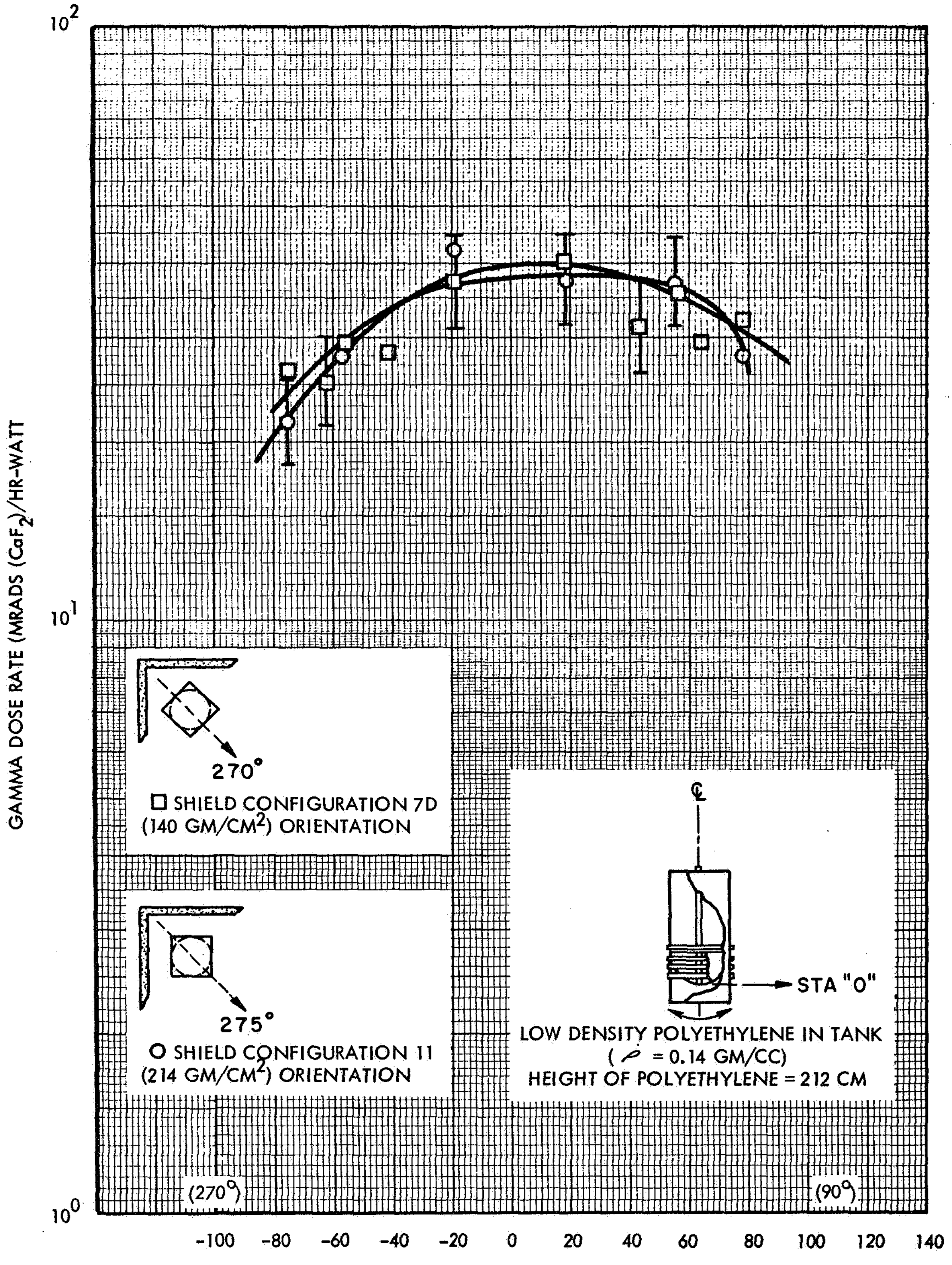

612601-42B

Figure 6-30. Gamma Dose Rate as Measured with CaF_2:Mn TLD's vs Radial Distance from Tank Axial Centerline on Tank Hemisphere

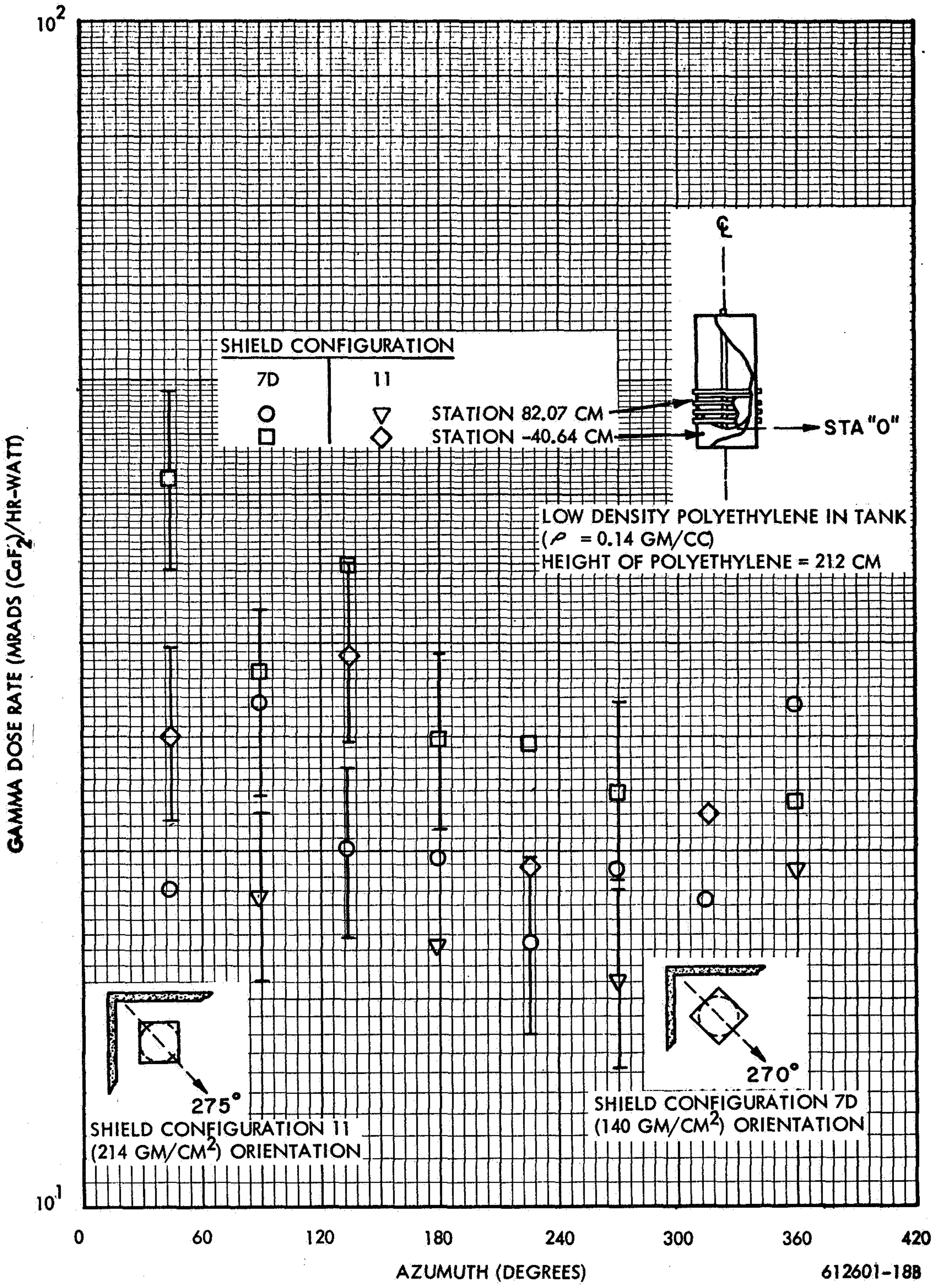

Figure 6-31. Gamma Dose Rate as Measured with CaF_2:Mn TLD's vs. Azimuth on Tank External Skin

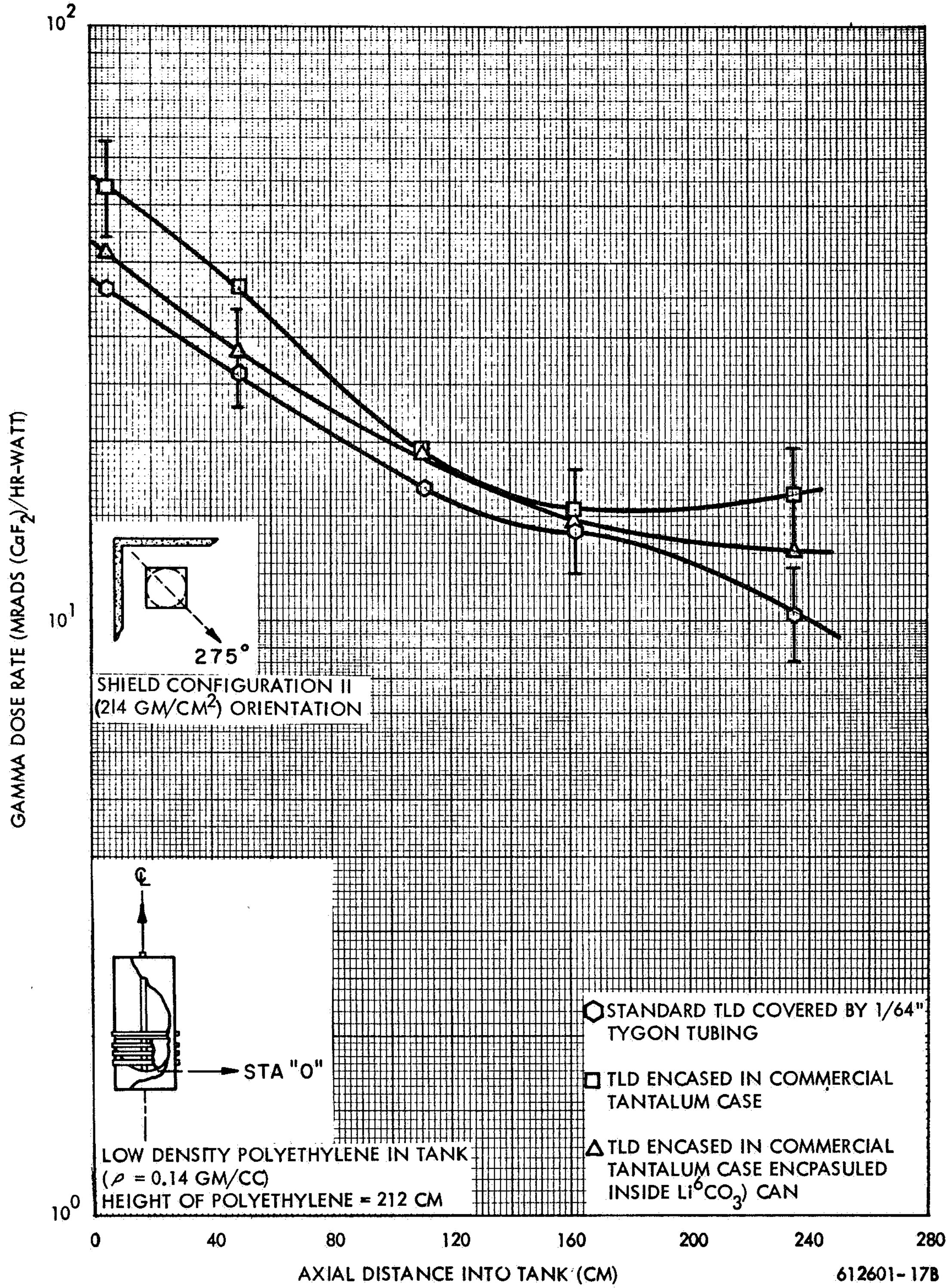

Figure 6-32. Gamma Dose Rate as Measured with CaF_2:Mn TLD's Having Different Energy Flatteners vs Axial Distance into Tank

enriched Li_2CO_3 shield. Upon inspection of Figure 6-32, it may be seen that without exception the Tygon encapsulated TLD's give the lowest readings. It may be seen from Figure 6-33 that for the unshielded case, the TLD response rises by nearly an order of magnitude at 0.03 Mev over a desired energy independent response. It is suspected that this rise in response for the low photon energies is the primary reason why the TLD data is higher than corresponding CO_2 data. On the other hand, the tantalum shields which are presumably designed to flatten this energy response, have a considerable neutron absorption cross-section with the attendant capture gamma rays. Furthermore, a substantial epithermal neutron cross-section also exists for tantalum; thus, in reference to Figure 6-32 it may be noticed that where the percentage of thermal neutrons is the greatest, i.e., on the outside of the tank, the difference between the bare, the tantalum-covered, and the lithium carbonate encapsulated tantalum-covered TLD's is the greatest. On the other hand, where the neutron spectrum is composed primarily of the fast or epithermal neutrons, i.e., at some distance into the polyethylene, the lithium carbonate can has very little effect. However, encapsulated TLD's are still higher than the Tygon-covered TLD's.

6.2.1.3 Discussion of Gamma Dose Rate Results

Figure 6-34 indicates the results of the subtraction process between the Configuration 7D and the Configuration 11 gamma dose for Tubes 1 and 3 for the CO_2 chamber data. Because the differences are on the order of only 1-10 percent of the magnitude of the original data, it appears that test cell background is primarily being measured. These subtracted values are well within the precision of the individual measurements and thus, the scatter obtained is not surprising. The data are included, however, to indicate an order of magnitude of about 1 mrad(C)/watt-hr throughout the tank.

6.2.2 Thermal Neutron Flux Measurements

Thermal neutron flux measurements were made with both active and passive dosimetry techniques for the low density polyethylene case. Measurements with the low density polyethylene were made with Shield Configuration 7D and Configuration 11. As

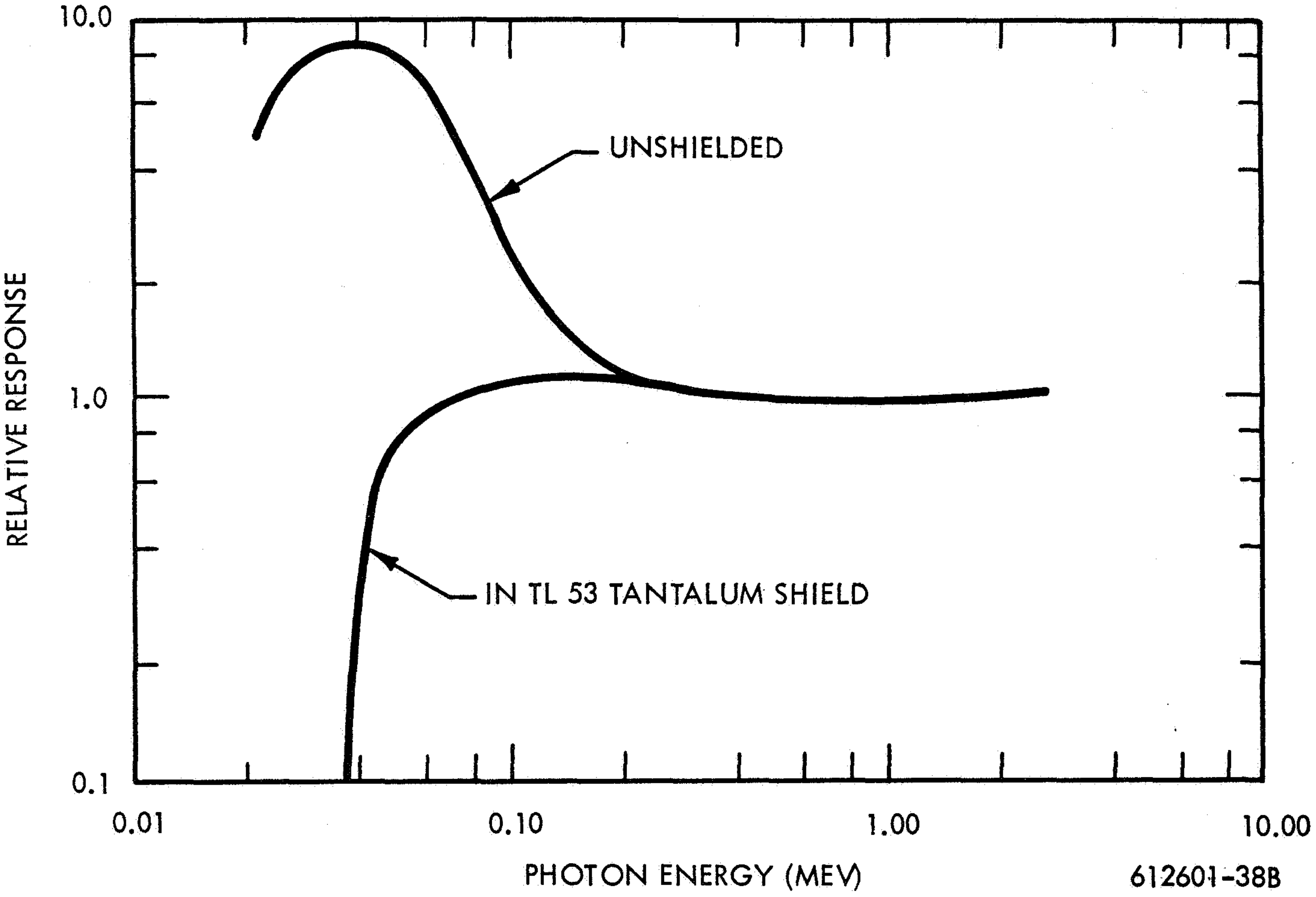

Figure 6-33. Response Vs Photon Energy for CaF_2:Mn Hot Press Thermoluminescent Detector

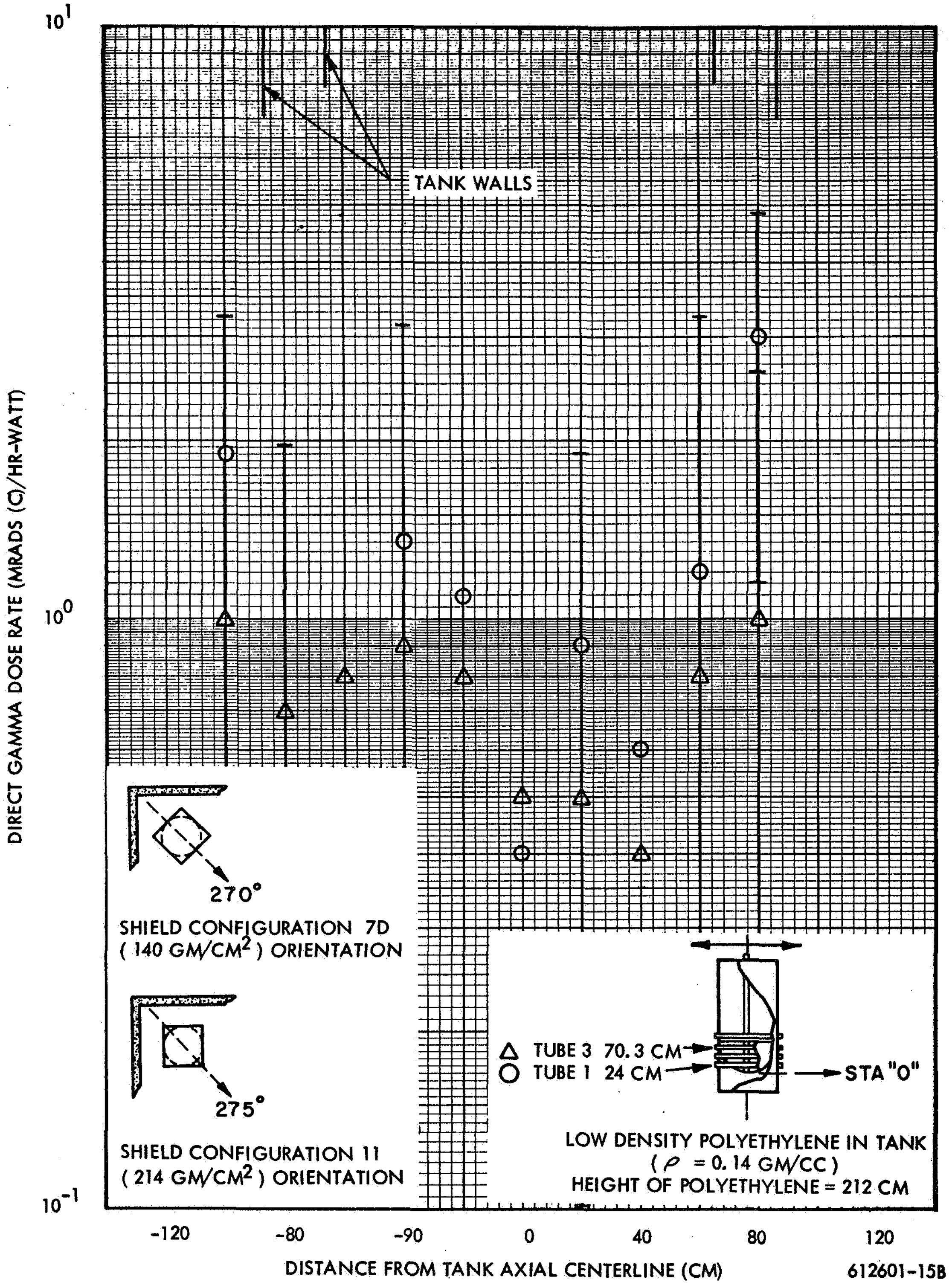

Figure 6-34. Direct Gamma Dose Rate as Measured with RSG-8A Carbon Wall Ion Chamber vs Distance from Tank Axial Centerline

was the case in the gamma dose data, differences in the flux data between Configurations 7D and 11 are small and within the uncertainty of the data. Thus, the method of subtracting Configuration 11 from Configuration 7D data to obtain the direct environment, i.e., without test cell radiation background, leads to results which are uncertain. The thermal neutron data is presented in an effort to support the gamma dose measurements and analysis.

6.2.2.1 Thermal Neutron Flux Measured with a Compensated Boron-Lined Ion Chamber

Figure 6-35 shows the thermal neutron flux as measured with the WX-5362 compensated ion chamber as a function of distance from the axial centerline in the tank. These data were obtained with Shield Configuration 7D. Figure 6-36 shows similar data for Shield Configuration 11. The data are essentially the same within the uncertainties of the measurement. Both figures show the dosimetry about the centerline with the data in the direction towards the test cell corner being the highest. Unlike the thermal data obtained with the high density polyethylene,the thermal flux here continues to decrease with increasing station along the tank centerline because the polyethylene foam extended to a height of approximately 212 cm.

6.2.2.2 Thermal Neutron Flux Measured with Dysprosium Foils

Thermal neutron flux measurements made with Dysprosium as a function of axial distance in the tank were performed and the data are presented in Figure 6-37. Data for both bare and Cd-covered foils and for both Shield Configurations 7D and 11 were obtained. As with the results obtained with the compensated ion chamber, the data obtained with Shield Configurations 7D and 11 are essentially the same. The flux, as indicated by the bare Dysprosium foils, increases slightly as a function of initial distance into the tank and then rapdily drops off and reaches a minimum around 125 to 150 cm. It then increases again as the top surface of the polyethylene is approached. (approximately 212 cm) The behavior of the neutron fluxes indicated by the bare foils is essentially identical to that obtained with the WX-5362 boron-lined compensated ion chamber.

The fluxes indicated by the cadmium-covered Dysprosium falls off smoothly with axial distance until it too reaches a minimum value at about 125 to 150 cm. The flux then

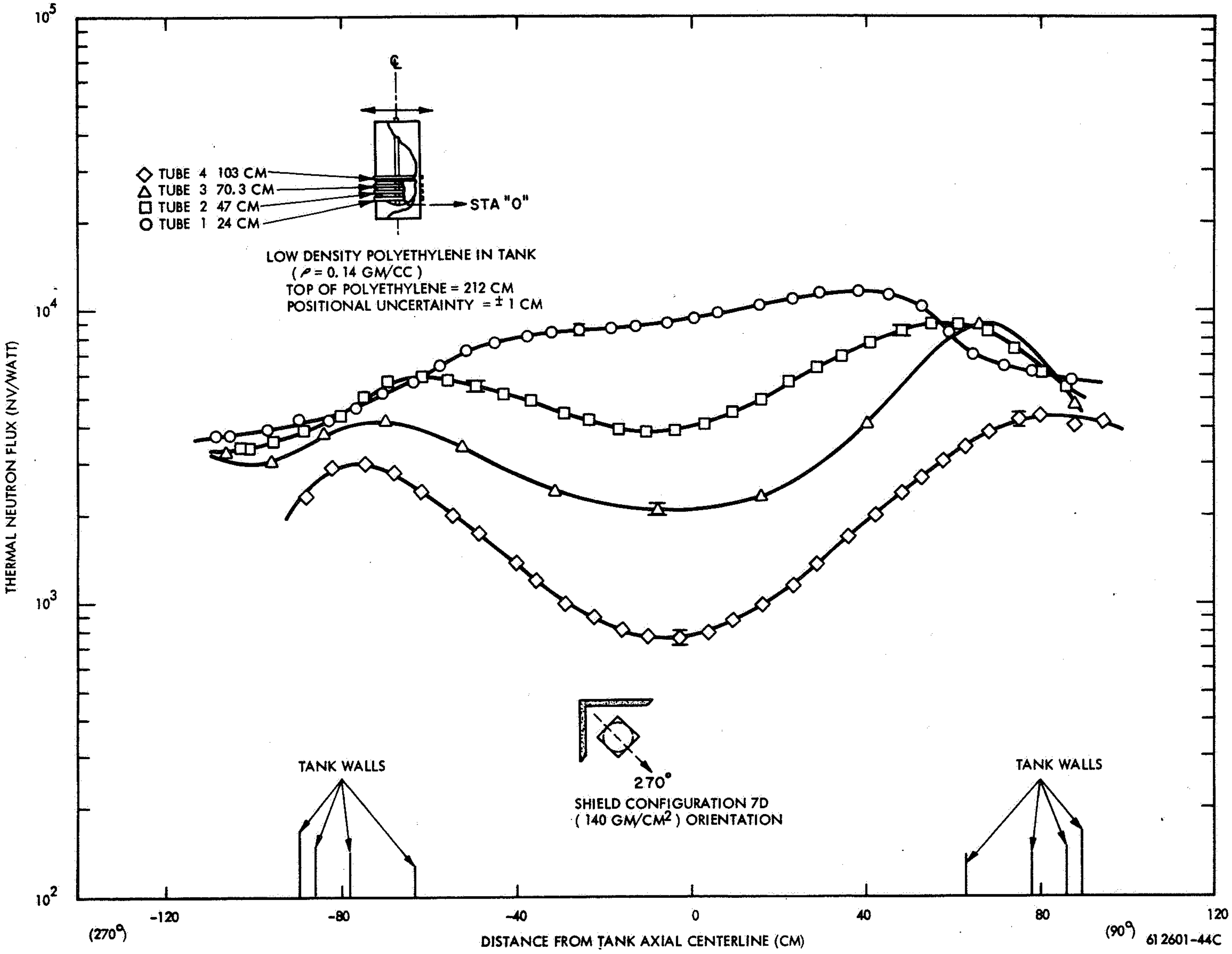

Figure 6-35. Thermal Neutron Flux as Measured with a WX-5362 Boron-Lined Compensated Ion Chamber vs Distance from Axial Centerline of Tank

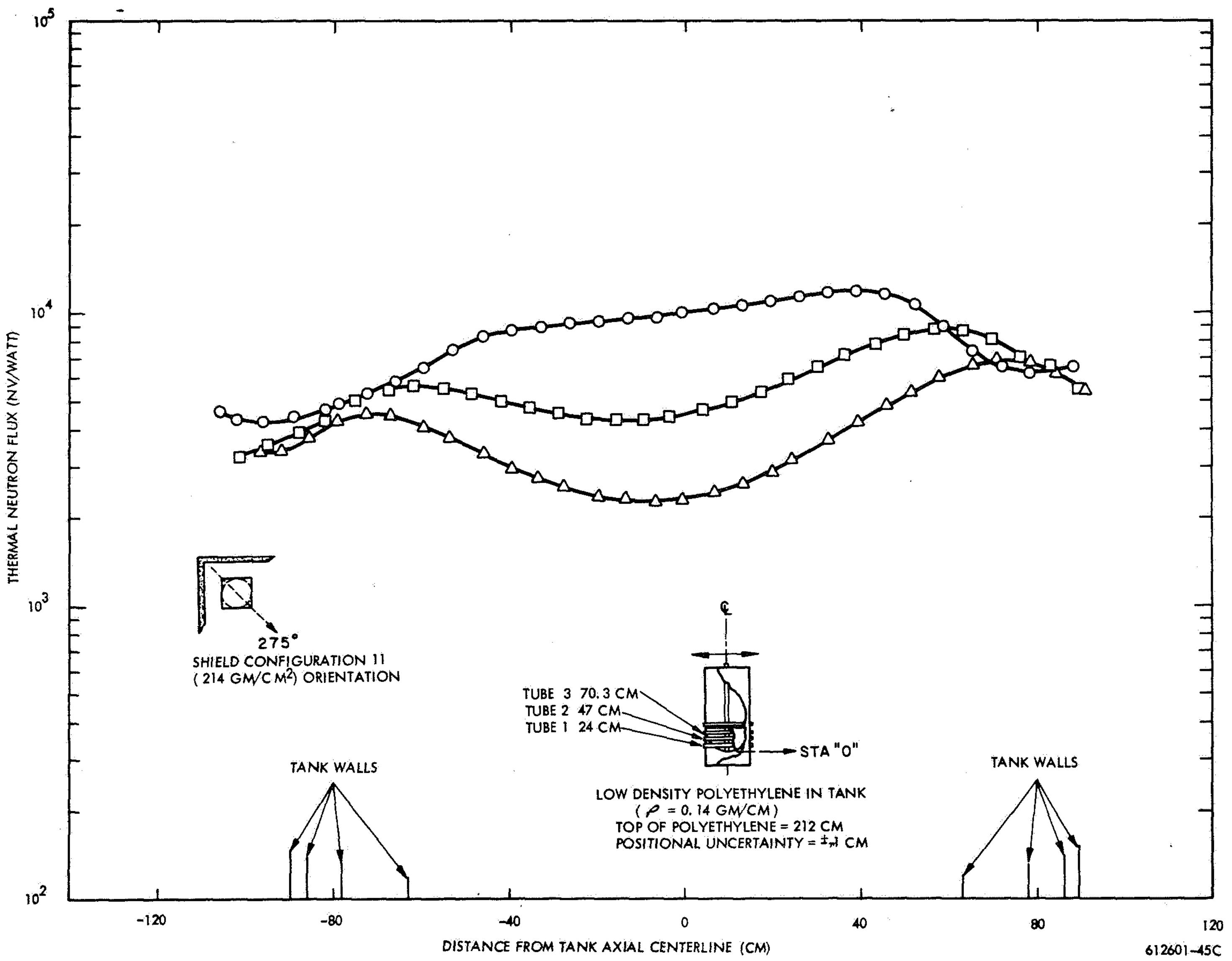

Figure 6-36. Thermal Neutron Flux Measured with a WX-5362 Boron-Lined Compensated Ion Chamber vs Distance from Axial Centerline of Tank

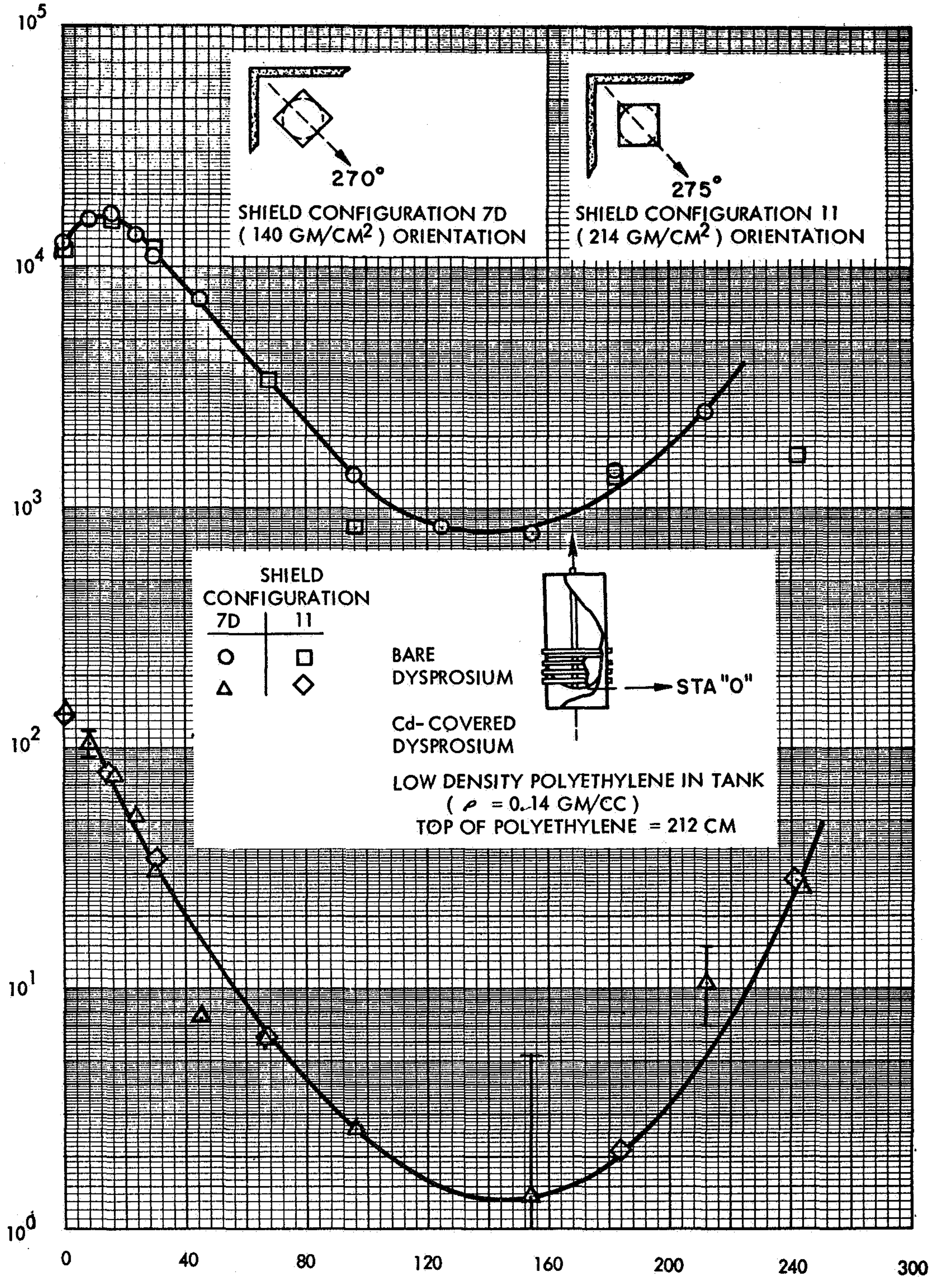

Figure 6-37. Thermal Neutron Flux as Measured with Dysprosium vs Axial Distance into Tank

rises again as the top of the polyethylene is approached.

This upswing in both the bare and cadmium-covered activities as the top of the polyethylene is approached is presumably due to the neutron background that exists above the propellant tank.

Dysprosium measurements were also taken on the bottom hemisphere of the tank. Figure 6-38 shows both bare and cadmium-covered results for Shield Configurations 7D and 11. No significant differences occur for the two shield configurations. Again, the data indicates an asymmetry about the centerline with the data being higher on the side towards the test cell corner.

A measurement of the thermal neutron flux was made radially with Dysprosium through Tube 4 at Station 103 cm. This data for both bare and cadmium-covered foils was obtained on Shield Configuration 11 and is shown in Figure 6-39. This can be compared with the thermal fluxes measured by the WX 5362 compensated ion chamber shown in Figure 6-35. Although the flux data as indicated by the WX-5362 for Tube 4 was obtained on Shield Configuration 7D, it is believed that there is no significant difference between the data here and that which would have been obtained had the chamber been run in Tube 4 for Configuration 11. The dysprosium data shows a characteristic behavior as a function of radial distance from the axial centerline. Again, the asymmetry about the centerline occurs with the flux being highest at the edge of the tank in a direction towards the test cell corner.

Figure 6-40 shows the neutron fluxes measured by bare and cadmium-covered dysprosium foils on the circumference of the tank at 2 stations. These measurements were performed with both Shield Configurations 7D and 11. The data for 11 was essentially identical with that given for Configuration 7D and is therefore not presented. The bare foil data shows a scalloping effect with a small peak at around 90 degrees and a minima around 240 to 270. This is believed to be due to the effects of the test cell wall upon the radiation environment. A similar effect was noted with the Dysprosium data with the high density polyethylene in the tank. The cadmium-covered foil data appears to have a slight scalloping but the differences are well within the measurement uncertainties.

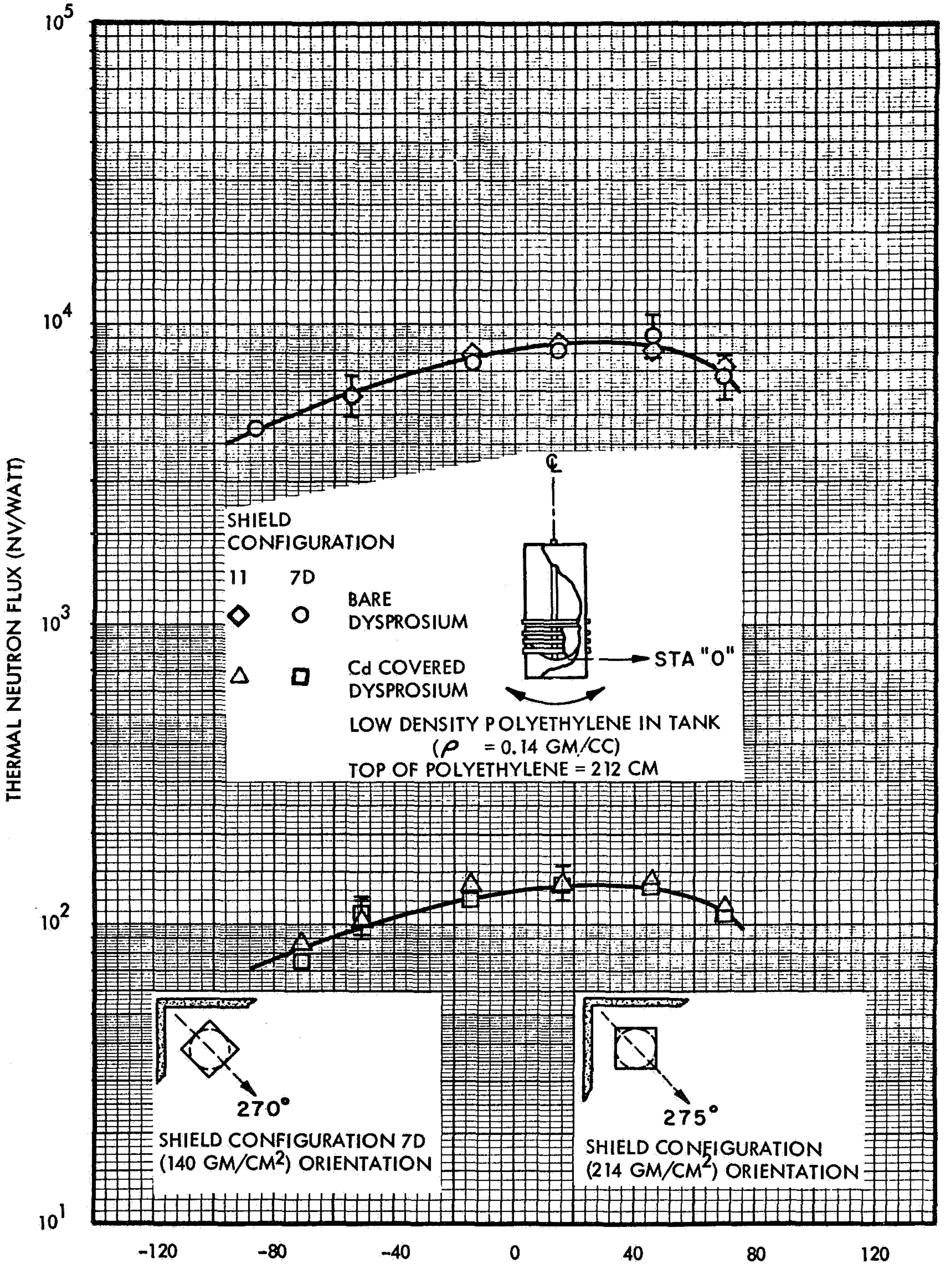

612601-14B

Figure 6-38. Thermal Neutron Flux as Measured with Dysprosium Vs Radial Distance from Centerline on Tank Hemisphere

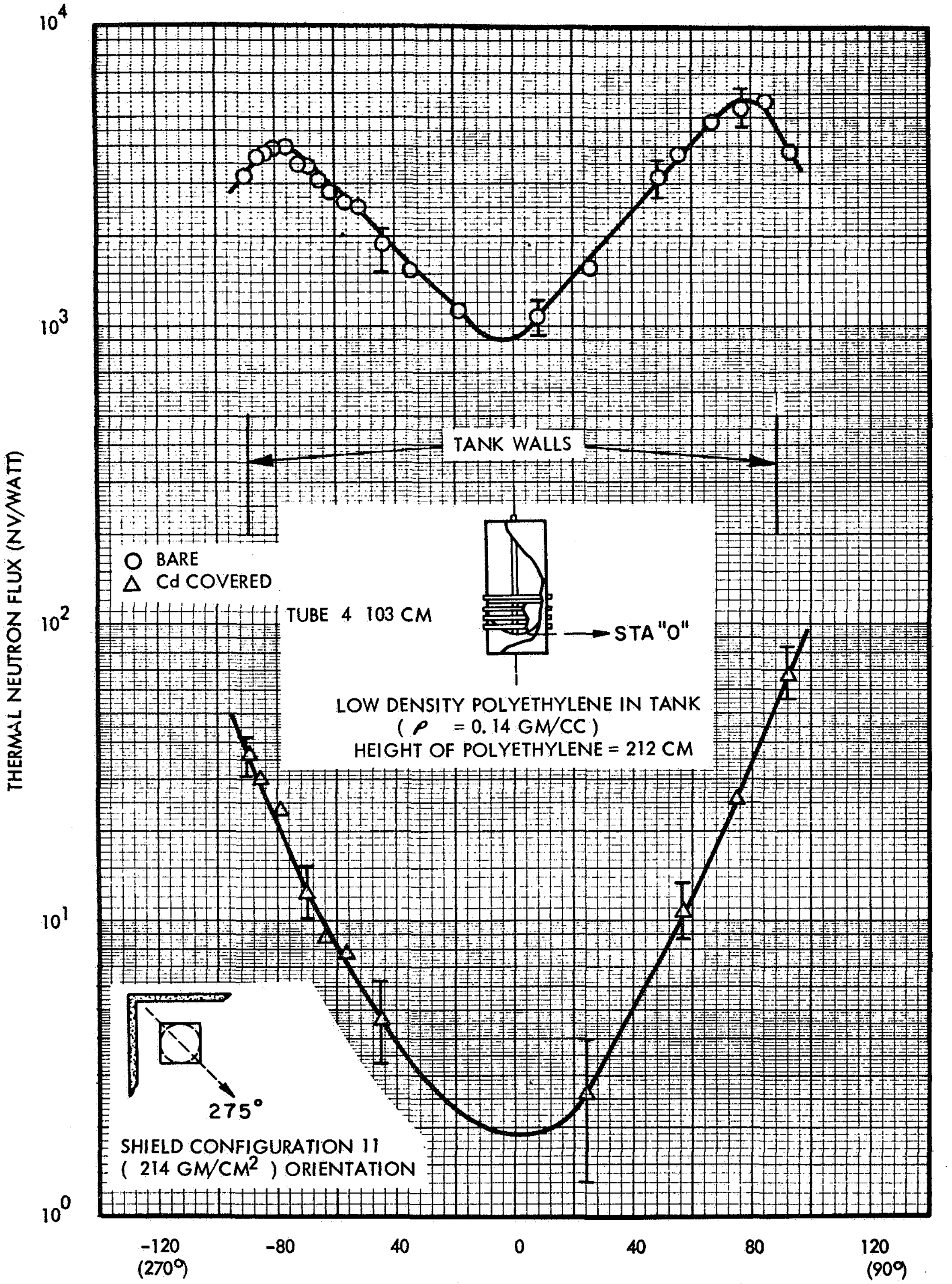

Figure 6-39. Thermal Neutron Flux as Measured with Dysprosium vs Radial Distance from Tank Axial Centerline (Tube 4)

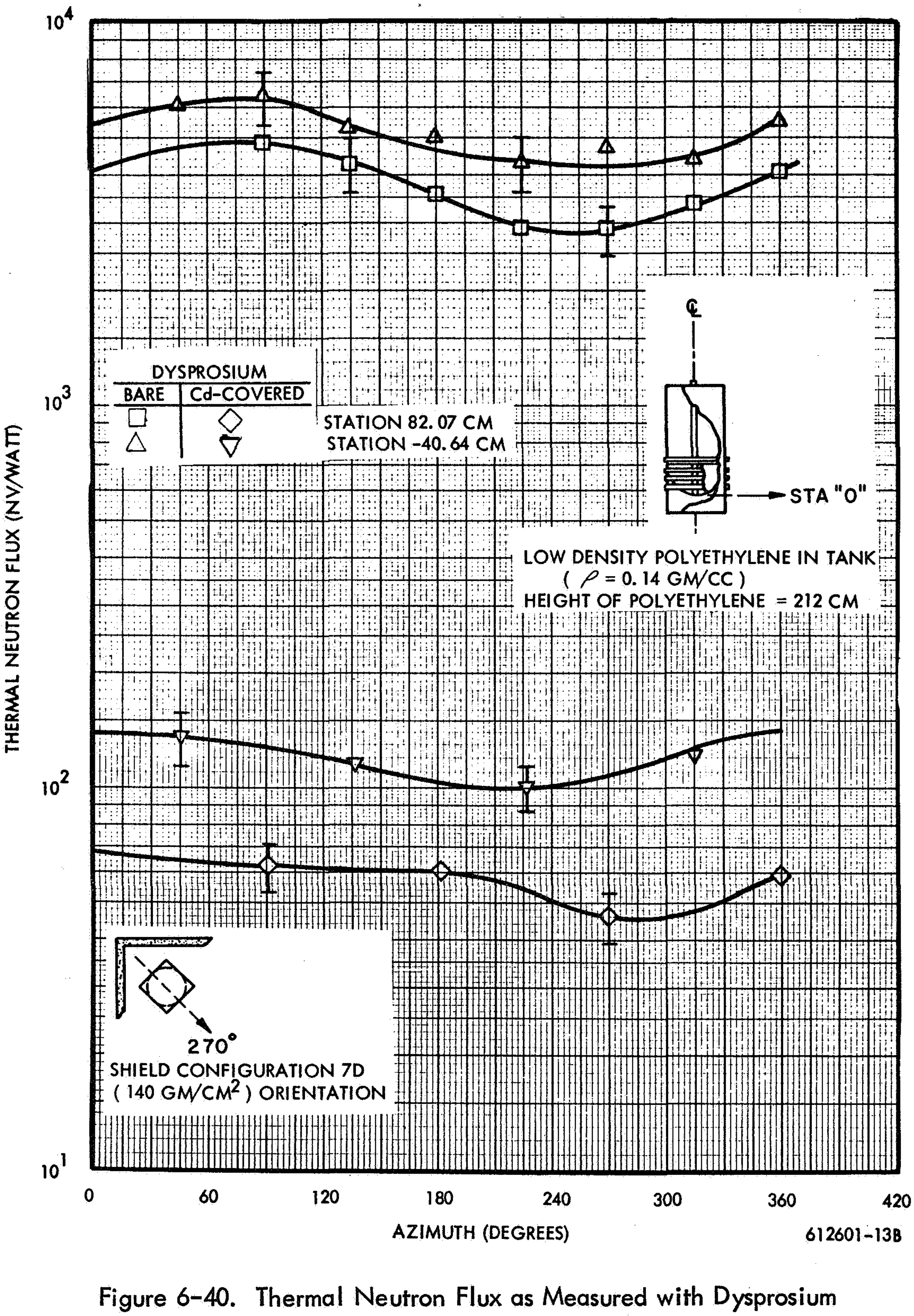

Figure 6-40. Thermal Neutron Flux as Measured with Dysprosium Vs Azimuth on Tank External Skin

6.3 SPECTRAL MEASUREMENTS

One purpose of the passive dosimetry data was to supplement the active dosimetry data in terms of providing better definition of the neutron spectra on the surface of the propellant tank. Some indication of a neutron spectra for Configurations 4B, 7D and 11 were obtained using threshold and resonance type foils. These foils included sulfur, boron-covered plutonium, dysprosium (bare and cadmium-covered) and gold (bare and cadmium-covered). In addition, a measurement was made with a U-238 fast fission chamber (containing 2 ppm U-235). The results of exposure of these detectors at approximately the bottom of the propellant tank near the axial centerline, is shown in Table 6-2. Also indicated in this table are the approximate energy ranges for which these foils apply. For example, sulfur has a threshold energy of 2.9 Mev, the U-238 is assumed to have an energy threshold of 1.5 Mev and the plutonium with 1 cm of B-10 is quoted* to have approximately 0.5 Kev threshold energy. The dysprosium and gold are resonance type foils with the gold having a resonance about 5 ev.

Both gold and dysprosium are close to a 1/v absorber for energies below approximately 1 ev. Hence, by utilizing the difference between the bare and cadmium-covered results, both these foils may be utilized as ~1/v thermal neutron flux detectors.

The results of the spectral induces measurements as shown in Table 6-2 show several features of interest. For example, in the fast energy range, comparison of the data for the three configurations --4B(high density polyethylene), 7D (low density polyethylene) and 11 (low density polyethylene)--shows the following:

The sulfur data ($E > 2.9$ Mev) are about a factor of 4 higher for Configuration 4B as opposed to Configurations 7D or 11. Similarly, the fast neutron data from the U-238 fast fission chamber ($E > 1.5$ Mev)are about a factor of 3 higher for Configuration 4B compared with 7D or 11.

The Pu-239 data ($E > 0.5$ Kev), however, are essentially the same (within the uncertainties of the results) for Configuration 4B as opposed to Configurations 7D and 11.

---

*"Fast Neutron Physics", P.489, Part 1, Volume IV, edited by Marion, J. B. and J. L. Fowler. Interscience monographs and texts in Physics and Astronomy.

TABLE 6-2

NEUTRON SPECTRAL RESPONSES MEASURED WITH ENERGY DEPENDENT DETECTORS NEAR THE BOTTOM OF THE TANK HEMISPHERE

Type of Detector	Energy Response	Configuration Equivalent flux*, n/cm^2 sec-w 4B	 7D	 11**
Sulfur	E > 2.9 Mev	224 ± 13%	50.3 ± 14%	46.8 ± 15%
U-238 Chamber (2ppm-235) (Cd-wrapped, in Boral box)	E > 1.5 Mev	768 ± 10%	270 ± 10%	210 ± 10%
Pu-239 foils in 1 cm B^{10}	E > 0.5 Kev	2770 ± 28%	3001 ± 28%	2190 ± 28%
Dy, bare	Thermal	9950 ± 13%	7910 ± 13%	7830 ± 13%
Dy, Cd-covered	E > 0.4 ev	162 ± 13%	144 ± 15%	129 ± 13%
Au, bare	Thermal	9300 ± 17%	8410 ± 9.2%	7090 ± 9.2%
Au, Cd-covered	E ~ 5 ev	2810 ± 9.2%	3460 ± 9.2%	2250 ± 9.2%

* Equivalent flux was obtained from saturated activity by use of the cross sections given in Table A-4.

** Low density polyethylene only.

And, if the flux in the energy interval 0.5 Kev $>$ E $<$ 1.5 Mev obtained by taking the difference between the Pu-239 and the U-238 values, the result is a slightly lower value for Configuration 4B as compared with the other two configurations. This result is not fully understood at this time, but it seems to indicate that the intermediate energy flux (0.5 Kev $>$ E $<$ 1.5 Mev) remains essentially constant for all three configurations. This is believed to be due to test cell scattering background.

It should be noted in Table 6-2 that a relatively large error exists in the quoted accuracy of plutonium data. This was due primarily (~25 percent) to the uncertainty in the absolute calibration of the detector.

Comparison of the thermal measured neutron fluxes by bare and cadmium-covered gold and dysprosium show that 1) the thermal neutron flux (E $<$ 0.4 ev) obtained by subtracting the corresponding cadmium-covered from the bare foil measurement are about 20-30 percent higher for dysprosium as compared to gold; 2) the measured thermal fluxes (E $<$ 0.4 ev are about 20 percent higher for Configuration 4B as compared with Configurations 7D and 11; and 3) the cadmium-covered gold and dysprosium measured epicadmium fluxes are about 30 percent higher for Configuration 4B as compared with Configuration11. Again, these differences are so small as to be essentially within the quoted accuracies of the measurements and thus the subcadmium and epicadmium thermal fluxes can be said to be essentially the same for all three configurations, again indicating a relatively large cell background scattering effect. Table A-4 in Appendix A of this report provides a listing of the cross-sections which were used to obtain the average fluxes in Table 6-2. By use of these cross-sections, one can obtain the saturated activity of the foils which could be used to compare directly with calculated foil activites.

An index of the thermal spectra is given by the cadmium ratio* of gold and dysprosium. The measured cadmium difference fluxes obtained by taking the difference of the bare minus the cadmium-covered foils for gold and dysprosium agree within about 30 percent at the location below the propellant tank. This is within the quoted accuracy of these data which thus lends confidence to the thermal flux measurements. It should be noted that the cadmium ratio for the gold is 3.3 at this location while that for dysprosium is about 61. This type of difference is to be expected since the dysprosium cross-section decreases slightly faster than the reciprical of the velocity of the neutron energy, i. e., 1/v, while that of gold is essentially a 1/v cross-section to the 5 ev resonance. Thus, the fact that the gold has a much lower cadmium ratio than that of dysprosium is to be expected and is some indication of the relative number of neutrons in the 0.4 to 5 ev range. The dysprosium cadmium ratios are somewhat larger and thus easier to measure. Thus, the cadmium ratio of dysprosium has been used as an index to changes in the thermal flux spectra in and around the propellant tank. Figures 6-41, 6-42, and 6-43 thus show the variation of cadmium ratio for dysprosium as plotted on the tank external skin vs. axial distance, vs azimuthal angle, and vs radial distance on the tank hemisphere. All of these data apply to Shield Configuration 4B with high

---

* The cadmium ratio, R_{cd}, was obtained from the formula:

$$R_{cd} = \frac{A_B}{F_{cd} A_{cd}}$$

where: A_B = Saturated activity of a bare foil
A_{cd} = Saturated activity of a cadmium-covered foil
F_{cd} = a correction factor

The need for F_{cd} arises from the fact that contrary to the ideal case, a certain number of epicadmium neutrons are absorbed by the cadmium covering and that a certain number of thermal neutrons succeed in passing through the cadmium. F_{cd} is typically a small correction, however, and was chosen for these measurements as 1.05 based on values given in ANL-5800, Section 9.1.7.

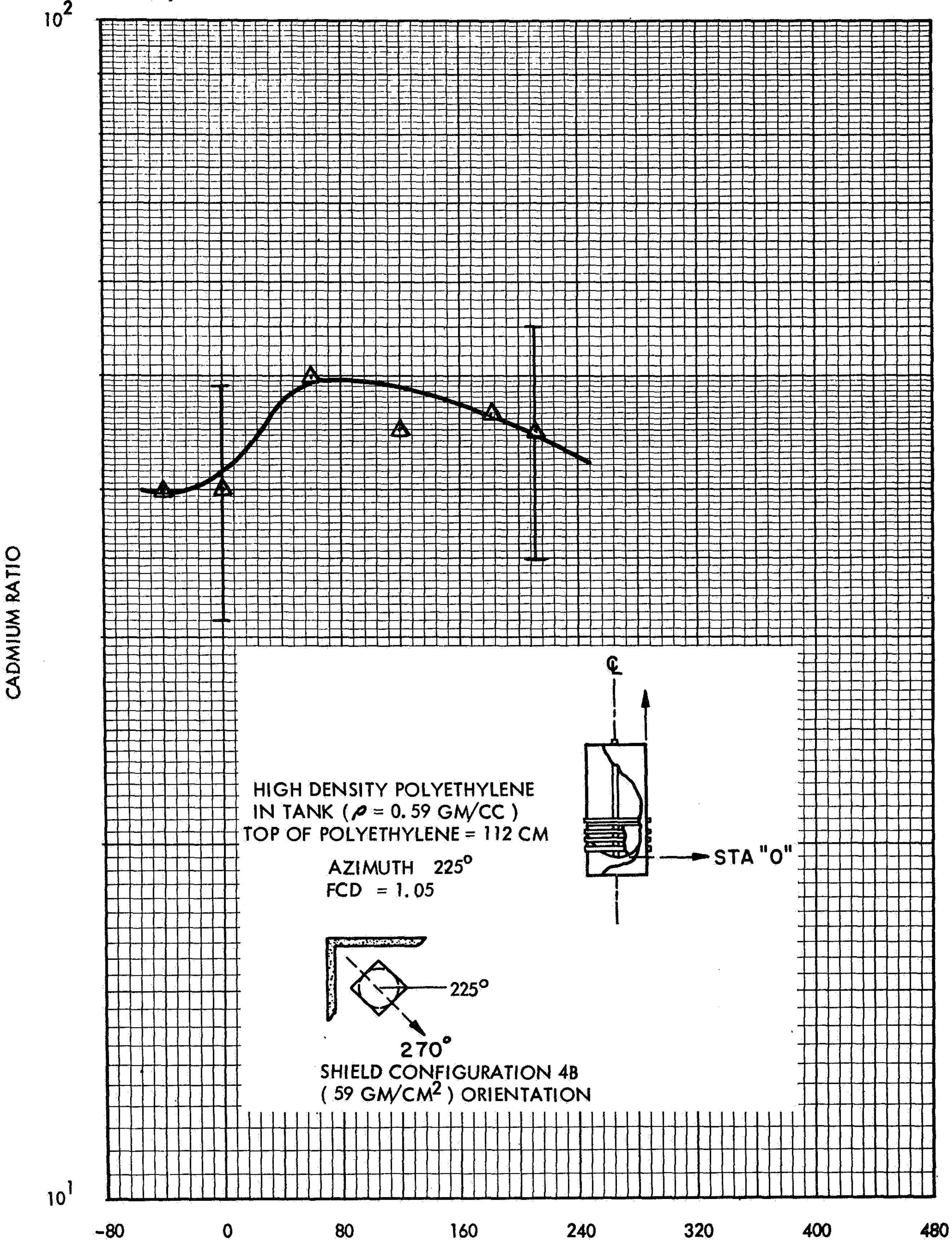

Figure 6-41. Cadmium Ratio as Measured with Dysprosium Vs Axial Distance on Tank External Skin

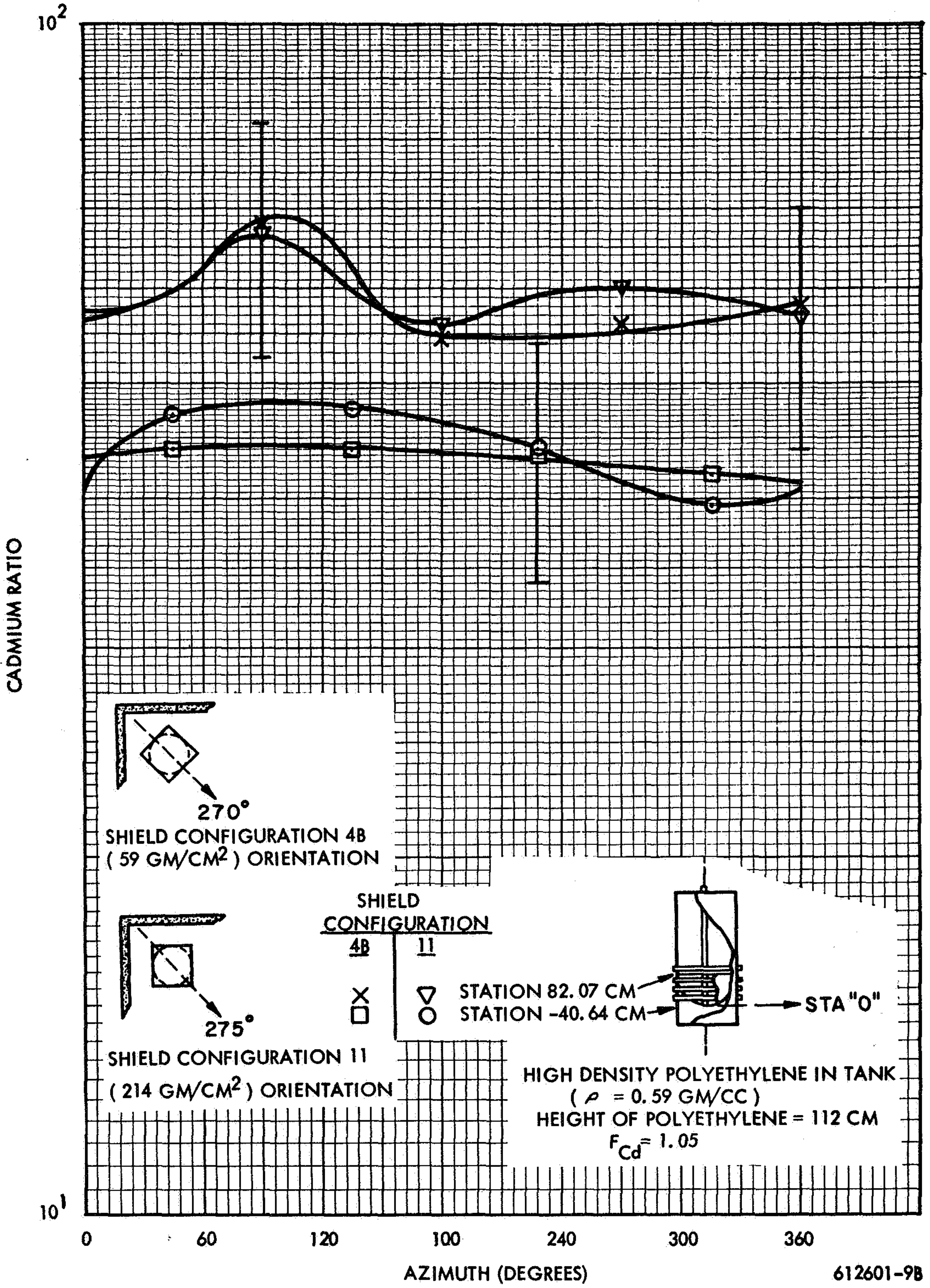

Fiaure 6-42. Cadmium Ratio as Measured with Dysprosium Vs Azimuth on Tank External Skin

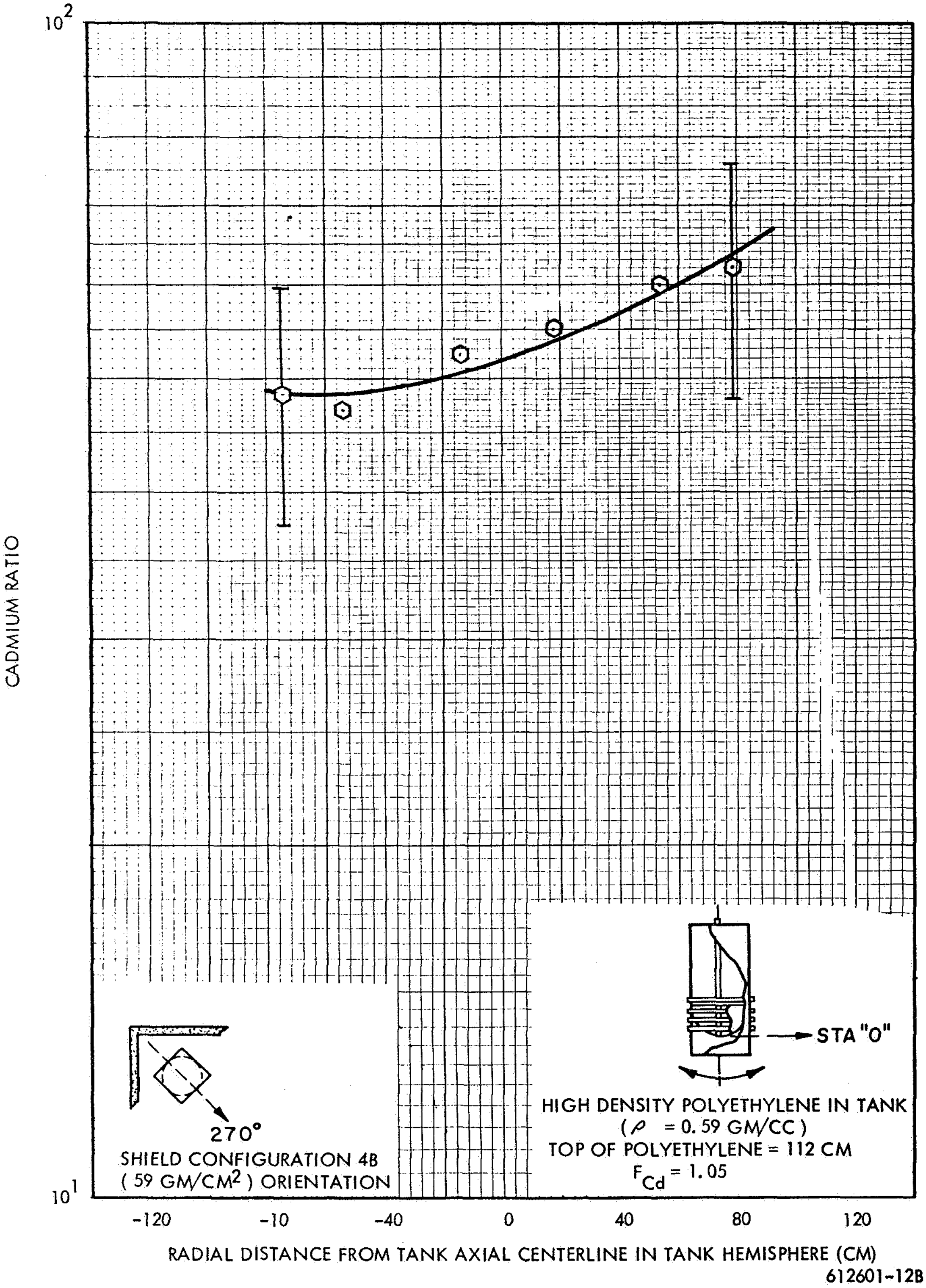

Figure 6-43. Cadmium Ratio as Measured with Dysprosium vs Radial Distance from Tank Axial Centerline on Tank Hemisphere

density polyethylene in the tank. Figure 6-41 indicates a cadmium ratio from station -40 cm to 0 cm of about 40. At station 60 cm, this cadmium ratio increases to approximately 50 and then decreases with increasing station from 50 to approximately 45 at 250 cm. Data were taken at an azimuthal angle of 225 degrees, i.e., in a direction away from the test cell walls. The lower cadmium ratio at the lower station, i.e., from -40 to 0, appears to be due to the fact that in this region there is no polyethylene in close contact to the detector. At an axial station of + 60 cm the cadmium ratio approaches 50. The increased thermalization as indicated by the larger cadmium ratio is believed to be due to the fact that in this area the polyethylene is much closer to the detector, i.e., the detector at + 60 cm is very close to the cylindrical portion of the polyethylene in the propellant tank. The slight decrease in cadmium ratio above a station of 60 cm is possibly due to self shielding effects of the tank.

Figure 6-43 shows the cadmium ratio as a function of radial distance on the tank hemisphere. It can be easily seen from these data that the cadmium ratio increases as we go toward the test cell wall as might be expected. This is of course due to the thermal neutrons produced in the test cell walls.

Figure 6-42 shows a plot of the cadmium ratio vs the azimuthal angle at two stations on the propellant tank for both Configurations 4B and 11. These data indicate that for the upper station, i.e., at 82.07 cm, there is a sharp increase in cadmium ratio to about 70 at an azimuthal angle of about 90 degrees corresponding roughly with the corner of the test cell in the direction towards the nearby test cell walls. No values exist at this elevation in the directions perpendicular to the test cell walls. Away from the test cell walls, i.e., an azimuthal angle of 270 degrees, the cadmium ratio drops off to about 55 or 60, thus indicating again an increase in thermal flux in a direction towards the test cell walls. At the lower station, however, i.e., at -40.64 cm, no such increase is shown to exist at the 90 degree azimuthal angle. It is believed to be due again to the fact that at the lower station more of the radiation is coming from the shield as opposed to the thermal neutrons coming from the test cell wall. Thus, the increase in the direction towards the test cell wall is not as marked as it is for the higher station. Overall, these data again indicate that a sizable thermal neutron background is produced from thermalization and scattering from the test cell walls. The magnitude of this thermal flux background is discussed more fully in the section on thermal neutron measurements.

6.4 UNCERTAINTIES IN ACTIVE AND PASSIVE MEASUREMENTS

6.4.1 Active Measurements

The accuracy of active dosimetry measurements has been estimated for each of the detectors used. Table 6-3 summarizes the contributing sources of uncertainty on the basis of one-sigma estimates given in percent. Since these are independent in nature, the total uncertainty is taken to be the square root of the sum of the squares of the individual uncertainties.

Estimated measurement uncertainties in the CO_2 ionization chamber (RSG-8A) data include the statistical summation of the uncertainties due to calibration (± 2 percent), reactor power (± 5 percent) the accuracy of the readout of the detector current (± 3 percent), and the power reading (± 3 percent) for a total uncertainty of ± 9 percent.

Estimated uncertainties in the WX-5362 boron-lined ion chamber are the same as for the CO_2 ion chamber except for the calibration uncertainty of ± 5 percent (see Appendix A) to yield a total uncertainty of ± 8 percent.

Estimated uncertainties in the U-238 fast fission chamber include the statistical summation of the uncertainties due to calibration (± 7 percent), reactor power determination (± 5 percent), accuracy of readout of power level (± 3 percent), and the uncertainties due to counting statistics. The latter is, in general, small compared to the first three. This is especially true since an effort was made to take the same number of total counts regardless of counting rate. Hence, the counting statistics uncertainty is neglected and the overall uncertainty is estimated to be ± 9 percent.

6.4.2 Passive Measurements

The accuracy of the passive dosimetry neutron flux data has been estimated for each of the foil types used. Tables 6-4 and 6-5 summarize the principal sources of uncertainty on the basis of one-sigma estimates given in percent. Since these are independent

TABLE 6-3

ACTIVE MEASUREMENT UNCERTAINTIES

Source of Uncertainty	One-Sigma Uncertainty in Percent			
	Detector			
	CO_2	Hurst	WX-5362	Fast Fission
Instrument Calibration	2	5	5	7
Reactor Power Calibration	5	5	5	5
Accuracy of Instrument Readout	3	4 (max.)	3	
Power Reading	3	3	3	3
Total	7	9	8	9

TABLE 6-4

PASSIVE MEASUREMENT UNCERTAINTIES

	One-Sigma Uncertainty in Percent			
	Detector			
Source of Uncertainty	Dy	Au	S	Pu-239
Cross-Section	7.5	3.1	9.9	10
Alloy Content	7.3	--	--	--
Reactor Power Calibration	5	5	5	5
Absolute Efficiency Calibration	5	5	5	24.3
Misc. Electronics Effects	3.7	3.7	3.2	3.6
Epithermal Correction	2	10	--	--
Totals	13.3	13.2	12.6	27.0

TABLE 6-5

TLD AND PHYLATRON MEASUREMENT UNCERTAINTIES

Source of Uncertainty	One Sigma Percent TLD*	 Phylatron
Reproducibility	5	2
Uniformity	10	< 10
Power	5	5
Calibration	10	20
Readout Accuracy	1 to 10	5**
TOTAL	16 to 19	23% + 5**

---

*An additional uncertainty results from use in a mixed gamma neutron field as a direct consequence of the 3 mole percent $Mn:F_2$ contained in the $CaF_2:Mn$ TLD's. It is felt, however, that an upper limit of approximately 30 percent (due to neutron capture by the Mn) would be a reasonable assumption for those measurements.

**Absolute uncertainties [Rads (tissue)] in nature, the total uncertainty is taken to be the square root of the sum of the squares of the individual uncertainties. The resultant uncertainties, on a one-sigma basis, are ± 13.3 percent for dysprosium thermal flux, ± 13.2 percent for gold thermal flux, ± 12.6 percent for sulfur fast flux, ± 27.0 percent for Pu-239 fast flux, ± 23 percent for Phylatron fast dose, and ± 19 percent for TLD gamma dose. These uncertainties are in addition to those uncertainties due to counting statistics which are calculated separately for each data point. The error bars appearing on selected data points in the figures represent the statistical sum of the counting statistics and the above estimated statistical uncertainties on a one-sigma basis.

6.5 HEATING RATES

By the method described in Section 3.6 of this volume, heating rates have been calculated from the data just presented. The results are given in Table 6-6.

TABLE 6-6

DERIVED HEATING RATES IN LH_2

	Heating Rate in LH_2 (watts/cc)			
	Gamma		Neutron	
	Reactor Power		Reactor Power	
Configuration	1 Watt	1575 MW	1 Watt	1575 MW
7D*	7.5×10^{-13}	1.2×10^{-3}	-	-
4B**	7.5×10^{-12}	1.2×10^{-2}	1.5×10^{-11}	2.4×10^{-2}

All heating rates are given for a point located on the bottom of the tank hemisphere on the tank axial centerline and are derived for the "direct" radiation measurements.

* ± 100 percent

** ± 20 percent

APPENDIX A

DETECTOR CALIBRATION

A. 1 CALIBRATION OF WX-5362 BORON-LINED COMPENSATED ION CHAMBER

A WX-5362 compensated ion chamber (S/N 654402) was taken to ORNL* for calibration. It was placed in a Tower Shielding Facility beam port location where the $\phi_{th} = 49.5$ n/cm^2-sec-W ($\pm$ 5 percent). The TSF-II reactor was operated at a power level of 100 kw. Table A-1 presents the results of the operations.

TABLE A-1

Power Level (kw)	Experimental Arrangement	WX-5362 (AMPS)	Current Determination
100	Bare Beam Port	$2.92 \times 10^{-8} \pm (0.5\%)$	Zero Null
100	Cd over Beam Port	$1.26 \times 10^{-9} \pm (0.5\%)$	Zero Null
100	1 cm B-10 over Beam Port (Background)	$5 \times 10^{-11} \pm (1.0\%)$	Zero Null

$$\text{Calibration factor} = \frac{2.9 \times 10^{-8} - 1.21 \times 10^{-9}}{4.95 \times 10^{6}} \ \text{Amps/nv}_{th}$$

Thermal neutron calibration factor = 5.65×10^{-15} Amps/n/cm^2-sec $\pm$ 5.2 percent.

The WX-5362 measured Cd ratio is 24.2. This agrees with the ORNL value of 25.8 measured with a BF_3 detector.

As a method of intercomparison of the thermal neutron sensitivity of the three existing WX-5362 detectors, a series of measurements was made at the WANEF Radiation Calibration Facility (RCF). One WX-5362 at a time was placed in a paraffin-filled barrel together with the WANEF NBS standard 5 Ci PuBe neutron source. Approximately one inch

---

* Arrangements were made through C. Clifford of the Neutron Physics Division of the Oak Ridge National Laboratory.

of paraffin separated the detector and source. The detector currents were then read by the null method using a Keithley 417A picoammeter and a Keithley 261 picoammeter current source. Background current was negligible.

Factory calibration data was also obtained for two of the detectors. The factory calibration procedure consists of placing the detector in a three foot hollow cube which is surrounded on all sides by six inches of paraffin. A 2-1/2 Ci PuBe neutron source is also located within the cube. Flux mapping to determine the flux within this cube was done with gold and magnesium foils to measure the thermal and fast neutron flux, respectively.

Final results of all calibrations are given in Table A-2.

TABLE A-2

WX-5362 Detector	ORNL Calibration ($amps/n-cm^2-sec$)	Factory Calibration ($amps/n/cm^2-sec$)	WANEF Calibration* ($amps/n-cm^2-sec$)
SN 108	----	$(2.1 \pm 0.2) \times 10^{-15}$	$(2.23 \pm 0.1) \times 10^{-15}$
SN 104	----	$(1.5 \pm 0.15) \times 10^{-15}$	$(1.58 \pm 0.08) \times 10^{-15}$
654-402	$(5.65 \pm 0.28) \times 10^{-15}$	----	$(5.65 \pm 0.28) \times 10^{-15}$

A.2 CALIBRATION OF RSG-8A CARBON WALL IONIZATION CHAMBER

The RSG-8A, SN G-928 carbon wall ionization chamber was calibrated for WANEF by the National Bureau of Standards.

The RSG-8A, SN G929 detector was then calibrated against the above NBS calibrated detector using the 30 Ci Co^{60} source located at the WANEF RCF. Measurements at several distances verified close adherence to the inverse square law indicating an insignificant amount of scattering.

The calibration of the Co^{60} source radiation field (38.25 ± 0.9 RHM**) thus obtained gave very good agreement with the manufacturers calibration (38.0 ± 1.1 RHM).

---

* Calculated from ORNL calibration and intercompaired through WANEF paraffin barrel.

** Roentgen per hour at a distance of one meter.

This source strength is as of April 1, 1968.

Sensitivities of the detectors are given in Table A-3.

TABLE A-3

Detector	Co^{60} Calibration (R/amp-hr)	Cs^{137} Calibration (R/amp-hr)
SNG-928	$(2.36_4 \pm 0.04_7) \times 10^{11}$	$(2.43_6 \pm 0.04_9) \times 10^{11}$
SNG-929	$(2.24_6 \pm 0.04) \times 10^{11}$	----

A.3 CALIBRATION OF U-238 (2 PPM U-235) FISSION DETECTOR

The U-238 fission detector SN 672602 was calibrated with the 5 Ci PuBe neutron source. The PuBe source was calibrated at NBS for total neutron emission rate. This value was $8.68 \times 10^6 \pm 1.6$ percent neutrons/second. The U-238 detector was wrapped in 20 mil cadmium for the calibration. The counting rate was then taken as a function of separation distance. The background of the detector was taken and subtracted from the total counting rate. The results of this procedure are plotted in Figure A-1. A $1/r^2$ fall-off with radial distance r from the source is also plotted. Good agreement of the counting rate versus position with the $1/r^2$ value is obtained for separation distances greater than 25 cm.

Since the fall off in flux follows the $1/r^2$ law, the neutron flux from the PuBe source at the detector position can be obtained from the following equation.

$$\phi_{PuBe} = \frac{S_o}{4\pi r^2} \tag{1}$$

where:

S_o = 8.68×10^6 n/sec emission rate of PuBe neutrons

r = source detector separation distance in cm.

The efficiency of the detector for PuBe spectrum neutrons becomes

$$\epsilon_{PuBe} = (\text{Counts/sec})/(\text{n/cm}^2\text{-sec}) \tag{2}$$

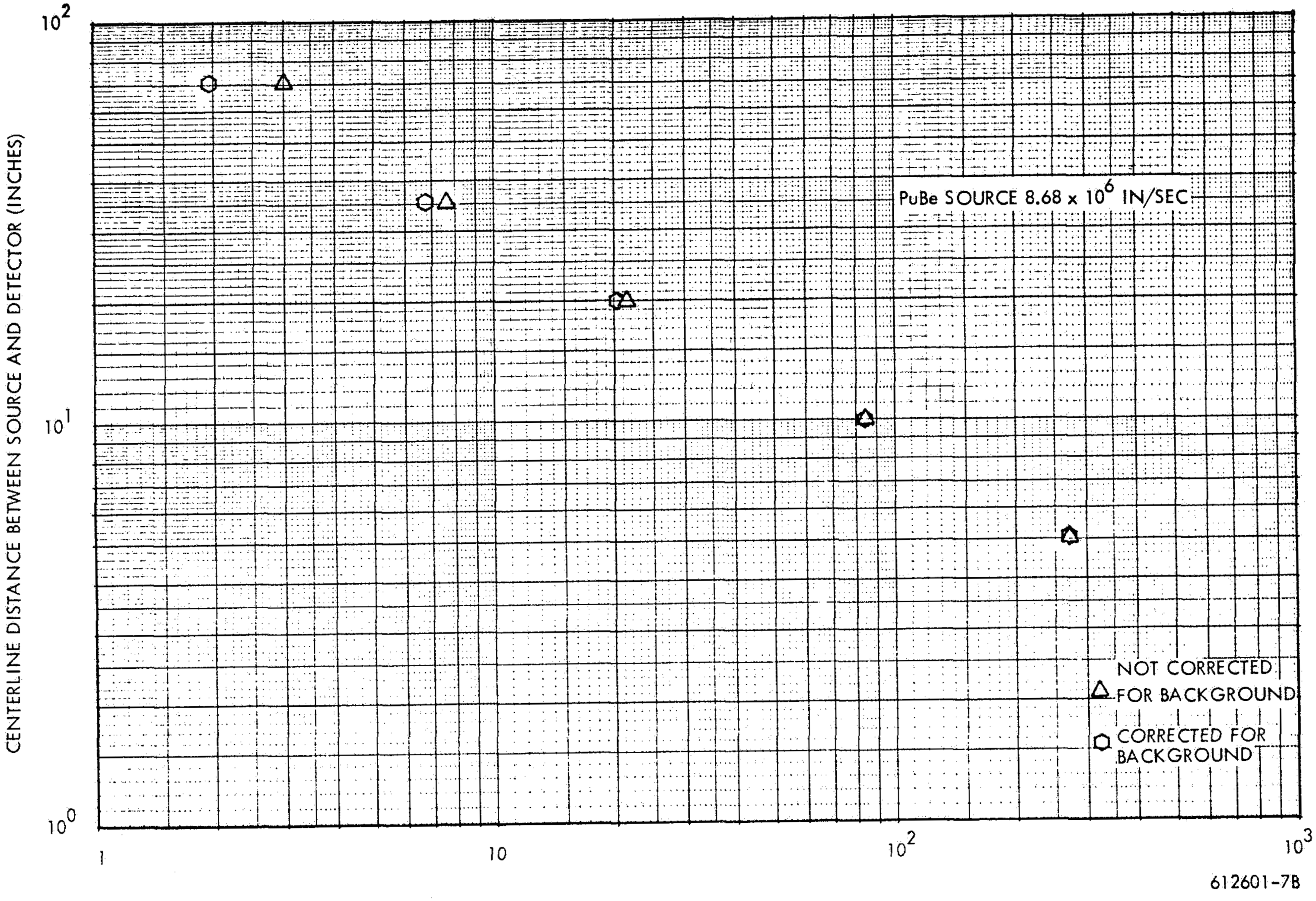

Figure A-1. Counting Rate as Outlined by a WX-30748 Fast Fission Detector Versus Detector - Source Distance or

$$\epsilon_{PuBe} = CPS/\phi_{PuBe} \qquad (3)$$

The quantity desired in the measurements with the detector is the flux at the detector location. Since the spectrum of neutrons is not the same as the PuBe spectrum, a correction for the U-238 fission cross section must be made.

Due to absorption and electronic bias in the operation of the detector, there will be fission fragments that are not detected or registered as a count. Neglecting anisotropic emission of the fission fragments, the following relationship is valid.

$$\frac{\text{Observed Fiss/sec}}{\text{Actual Fiss/sec}} = \text{Constant} = K$$

Since there are two fragments emitted per fission (but one is absorbed in the walls), the observed fissions per second are actually counts per second. The constant K is independent of the neutron spectrum if anisotropic emission of fission fragments is ignored. Therefore to obtain a relationship for fission spectrum neutrons, the following relationship holds.

$$\frac{FCPS}{PFPS} = \frac{FSCPS}{FSFPS} = K \qquad (4)$$

where

PCPS = Counts per second (Observed fissions per second for PuBe neutrons.

PFPS = Actual fissions per second for PuBe neutrons.

FSCPS = Counts per second = observed fissions per second for fission spectrum neutrons

FSFPS = Actual fissions per second for fission spectrum neutrons

$$PFPS = \frac{Na}{A} M \phi_{PuBe} \bar{\sigma}_{PuBe} \qquad (5)$$

$$FSFPS = \frac{Na}{A} M \phi_{FS} \bar{\sigma}_{FS} \qquad (6)$$

where

Na = Avogadros' number

A = Atomic weight - 238

M = Mass of U-238

ϕ_{PuBe} = n/cm^2-sec of PuBe spectrum neutrons

$\bar{\sigma}_{PuBe}$ = PuBe neutron spectrum weighted fission cross section of U-238

ϕ_{FS} = n/cm^2-sec of fission spectrum neutrons

$\bar{\sigma}_{FS}$ = Fission neutron spectrum weighted fission cross section of U-238

Inserting the equations 5 and 6 into 4 yields

$$\frac{PCPS}{\phi_{PuBe}\;\bar{\sigma}_{PuBe}} = \frac{FSCPS}{FS\;\;\bar{\sigma}_{FS}}$$

From equation 3, it is seen that

$$\frac{PCPS}{\phi_{PuBe}} = \epsilon_{PuBe}$$

Therefore,

$$\epsilon_{FS} = \frac{FSCPS}{\phi_{FS}} = \epsilon_{PuBe}\;\frac{\bar{\sigma}_{FS}}{\bar{\sigma}_{PuBe}} \qquad (7)$$

From ANL-5800, $\bar{\sigma}_{FS}$ = 0.555 barns.

The PuBe neutron spectrum fission weighted cross section was obtained by using the PuBe neutron spectrum given in ORNL-4134 and the fission cross section of U-238 given in BNL-325, 2nd Edition. Equation (8) was used to obtain the value of $\bar{\sigma}_{PuBe}$.

$$\bar{\sigma}_{PuBe} = \frac{\int_{1\ Mev}^{12\ Mev} \sigma_F \ \phi_{PuBe} (E) \ dE}{\int_{1\ Mev}^{12\ Mev} \phi_{PuBe} (E) \ dE} \qquad (8)$$

The hand calculation was performed by taking a mean ϕ and $\bar{\sigma}_F$ for 0.5 Mev intervals from 1-12 Mev.

A value of $\bar{\sigma}_{PuBe}$ = 0.648 barns was obtained. Therefore,

$\epsilon_{FS} = \epsilon_{PuBe} \dfrac{0.555}{0.648} = 1.078 \times 10^{-3}$ (Counts/sec)/(n/cm^2-sec) for the U-238 fission detector.

Based upon an intercomparison in the test fixture, the sensitivity of detector S. N. 680401 is 1.06×10^{-3} (counts/sec)/(n/cm^2-sec).

A.4 CALIBRATION OF THE HURST PROPORTIONAL COUNTER

The Hurst proportional counter (Reuter-Stokes RSN-48) was calibrated using the NBS calibrated 5 Ci PuBe neutron source. The calibration procedure is described as follows: The RSN-48 has an internal Pu-239 α source that can be exposed by the operation of a solenoid. Since the counter sensitivity is affected by temperature and ingassing of the cyclopropane into the polyethylene liner, the chamber had to be calibrated prior to its use. Rather than expose the chamber to the PuBe source prior to taking data, the internal Pu-239 α source was used as the standard to determine day-to-day changes in the detector characteristics. The following procedure was used to determine the detector calibration with a PuBe source.

1) The detector was exposed to a known PuBe neutron flux from a PuBe source and data was obtained.

2) Immediately after this data was obtained, the internal Pu-239 α source was exposed and data again was obtained.

Prior to obtaining data on a reactor run, the following procedure was used:

1) The internal α source was exposed and data was obtained.

2) The data for the reactor run was obtained with the shutter to the α source closed.

The principle of operation of the detector to obtain energy deposition is based on the Bragg-Gray principle. When the detector is exposed in a known neutron field, the dose measured by the detector is*

$$D_o \left[\frac{\text{Rads (Tiss)}}{\text{n/cm}^2}\right] = \frac{E_a, \text{ (Mev)} \quad (1.6021 \times 10^{-6} \left(\frac{\text{Ergs}}{\text{Mev}}\right)}{M_{\text{gross}} \bullet 100 \left(\frac{\text{Ergs}}{\text{gm-rad}}\right) \bullet 1.45 \bullet T, \text{ (sec)}} \; \phi_n, \left(\frac{n}{\text{cm}^2\text{-sec}}\right) \qquad (1)$$

where

D_o = Rads (tissue) measured by the detector per n/cm^2 incident

E_a = Energy absorbed by the gas in Mev

1.6021×10^{-6} = Conversion factor from Mev to Ergs

M(gms) = Mass of cyclopropane gas in the detector

100 = Conversion of Ergs/gm to Rads

1.45 = Conversion of Rads (cyclopropane) to Rads (Tissue).

T = Counting time

ϕ_n = Neutron flux incident on the detector.

Since the detector is a Bragg-Gray chamber with polyethylene walls and cyclopropane gas, it measures directly the absorption of neutron kinetic energy in units of Rads (cyclopropane) and to obtain Rads (tissue), the conversion factor 1.45 was used. This factor is within a few percent of being independent of the neutron energy.

---

* T. D. Hones, D. R. Johnson & J. H. Thorngate, "Neutron Dose Conversion Factors for PuBe and PoBe Sources", Health Physics, Volume II, pp, 519-522, 1964.

The dose rate for the PuBe neutrons at the detector was calculated from the flux of neutrons obtained from the known emission rate and an appropriate flux-to-dose conversion factor.

$$K_n (T_c) = \left(\frac{\text{Rads (Tiss)}}{n/\text{cm}^2}\right) \times \left(\frac{n}{\text{cm}^2\text{-sec}}\right) \qquad (3)$$

$$\frac{n}{\text{cm}^2\text{-sec}} = \frac{8.68 \times 10^6}{4 \pi r^2} \quad \frac{n}{\text{cm}^2\text{-sec}}$$

$$\frac{\text{Rads (Tiss)}}{n/\text{cm}^2} = 3.9 \times 10^{-9} \quad \frac{\text{Rads (Tiss)}}{n/\text{cm}^2}$$

The source detector separation distance was 52.07 cm for the calibration. Since the source and detector dimensions are ≈ one-tenth this value, the use of the $1/r^2$ law is appropriate to determine the neutron flux. From the analyzer data and equations (2) and (3), the K_n (T_c) value was determined.

A.5 CALIBRATION OF THE PASSIVE DOSIMETRY

The calibration of the thermoluminescent dosimeters was accomplished by exposing a representative sample of them to a Co^{60} source of known dose rate at various distances. The accuracy of the determination including problems of reproducibility is then estimated at ± 10 percent.

The calibration of the sulfur dosimeters in terms of absolute disintegration rate was established by radiochemical means involving chemical separation of the P-32 activity of an irradiated pellet and absolute counting techniques. This was then used as a reference to establish the absolute efficiency of the beta counters in which the samples were counted. The accuracy of the calibration was ± 5 percent.

The calibration of the dysprosium-aluminum, plutonium, and the gold foils was accomplished by gamma spectrometry of irradiated foils to establish absolute disintegration rates which were then used to determine the efficiency of the beta counting system used for the experiment. The accuracy of the calibration of all foils except Pu-237, was ± 5 percent. The Pu-239 calibration accuracy was ± 25 percent.

The dysprosium-aluminum foils had been supplied as having a nominal content of 5 percent dysprosium by weight. A representative sample of the foils was analyzed by x-ray fluorescence techniques which compared them with a known standard of dysprosium-aluminum. The results indicated a content of 3.75 percent to an estimated accuracy of ± 7 percent.

Astronuclear Laboratory

APPENDIX B

DATA REDUCTION

B.1 ACTIVE DOSIMETRY DATA

A computer code for the WANEF PB-250 digital computers (Figure B-12) was written for data reduction of the RSG-8A gamma dose rate and the WX-5362 thermal neutron flux data. As a result, the preliminary results were generally available in units of Rads (carbon)/hr-watt and nv/watt, respectively within a few hours after the end of the run. The code also converted the voltage "position readout" into actual distance. After the actual power and detector calibration data became available, the data was then reprocessed to yield the final results.

Data from the WX-30748 fast fission detector was processed by hand to give threshold flux (E >1.5 Mev) primarily because of the relatively small number of points. Also, since many different counting times were used within any one run, it was not feasible to use the same data reduction code as was used for the RSG-8A and the WX-5362 data.

The RSN-48 data was reduced by the WANEF PB-250 computers and the WANG-370 calculator. The final results were obtained in mrads (tissue)/hr-watt.

All data is referenced to either the outside bottom of the tank hemisphere and/or the axial centerline, whichever is appropriate.

B.2 Au, Dy AND S PASSIVE FOIL DOSIMETRY DATA

When an appropriate detector is placed in a position where the neutron flux is ϕ (E,x,y,z), the activity of the detector at any time during its irradiation can be calculated by writing an equation expressing the rate of change of a radioactive species.

$$\frac{dn}{dt} = R - \lambda n \qquad (1)$$

TABLE B-1

CONSTANTS USED IN DATA REDUCTION

	$Dy^{164} \longrightarrow$	Dy^{165}	$S^{32} \longrightarrow$	P^{32}	$Au^{197} \longrightarrow$	Au^{198}	Pu^{239}	U^{238}
Atomic Number	66	66	16	15	79	79	94	92
Isotopic Weight (1)	163.9392		31.97207		196.96654			238.0508
Abundance (1)	0.2818		0.950		1.000			
Half Life (1)		141 min.		14.3 days		64.8 hours		
Decay Constant		4.9159×10^{-3} min.^{-1}		3.3661×10^{-5} min.^{-1}		1.7828×10^{-4} min^{-1}	239.0522	
Thermal Cross-Section (2)	2700 barns				98.8 barns			
Fast Cross-Section			0.300 barns				1.8 barns	0.555 barns 3)
Effective Threshold Energy	Thermal		2.9 Mev		Thermal		1/2 Kev	1.5 Mev 3)

(1) Chart of Nuclides, July 1966

(2) BNL 325, 2nd Edition, Supp. 2

(3) ANL-5800, 2nd Edition, Reactor Physics Constants, July 1963

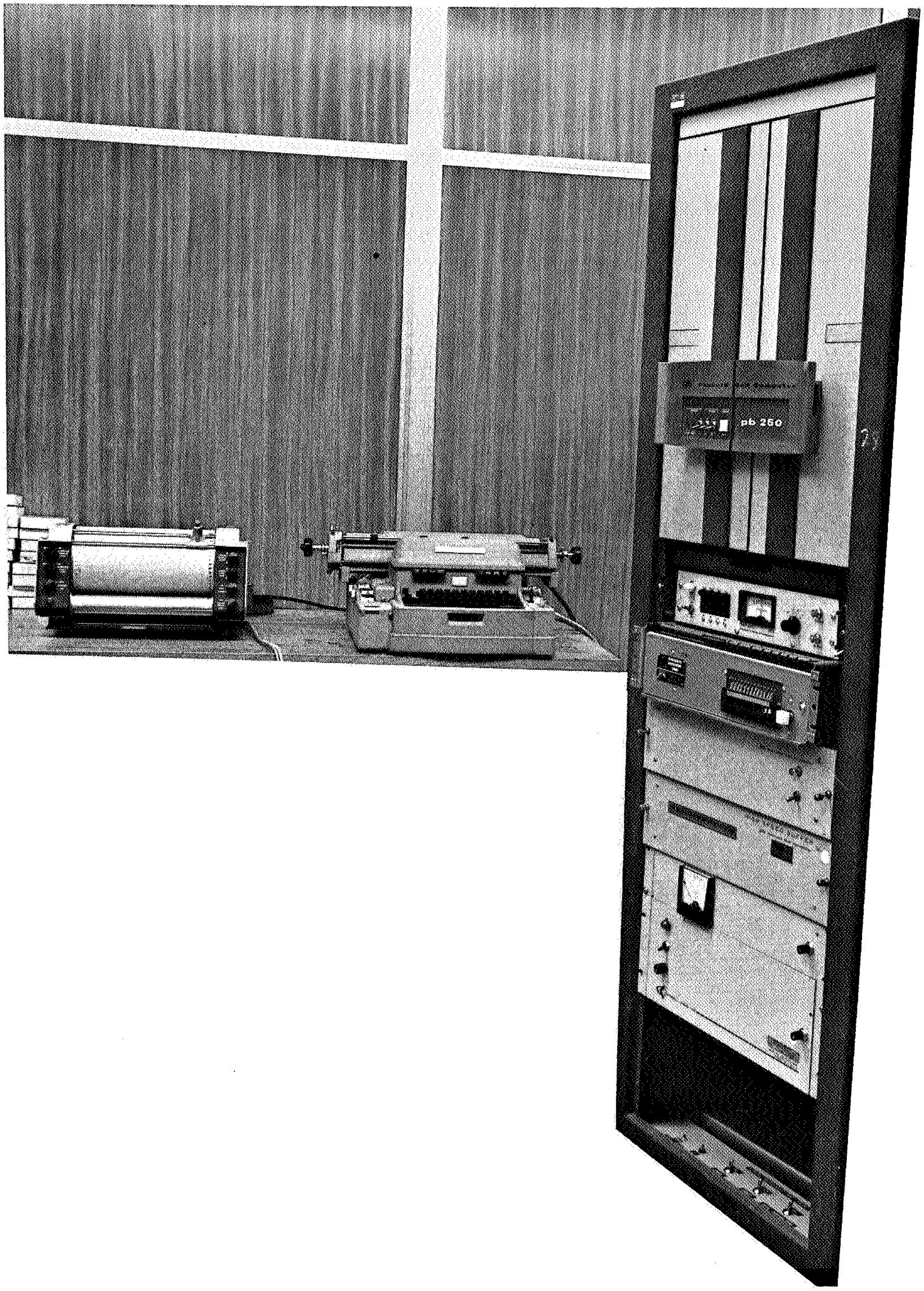

Figure B-1. One of the PB-250 Data Reduction Computers where

n is the number of radioactive atoms at time t

R is the radioactive atom rate of production

λn is the rate of decay or the activity A of the detector

The rate of production,

$$R = \int_{VOL} \int_{0}^{\infty} N(x,y,z) \; {}_{a} \; (E,x,y,z) dV dE \qquad (2)$$

where

σ_a is the microscopic activation cross-section

$N(x,y,z)$ is the number of atoms per unit volume of the type being activated. The solution of Equation (1) assuming constant R and neglecting the small decrease in the number of stable atoms N is:

$$A = \lambda n = R \left(1-e^{-\lambda t}\right) \qquad (3)$$

where t is measured from the start of the irradiation and the activity is zero at $t = 0$. If a detector is irradiated for a very long time, i.e., $t = \infty$, then Equation (3) becomes

$$A = R\,(1 - e^{-\lambda.\infty}) = R = A_s \qquad (4)$$

where A_s is the saturation activity or the activity approached for an irradiation long compared with the mean life $1/\lambda$. Then Equation (3) can be written as

$$A_o = A_s\,(1 - e^{-\lambda t_o}) \qquad (5)$$

where A_o is the activity at the end of irradiation and t_o is the irradiation time.

If the detector is counted between times t_1 and t_2 measured from the end of the exposure, the number of total counts C* will be

---

* Corrected for counting system resolving time, i.e., $C_{corr.} = C_{unc}/1-C_{unc}T_c$

$$C = E\int_{t_1}^{t_2} A_o e^{-\lambda t'} dt' + B = E \frac{A_o}{\lambda} (e^{-\lambda t_1} - e^{-\lambda t_2}) + B \qquad (6)$$

where

C_{corr} = true counts/unit time
C_{unc} = observed counts/unit time
T_c = resolving time/count
E is the efficiency of the counting system for the particular detector of interest.
B is the total background counts between t_1 and t_2.

Combining Equations (5) and (6) we get:

$$A_s = \frac{\lambda(C - B)}{E(1 - e^{-\lambda t_o})(e^{-\lambda t} - e^{-\lambda t_2})} \qquad (7)$$

where A_s is the saturation activity per second (if λ is in units of sec^{-1}). The saturation activity per second, per watt of irradiation power, per gram of foil material used is

$$A_s = \frac{\lambda(C - B)}{E(1 - e^{-\lambda t_o})(e^{-\lambda t_1} - e^{-\lambda t_2}) P W} \qquad (8)$$

where P is the irradiation power in watts and
W is the foil weight in grams

Assuming energy independent flux and cross section or a spectrum weighted cross section, the flux can be calculated by

$$\phi = \frac{A_S}{\sigma_a NT} \quad \text{where: T is the foil thickness} \qquad (9)$$

Equations (8) and (9) were programmed for the Raytheon 250 computer to reduce the data.

Again, all data is reported in cylindrical coordinates with the origin located at the bottom of the tank hemisphere on the tank axial centerline. Table B-1 gives the constants used in the data reduction process.

B. 3 TLD AND PHYLATRON DATA

All TLD and Phylatron data were reduced by the use of calibration curves. The TLD calibration curve was obtained at WANEF by exposing TLD's in a known field and then plotting the reading obtained against the exposure dose. The actual data reported in this document are then generated by the inverse of this process.

The Phylatron calibration curves were supplied by the device manufacturer. Although an additional correction based upon neutron spectra factor is possible, preliminary calculations indicate at most a small correction and so it was not employed.

APPENDIX C

ELEMENTAL ANALYSIS OF TANK STRUCTURE

An analysis was obtained for various material samples on the tank. The results are shown in Table C-1.

TABLE C-1

ELEMENT ANALYSIS OF TANK STRUCTURE*

Element	Tank Skin Skirt	Tank Skin Near Skirt	Tank Internal Angle	Cover Flange on Tank Hemisphere	Rivets**	Sleeves	Rivets	Reinforcing Ring on Bottom of Tank	Tank Skin on Hemisphere	Green*** Paint	White Paint
Ag										0.003	0.003
Al	Balance	Balance	Balance	Balance		Balance	Balance	Balance	Balance	0.08	1.0
As											
Au										0.1	0.1
B										0.003	0.003
Ba										0.01	0.06
Be										0.0003	0.0003
Bi										0.03	0.03
Ca										0.30	2.0
Cd										0.03	0.03
Co					0.01					0.03	0.03
Cr	0.2	0.2	0.2	0.2	0.04	0.2	0.2	0.30	0.2	5.5	0.06
Cs										0.1	0.1
Cu	0.06	0.08	1.68	0.27	0.07	0.31	1.5	2.0	0.09	0.01	0.01
Fe	0.21	0.23	0.18	0.37	Balance	0.38	0.15	0.17	0.19	1.5	3.0
Ga											
Ge										0.03	0.03
Hf											
Hg											
In										0.03	0.03
K										3.0	0.30
Li										0.001	0.005
Mg	5.20	5.05	0.95	0.90				1.02	4.80	0.56	2.3
Mn	0.64	0.75	0.1	0.20	0.75	0.1	0.1	0.20	0.45	0.04	0.06
Mo					0.25					0.03	0.03
Na										0.28	0.43
Nb					0.006					0.01	0.01
Ni	0.005	0.01	0.01	0.005	0.06	0.01	0.005	0.02	0.005	0.03	0.03
P										0.03	0.03
Pb					0.001					0.07	0.43
Rb										0.01	0.01
Sb										0.01	0.01
Si	0.19	0.20	0.60	0.70				0.68	0.17	2.0	3.2
Sn										0.03	0.05
Sr										0.01	0.01
Ta										0.01	0.1
Th										0.03	0.03
Ti	0.2	0.2	0.2	0.02		0.02				0.03	15
Tl										0.1	0.1
U										0.1	0.1
V					0.2					0.03	0.03
W										0.1	0.1
Zn	0.03	0.09	5.9	0.10		0.05	6.0	5.8	0.03	3.0	0.03
Zr					0.01					0.10	0.03

* Values shown are in w/o ± 10-30 percent relative as received.

** Rivet is possibly low alloy steel.

*** Paint was removed by gently scraping with a stainless steel spatula and then mixed with graphite for analysis.

APPENDIX D

A COMPARISON OF RADIATION MEASUREMENTS MADE IN LH_2 VERSUS THOSE MADE IN POLYETHYLENE SIMULATED IN LH_2

A series of radiation measurements* has been made in LH_2 using the ASTR reactor operated by General Dynamics/Fort Worth. Although these data are not directly comparable with the data contained in this report, some worthwhile insights may be obtained through a few simple comparisons. These will, to a first approximation, enable a comparison of the LH_2 and polyethylene simulated LH_2 data. Because of the vast differences in the experimental condition, only relative attenuations along the tank axial centerlines will be compared.

D.1 NEUTRON MEASUREMENTS

The only comparable data available for fast neutron attenuation is the fast neutron flux ($E > 2.9$ Mev) measured with sulfur. Figure D-1 shows the sulfur flux for the empty and LH_2 filled tank as measured at Fort Worth with the ASTR Reactor.

Figure D-2 shows the corresponding data obtained for the polyethylene ($\rho = 0.59$ gm/cc) filled tank with Shield Configuration 4B as obtained under the current series of measurements at WANEF.

Before making a comparison between these two sets of data, several experimental differences should be mentioned. They are as follows:

1) The separation distance between the reactor and the tank bottom is 14 inches for Configuration 2 of the Fort Worth data but is > 100 inches for the simulated LH_2 data.

2) The simulated LH_2 has slightly higher hydrogen density and contains carbon.

3) The LH_2 Configuration 2 interposed ~ 41 gms/cm^2 between the top of the reactor and the tank bottom while Configuration 4B interposed 59 gm/cm^2.

---

* Nuclear Radiation Heating in Liquid Hydrogen", NASA CR-54078

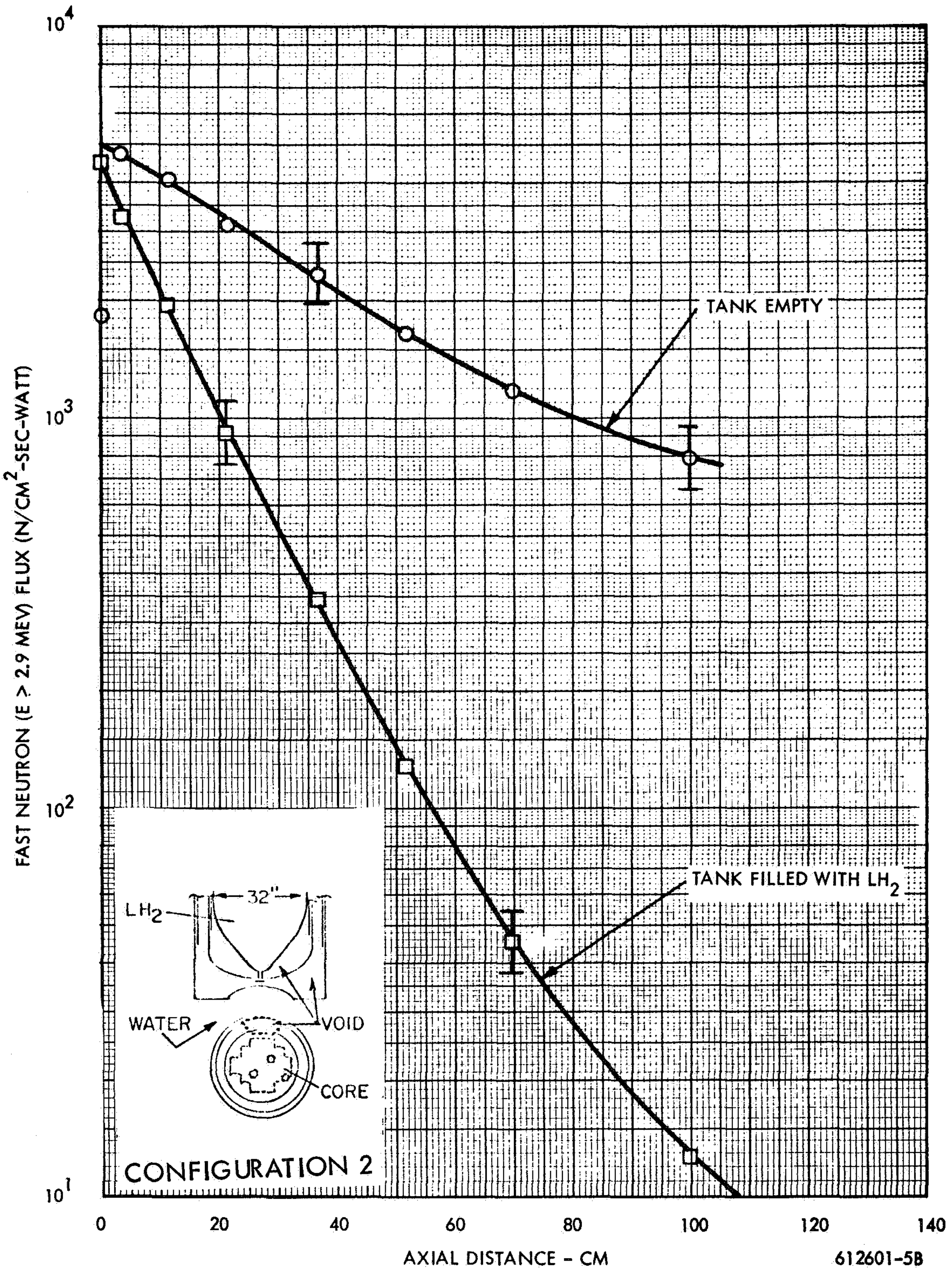

Figure D-1. Fast Neutron (E > 2.9 Mev) Flux in LH_2 versus Axial Distance for Configuration 2

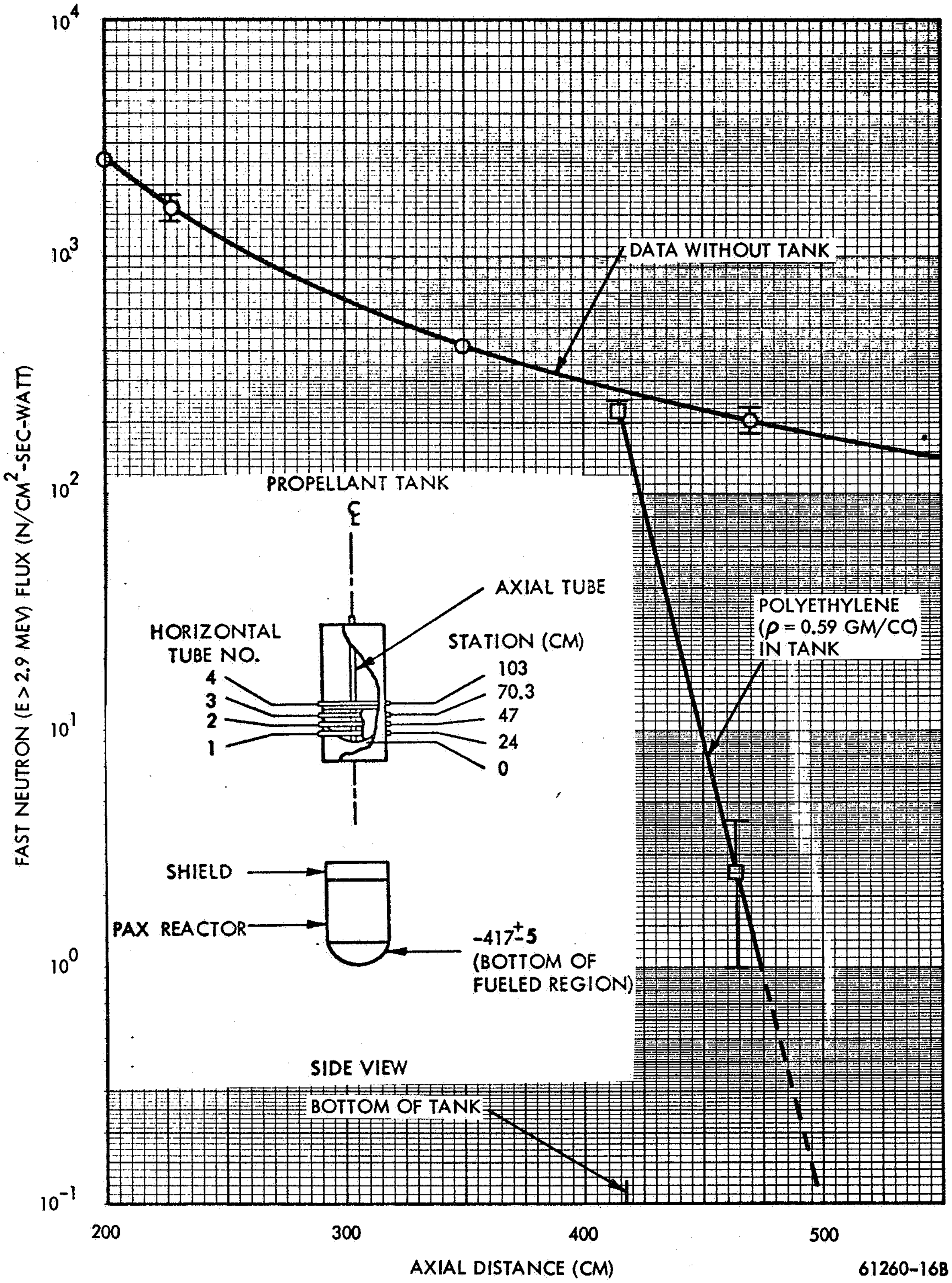

Figure D-2. Fast Neutron (E >2.9 Mev) Flux in Polyethylene versus Axial Distance

4) The base of the LH_2 dewar was conical in shape while that of the polyethylene tank was nearly a hemisphere.

5) The incident reactor neutron and gamma spectrum were not the same in the two cases since the Fort Worth experiments utilized a water moderated reactor (the ASTR) while the WANEF experiments utilized a NERVA type graphite moderated critical mockup.

Unfortunately, only Conditions 1 and 2 are at all amenable to simple hand calculations. Hence, these are the only factors for which corrections will be calculated.

In order to remove, to a first approximation, the effect of source-to-tank distance, let us divide the data taken with LH_2 (real or simulated) by the corresponding data where no hydrogen media is present. To aid in the comparison, the resultant curves will be normalized arbitrarily to unity at zero depth into the tank.

In order to remove the carbon fast neutron attenuation effects in the polyethylene simulated LH_2, effective carbon removal cross-section was utilized as follows: the lower curve in Figure D-3 was multiplied by exp (0.0256 X)

where X is the distance into the polyethylene (in cm)

and $0.0256 = \Sigma_r (C) \times \frac{\rho_p}{\rho_c} \times \frac{A_c}{M_p}$

where Σ_r (C) = the microscopic removal cross-section (0.08 cm^{-1}) for carbon having a density ρ_c of (1.6 gm/cc)

ρ_p = density of polyethylene (0.59 gm/cc)

A_c = Atomic Mass of carbon (12)

M_p = Unit molecular weight of polyethylene (14)

In order to correct for the slightly higher hydrogen density in polyethylene, the following correction was also made to the distance scale (after removal of carbon) on the simulated LH_2 data.

$$X_{corr} = \frac{\rho_p}{\rho_H} \times \frac{A_H}{M_p} \times X_{meas}$$

Figure D-3 shows the comparison of the distance corrected LH_2 data and the simulated LH_2 data corrected as mentioned above. The steeper slope exhibited by the simulated LH_2 data is felt to arise as a result of difference in tank bottom shape and for differences in leakage spectrum. This would be likely to cause a somewhat shallower attenuation curve for the conical bottom, then for the hemispherical bottom.

D.2 GAMMA MEASUREMENTS

A comparison between the LH_2 gamma data and the polyethylene simulated ($\rho = 0.59$ gm/cc) LH_2 gamma data was made in the manner previously described for neutrons. Here, however, the step dealing with the carbon removal cross section was omitted since the differences between LH_2 and CH_2 can be adjusted, presumably, simply by equating electron densities. The high density polyethylene data was used since the uncertainties associated with the "direct" radiation measurements in the appropriate density ($\rho = 0.14$ gm/cc) polyethylene were so large. Figure D-4 shows the LH_2 gamma data (as measured with cobalt glass) for Configuration 2 with and without LH_2 in the tank. Figure D-5 shows the corresponding data for the high density polyethylene LH_2 simulation with and without the tank.

The LH_2 data corrected for source-detector distance are shown in Figure D-6 as is the polyethylene data as corrected for density. It may be seen that the agreement is quite good up to 80 cm or so, in spite of the large correction made for differing densities. There are, however, at least two problems. In the LH_2 experiments, it was noted that the LH_2 appeared to shield some of the low energy gammas which presumably arose from capture in the water surrounding the tank. Another possibility is the thermal neutron capture gammas arising from the boroxy tank lining. Also, the polyethylene simulated LH_2 "empty tank" measurements were made without any tank in place. Hence, the capture gamma background is not consistent between the two sets of data. Also, a considerable difference also exists in the relative thermal neutron background fluxes between the two experiments.

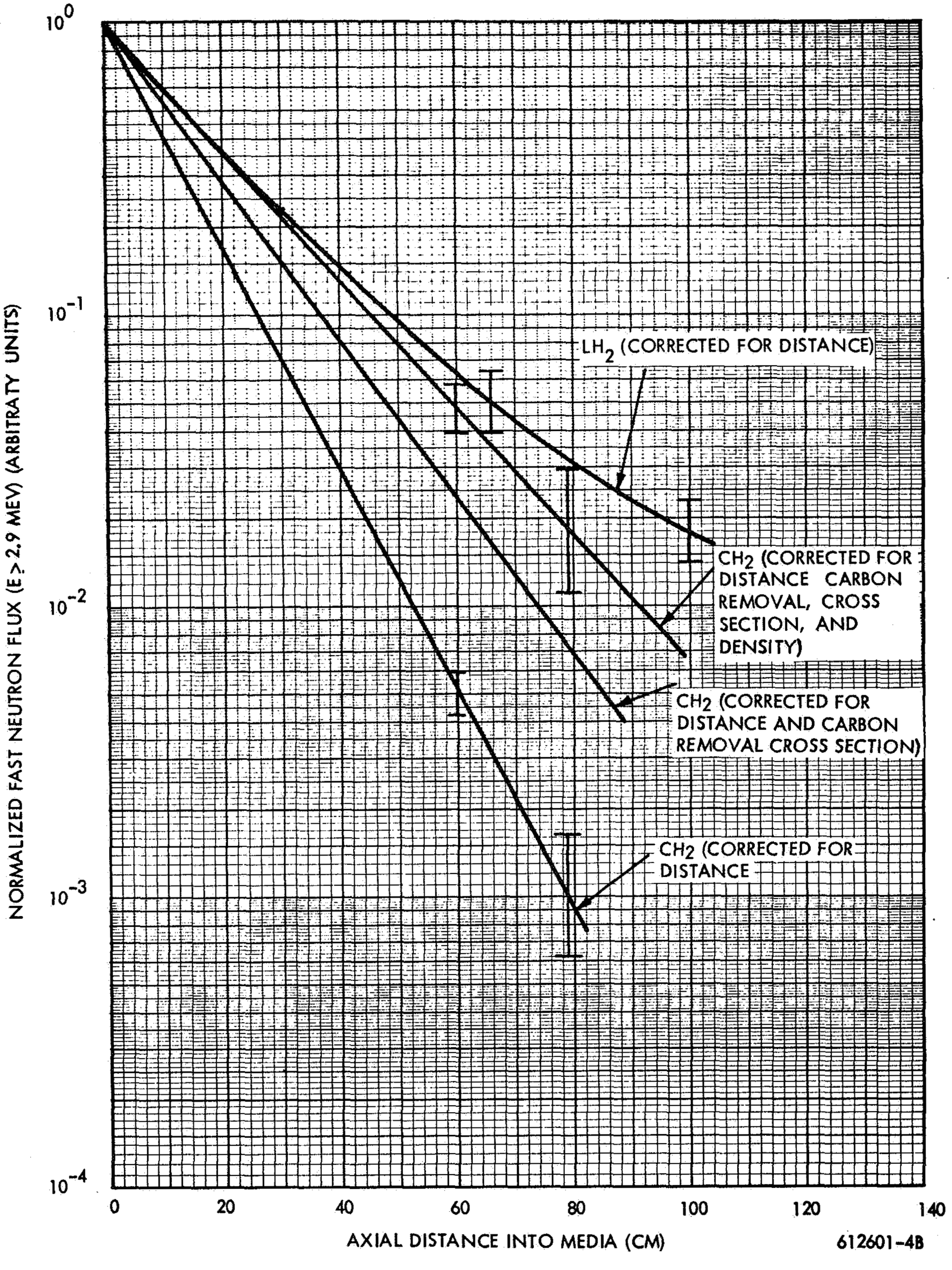

Figure D-3. A Comparison of Fast Neutron (E > 2.9 Mev) Flux in LH_2 and Polyethylene Simulated LH_2 versus Axial Distance into Media

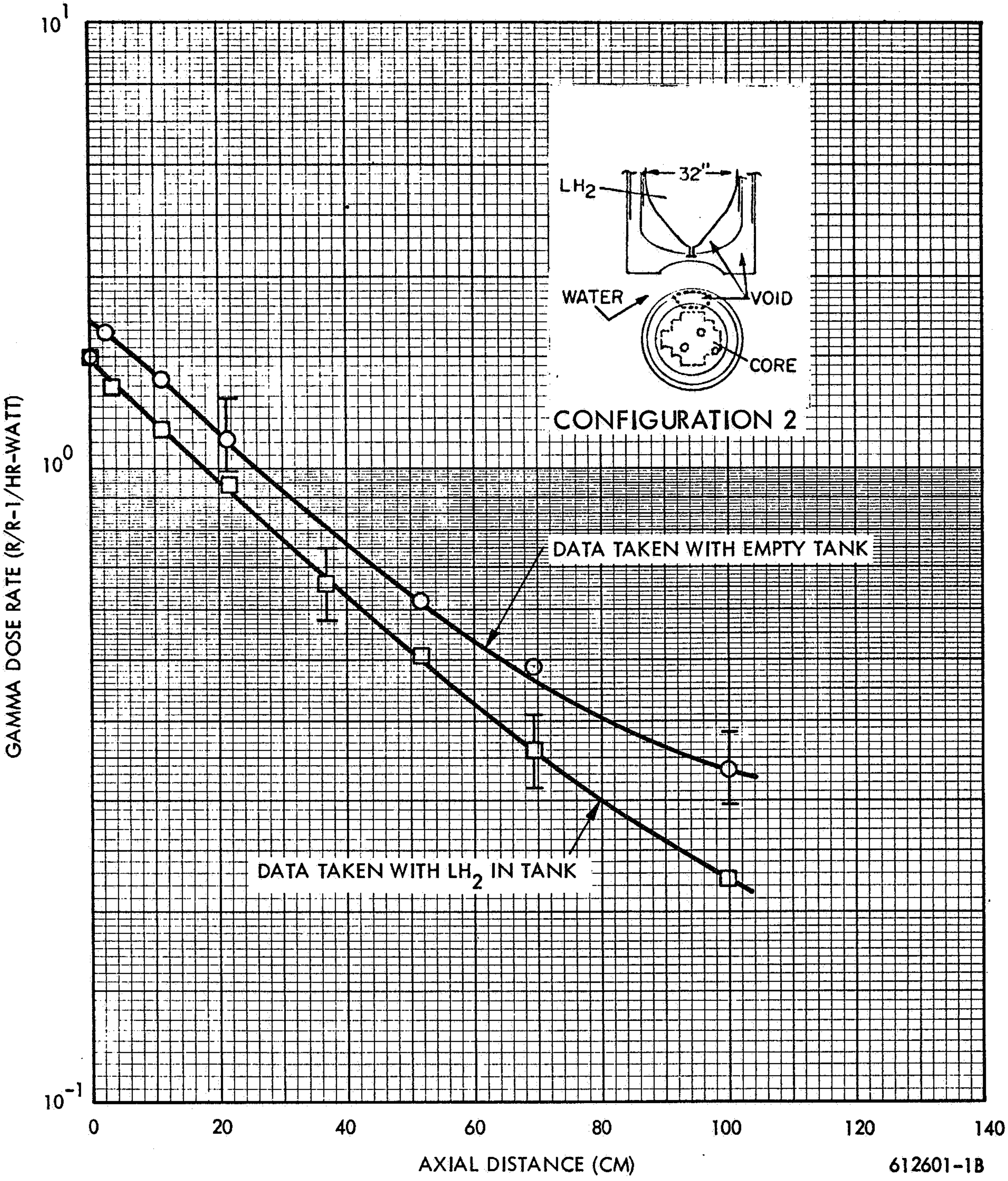

Figure D-4. Gamma Dose Rate as Measured with Cobalt Gloss versus Axial Distance

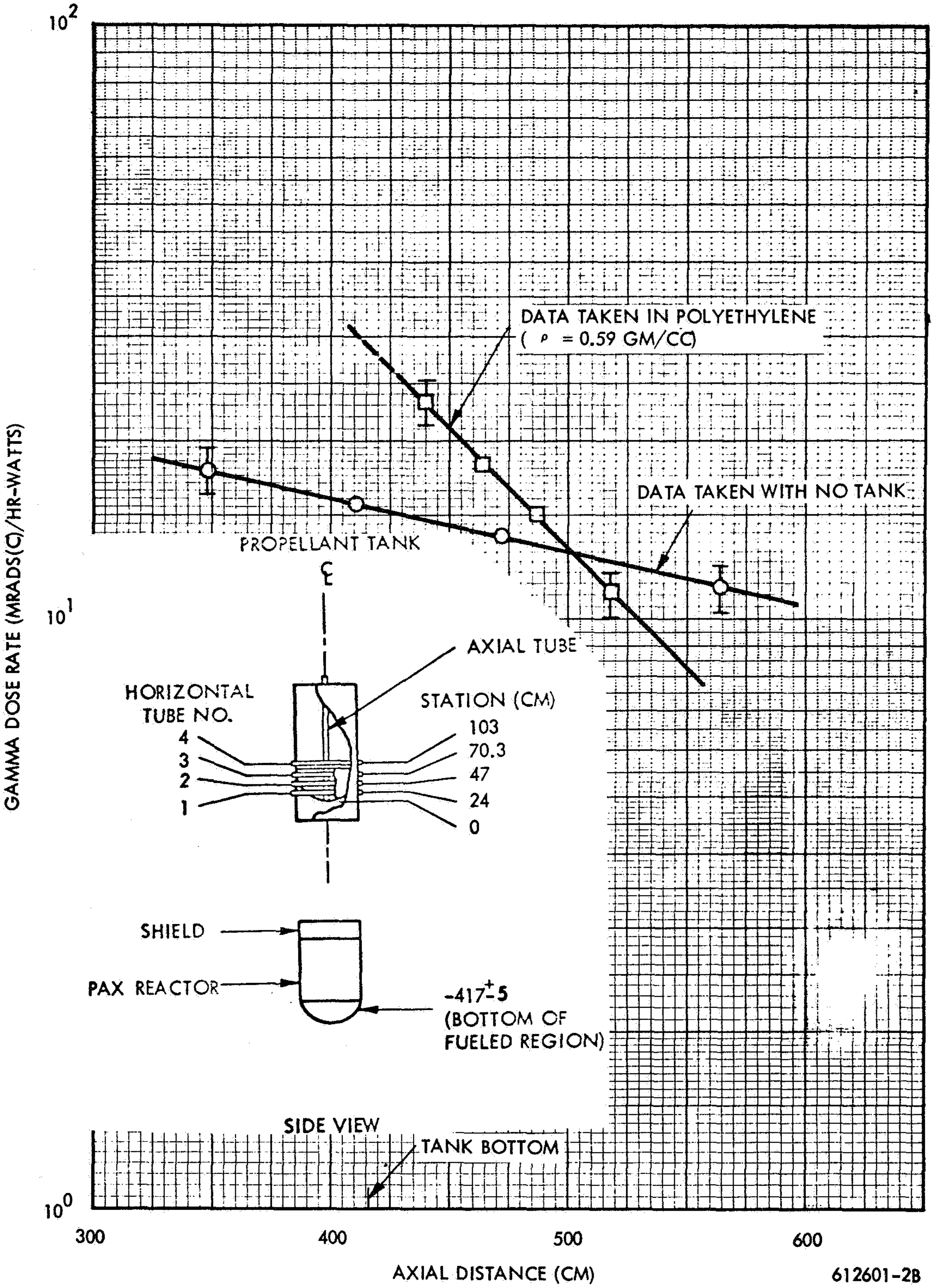

Figure D-5. Gamma Dose Rate as Measured with a Carbon Wall Ion Chamber versus Axial Distance

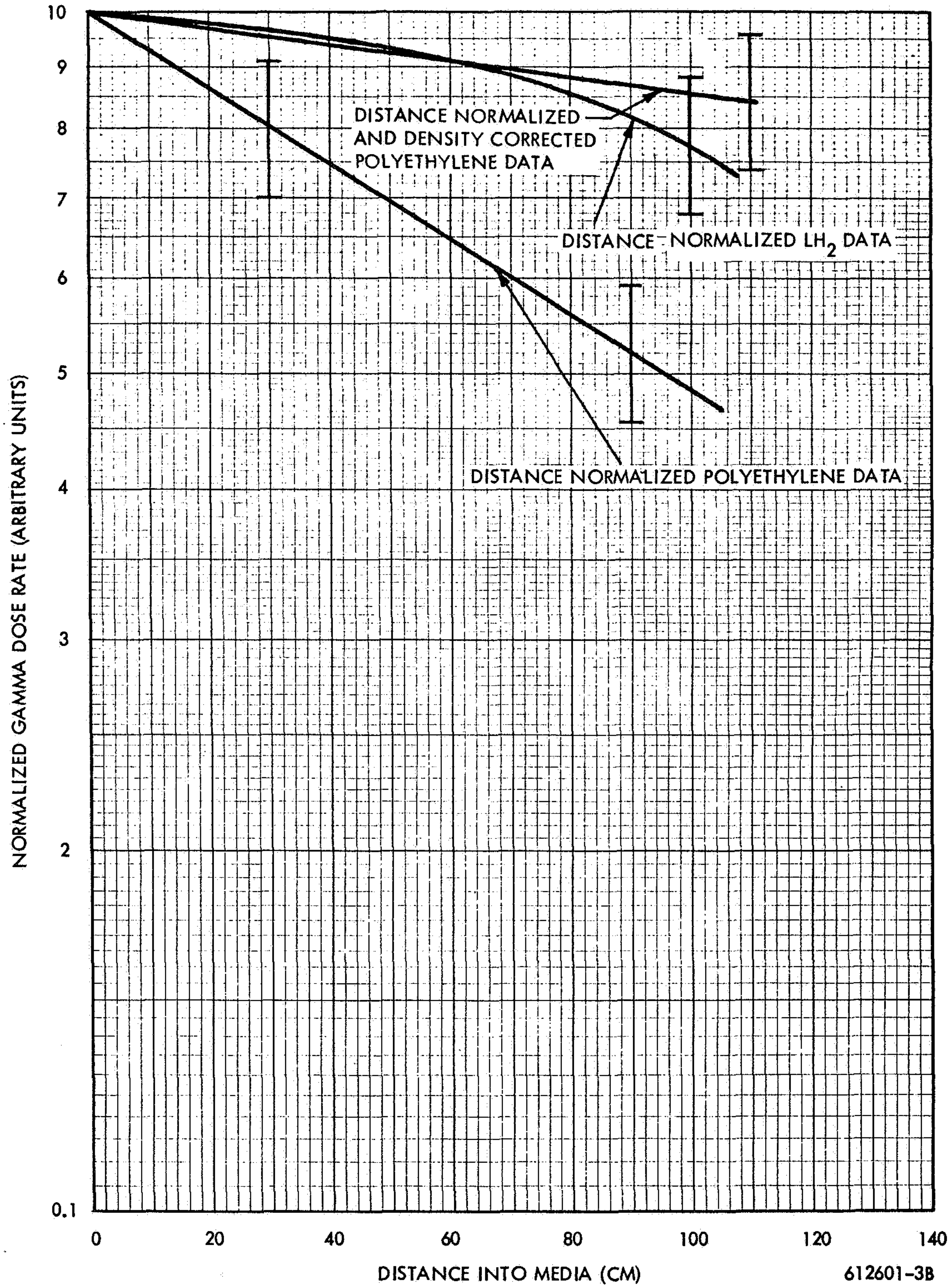

Figure D-6. Normalized Gamma Dose Rate versus Distance into Media